BARC/2001/E/034

BARC/2001/E/034

भारत सरकार
GOVERNMENT OF INDIA
भाभा परमाणु अनुसंधान केन्द्र
BHABHA ATOMIC RESEARCH CENTRE

INVESTIGATIONS ON THE EFFECT OF HEATER AND COOLER ORIENTATION ON THE STEADY STATE, TRANSIENT AND STABILITY BEHAVIOUR OF SINGLE-PHASE NATURAL CIRCULATION IN A RECTANGULAR LOOP

by

P. K Vijayan, V. K. Bhojwani, M H. Bade, M. Sharma,
A. K. Nayak, D. Saha and R. K. Sinha
Reactor Engineering Division

2001

BARC/2001/E/034

BARC/2001/E/034

GOVERNMENT OF INDIA
ATOMIC ENERGY COMMISSION

INVESTIGATIONS ON THE EFFECT OF HEATER AND COOLER ORIENTATION ON THE STEADY STATE, TRANSIENT AND STABILITY BEHAVIOUR OF SINGLE - PHASE NATURAL CIRCULATION IN A RECTANGULAR LOOP

by

P. K. Vijayan, V. K. Bhojwani, M. H. Bade, M. Sharma,
A. K. Nayak, D. Saha and R. K. Sinha
Reactor Engineering Division

BHABHA ATOMIC RESEARCH CENTRE
MUMBAI, INDIA
2001

BIBLIOGRAPHIC DESCRIPTION SHEET FOR TECHNICAL REPORT
(as per IS : 9400 - 1980)

01	*Security classification*	Unclassified
02	*Distribution*	External
03	*Report status*	New
04	*Series*	BARC External
05	*Report type*	Technical Report
06	*Report No*	BARC/2001/E/034
07	*Part No or Volume No*	
08	*Contract No*	
10	*Title and subtitle*	Investigations on the effect of heater and cooler orientation on the steady state, transient and stability behaviour of single-phase natural circulation in a rectangular loop
11	*Collation*	136 p , 62 figs , 12 tabs , 5 ills
13	*Project No*	
20	*Personal author(s)*	P K Vijayan, V K Bhojwani, M H Bade, M Sharma, A K Nayak, D Saha, R K Sinha
21	*Affiliation of author(s)*	Reactor Engineering Division, Bhabha Atomic Research Centre, Mumbai-400 085
22	*Corporate author(s)*	Bhabha Atomic Research Centre, Mumbai-400 085
23	*Originating unit*	Reactor Engineering Division, BARC, Mumbai
24	*Sponsor(s) Name*	Department of Atomic Energy
	Type	Government

Contd (ii)

30	*Date of submission*	December 2001
31	*Publication / Issue date*	January 2002
40	*Publisher / Distributor*	Head, Library and Information Services Division, Bhabha Atomic Research Centre, Mumbai
42	*Form of distribution*	Hard copy
50	*Language of text*	English
51	*Language of summary*	English
52	*No. of references*	32 refs.
53	*Gives data on*	
60	*Abstract*	An instability demonstration facility has been in operation in the Heat Transfer Laboratory of the Reactor Engineering Division for the past few years. This report deals with the investigations carried out in this facility so far. The facility is essentially a rectangular loop designed to generate single-phase natural circulation data on the steady state and stability behaviour for different orientations of the heat source and the heat sink. Effect of different heat addition paths and flow direction on the stability behaviour was also studied. The stability map of the system was generated both by the linear and the nonlinear methods
70	*Keywords/Descriptors*	REACTOR COOLING SYSTEMS; UNSTEADY FLOW; STEADY-STATE CONDITIONS; STABILITY; PHWR TYPE REACTORS; TRANSIENTS; NATURAL CONVECTION; INSTABILITY; VALIDATION; HEAT TRANSFER; OSCILLATION MODES; FLOW MODELS
71	*INIS Subject Category*	S21
99	*Supplementary elements*	

Abstract

An instability demonstration facility has been in operation in the Heat Transfer Laboratory of the Reactor Engineering Division for the past few years. This report deals with the investigations carried out in this facility so far. The facility is essentially a rectangular loop designed to generate single-phase natural circulation data on the steady state and stability behaviour for different orientations of the heat source and the heat sink. Effect of different heat addition paths (i.e. start-up from rest, power raising from initial stable steady state and decay of instability due to power step back) and flow direction on the stability behaviour was also studied. The stability map of the system was generated both by the linear and the nonlinear methods. The findings can be summarised as follows

Instability was only observed for the orientation with both the heater and cooler horizontal. Three distinctive oscillatory flow regimes were identified near the lower stability threshold. The predominant oscillatory regimes are unidirectional pulsing and bi-directional pulsing both of which are nearly periodic. Between these two a regime with chaotic switching between unidirectional and bi-directional pulsing is observed. Unidirectional pulsing is characterized by repetitive flow initiations in the same direction followed by a period of near stagnant flow. Bidirectional pulsing is characterized by the occurrence of alternate forward and reverse (clockwise and anticlockwise) flow pulses. On the phase space (ΔP-W plane), unidirectional pulsing portrays a bean shaped limit cycle whereas bi-directional pulsing portrays a dumbbell shaped limit cycle. The phase portrait for the unstable flow regime with chaotic switching (between unidirectional and bi-directional pulsing) shows a dumbbell shape with a spread around the periphery. The shape of the limit cycle, however, depends on the chosen parameter space. Depending on the chosen parameter space, unidirectional pulsing can portray the hood of a cobra, the jaws of a shark, the sole of a shoe or a bean shaped limit cycle. Similarly, bi-directional pulsing can portray a squirrel, a butterfly, a duck or a dumbbell. As the power increases, the phase plots deform.

Out of the two predominant unstable regimes, unidirectional pulsing was experimentally observed for the first time although Keller (1966) predicted its existence. First experimental confirmation that natural circulation instability exhibits hysteresis was also obtained. The existence of a conditionally stable regime (where the instability threshold depends on the heat addition path) was experimentally confirmed and its thresholds established for the first time. A specified operating point in the conditionally stable regime can be stable or unstable depending on the operating procedure. An operating procedure to achieve stable or unstable operation in the conditionally stable regime was experimentally established. In the conditionally stable regime, the heat transport capability of the unstable flow was found to be inferior to the stable flow at the same power. Both unidirectional pulsing and the chaotic switching between unidirectional and bi-directional pulsing are observable only in the conditionally stable regime. For the unconditionally unstable regime, the observed oscillatory mode is always bi-directional pulsing.

Three distinct mechanisms for instability development were observed. In the first two, instability was observed right from flow initiation. In one of these, the oscillation growth terminates after a few cycles and unidirectional oscillations with practically the same amplitude is observed. In the second mechanism observed at a higher power, a switch to bi-directional pulsing terminates the oscillation growth. Both the above mechanisms are found only for start-up from rest. The third mechanism is observed when power is increased to an unstable value from a stable steady state. Here the growth of small amplitude oscillations as described by Welander (1967) is the mechanism causing instability. Here also a switch to bi-directional pulsing terminates the oscillation growth.

Period doubling is observed while the oscillatory mode switches from unidirectional to bi-directional pulsing at low powers. As the power is increased the period enhancement reduces (i.e less than 2). Although the magnitude of the period *before and after switching is not reproducible, the period ratio is* nearly reproducible. For the development of instability following an oscillation growth mechanism also, period enhancement is observed while switching from the unidirectional to the bi-directional pulsing. In this case, period doubling and even tripling is observed. For all cases tested, the period enhancement ratio is found to vary between 2 and 3 only. Although the period enhancement ratio is nearly reproducible for a given power, it is found to change randomly with small changes in power.

Before the transition to fully developed two-phase flow instability, a region of compound single phase-two phase instability, which is characterized by the occurrence of a subcooled boiling region during the low flow period of the oscillation cycle is observed. Three distinctive regimes were identified for this case: (a) compound instability with sporadic subcooled boiling at low power, (b) compound instability with a two-phase region once in every cycle at intermediate power and (c) compound instability with two-phase region occurring twice in every cycle at high power. In the present experiments, power was not sufficient to cause boiling for the complete duration of the oscillation cycle. The oscillatory regime is bi-directional pulsing for the entire compound single phase-two phase instability. With the inception of subcooled boiling, bi-directional pulsing becomes chaotic leading to the formation of cusps on the phase plot.

The steady state data for all orientations were found to be in good agreement with the theoretical flow correlation. Linear and nonlinear analyses for the stability of the steady states gave almost identical thresholds. With the nonlinear analysis code, it was possible to identify the different unstable flow regimes. It also helped to identify the thresholds of the conditionally stable region. However, there is significant deviation in the predicted and measured thresholds for the different unstable flow regimes and the conditionally stable regime. This is attributed to the simplified analysis, which neglects wall effects and 3-D nature of the flow. The significance of the conditionally stable regime is that the linear analysis alone is not sufficient to ensure stable operation. To ensure this, an appropriate operating procedure needs to be established by nonlinear analysis.

Linear analysis showed that the orientation with both heater and cooler vertical is most stable and the orientation with both cooler and heater horizontal is least stable although the latter is capable of the highest flow (from steady state analysis). For a given heater orientation, the loop with vertical cooler is more stable than the one with horizontal cooler. For a specified cooler orientation, the loop with heater vertical is more stable than the one with heater horizontal. Comparison of the data with the predicted stability map showed that the 1-D analysis is conservative (in that it predicts larger unstable zone than experimentally observed). This is attributed to the neglect of wall effects and 3-D nature of the flow.

Another significant finding from the theoretical model as well as the experiment is that the instability is due to thermal stratification, which causes the hot plug to remain stranded just below the elbow in the vertical down leg. Therefore, locating the cooler just below the elbow in the vertical down leg enhances stability. Other methods to suppress the instability are to enhance the L_v/D and St_{in}. Enhancing the St_{in} beyond a certain value can completely eliminate the instability. However, enhancing the L_v/D can only shift the unstable zone but *cannot eliminate it altogether. Effect of* the heater and cooler lengths on the stability behaviour was studied using the linear method for the orientation with both heater and cooler horizontal. The heater length is found to have only a marginal effect on the stability whereas the effect of cooler length is significant. Increasing the length of both heater and cooler is found to enhance stability.

CONTENTS

1. INTRODUCTION

A heat source and a heat sink connected by piping forms the essential hardware of a natural circulation loop (NCL). Usually the heat sink is placed at a higher elevation to promote natural circulation. The flow takes place due to the buoyancy force caused by the density gradient resulting from heat transfer. The fluid circulation can continue as long as the heat source and the heat sink are available without the help of a fluid moving machinery. Due to this, natural circulation loops find extensive application in several industries. It includes nuclear reactor core cooling, solar water heaters, transformer cooling, cooling of internal combustion engines and rotating machinery like the gas turbine. Other traditional applications include geothermal power extraction, permafrost protection and low flow corrosion studies. Emerging new applications include computer-cooling, study of deterministic chaos and heat dissipation with the help of so called "liquid-fins".

Current generation of nuclear reactors are designed to remove core heat by natural circulation in the event of a pump failure. The predicted and observed mode of core cooling is by single-phase natural circulation in PWRs (Pressurised Water Reactors) and PHWRs (Pressurised Heavy Water Reactors) during a power failure to the circulating pumps. Calculations show that the current designs of PWRs can remove as much as 20% of core power by single-phase natural circulation (D'Auria et al. (1999)). Advanced designs of PWRs like the CAREM reactor employs single-phase natural circulation as the normal mode of core cooling (Delmastro (2000)). In addition, many reactors used to produce hot water for the district heating system in cold countries employs single-phase natural circulation as the normal mode of core cooling (Gureeva et al. (1989)).

In different types of nuclear reactors the orientation of the heat source (core) and the heat sink (steam generator) are different. For example, PHWRs have horizontal core and vertical steam generators, PWRs have vertical core and vertical steam generator and VVERs have vertical core and horizontal steam generators. In view of this an experimental program was initiated to study the effect of heater and cooler orientation in a rectangular natural circulation loop.

It is of interest to study how the flow develops following the application of heating to initially motionless and isothermal fluid in the loop with different heater and cooler orientations. It may be noted that natural circulation flow can initiate only after the generation of a buoyancy force. This will happen only when there is a temperature difference between the vertical limbs of the loop. With the vertical heater, a temperature difference and hence a buoyancy force is generated almost instantaneously following the application of heating. However, in the case of horizontal heating with quiescent initial state, axial conduction is the only heat transfer mechanism, which can cause heating up of the vertical limbs. Pure conduction, however, will generate identical temperatures in the vertical limbs (if the unheated portion of the horizontal tube is same on either side of the heater), which will not generate a net buoyancy force in one direction to initiate loop flow. Hence it will be interesting to study the effect of heater and cooler orientation on the start-up (flow initiation) transient.

Natural circulation loops are susceptible to instability. Operation with an unstable natural circulation loop is undesirable as it can lead to problems in control and occurrence of CHF during low flow periods. Generally, restricting operation within the stable zone ensures smooth operation of the reactor. The stable and unstable zones are usually identified with the help of stability maps obtained by a linear stability analysis. The linear stability analysis generally predicts a lower and an upper stable zone. However, it is of interest to investigate

the nature of the unstable oscillatory behaviour as these systems can pass through an unstable zone at least temporarily during start-up, power raising or pressure raising. Hence an experimental investigation of the unstable oscillatory behaviour has been carried out in a simple rectangular loop near the lower stability threshold predicted by the linear stability analysis. In addition to the stability characteristics, the steady state and transient behaviours were experimentally studied for different orientations of the heater and cooler. The experimental results have been compared with theoretical predictions obtained by the one-dimensional theory. The adequacy of the linear stability analysis to predict the stability thresholds of the non-linear single-phase density wave oscillations in a simple rectangular loop has been examined by comparing it with nonlinear analysis using finite difference technique. The results of these studies are documented in this report.

2. REVIEW OF PREVIOUS WORK

Keller (1966) theoretically studied a rectangular natural circulation loop with point heat source and sink located at the centre of the bottom and top horizontal sections respectively. He predicted unidirectional periodic flow oscillations that depend on the interplay between friction and buoyancy forces but is unaffected by inertia. Theoretical investigations by Welander (1967) studied the oscillatory behaviour in a somewhat similar rectangular loop (the only difference was that the two vertical pipes were joined by horizontal bottom and top sections of zero length where the point source and sink were located) and proposed a mechanism for the instability based on growth of small amplitude oscillations. For the sake of convenience we refer to it Welander mechanism of instability.

Experiments by Creveling et al. (1975) showed for the first time the occurrence of the instability for ordinary fluids albeit in a toroidal loop. The mechanism for the instability was observed to be that proposed by Welander. Subsequent experimental work by Gorman et al. (1986) in the toroidal loop of Creveling observed three different chaotic flow regimes: a globally chaotic regime whose essential features can be described by a one-dimensional cusp-shaped map, a subcritical regime in which flow can be either chaotic or steady, and a transient regime in which the flow remains chaotic for a time and then decays into a steady flow.

Coming back to the stability characteristics of rectangular loops, the work by Chen (1985) showed that the aspect ratio (height/width) plays an important role on the stability of a rectangular loop. In Chen's work, the loop considered had the entire bottom horizontal pipe heated and the entire top horizontal pipe cooled. His predictions showed that the loop became more unstable as the aspect ratio approached unity. The earliest experimental work in a rectangular loop with vertical heater and cooler by Holman and Boggs did not study the instability. Subsequent work in rectangular loops by Huang-Zelaya (1988), Misale et al. (1991), Bernier-Baliga (1992) and Ho et al. (1997) also concentrated on the steady state behaviour. Vijayan et al. (1992) observed instability for the largest diameter loop while experimenting with three rectangular loops of diameter 6, 11 and 23.2 mm respectively. All the three loops had the same length with the central portions of the bottom and top horizontal pipes acting as source and sink respectively. The observed instability behaviour involved repetitive flow reversals. They also observed a conditionally stable regime in which the flow can be steady or oscillatory depending on the path followed in the experiment for changing the power. However, experiments were not conducted for very low powers and unidirectional oscillations as proposed by Keller (1966) were not observed. Subsequently Misale et al. (1999) observed instability in rectangular loops that also showed repetitive flow reversals. Experiments by Nishihara (1997), however, obtained unidirectional oscillatory instability in a

rectangular loop with both the source and sink vertical This showed that single-phase natural circulation instability can be observed in loops with asymmetric heating and cooling conditions just as two-phase natural circulation instability This raised the following question Why single-phase instability is not observed in large systems such as the nuclear reactor loop? This is especially important now since a few new designs like the CAREM reactor are being developed with single-phase natural circulation as the normal mode of core cooling Hence a new study has been undertaken to characterise the oscillatory behaviour in rectangular loops with different orientations of the heat source and sink

3. EXPERIMENTAL INVESTIGATIONS

3.1 Description of the Test Loop

The experiments were carried out in a uniform diameter rectangular natural circulation loop It was built with borosilicate glass tube of inside diameter 26 9 mm and outside diameter 28 9 mm Fig 1a and b show a schematic diagram and photograph respectively of the test loop The loop had two heaters and two coolers One of the heaters was constructed horizontally at the lowest elevation and the other was vertical The heaters rated at 2 kW each, were made of 1 mm diameter nichrome wire evenly wound on the outside of the glass tubes The lengths of the horizontal and the vertical heaters were 620 mm and 735mm respectively The coolers were tube-in-tube type with the coolant (water) flowing through the annulus One of the coolers was constructed horizontally at the upper most elevation and other vertical on the right side limb as shown in Fig 1a Each cooler is 800 mm long with the outer tube inside diameter of 49.2 mm and 1 5 mm wall thickness The coolant flow to the secondary side of the cooler was provided from an overhead tank The coolant inlet line had three valves in series, two of which were used to adjust the coolant flow while the third was used to valve-in or valve-out the cooler

The loop also had an expansion tank located at the highest elevation to take care of the thermal expansion of water It was kept open to atmosphere, so that during experiments the primary loop pressure was near atmospheric The same valve located in the bottom horizontal tube was used for both filling and draining operations In addition to the expansion tank, another vent connection was provided after the horizontal cooler as shown in Fig 1a To reduce the heat losses, the loop was insulated by ceramic mat except for the operating cooler The uninsulated cooler helped in the visualisation of flow

3.2 Instrumentation

Mineral insulated 0 5mm diameter chromel-alumel thermocouples (K-type) were used to measure the temperatures The loop was instrumented with 12 thermocouples (denoted as TC1 to TC12 in Fig 1a) to measure pipe centre temperature at different locations The thermocouples were inserted through a capillary glass tube Measuring accuracy of the thermocouples was 0 4% (± 1 1 ^{0}C) The thermocouples were calibrated in the range 0-150 ^{0}C, which is well within the operating range of the present experiments The pressure difference across a 1065 mm long section of the bottom horizontal tube was measured with the help of a calibrated differential pressure transmitter (DPT), which had a measuring accuracy of 0 25% of the span The impulse lines connected to the DPT (Rosemount make) were branched-off from the bottom of the horizontal glass tube to prevent ingress of air and steam The differential pressure transmitter was calibrated in the range of – 100 to + 100 Pa (– 10 to + 10 mm of water column) The negative range was included to indicate flow reversal

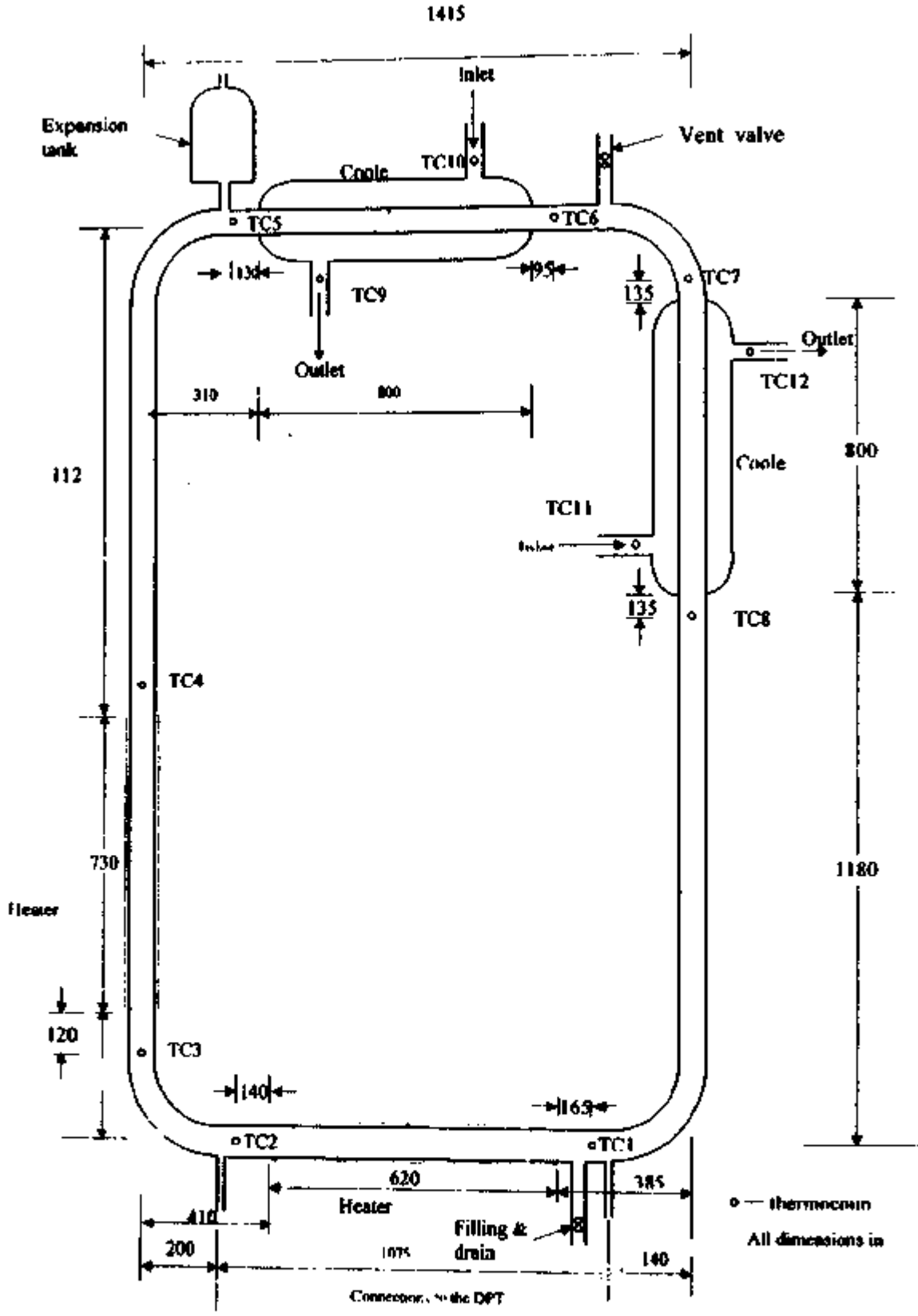

Fig.1a: Schematic of the test

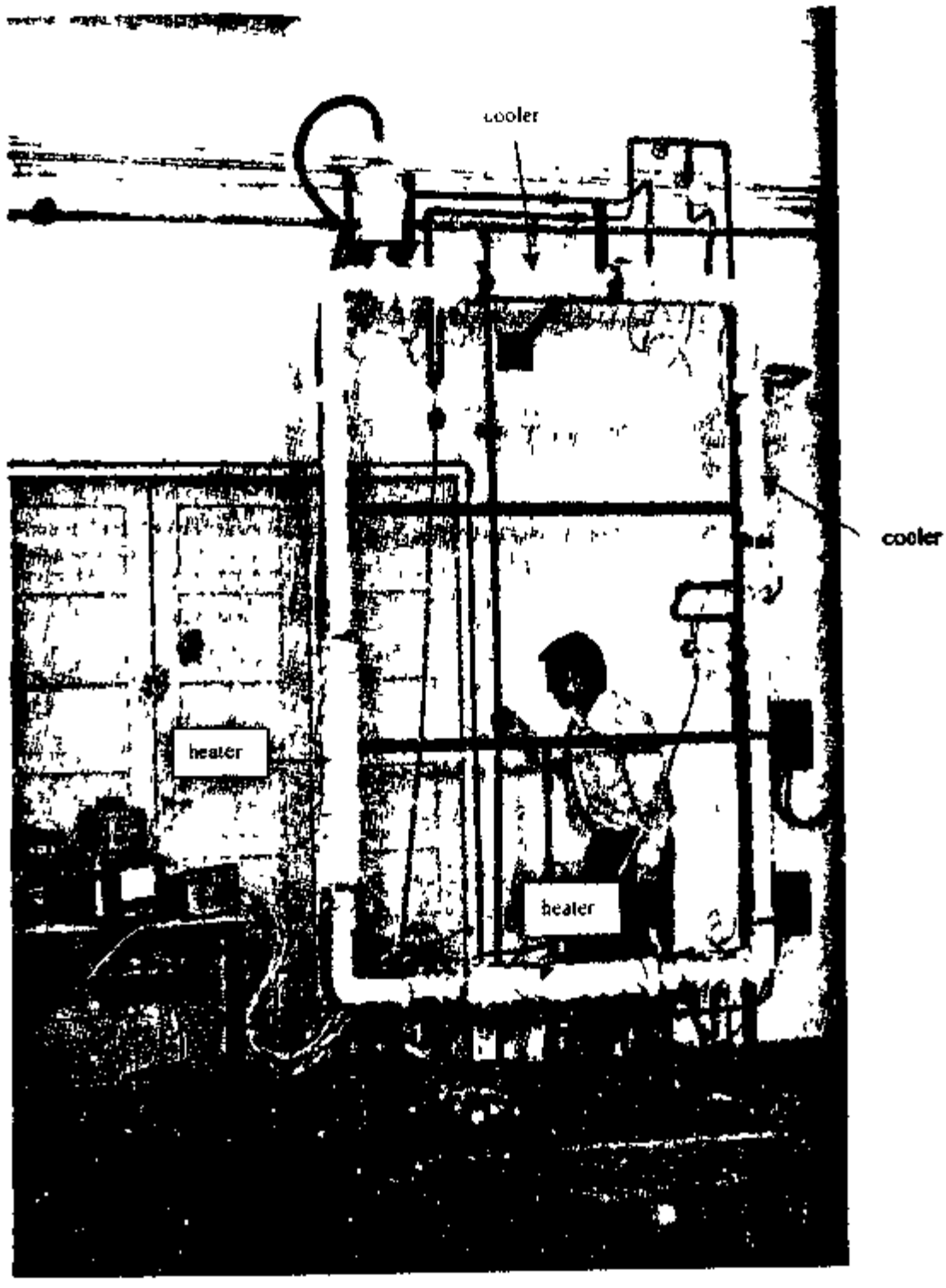

Fig. 1b: Photograph of the experimental loop

The coolant flow rate was measured directly by collecting the water in a measuring flask and noting the time required using a stopwatch. The heater power could be varied with the help of a dimmerstat and was measured using a wattmeter, which had an accuracy of 0.5% of the span (0-1250 W). For recording the steady state experimental data a Graphtec Digital Multicorder was used, on which five temperature readings and the pressure drop across the heater were recorded as it had only six channels. The accuracy of this instrument was 0.05% of the range for pressure drop (ΔP) and 1^0C for temperature. The Graphtec Recorder also had a graphic display screen of all the channels available on it. During recording a chart speed of 60 mm per minute was used. Other channels were monitored at regular intervals with a digital temperature indicator, which had an accuracy of $\pm$ 1^0C. To enable the digital recording of the unstable behaviour, a Penny+Giles Multitrend data logger was used. The data logger had eight channels (one ΔP and the remaining seven thermocouples) with a scanning rate of 1.5 s. Data could be stored in a 3.5" floppy disc and analysed to obtain time trace of the parameters. Accuracy of the instrument was $\pm$ 1^0C for temperatures. During the transient and stability experiments, the digital data were acquired on floppy disk.

3.3 Experimental Procedure

To avoid heat loss through the non-operating cooler, its outer glass tube was insulated and the secondary side (i.e. the annulus) was completely drained. Then the primary loop was filled with tap water. To drive out the air bubbles, the filling flow was continued for some more time with pulsing. To remove the dissolved gases in the water, the loop was run under natural circulation condition at a power significantly higher than that of the proposed test for some time (1 to 2 hours). This procedure was followed in all the tests to drive out the dissolved gases. Before the experiment, the secondary cooling water flow rate was set at the required value. Sufficient time (1 to 2 hours) was given for the test loop to stabilise at room temperature without heating.

3.3.1 Steady state test procedure

When steady initial conditions were reached, the reading was noted with zero power. Then, the heater was put on and set at the required power using the dimmerstat. By observing the trend of the pressure drop (ΔP) and temperature variation in graphical display mode on the Graphtec recorder, the steady state condition can be judged. At the steady state condition, all the temperature and ΔP data were collected. Then, the power was increased in steps of 100 W and allowed to attain the steady state. The same procedure was repeated till the power reached 1000 W. The power was then brought down to 950 W. After achieving steady state, the power was brought down in steps of 100 W allowing to attain the steady state for each power. The procedure was repeated till power reached 50W. Thus steady state data could be generated in the range of power from 50 to 1000 W. Repeatability of the test results was also checked.

3.3.2 Procedure for Generating Data on the Flow Initiation Transient

These experiments were carried out by suddenly switching on the heater when the fluid was stagnant at uniform initial temperature throughout the loop. To achieve uniform initial temperature, the cooling water was valved-in one to two hours before the actual tests as mentioned before. After achieving uniform temperatures (indicated by the temperature trends in the Penny+Giles Multitrend data logger) the power was switched on. The dimmerstat position was preset to obtain the required power before switching on the heater. Immediately

after the power was put on the digital recording of the data began. Usually, the time delay between the instants of switching on the heater and the start of recording was less than one second. The system was allowed to continue like this till the attainment of the steady state. The pressure drop across the heater and seven temperatures (TC-1 to TC-6 and TC-8) were recorded on the floppy disc during the experiment.

3.3.3 Procedure for the Stability tests

Preliminary experiments have established that single-phase instability occurs only for the case of horizontal heater and horizontal cooler (HHHC) orientation. The instability threshold was found to be different for different heat addition paths. Hence we studied the oscillatory scenario for the following heat addition paths:

1) start-up from stagnant conditions (designated as test series # 1),
2) Power Raising from Stable Steady state conditions (PRSS) (test series # 2) and
3) Decay of Instability due to Power Step-back (DIPS) (test series # 3).

All the above tests were carried out with the same cooling water flow rate (5 lpm) and inlet temperature (around 34 ^{0}C). The pressure drop across the heater and seven temperatures (TC-1 to TC-6 and TC-8) were recorded on the floppy disc during the experiment. In order to appreciate the oscillatory scenario better, the nominal fluctuations in the various measured quantities were established first for the steady state and stagnant initial conditions. The fluctuation in the controlled coolant flow rate was within $\pm$ 3% of the set value. The coolant inlet temperature was not controlled and was found to vary by 1 to 3 ^{0}C during the 12-hour duration of the test. For the steady state condition, the fluctuation in the temperatures at various locations in the loop was within $\pm$ 1^{0}C from the mean value. Even for the unheated initial condition, a maximum fluctuation of $\pm$ 0.5 ^{0}C was observed instead of a uniform temperature throughout the loop. The steady state fluctuations in the wattmeter reading was $\pm$ 2.5W. Similarly, steady state fluctuations in the ΔP reading was $\pm$ 0.15 Pa ($\pm$ 0.015 mm of water column). During stagnant conditions, the ΔP fluctuations were of the same order. A brief experimental procedure is given below for each test.

3.3.3.1 Start-up from stagnant conditions (Test Series # 1)

The experimental procedure followed was same as that described in section 3.3.2 except that the system was allowed to continue operation in the unstable state for a period of six to ten hours for every test. In the following morning, the same procedure was repeated for another power. The primary objective of these tests was to obtain the threshold power at which the system can be started up without encountering instability.

3.3.3.2 Power Raising from Stable Steady state Conditions (PRSS Test Series # 2)

In these experiments, an initial stable steady state with unidirectional flow was achieved first. For achieving the initial steady state, the procedure followed in the previous test series (i.e. 3.3.3.1) was adopted. After achieving the initial steady state, a step increase in power was given. Sufficient time was given to achieve a steady or oscillatory behaviour. If the system remains stable another step increase in power was given. The process was repeated till the instability was observed. The objective was to determine the threshold value upto which power can be raised smoothly (in single or several steps) without encountering instability.

3.3.3 3 Decay of instability due to power step back (DIPS) (Test series # 3)

Here an initial oscillatory condition was established first. To establish this condition, the procedure followed was the same as that employed in series # 1 tests (i.e. 3.3.3.1). After the oscillatory behaviour sets in sufficient time was allowed for the initial transients to die out. Then a step decrease in power was given. Sufficient time was allowed to achieve a stable state. If a stable state is not achieved another step decrease in power was given. The procedure was repeated until a unidirectional steady flow is achieved. The test was repeated for different initial oscillatory flow conditions. The objective of these tests was to obtain the threshold value to which the power must be brought down to achieve stability from an unstable state.

3.4 Experiments Conducted

Steady state, transient and stability tests were carried out for various orientations in the loop.

3.4.1 Steady State Experiments

The objective of these tests were to check the adequacy of the generalised flow correlation (see Vijayan (1999)) to represent data generated with various heater and cooler orientations. Steady state experiments were carried out for the following orientations of the heater and cooler:

1) Horizontal Heater and Horizontal Cooler (HHHC)
2) Horizontal Heater and Vertical Cooler (HHVC)
3) Vertical Heater and Horizontal Cooler (VHHC)
4) Vertical Heater and Vertical Cooler (VHVC)

The centre line elevation difference between the cooler and the heater is given in Table 1 for the various orientations of the cooler and heater. The analysis of the steady state data is given in section 4.

Table 1: Centre line elevation difference (Δz_c) between the cooler and heater for different orientations:

Orientation	Δz_c - m
HHHC	2.185
HHVC	1.580
VHHC	1.5075
VHVC	0.9025

3.4.2 Transient Behaviour

These are basically the flow initiation transients, which were also conducted for all the four orientations mentioned above. Results of these tests are given in section 5.

3.4.3 Stability Experiments

As already stated, the stability tests were carried out for all orientations, i.e. HHHC, HHVC VHHC and VHVC. Out of these single-phase instability was observed only for the HHHC orientation. For this case, the stability behaviour was dependent on the heat addition mode. Three heat addition modes were investigated and their results are presented in section 6.

4. ANALYSIS OF STEADY STATE DATA

Prior studies (Vijayan (1999)) showed that the steady state flow in single-phase natural circulation loops could be expressed as

$$Re_{ss} = C\left[\frac{Gr_m I_{ss}}{N_G}\right]^Y \quad (1)$$

Where $Gr_m = D_r^3\rho^2\beta g\Delta T_r/\mu^2$, $\Delta T_r = QH/(A_r\mu C_p)$, $I_{ss} = \oint(\theta(S))_{ss}dZ$, C = $(2/p)^t$ and $t = 1/(3-b)$ with p and b obtained from a friction factor correlation of the following form.

$$f = p/Re^b \quad (2)$$

The geometric parameter, N_G is defined as

$$N_G = \frac{L_1}{D_r}\sum_{i=1}^{N}\left(\frac{l_{eff}}{d^{1+b}a^{2-b}}\right)_i \quad (3)$$

Where $D_r = \frac{1}{L_1}\sum_{i=1}^{N} D_i L_i$; $d_i = \frac{D_i}{D_r}$; $a_i = \frac{A_i}{A_r}$; $A_r = \frac{1}{L_1}\sum_{i=1}^{N} A_i L_i$ and $\left(l_{eff}\right)_i = \frac{\left(L_{eff}\right)_i}{L_1}$

For a uniform diameter loop with negligible local pressure losses (D_r = D, A_r = A and $(L_{eff})_i$=L_i. Hence, d =1, a = 1 and l_{eff} =1) N_G is obtained as

$$N_G = \frac{L_1}{D} \quad (4)$$

The local pressure losses has been accounted by introducing an equivalent length, Le, defined as

$$K = f\frac{Le}{D} \quad (5)$$

If the local pressure losses are significant, then

$$N_G = \frac{L_1}{D}\sum_{i=1}^{N}\left(l_{eff}\right)_i \quad (6)$$

where $(l_{eff})_i$ =(Leff)$_i$/L_1 and (Leff)$_i$= L_i + Le_i. The numerical value of the integral I_{ss}=1 for the HHHC orientation so that the steady state flow is given by

$$Re_{ss} = C\left[\frac{Gr_m}{N_G}\right]^Y \quad (7)$$

For other orientations, the value of $I_{ss} \neq 1$ and hence, Eq. (7) is not applicable. For orientations other than HHHC, Eq. (1) is to be used with the actual value of I_{ss}. The expressions for I_{ss} are given in Appendix-1. However, if we assume that the temperature variation is linear in the cooler then the steady state flow rate can be calculated by the following expression (see Vijayan (2000) for its derivation).

$$Re_{ss} = C\left[\frac{(Gr_m)_{\Delta z_c}}{N_G}\right]^{\gamma} \tag{8}$$

Where $(Gr_m)_{\Delta z_c} = D^3\rho^2\beta g Q_h \Delta Z_c / A\mu^3 Cp$. If we replace H with Δz_c, the centre line elevation difference, then equation (1) can be rewritten as

$$Re_{ss} = C\left[\frac{(Gr_m)_{\Delta z_c}}{N_G}\frac{H}{\Delta z_c} I_{ss}\right]^{\gamma} \tag{9}$$

Comparing equations 8 and 9, it is easy to show that the error, E, introduced by the assumption of linear variation of temperature in the cooler is given by the following expression

$$E = \left[\frac{H}{\Delta z_c} I_{ss}\right]^{\gamma} \tag{10}$$

If the value of E is unity, then no error is introduced. For HHHC orientation, Δz_c=H and I_{ss}=1, hence E=1. For the VHHC orientation, I_{ss}= Δz_c/H, leading to E=1. For other orientations, the error of approximation is a function of the St_m. The error of approximation is found to be less than 1% (see Appendix –2) for the present loop where $0.2 < St_m < 0.6$. Therefore, the steady state flow rate for all orientations can be obtained from the following equations,

$$Re = 0.1768\left(\frac{(Gr_m)_{\Delta z_c}}{N_G}\right)^{0.5} \quad \text{for a fully laminar loop (p=64 and b=1)} \tag{11}$$

$$\text{and } Re = 1.96\left[\frac{(Gr_m)_{\Delta z_c}}{N_G}\right]^{\frac{1}{2.75}} \quad \text{for fully turbulent loop (p=0.316 and b=0.25)} \tag{12}$$

It is of interest to see how good are these relationships with respect to the present experimental data.

4.1 Testing of the Steady State Correlation with Present Experimental Data

From the experimental data, the steady state natural circulation mass flow rate, W_{ss}, is obtained as follows:

$$W_{ss} = \frac{Q_h}{Cp_h(\Delta T_h)_{ss}} \tag{9}$$

Where the specific heat, Cp_h was calculated based on the average temperature (T_h) of the heater section (taken as the mean of the inlet and the outlet temperatures). ΔT_h was obtained as the difference of the measured outlet and inlet temperatures of the heater at steady state.

Using this mass flow rate, the Reynolds number was calculated Both the Re and Gr_m were calculated using the fluid properties estimated at the loop average temperature (taken as the arithmetic mean of temperatures indicated by thermocouples TC1 to TC8) Geometric number (N_G) was calculated using equations 4 and 6 for the case without and with local pressure losses respectively (see appendix-3) Three 'Tee' joints (with blocked branch) and four 90^0 elbows were the sources of local pressure losses in the current experimental loop The 90^0 elbows were assigned a loss coefficient of 0 9 and the Tee junctions were assigned a loss coefficient of 0 4, so that the total local loss coefficient of the loop amounts to 4 8 (Streeter and Wylie (1983))

The steady state data are compared with the theoretical correlations in figures 2a and 2b without and with consideration of the local pressure losses respectively The experimental data is observed to be very close to the theoretical correlation for all orientations of the heater and cooler confirming the validity of the correlations (7) and (8) The local pressure losses affects the results only marginally (see Fig 2b)

5. FLOW INITIATION TRANSIENTS

These tests were carried out for all orientations of the heater and cooler and the results are described orientation-wise

5.1 HHHC Orientation

With this orientation, the flow can initiate in either direction In the present loop, however, the flow initiated most of the times in the clockwise direction unlike earlier experiments with horizontal heaters by Vijayan (1988 and 1992) This could be due to a very slight inclination of the horizontal tube near the elbow, which favoured clock-wise flow If, however, flow initiated in the counter-clockwise direction (observed only for power greater than 250 W, then flow continued in that direction In the present report, the results for the clockwise flow only are presented Several experimentally observed start-up transients are reported in Fig 3 for the HHHC orientation For this orientation, stable behaviour was observed only for very low power (see Fig 3) Following the application of power, the pressure drop (ΔP) begins to rise after a quiescent initial state ($\Delta P = 0$), indicating the initiation of flow through the loop A possible mechanism that causes the loop flow to initiate appears to be the following

Immediately after the start of heating local convection currents are set up in the horizontal heater, which are initially stable With continued heating, the local convection currents become unstable and begin to move side ward diffusing heat towards the unheated horizontal ends of the heater Eventually, a temperature difference is created between the vertical limbs, which causes the flow During the quiescent initial state a hot plug of fluid is formed in the heater During flow initiation, this hot plug issues out into one of the vertical limbs The ascending hot plug accelerates the fluid causing a rapid increase of the ΔP and hence the flow Simultaneously, cold fluid enters the heater As the hot plug enters the top horizontal section, the buoyancy force reduces decelerating the flow As the entire hot plug enters the top horizontal section, its contribution to buoyancy force is zero, but a low flow continues due to the warm fluid issuing out of the heater During the low flow period another hot fluid plug begins to form in the heater The second peak in ΔP is obtained when this hot plug is ascending the hot leg The second hot plug, however, is less hot (because it stayed for a less time in the heater) than the first leading to a smaller peak ΔP than the first This results in an

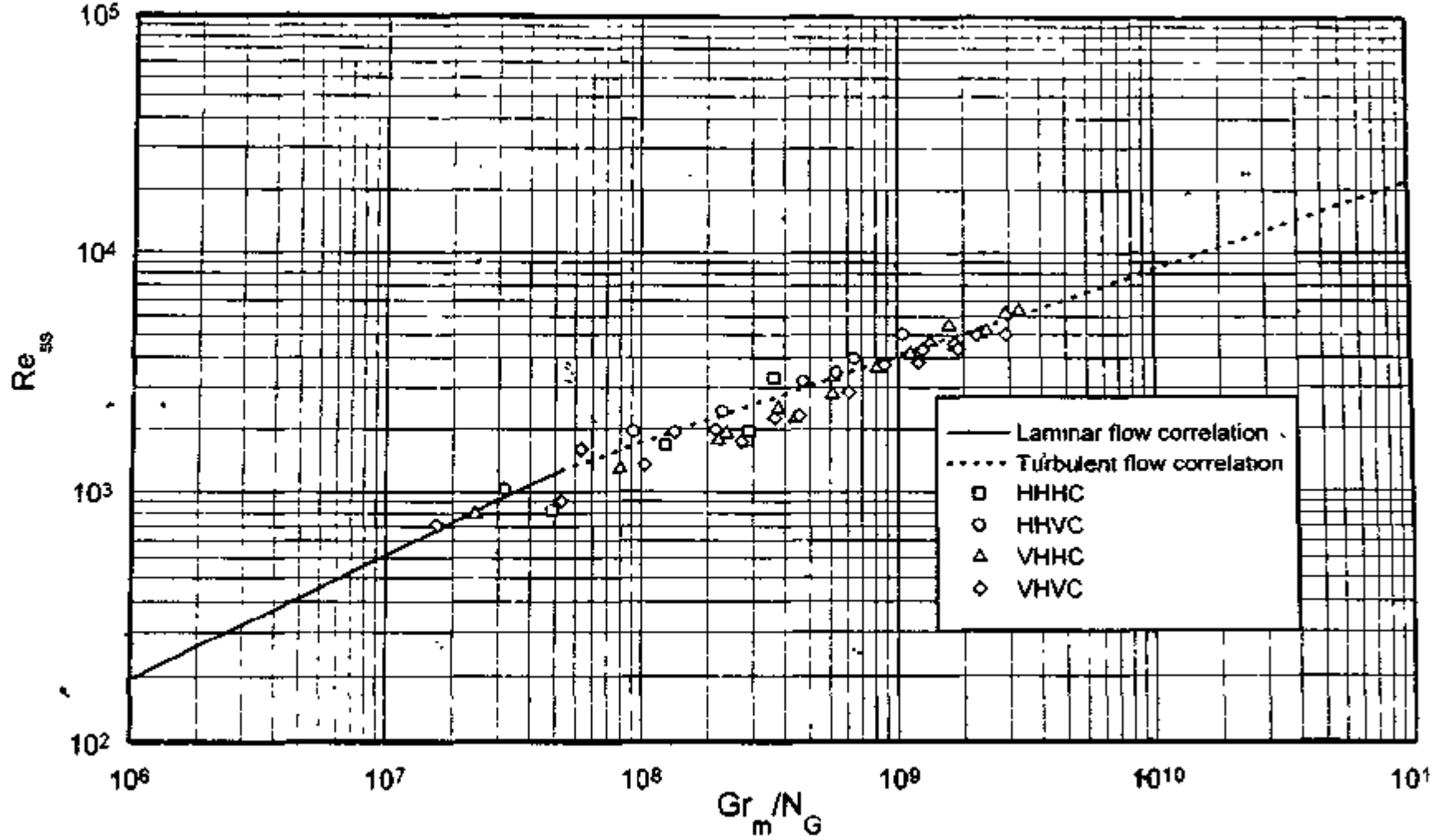

Fig. 2a: Steady state natural circulation data without considering the effect of local losses

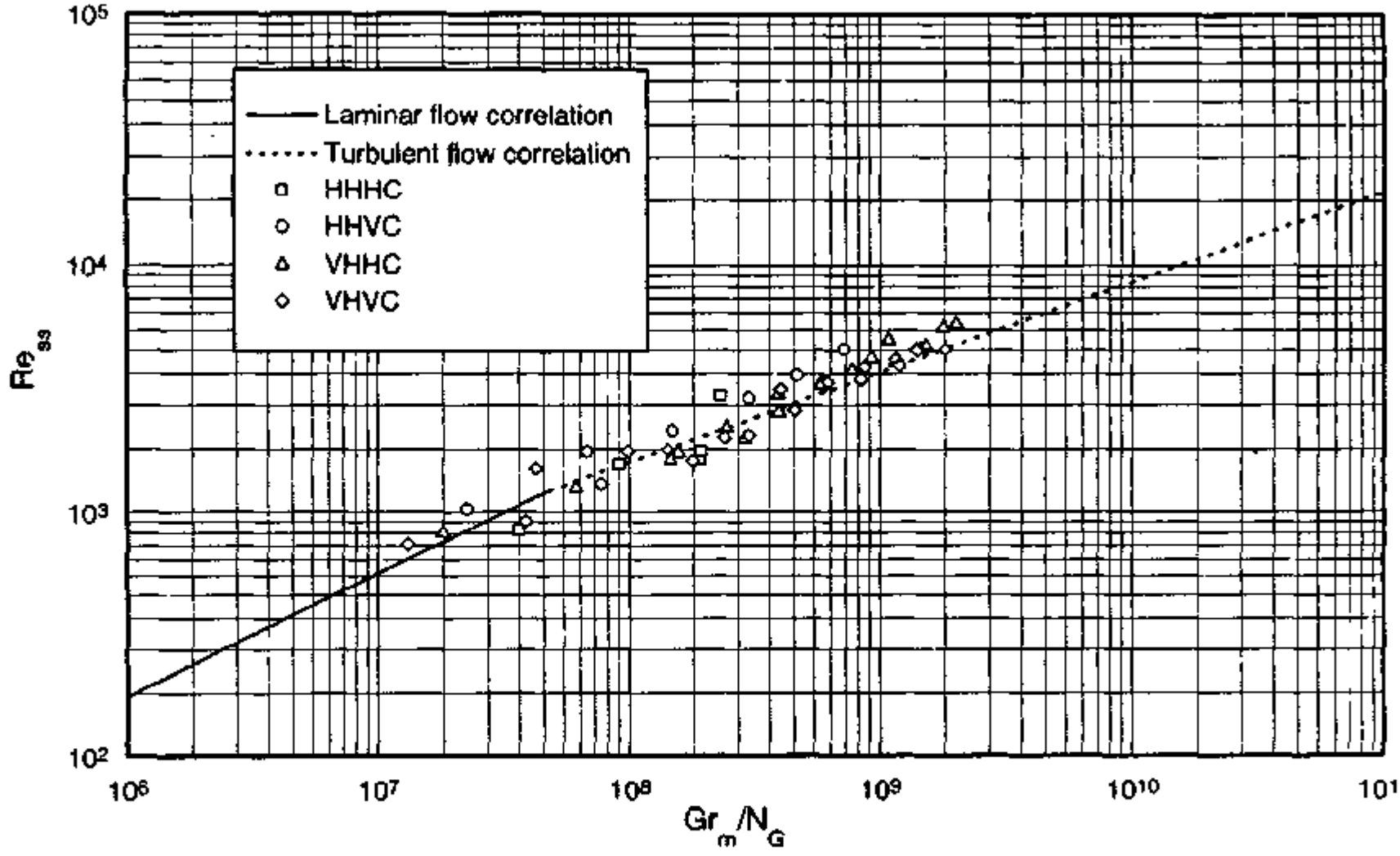

Fig. 2b: Steady state natural circulation data considering the effect of local losses

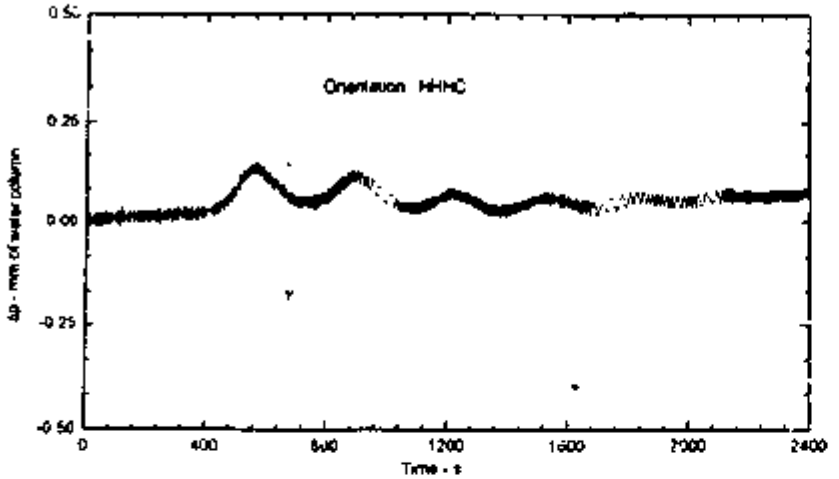

(a) 55 W

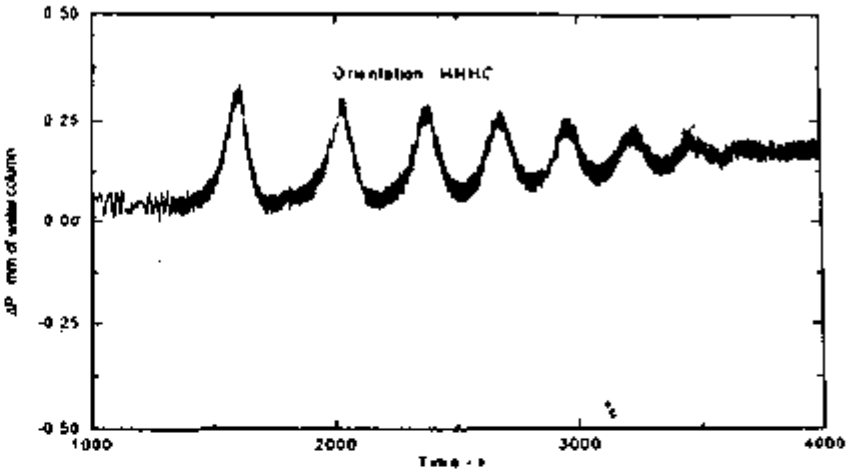

(b) 60 W

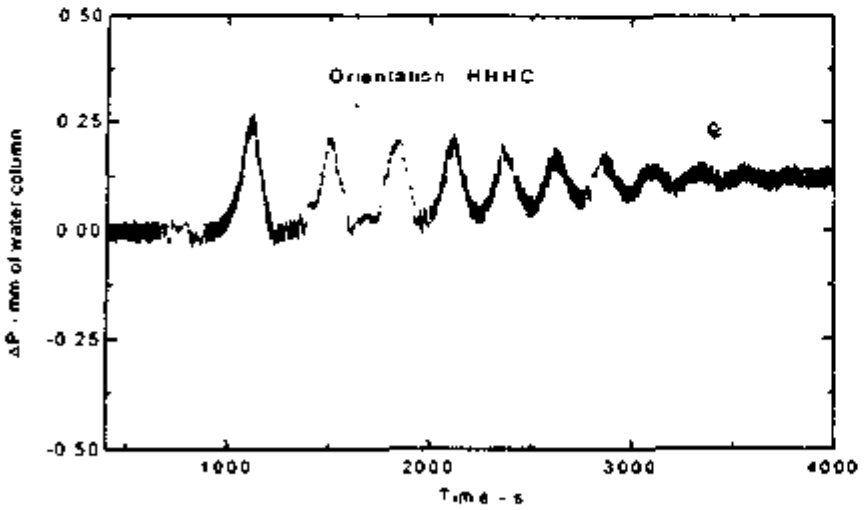

(c) 80 W

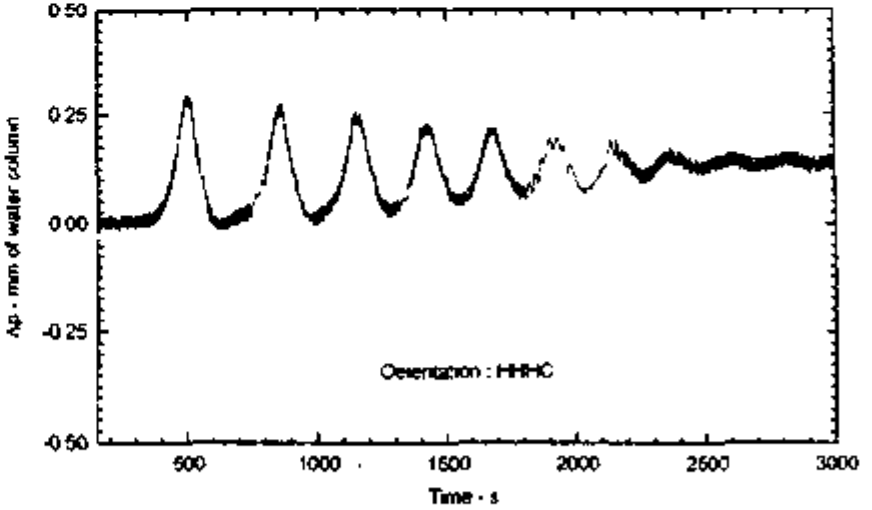

(d) 102 W

Fig. 3 : Start-up transient at different power with 5 ipm coolant flow rate at inlet temperature of 34 ^{0} C

oscillatory behaviour where every succeeding peak is smaller than the preceding one leading eventually to a stable state if the power is less than 105 W.

The duration of the initial quiescent state is found to decrease with power. Similar observations with horizontal heaters were made earlier by Bau-Torrance (1981) in an open square loop and Vijayan (1988) in a figure-of-eight loop.

5.2 HHVC Orientation

Typical start-up transients for the HHVC orientation (with coolant flow rate of 5 lpm) are shown in Fig. 4. For this orientation, sustained circulation in the anti-clockwise direction could not be achieved although flow initiated in the anti-clockwise direction in some cases. For example, the flow initiated in the anti-clock wise direction for the test at 257 W as shown in Fig. 4c. After the first oscillation, the flow reversed and subsequently the flow continued in the clockwise direction eventually leading to a steady state. The flow initiation for HHVC orientation always led to a stable steady state in contrast to the HHHC orientation for which no steady state was observed for heater power 105 W and above.

5.3 VHHC Orientation

In vertical heating the start-up transient is different from the one observed with horizontal heating. In this case, the time lag between the start of the heating process and flow initiation is far less than that for horizontal heating. As soon as the heating starts, the buoyancy force starts increasing, initiating the flow. With the start of heating, water near the wall gets first heated up and immediately starts to rise in the vertical limb due to the low density. The flow initiation transients for VHHC orientation at different powers are given in the Fig. 5. It is observed that after a single initial peak, there is an increasing trend of temperature up to the steady state level. The magnitude of the first peak is found to increase with power. Similar trend was observed for the VHVC orientation.

5.4 *Summary of Observed Behaviour during Flow Initiation*

During these experiments only the HHHC orientation showed single-phase instability. For VHHC and VHVC orientations, the flow remained stable up to a power of 1000 W for all cases studied. For the HHVC orientation, single-phase flow was observed up to about 650 W and a continuous stream of bubbles were observed above 700 W causing random oscillations in ΔP, whose amplitude was more than that in steady single-phase conditions (see Fig.6). Also it was confirmed that the bubbles, which cause the random oscillations are due to the localized boiling near the top wall of the horizontal heater with bulk liquid being highly subcooled. Since our work is restricted to only single-phase natural circulation special attention was not given to boiling natural circulation in this work. A summary of the observed behaviour during the start-up experiments is given in Table 2.

6. THE UNSTABLE FLOW REGIMES

Since single-phase instability is observed only for HHHC orientation, a detailed investigation of the unstable oscillatory behaviour was carried out for this orientation.

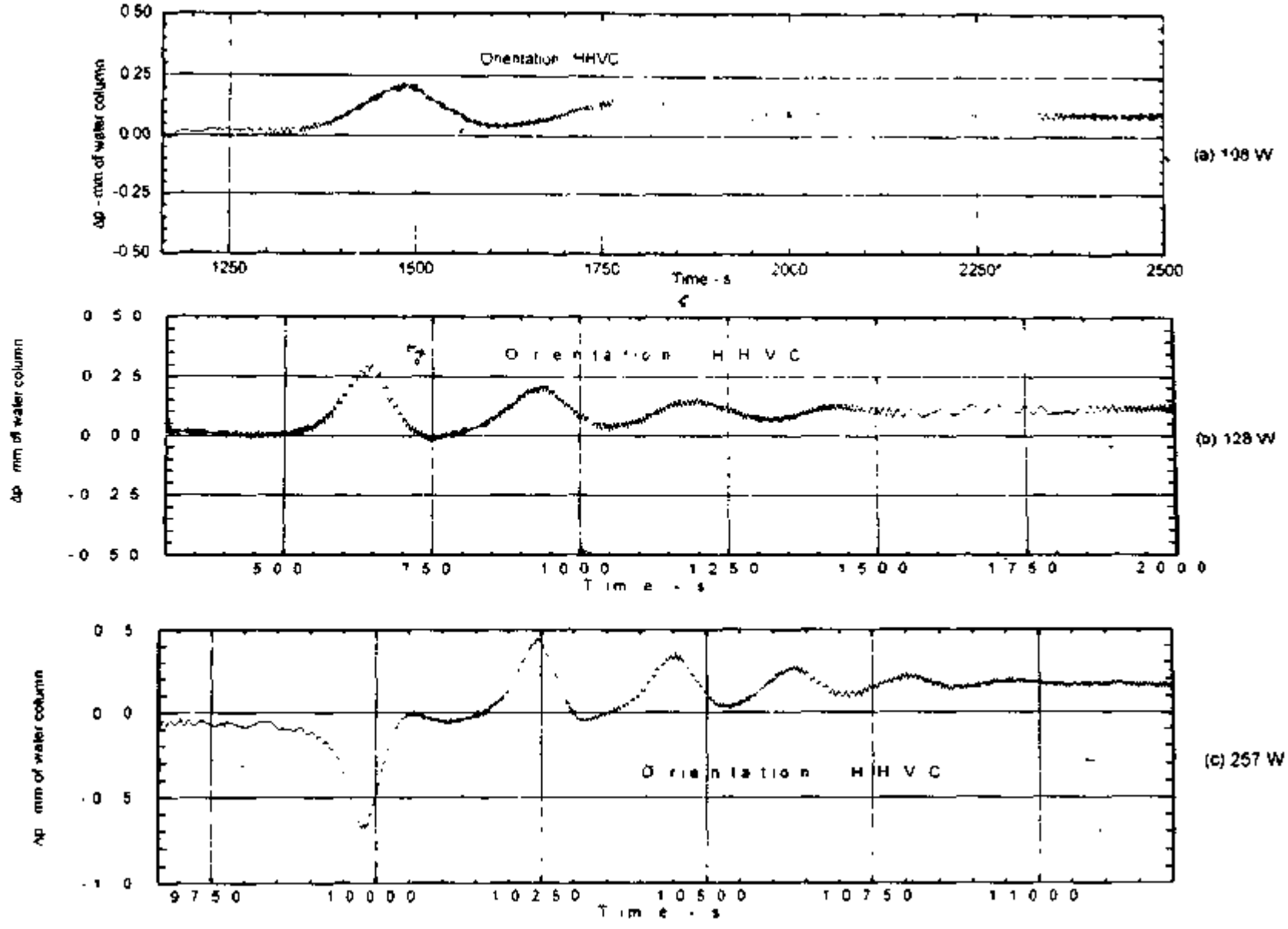

Fig. 4 : Flow initiation at different power with 5lpm coolant flw at inlet temperature of 34 °C

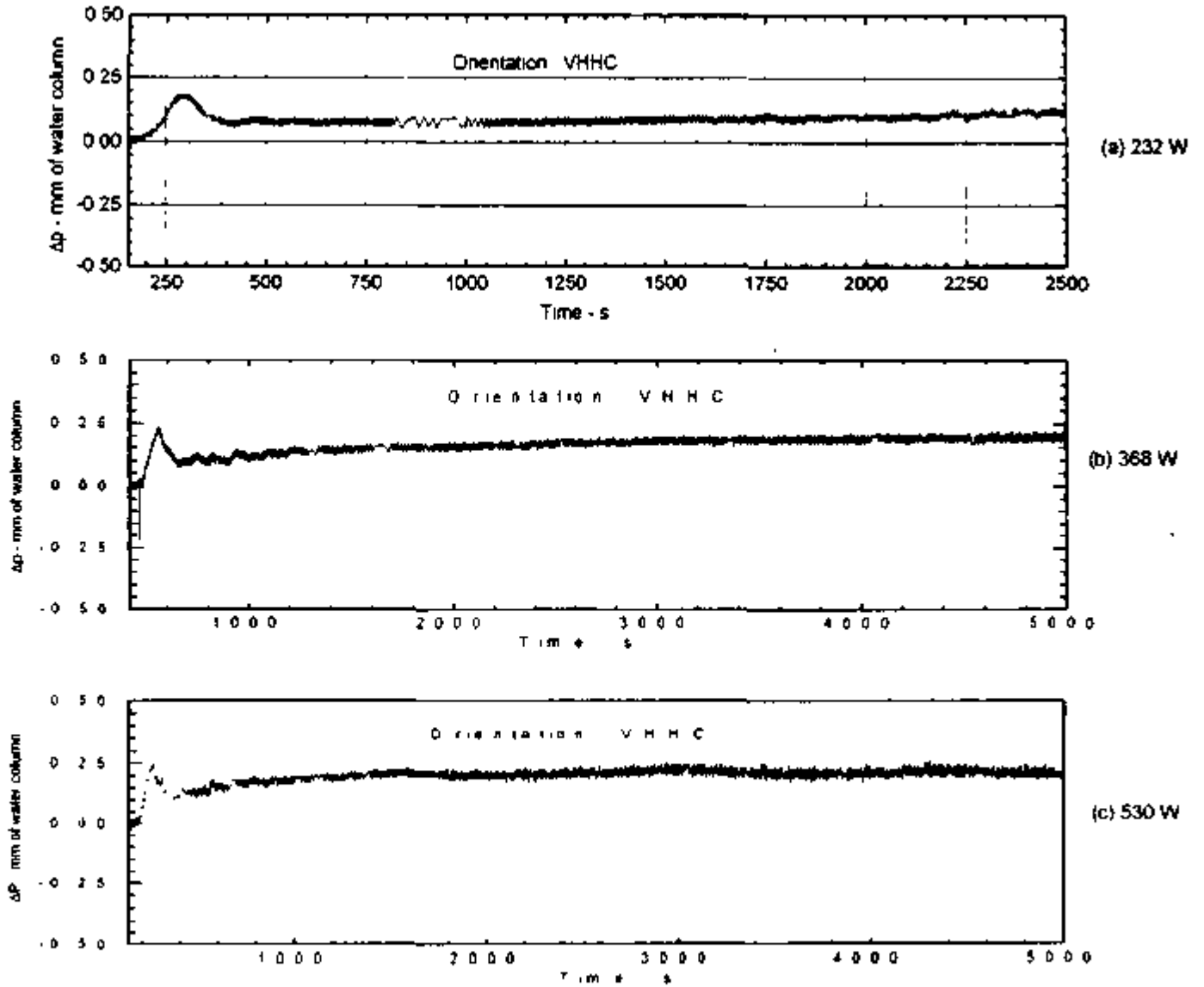

Fig 5 : Flow initiation transient at different powers with 5 lpm coolant flow at inlet temperature of 28 ^{0}C

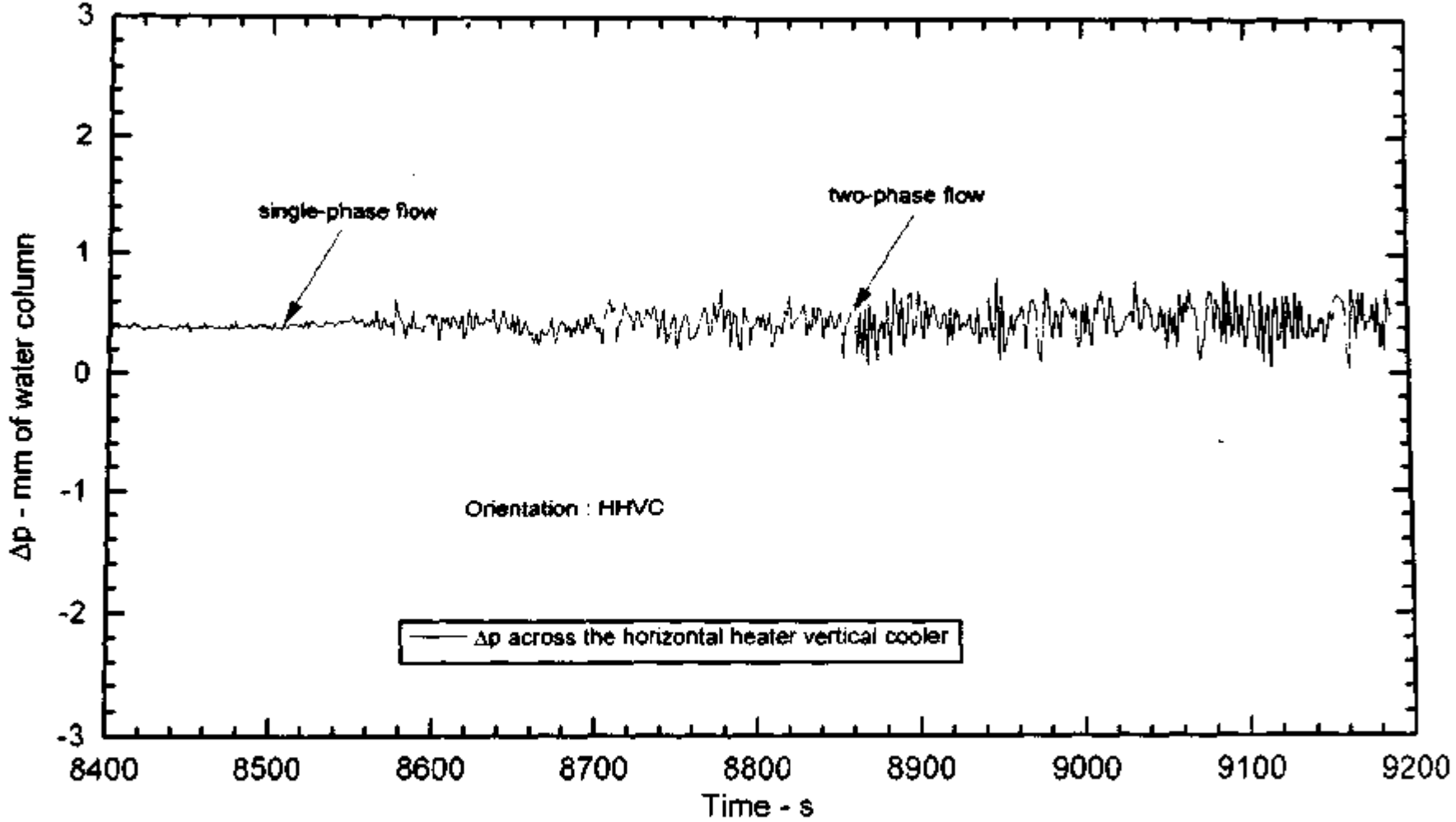

Fig. 6: Steady flow with and without boiling at 730 W and 4.92 lpm coolant flow rate with inlet temperature of 28 ^{0}C

Table 2: Summary of the results of the Start-up Experiments

Orientation	Threshold of instability	Nature of flow
HHHC	Between 102W and 105 W	Single-phase unstable flow for $Q_h \geq 105$ W
HHVC	Stable upto 1000 W*	Single-phase stable flow for $Q_h<585$ W, stable subcooled boiling for $Q_h>585$ W
VHHC	Stable up to 1000 W*	Stable without boiling
VHVC	Stable up to 1000 W*	Stable without boiling

* Experiments were not carried out beyond 1000 W, as it was feared that higher power might damage the glass loop as it did once for the HHHC orientation at 1225 W.

6.1 Summary of Observations

During the three series of tests described in section 3.3.3, the different flow regimes observed can be listed as below:

a) Steady unidirectional flow,
b) Periodic unidirectional pulsing flow,
c) Oscillatory flow with chaotic switching between unidirectional and bidirectional pulsing.
d) Periodic bi-directional pulsing flow and
e) Compound single phase-two phase instability with bi-directional pulsing.

Generally, theoretical prediction has shown an upper limit of heater power beyond which the system is stable. However, this upper limit was unachievable in the present loop in the single-phase condition as it starts boiling in the heater during the low flow period for powers greater than 408 W. It may be possible to reach this limit in single-phase condition in a pressurised water loop.

The range of heater power over which the above regimes were observed is different for the three heat addition paths studied. In some cases, all the above regimes were not observed. For example, the oscillatory flow regime with bi-directional pulsing only is observed while raising the power from a stable steady state. The phase plots given in Figures 7a, b and c clearly illustrate this. The experimental observations are summarized in Table-3. The threshold of instability is found to depend on the heat addition path. The thresholds for unidirectional and bi-directional pulsing are found to depend on the heat addition path. However, the threshold of compound instability is found to be independent of the heat addition path. Characteristics of each of the observed flow regimes are discussed below.

Table 3: Effect of heating mode on the instability

Mode of heating	Threshold of instability	Unidirection-al pulsing	Switching between UP* and BP+	Bidirection-al pulsing	Compound instability
Start up from rest	102 W < Q_h < 105 W	105 W < Q_h < 135 W	140 W < Q_h < 190 W	Q_h > 196 W	Q_h > 408W
Power raising from SSS*	260 < Q_h < 270 W	Not observed	Not observed	Q_h > 270 W	Q_h > 408W
Decay of instability due to PSB†	60 W < Q_h < 65 W+	65 W < Q_h < 140 W	Not established	Not established	Q_h > 408W

@ UP – Unidirectional Pulsing; + BP – Bidirectional Pulsing, * SSS – stable steady state, † PSB – Power step back
+ - These results are valid for a case where instability was initially established at 300 W.

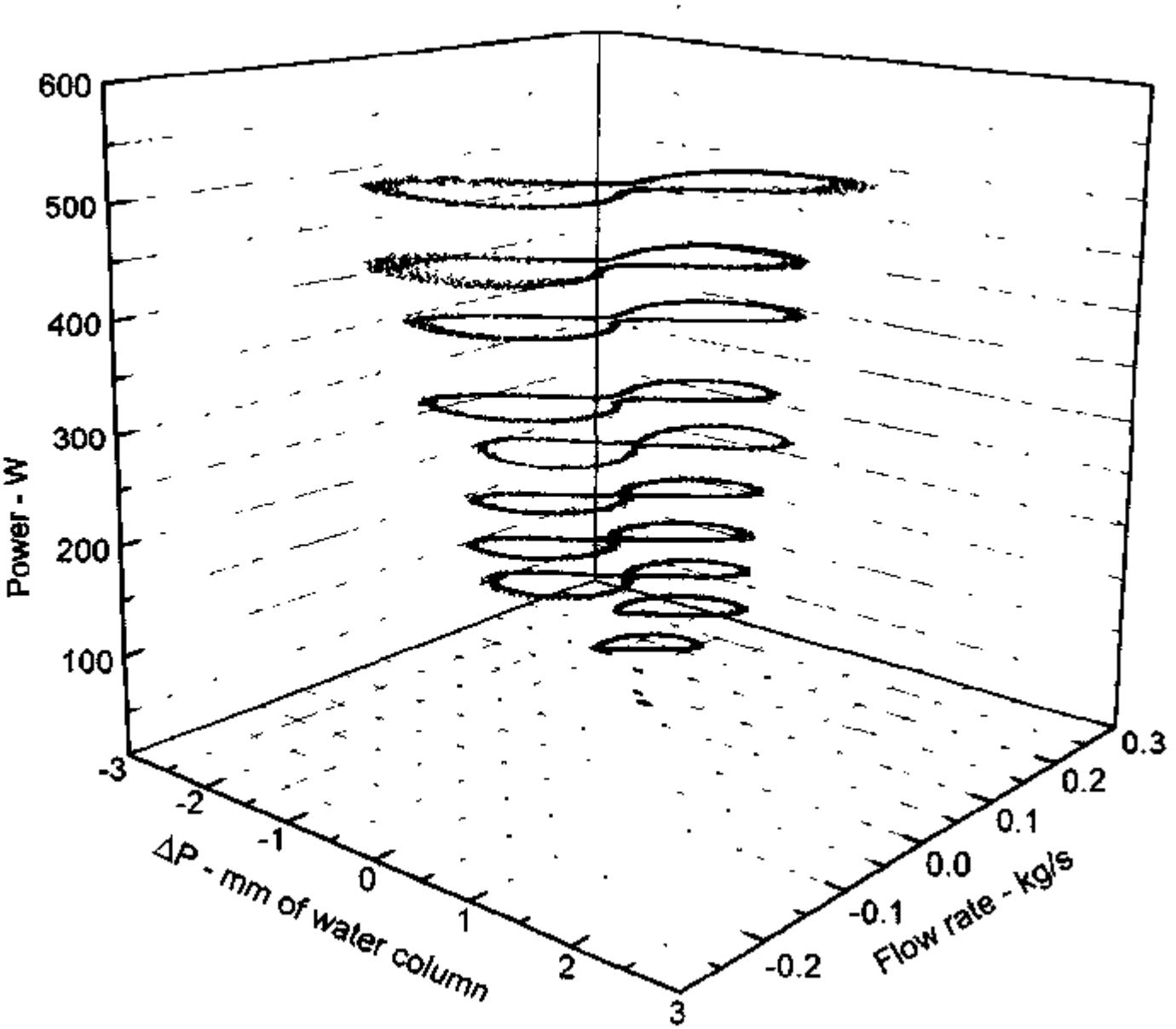

Fig. 7a: Phase space showing the total region of instability with power start up from rest
(Orientation : HHHC, Plot for 2500 seconds after neglecting initial transients)

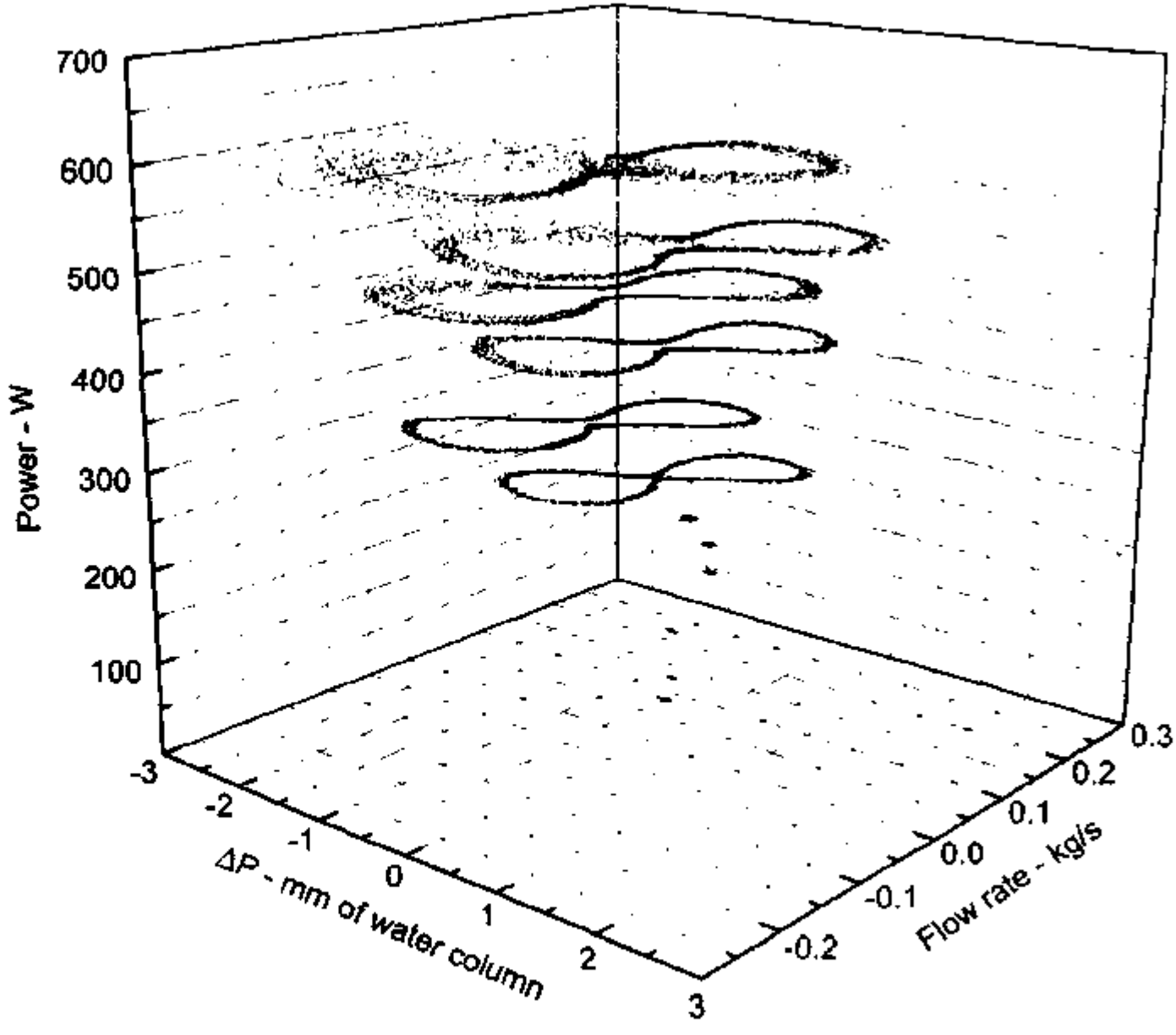

Fig. 7b: Phase space showing the total region of instability with Power raising from stable steady state flow condition (Orientation : HHHC. Plot for 2500 seconds after neglecting initial transients)

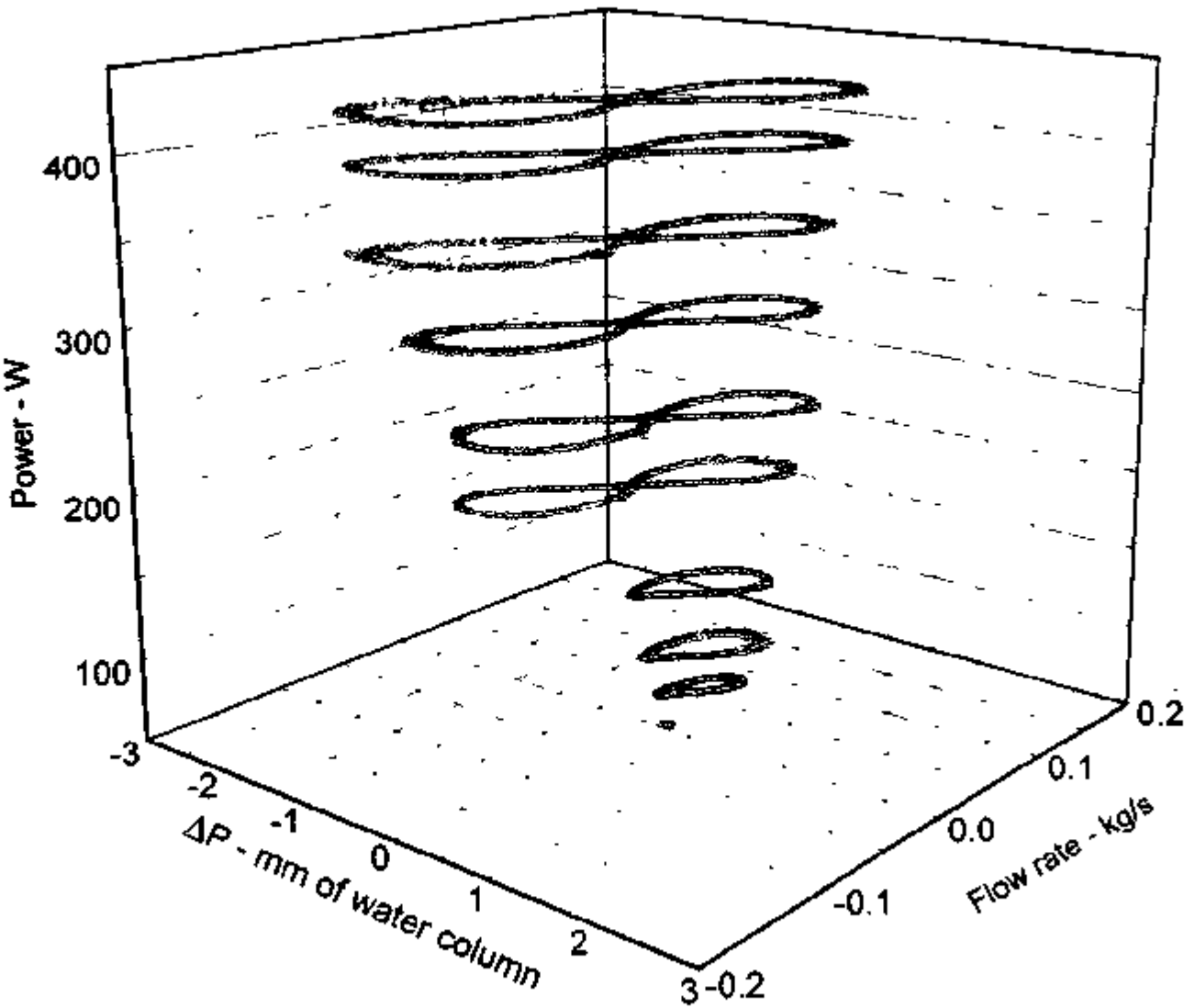

Fig. 7c : Decay of instability for various powers at 5 lpm coolant flow with inlet temperature of 34 ^{0}C

(Orientation : HHHC; Plot for 2500 seconds for each power after neglecting initial transients)

6.2 Stable Unidirectional Flow

Stable unidirectional flow is represented by fixed points on the phase plots (see figure 7) A characteristic feature of the oscillations that eventually die down to give a steady state is that the amplitude of every succeeding oscillation is less than that of the preceding one Since some deviations in the threshold of instability and the nature of the oscillatory behaviour prior to the attainment of steady state are noted depending on the heat addition path, the observed behaviour is described separately for each heat addition path

6 2 1 Start-up from Stagnant Conditions

The observed oscillatory behaviour following the application of heating leading to stable steady state was already discussed in section 5 The time lag between the heating process and the subsequent generation of buoyancy force results in an oscillatory behaviour These oscillations are damped if the power was less than 105 W resulting in a stable steady state (see Fig 8).

6 2.2 Power raising from an initially Stable Steady State

Figure 9 shows that the transient due to power raising from a stable steady state is shorter and milder than that for start-up (Compare the oscillatory behaviour prior to the first steady state with that corresponding to subsequent steady state following power raise in Fig 9) The main reason for this is that the prevailing low flow does not allow the formation of a very hot plug contrary to the case of flow initiation from rest Even the neutrally stable condition for this case results in small amplitude oscillations (see Fig 9b and c) Instability is observed if power is raised to 270 W (see Fig 9d), which is marginally dependent on the path followed in raising the power.

6 2 3 Decay of instability due to power step back

Figures 10a to c show some cases, where the instability decays into a steady state following a step back in power whereas Fig 10d shows a case where the instability does not decay to a steady state These tests showed that the power at which the instability decays to a stable steady state is only mildly dependent on the initial unstable state For example, at 200 W and 300 W the instability decays when the power is brought down to 60 W whereas for 400 W, the instability decays even at 65 W (not shown in figure) Above this power, the instability does not decay

It may be noted that while starting from stagnant initial conditions, stable unidirectional flow was observed up to 102 W while reducing power from an unstable condition stable flow was obtained only if power was below 65 W This indicates the occurrence of the hysteresis phenomenon Theoretically the possibility of occurrence of the hysteresis was reported by Lorenz (1963) and Bau-Wang (1992) Prior experiments conducted by Creveling et al (1975), Gorman et al. (1986) and Widman et al (1989) did not reveal hysteresis To our knowledge, the first experimental confirmation of the occurrence of hysteresis in natural circulation loops is reported here

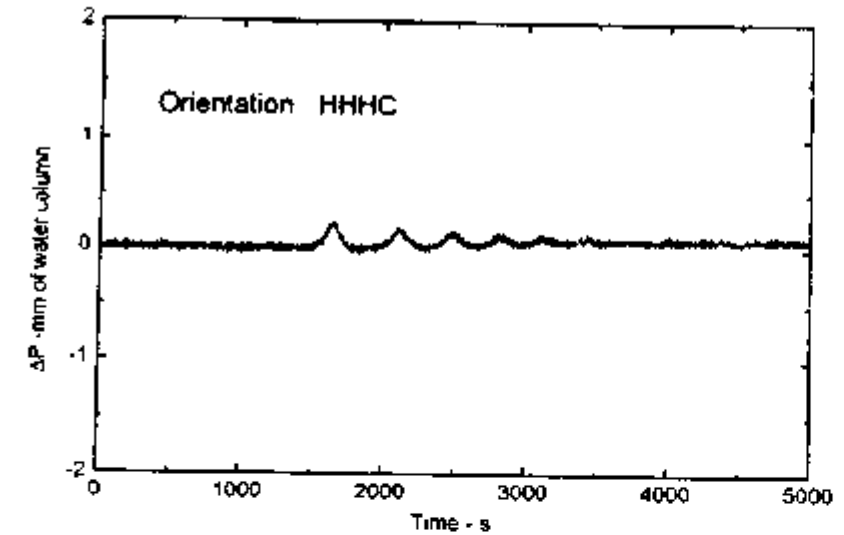

(a) Start-up from rest at 45 W

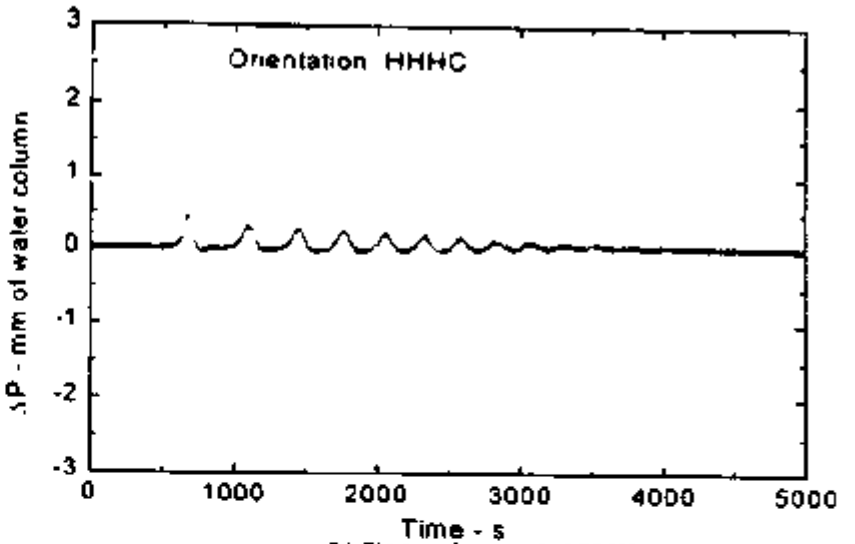

(b) Start-up from rest at 80 W

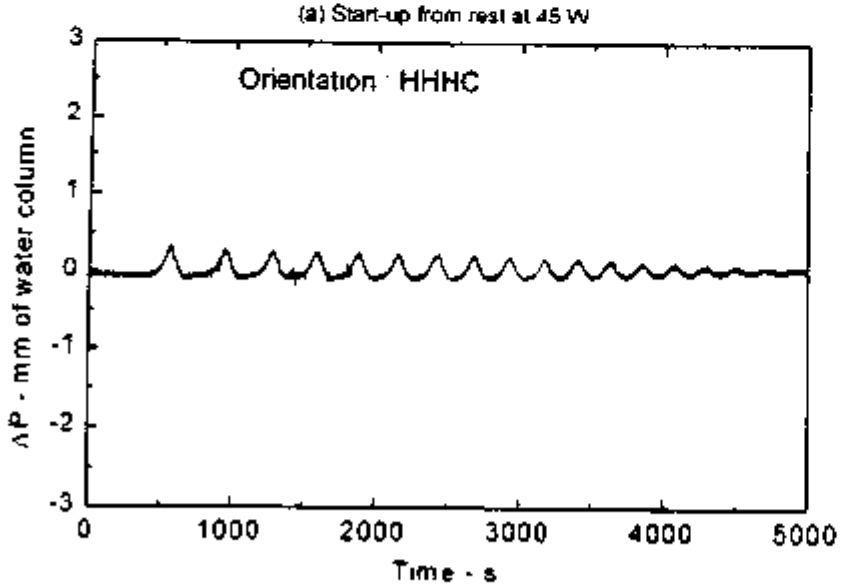

(b) Start-up from rest at 90 W

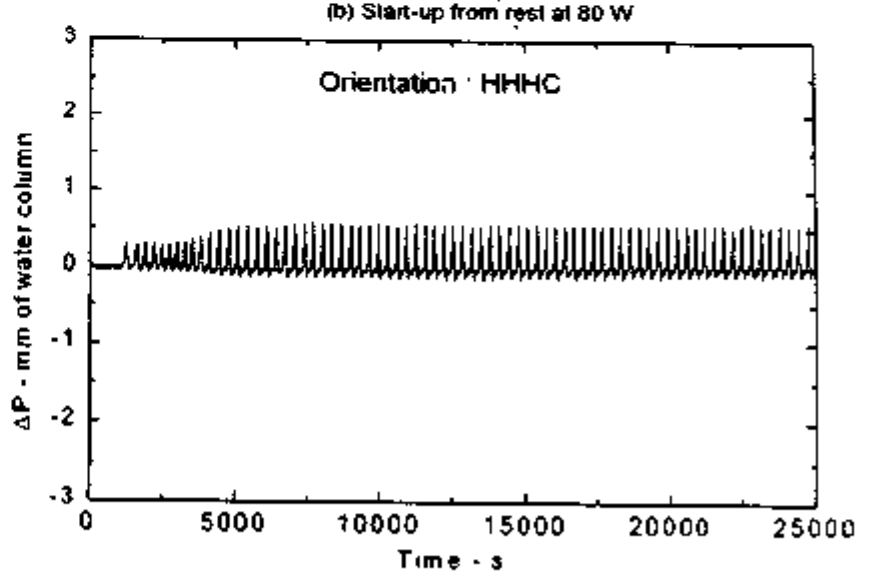

(d) Start-up from rest at 105 W

Fig. 8 : Start-up from rest for different powers at 5 lpm coolant flow and inlet temperature of 34 ^{0}C

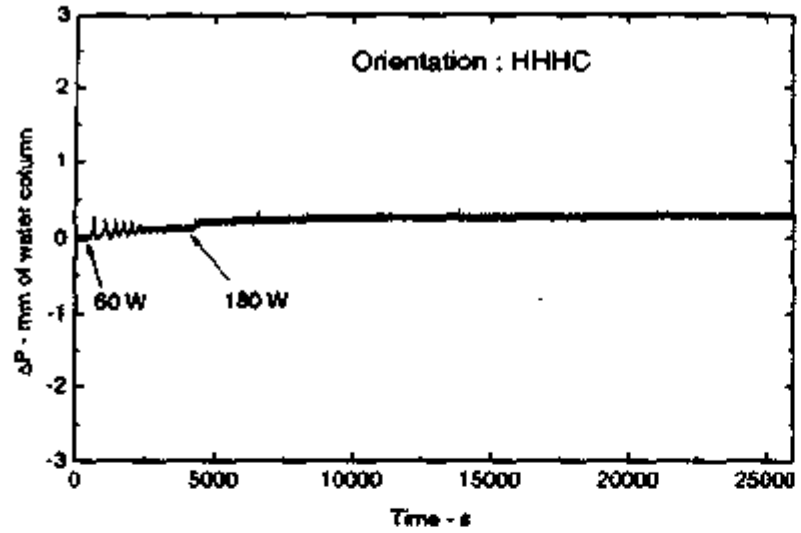

(a)

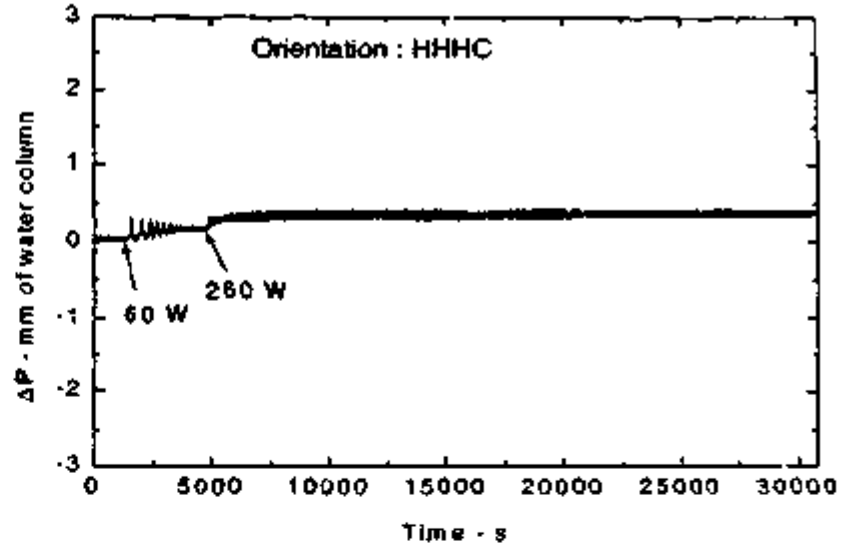

(b)

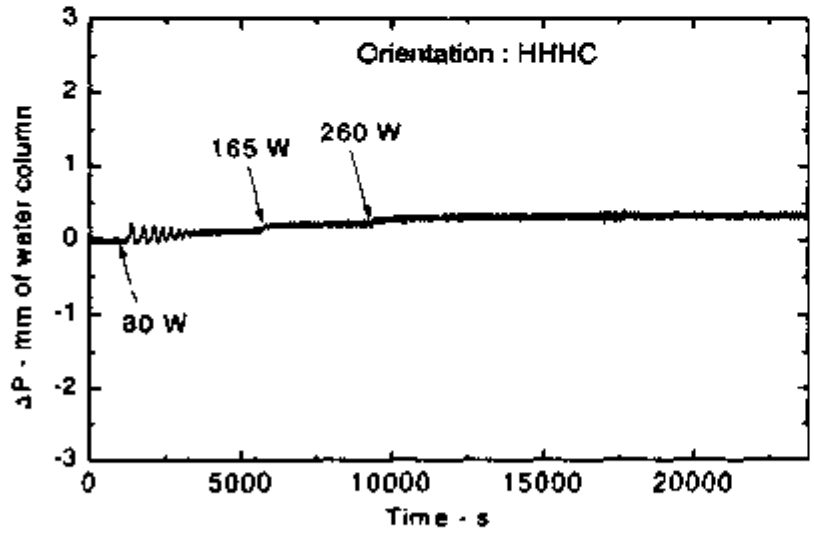

(c)

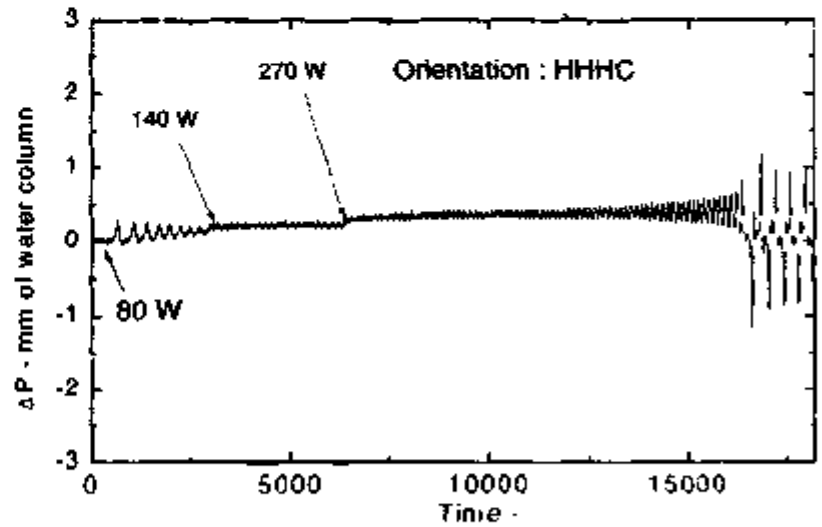

(d)

Fig. 9 : Development of stable behavior with 5 lpm coolant flow with inlet temprature of 34 °C

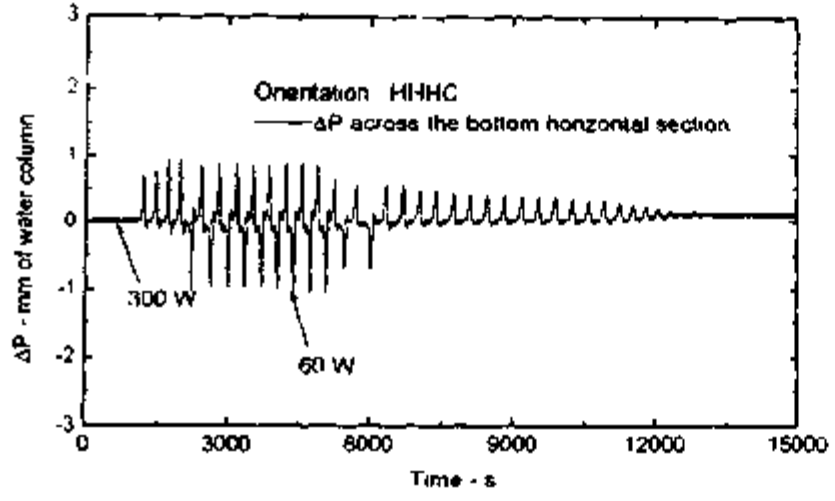

(a) Power step back from 300 W to 60 W

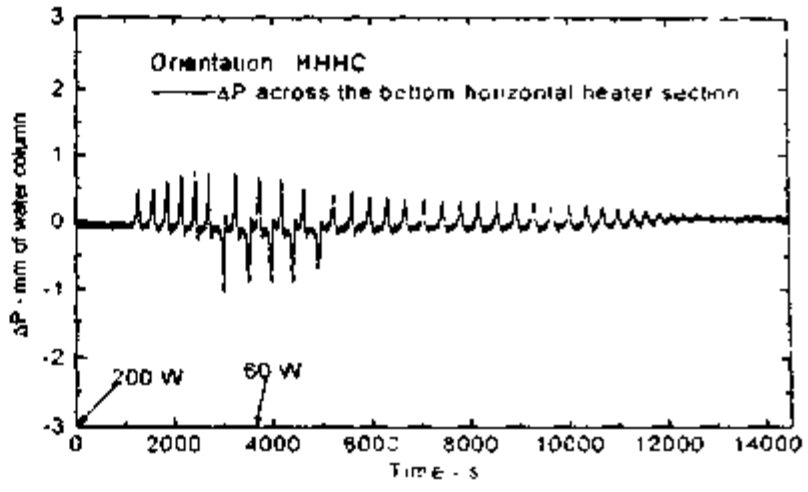

(b) Power step back from 200 W to 60 W

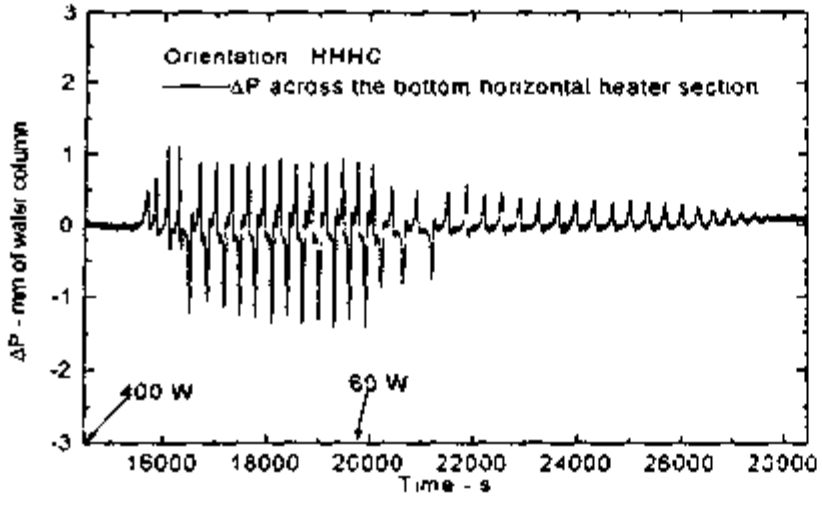

(c) Power step back from 400 W to 60 W

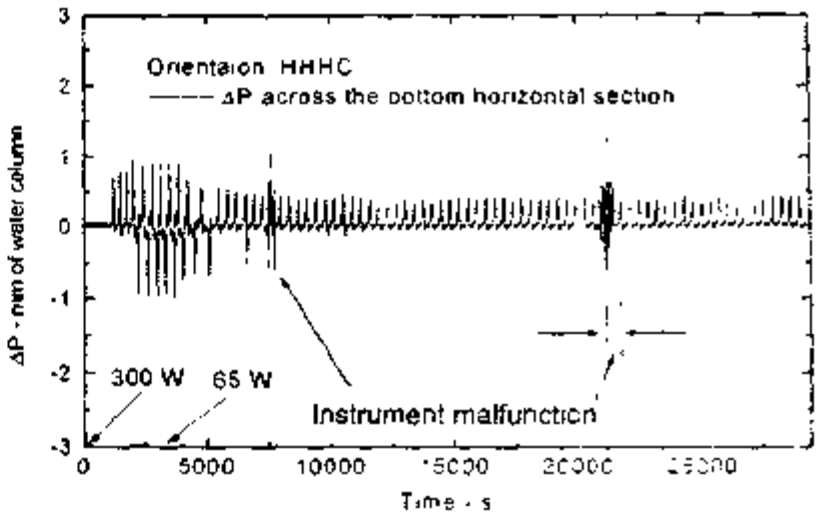

(d) Power step back from 300 W to 65 W

Fig 10 : Decay of instability due to Power step back at 4 9 lpm coolant flow and inlet temprature of 32 °C

6.3 Periodic Unidirectional Pulsing

Unidirectional pulsing is observed during start-up and decay of instability It was not observed for the case of power raising from stable steady state conditions

6.3 1 Start-up from Stagnant Conditions

The upper limit of steady unidirectional flow is observed for about 100 W at which the flow reduces to zero immediately after the first pulse This is caused by the inability of the cooler to sufficiently diffuse the hot plug (due to high velocity), with the result that the net buoyancy force reduces to almost zero when the hot plug of fluid descends down the cold leg During the near zero flow rate, another hot plug is generated in the heater which is nearly as hot as the first one Further increase in power causes continuous unidirectional pulsing that is periodic (see Fig. 11). Unidirectional pulsing was observed for $105 < Q_h < 135$ W At 140 W, the flow switches to bi-directional pulsing after remaining in the unidirectional pulsing mode for a long time

A characteristic feature of the unidirectional pulsing flow is that every large amplitude positive ΔP oscillation is succeeded by a small negative minimum and a plateau of near zero ΔP (see Fig. 12). The small negative minimum of ΔP necessarily indicates a very small reverse flow But its duration is small and the oscillatory nature is predominantly unidirectional. The near zero ΔP indicates stagnant conditions so that unidirectional pulsing appears to be repetitive flow initiations On the state space (see Fig. 13), the unidirectional pulsing flow forms a bean shaped limit cycle with a thicker shell for large time series plots The space enclosed by the limit cycle is found to increase with increase in power (see Fig 13) due to the increase in the amplitude of oscillations with power Unidirectional oscillatory motion was predicted by Keller (1966) in a rectangular loop like the present one albeit with a point heat source and heat sink at the centre of the bottom and top horizontal pipes respectively.

6.3 2 Decay of instability due to power step back

From an unstable oscillatory flow, unidirectional pulsing is observed in the range $65 < Q_h < 140$ W (see Fig 14) The unidirectional pulsing observed with different initial power are shown in Figs 15a and b. Fig 16 shows phase plots where a typical bidirectional pulsing instability decays into unidirectional pulsing. The spread in the trajectories shown in Fig 16 is due to the transient following the step back in power The darkness of the phase space corresponds to the duration of the pulsing mode Thus the phase spaces in Fig 16 indicate that the final unidirectional pulsing mode was of longer duration

6.4 Chaotic switching between unidirectional and bidirectional pulsing

Chaotic switching between unidirectional and bidirectional pulsing was observed during start-up and decay of instability due to step back in power It was not observed for power raising from stable steady state conditions.

6.4 1 Start-up from Stagnant Conditions

Typical examples of this type of behaviour are shown in figures 17a to d It appears that the two stable oscillatory modes for this loop is either unidirectional pulsing (at low powers (<135

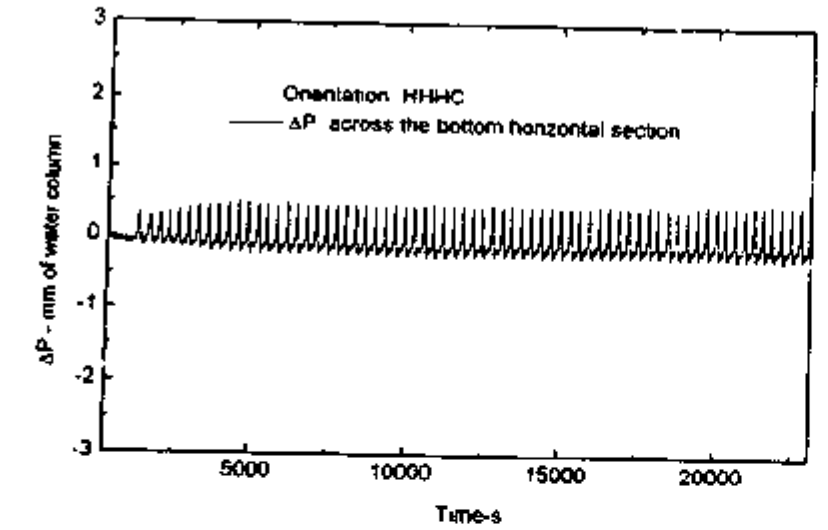

(a) Unidirectional pulsing at 115 W

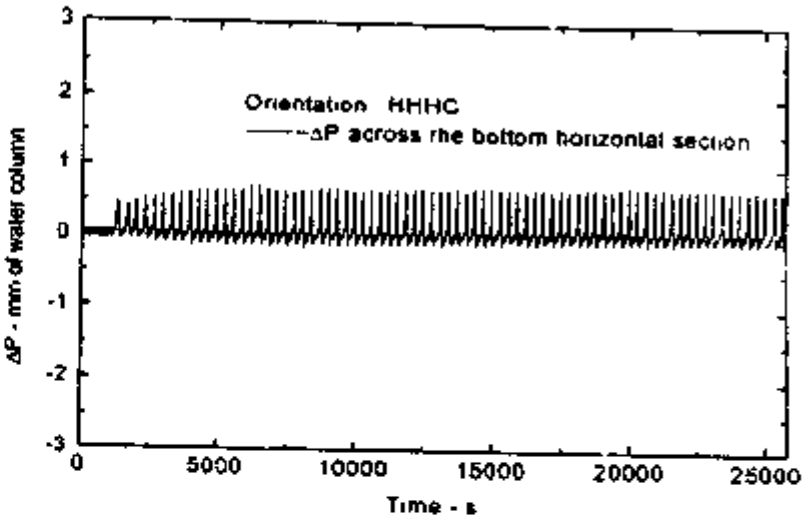

(b) Unidirectional pulsing at 120 W

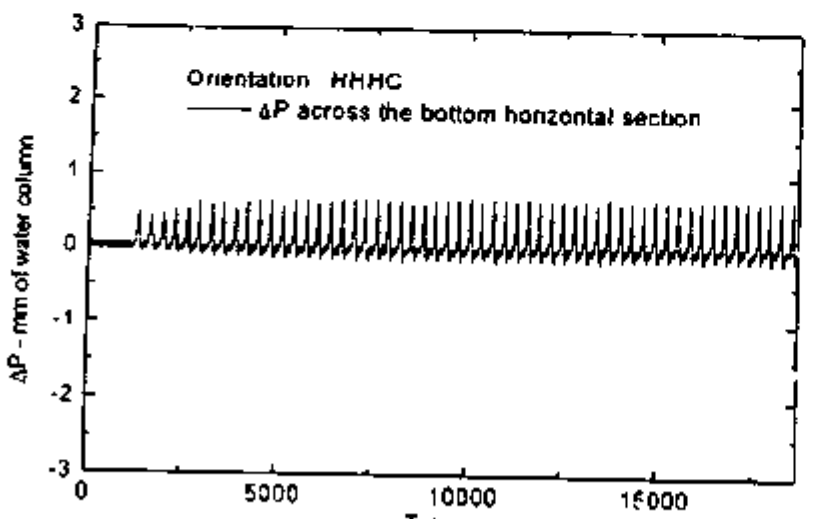

(c) Unidirectional pulsing at 130 W

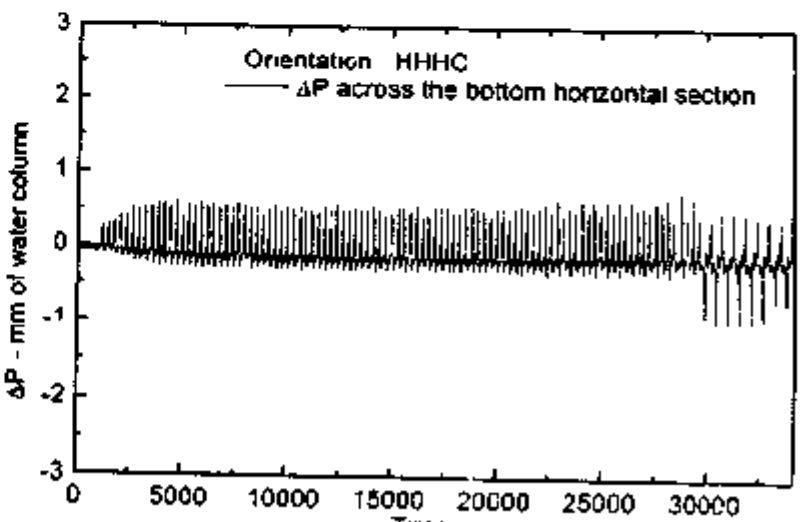

(d) Switching from unidirectional to bidirectional pulsing at 140 W

Fig. 11 : Unidirectional pulsing for various powers at 5 lpm coolant flow with inlet temprature of 34 ^{0}C

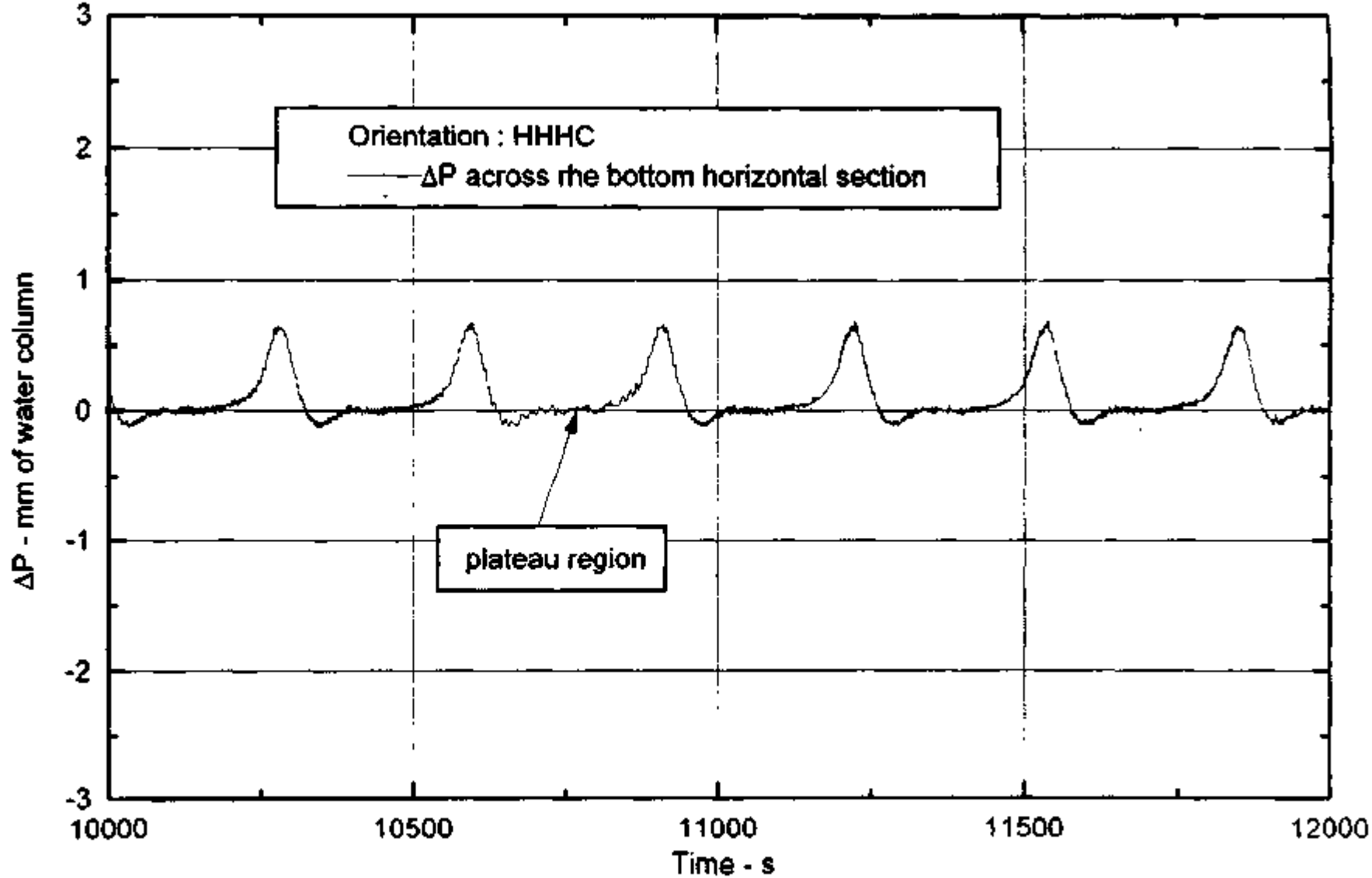

Fig. 12 : Unidirectional pulsing at 120 W and 5lpm coolant flow with inlet temperature of 35^{0}C

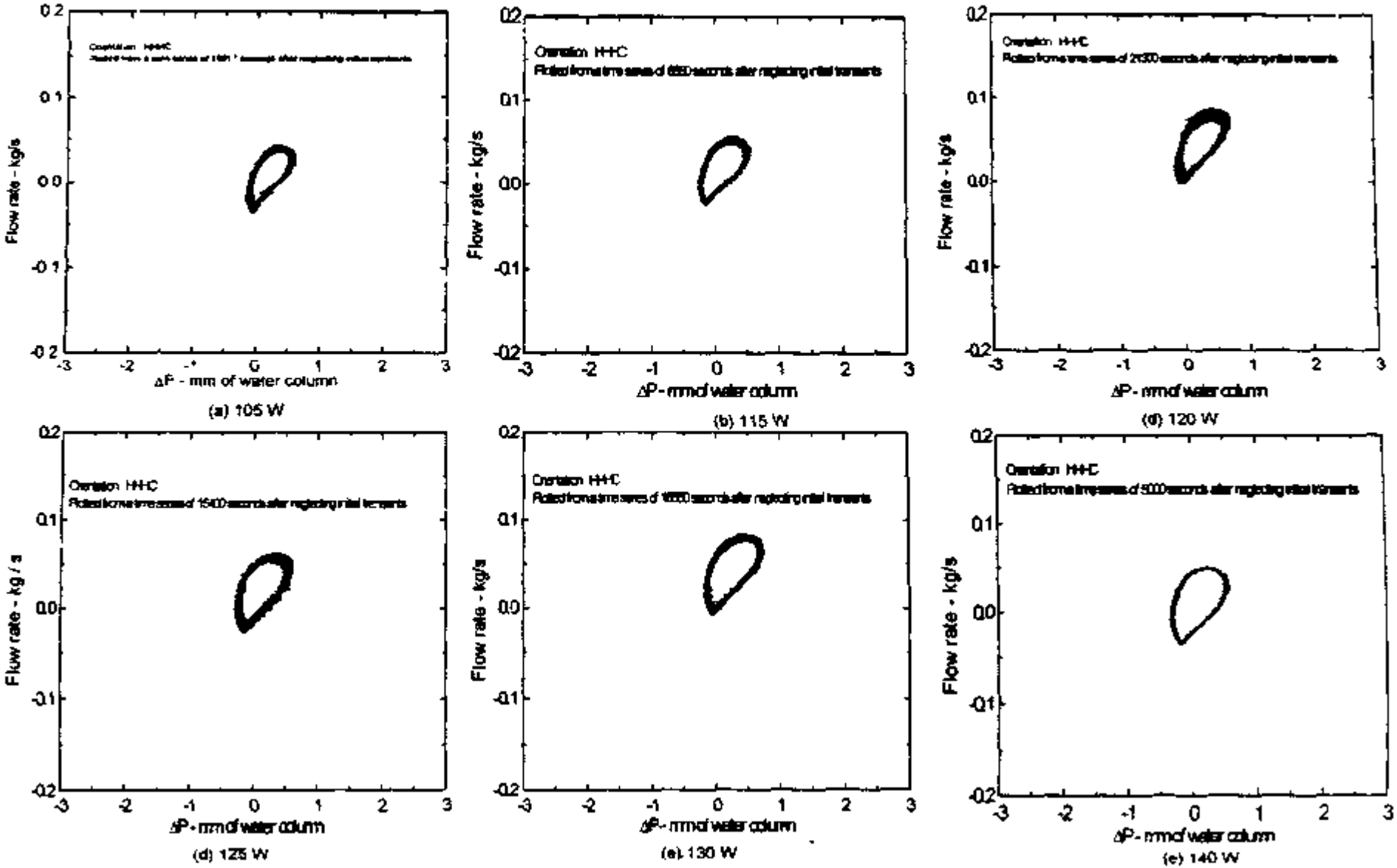

Fig 13 Unidirectional pulsing at different powers with 5 lpm coolant flow at inlet temprature of 34 °C

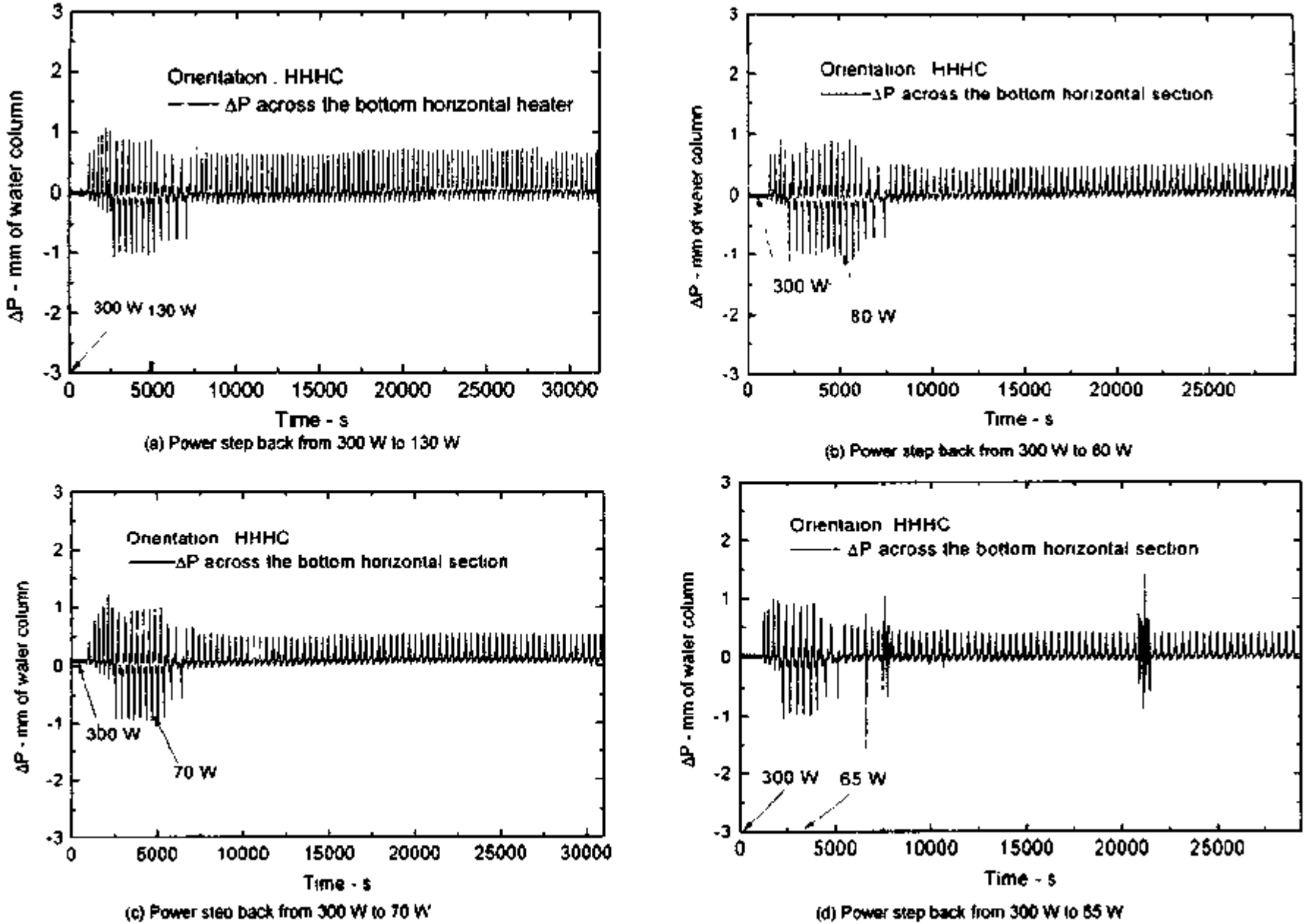

Fig. 14 : Decay of instability due to power step back at 5 lpm coolant flow and inlet temprature of 33 °C

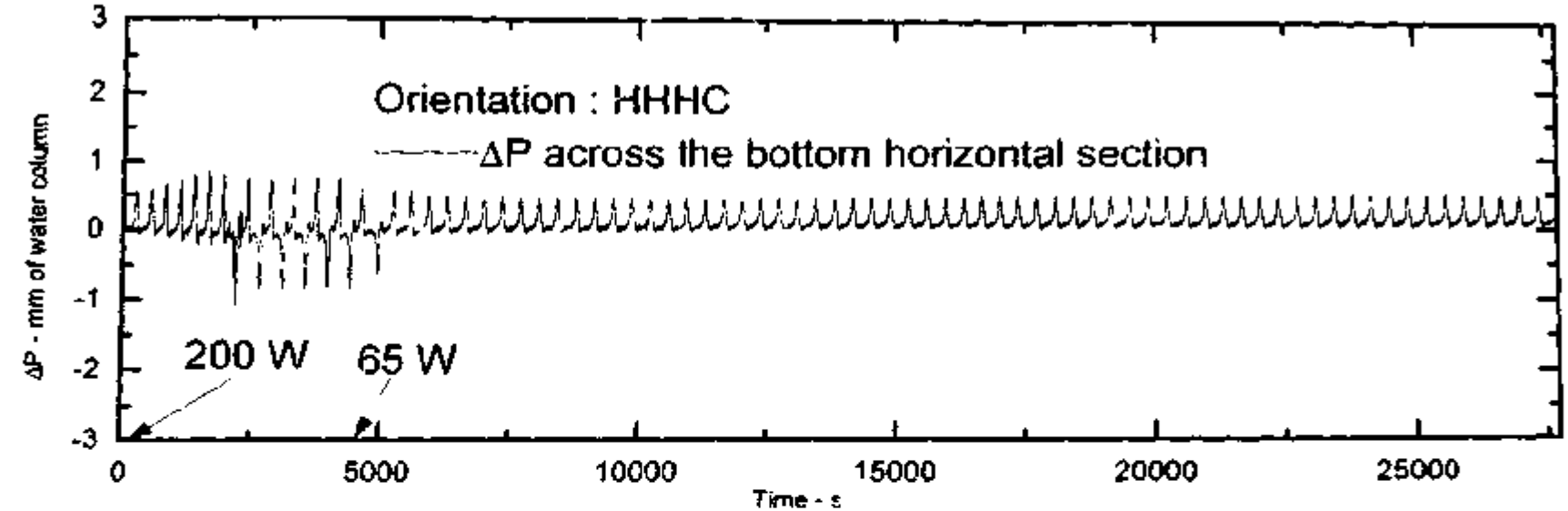

(a) Power step back from 200 W to 65 W

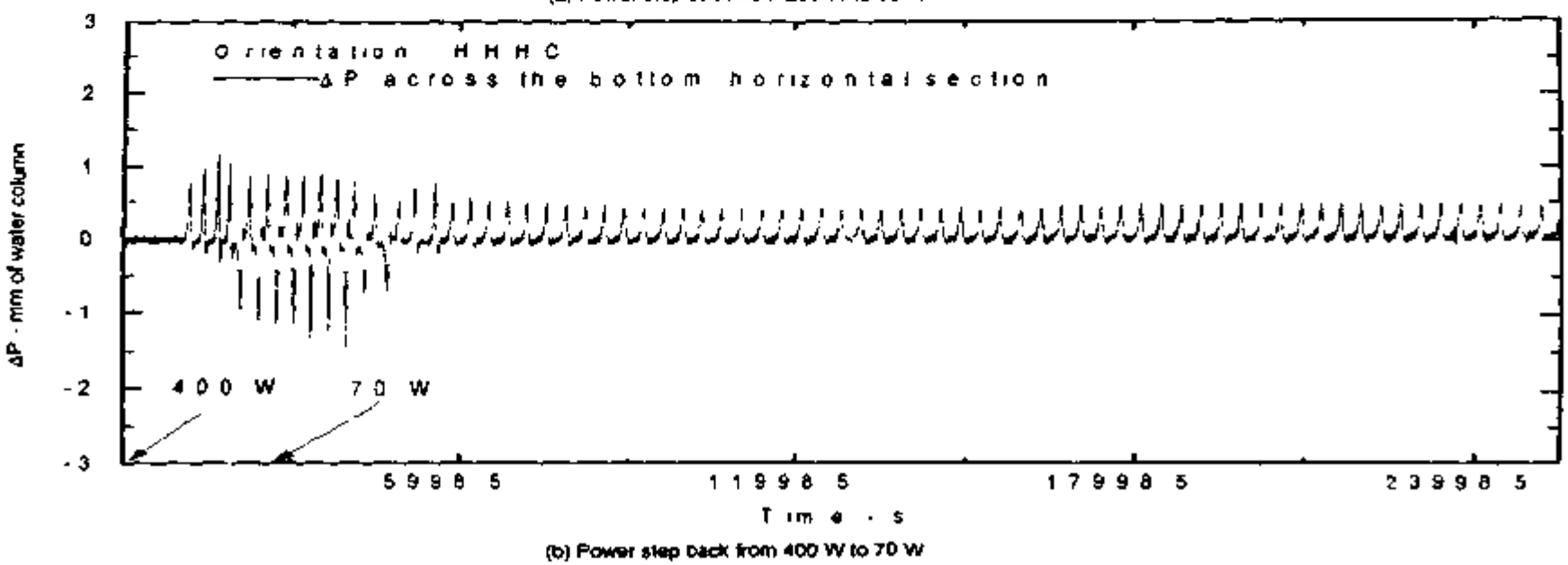

(b) Power step back from 400 W to 70 W

Fig. 15 : Effect of Power on Decay of instability stabilty

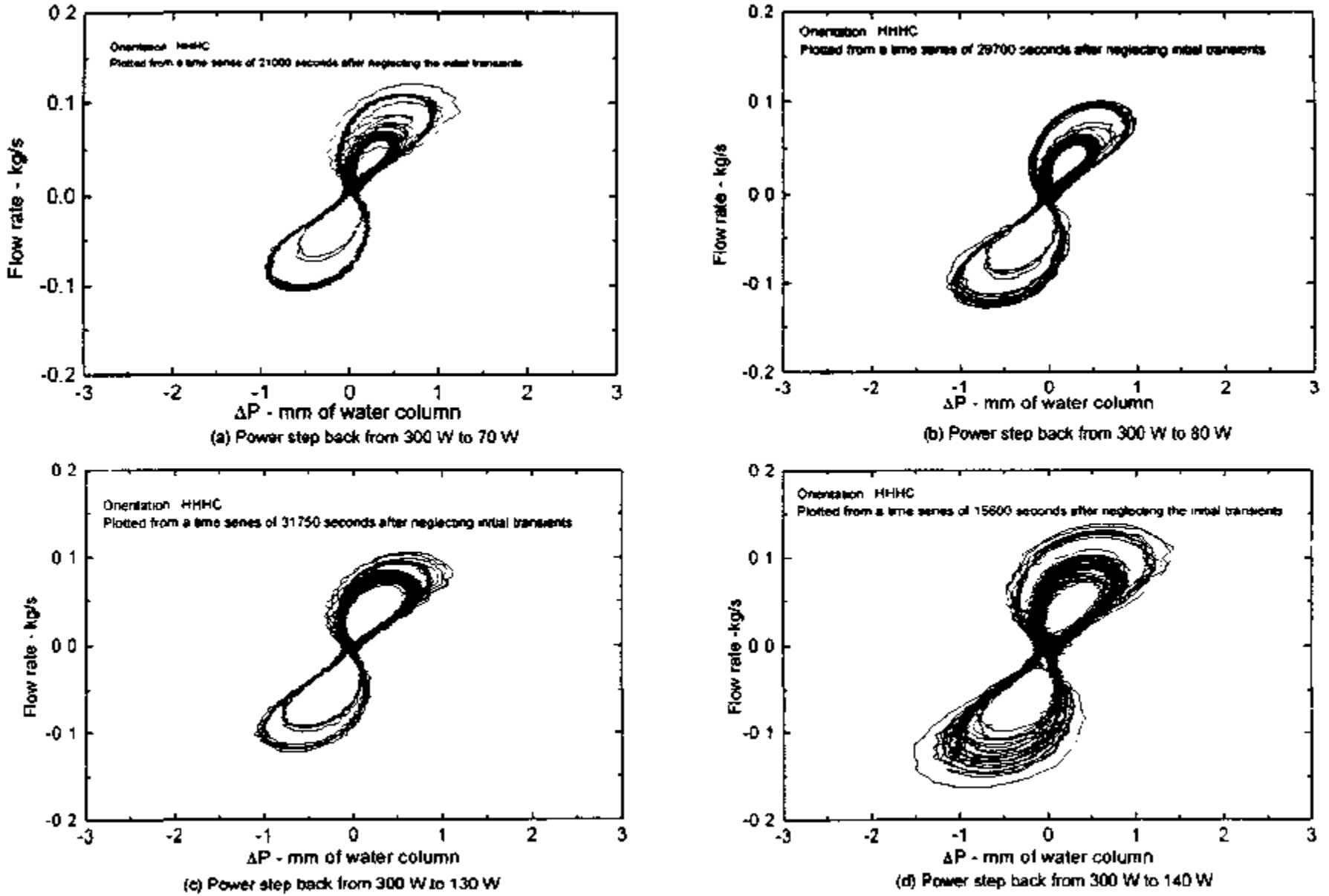

Fig 16 : Decay of bidirectional pulsing to unidirectional pulsing due to power step back at 5 lpm coolant flow with inle temprature 33 °C

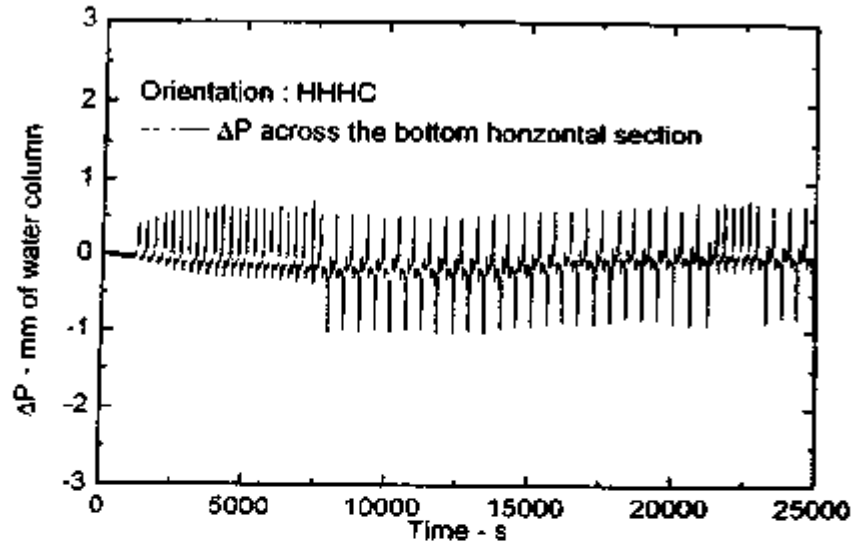

(a) Start-up from rest at 150 W

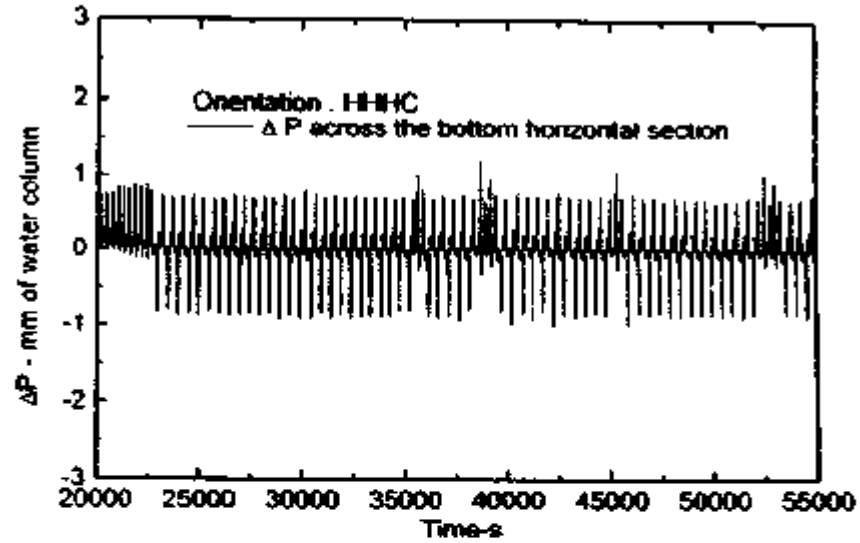

(b)Start-up from rest at 160 W

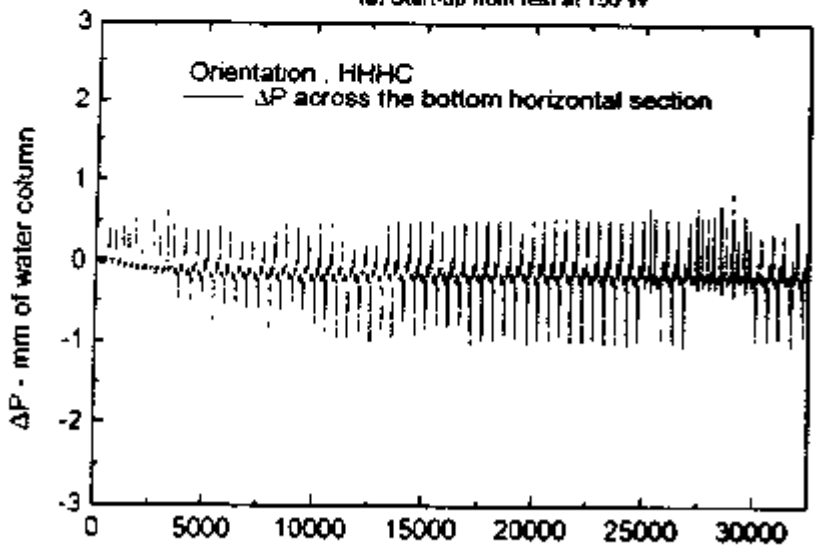

(c) Start-up at 165 W

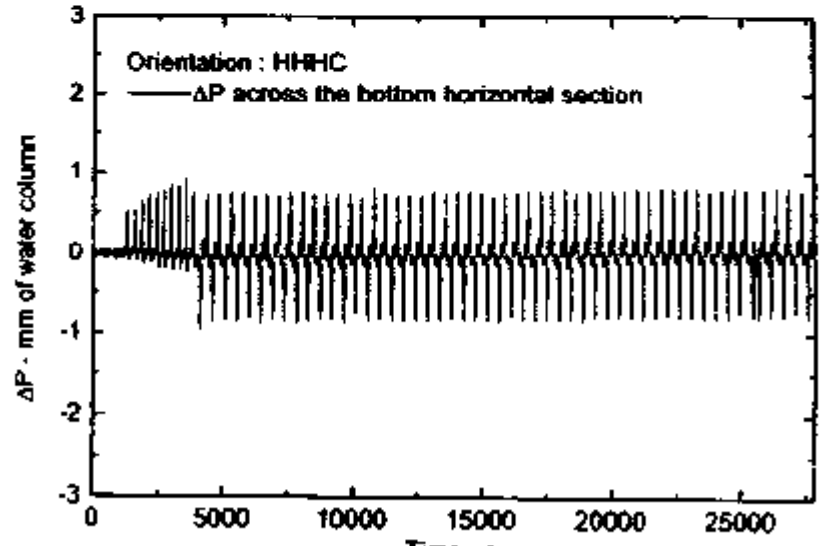

(d) Start-up from rest at 190 W

Fig 17 Chaotic switching between unidirectional and bidirectional pulsing for various powers at 5 lpm coolant flow with inlet temprature of 33C

W)) or bidirectional pulsing (at high powers (>196W)). Between these two limiting powers, it is natural to have a region where flow switches from unidirectional to bidirectional pulsing and vice versa. The frequency of the chaotic switching is found to decrease with increase in power. Chaotic switching is not observed for powers greater than 196 W. On the phase space, such plots do not show a single trajectory as in the case of periodic unidirectional or bidirectional pulsing. Instead, they show a spread around the mean trajetory (see Fig. 18).

6.4.2 Decay of instability due to power step back

Chaotic switching is observed for this case (Fig. 19). However, experiments were not carried out to establish the range of power in which chaotic switching occurs. It is also not known whether hysteresis phenomenon occurs for the chaotic switching mode.

6.5 Periodic Bidirectional Pulsing

6.5.1 Start-up from Stagnant Conditions

For powers greater than 196 W, the chaotic switching between unidirectional and bidirectional pulsing stops and a periodic bidirectional pulsing alone is observed after the first switching (see Figs 20 a to d). An interesting observation is that even for the unconditionally unstable case, a few unidirectional oscillations (whose amplitude increases with time) are observed before the switch to bidirectional pulsing (Fig 21). The characteristic feature of the bidirectional pulsing is the occurrence of repeated flow reversals resulting in alternate forward and reverse flow pulses. When the flow reversal occurs, both the ΔP and ΔT_h show negative values. Visual observation of the flow in the active cooler section (which was not insulated) confirmed the repetitive flow reversals. Neglecting the initial transients the shape of the long duration time series plots resembles a snake skeleton (Figs. 20 and 21).

On the phase space, the bidirectional pulsing flow neglecting the initial transients portrays a dumbbell that just touches each other at the centre at low power (22a to d). As the power increases, a separation is observed at the center (see figures 23a to d). The numerical investigations by Hart (1984 and 1985) have shown phase trajectories somewhat similar to those in Fig 23 for a toroidal loop. It may be noted that an exact periodic oscillation will trace out the same limit cycle every time. However, the phase portraits in Figs. 22, 23 and 13 reveal that bidirectional pulsing like unidirectional pulsing is only near periodic although Keller (1966) has termed unidirectional pulsing as periodic.

6.5.2 Power raising from an initially Stable Steady State

Typical results for the occurrence of instability for this case are shown in Figs 24a to d. A characteristic feature of this heat addition path is that the instability always develops by the growth of small amplitude oscillations (Welander Mechanism). The amplification period (defined as the time duration from the step increase in power (to unstable value) till the occurrence of the first flow reversal) is found to decrease with increase in power.

6.5.3 Decay of instability due to power step back

Bidirectional pulsing was not studied in detail in this heat addition mode. However, the available results indicate that bidirectional pulsing observed is practically same as that in section 6.5.1 (see Fig. 25).

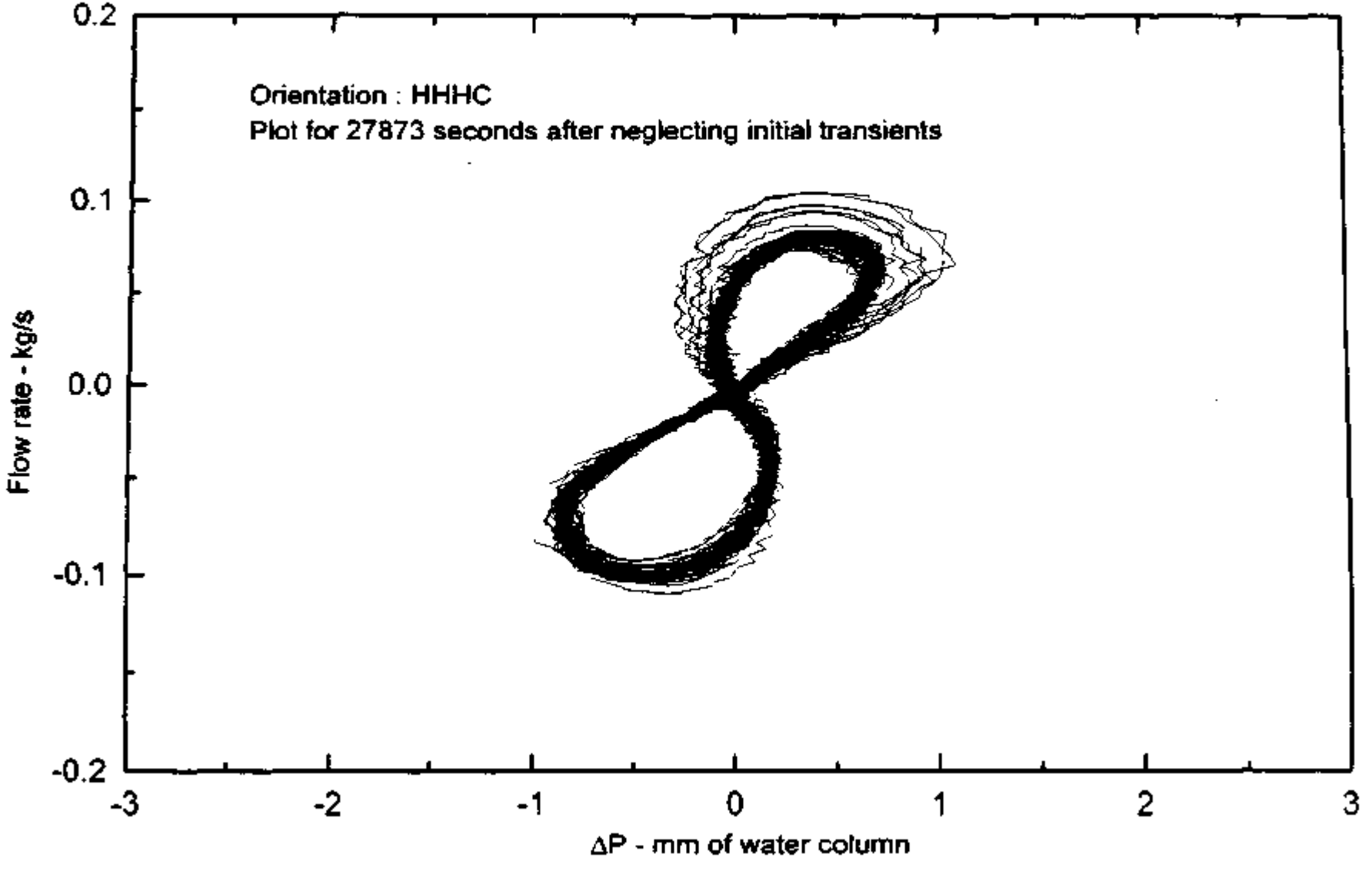

Fig.18 : Phase plot at 165 W and 5 lpm coolant flow with inlet temprature of 34 °C

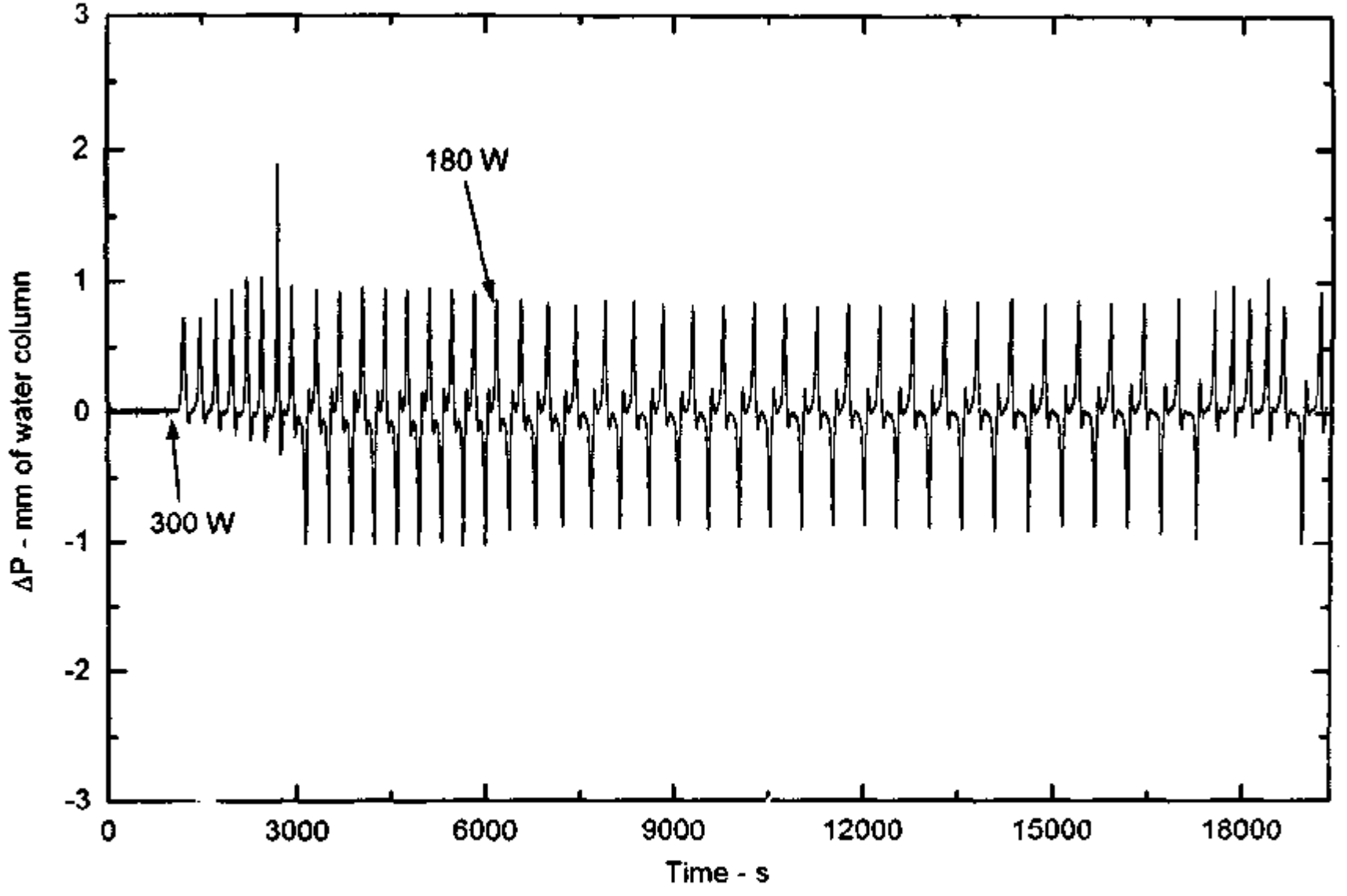

Fig. 19 : Chaotic switching during decay of instability due to step back in power from 300 W to 180 W and 4.94 lpm coolant flow at 27 ^{0}C

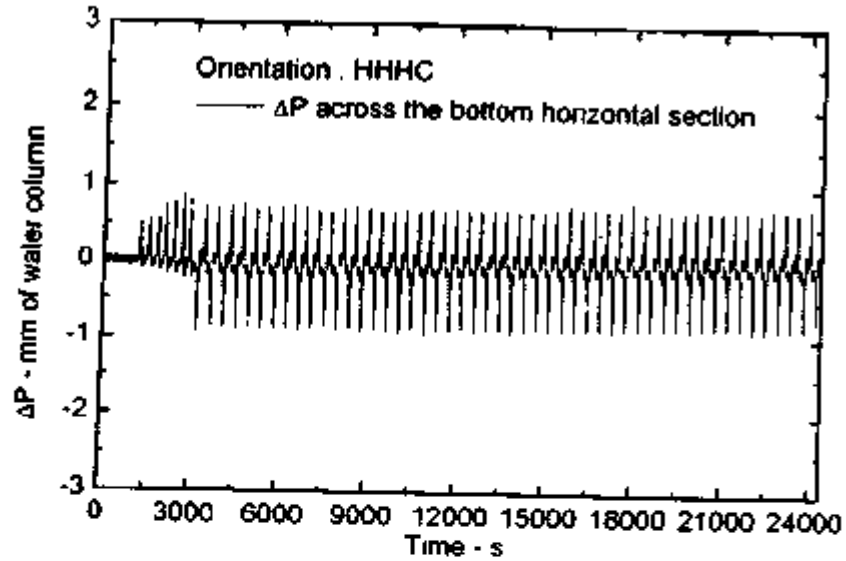

(a) Start-up from rest at 200 W

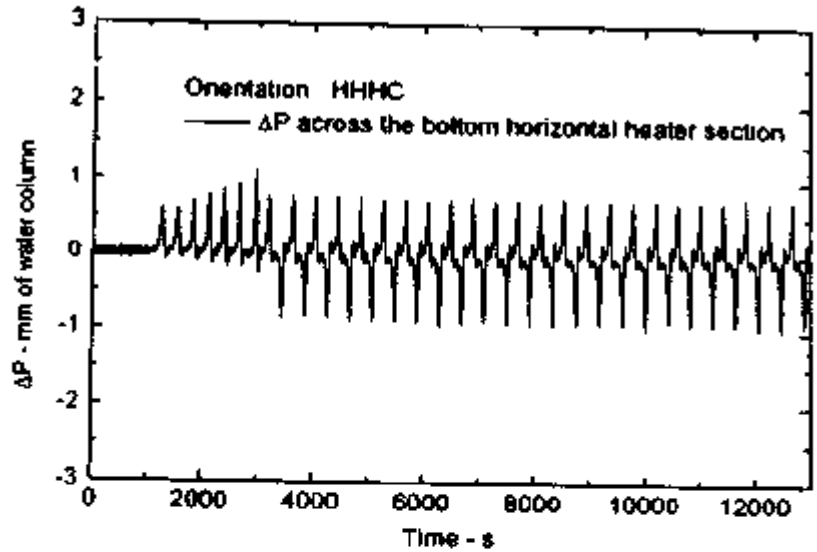

(b) Start-up from rest at 220 W

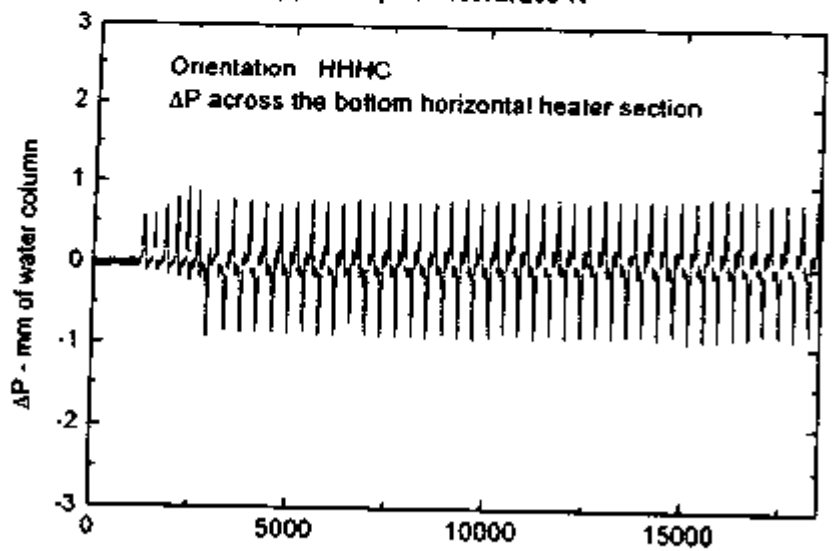

(c) Start-up from rest at 240 W

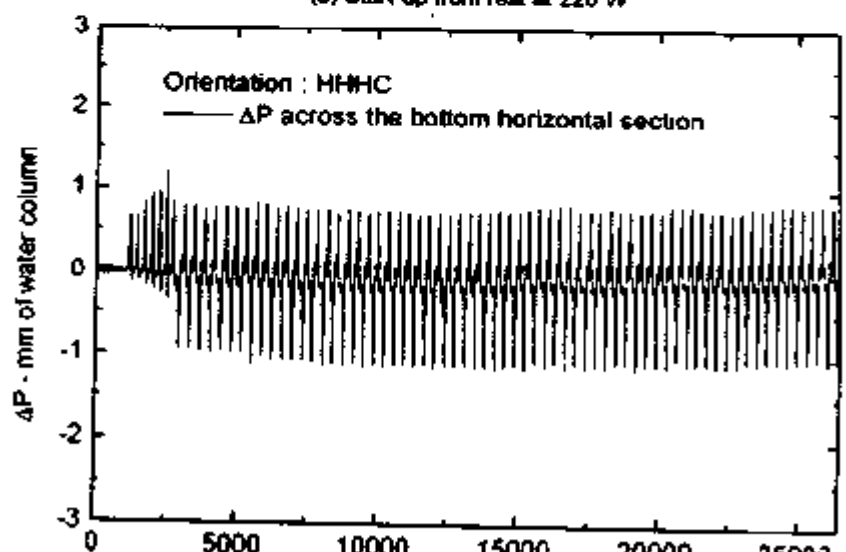

(d) Start-up from rest at 280 W

Fig. 20 : Bidirectional pulsing for different powers at 5 lpm coolant flow with inlet temprature of 33 °C

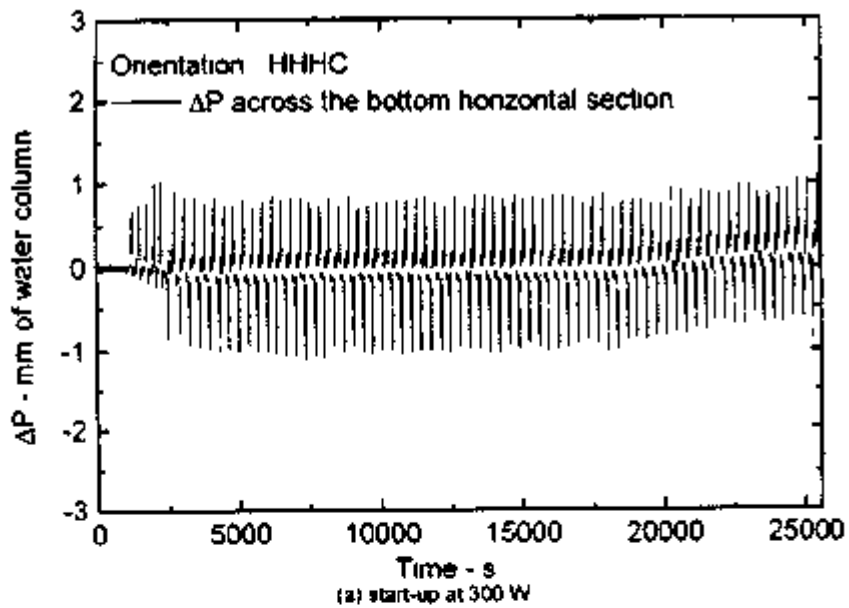

(a) start-up at 300 W

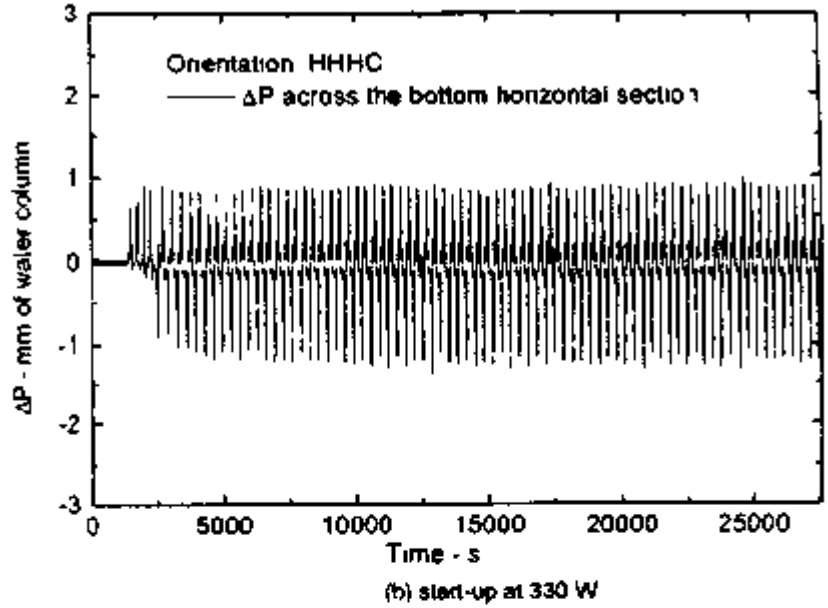

(b) start-up at 330 W

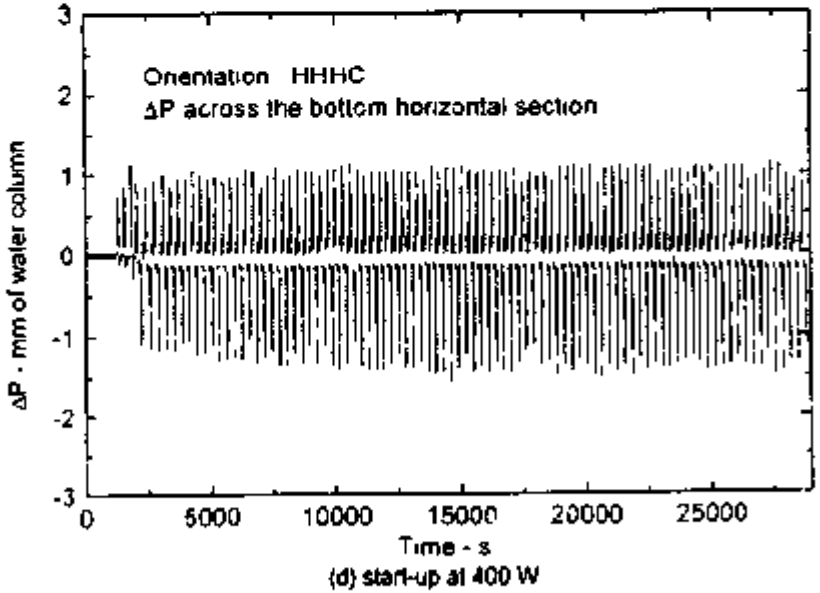

(d) start-up at 400 W

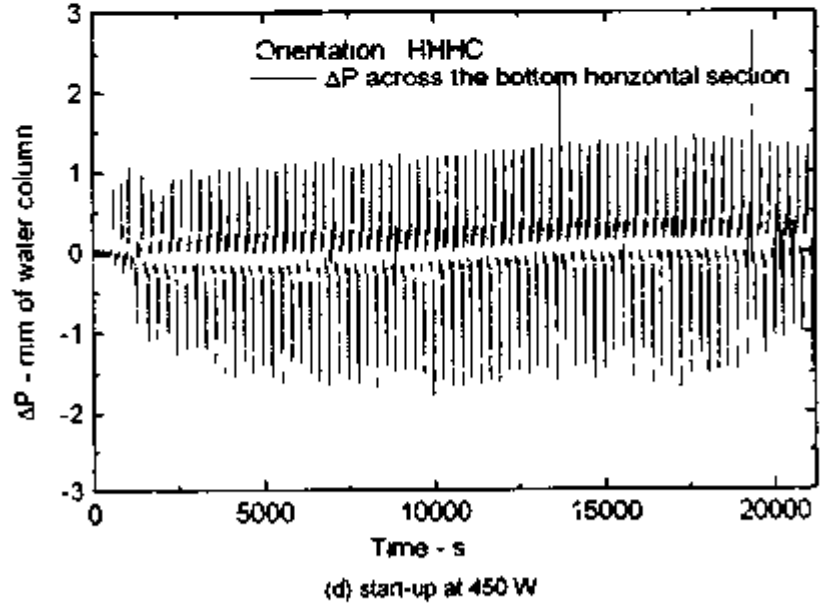

(d) start-up at 450 W

Fig 21 Development of unstable behavior at 300 W and 5 lpm coolant flow with inlet temperature of 33 °C

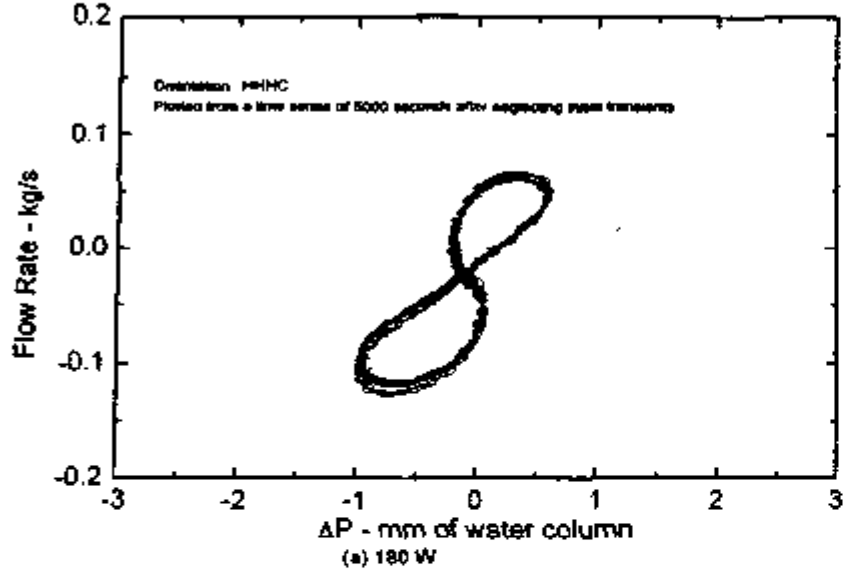

(a) 180 W

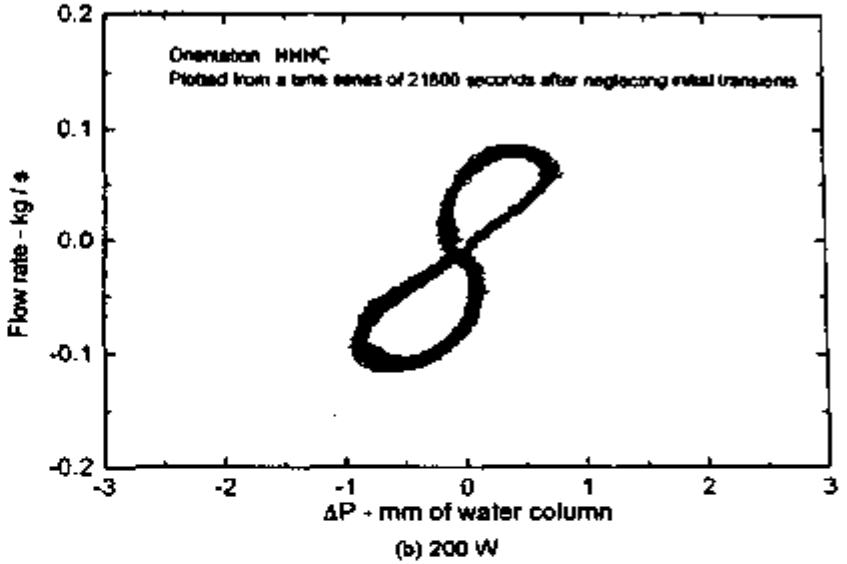

(b) 200 W

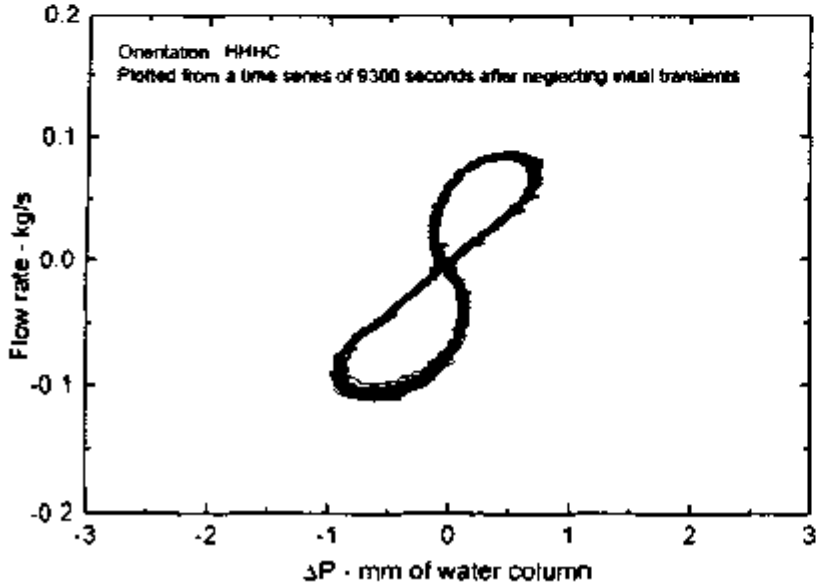

(c) 220 W

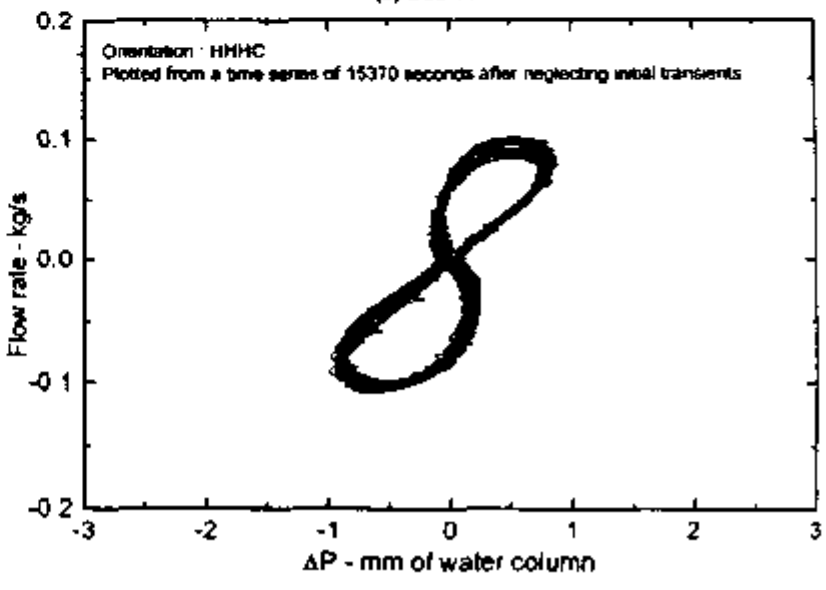

(d) 240 W

Fig. 22: Phase plots for bidirectional pulsing at 5 lpm coolant flow with inlet temprature of 34 °C

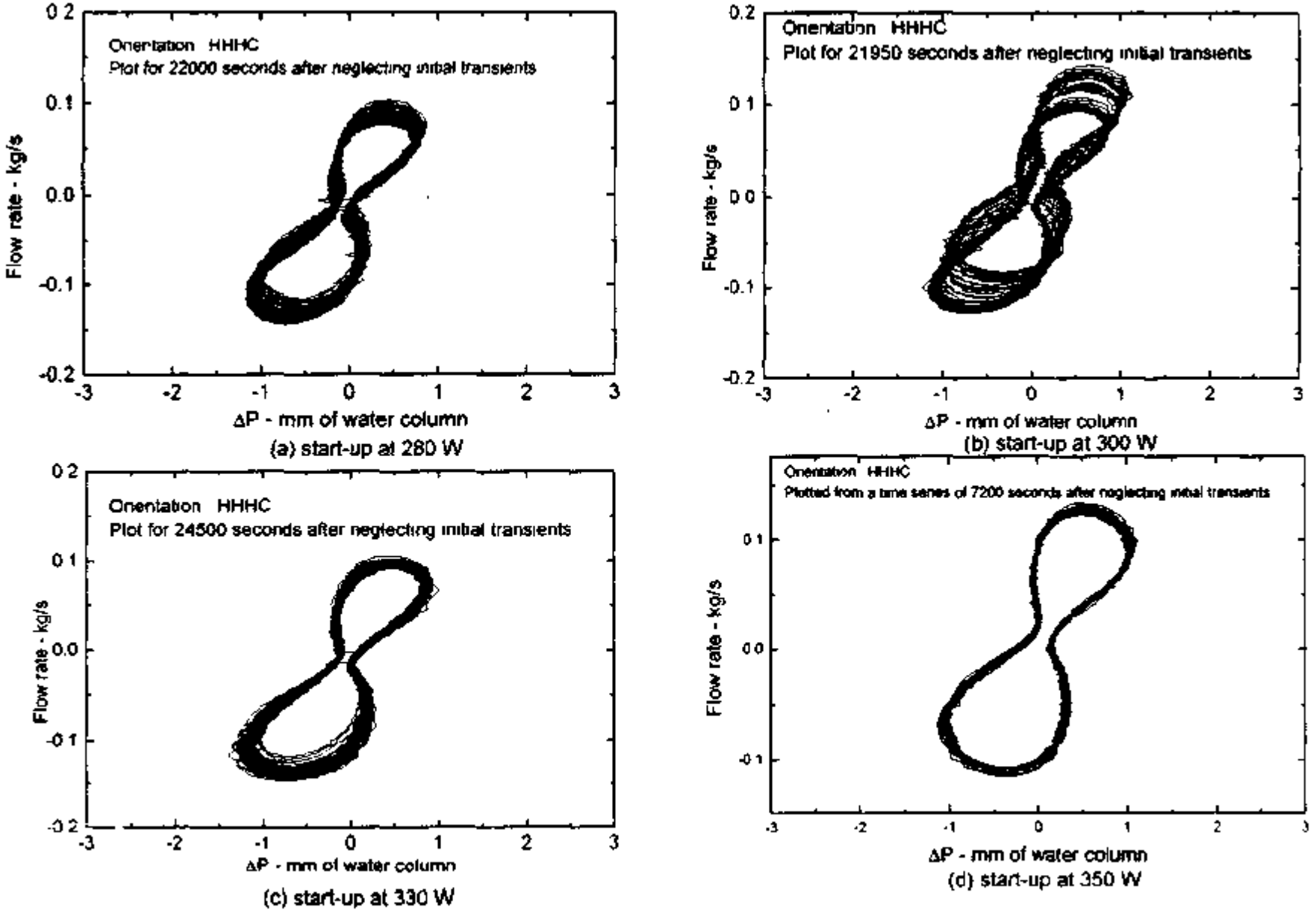

Fig.23 : Phase plots for different powers with 5 lpm coolant flow and inlet temperature of 32°C

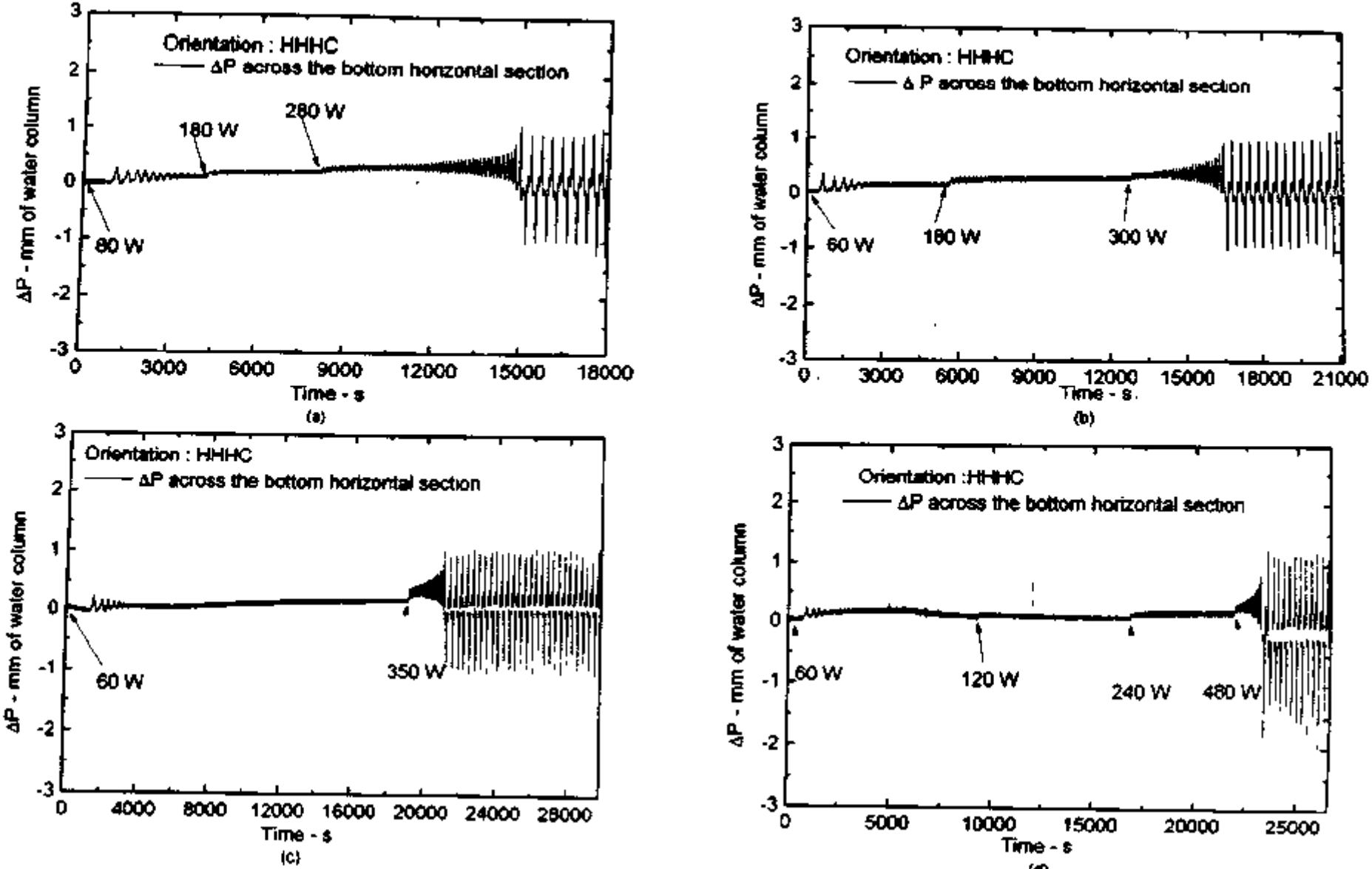

Fig. 24 : Development of unstable behavior at different powers with 5 lpm coolant flow rate at inlet temprature of 34 °C

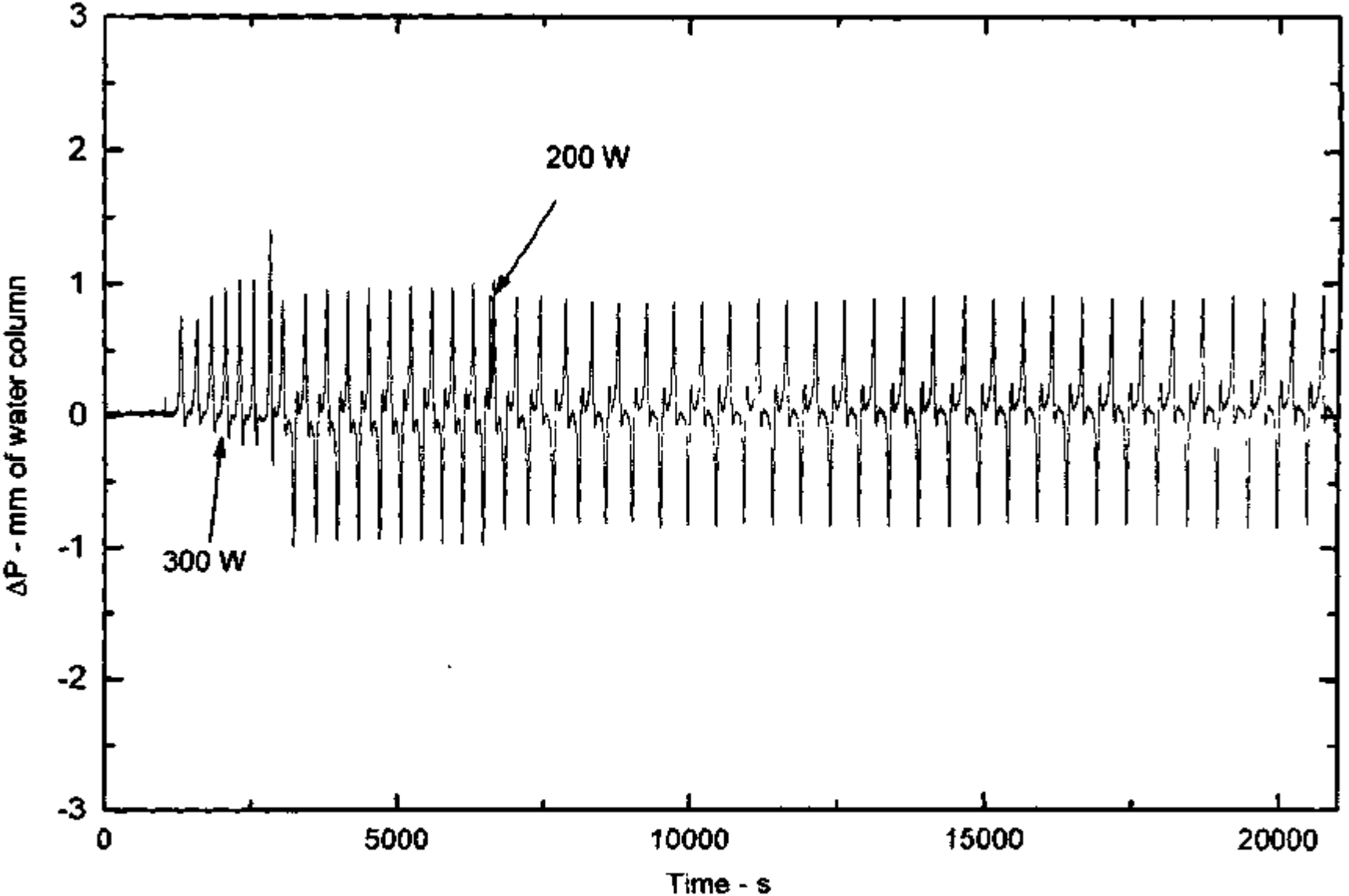

Fig. 25 : Decay of instability due to step back in power from 300 W to 200 W at 5 lpm coolant flow with inlet temperature of 28 ^{0}C

6.6 Compound Single Phase-Two phase instability with Bidirectional pulsing

At higher powers, the instability continues in the bidirectional pulsing mode superimposed by subcooled boiling. During the low flow part of the oscillation cycle; bubbles are formed near the top surface of the heater outlet, which are stationary to start with. When these bubbles are released high ΔP occurs since two-phase ΔP is significantly larger than single-phase ΔP. Boiling is indicated by the occurrence of sharp peaks in the ΔP due to bubble release, which was confirmed by visual observation (see Figs. 26 b, c and d. For the sake of comparison, a typical non-boiling case is shown in Fig. 26a). Due to the sudden increase of flow when the bubbles enter the vertical leg boiling is suppressed. In the range $408 < Q_h < 450$ W, the boiling is sporadic (see Figure 26b). Beyond about 450 W, the subcooled boiling becomes regular with every cycle having a two-phase part (see Fig. 26c). Beyond about 600 W, two two-phase regions are observed in every oscillation cycle (see Fig. 26d). With inception of subcooled boiling, the bidirectional pulsing becomes highly chaotic.

The bubbles generated at the top surface of the horizontal heater do not move until their size becomes more than a critical value (typically 2 to 5 mm in diameter). In the horizontal section at the heater outlet, the bubbles move almost in a line close to the top surface. During the high flow part of the cycle all bubbles in the horizontal heater are swept by the flow. In the vertical leg, most bubbles condense, but an occasional bubble reaches the top horizontal pipe and escape through the expansion tank. The threshold of the compound instability has not shown any significant dependence on the heat addition path.

On the phase space, the subcooled boiling leads to the formation of cusps in the dumbbell shaped trajectory (see Fig. 27). Both the time series and the phase plots show an increasingly chaotic behaviour with increase in power. Almost every trajectory depicts a separate line instead of the nearly overlapping trajectory observed at low powers. Ambrosini and Ferreri (1998) predict the formation of such cuspids for a rectangular loop even without boiling. In the present experiments also, smaller cusps are observed at low powers without boiling (see Figs. 22 and 23).

7. NATURE OF THE OSCILLATORY BEHAVIOUR

7.1 Metastable or Conditionally stable Regime

Experiments showed that the threshold power, at which the flow becomes unstable, is dependent on the heat addition path followed in the experiment. The region in which the instability threshold shows path dependence is referred to as the metastable or conditionally stable regime. If we consider only the first two heat addition paths (i.e. start-up from rest and power raising from a stable steady state) then the region between $105 < Q_h < 270$ W can be considered as subcritical regime if we borrow the terminology of Widmann et al (1989). The characteristics of this region is similar to the subcritical regime of Widmann et al. (1989) in that it is stable if power is increased in small steps, but unstable for large power increase (in our case start-up from rest). However, if we consider the third heat addition path (i.e. decay of instability due to power step-back), then we find that the instability does not decay even if we bring down the power in very small steps until the power is brought below a threshold value (65 W). Hence the entire region between 65 W to 270 W is considered as conditionally stable (metastable) region in this report. In the conditionally stable region, stable or unstable operation can be obtained depending on the heat addition path followed in the experiment

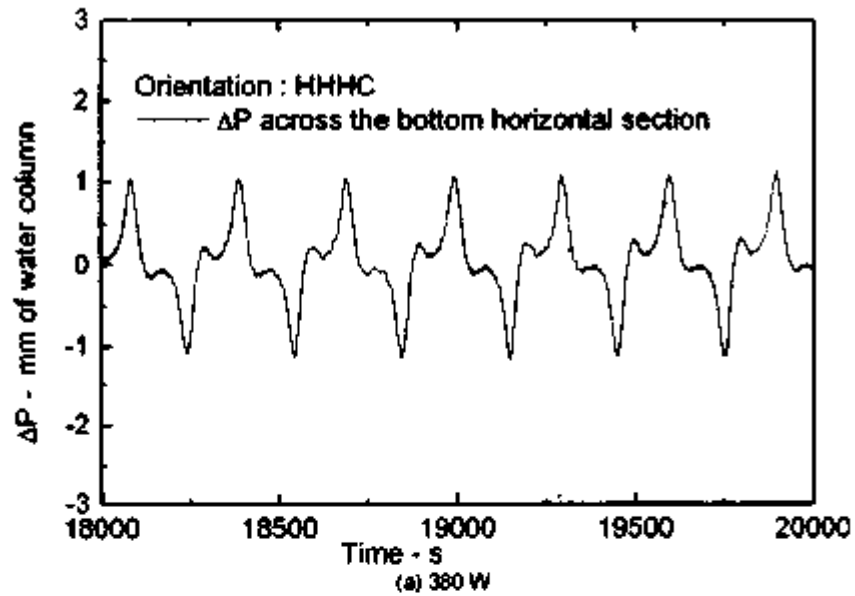

(a) 380 W

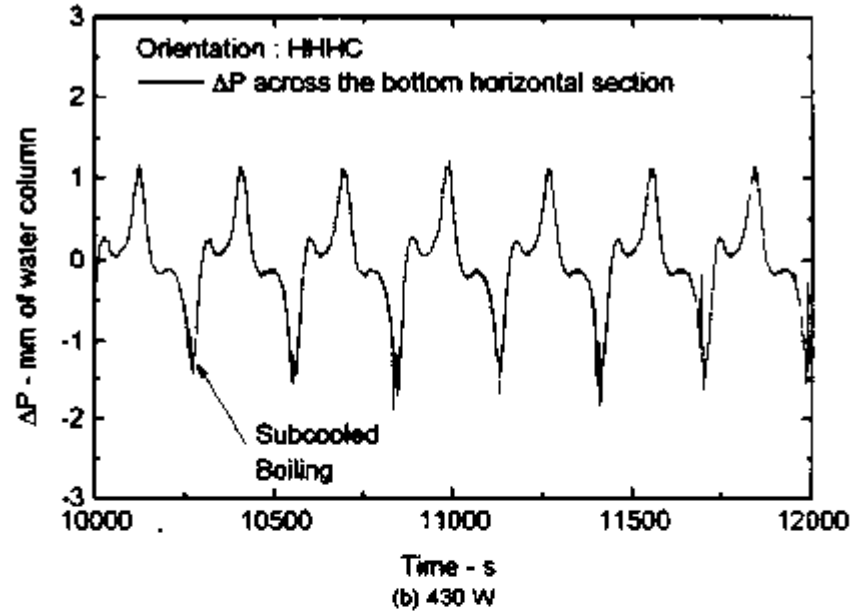

(b) 430 W

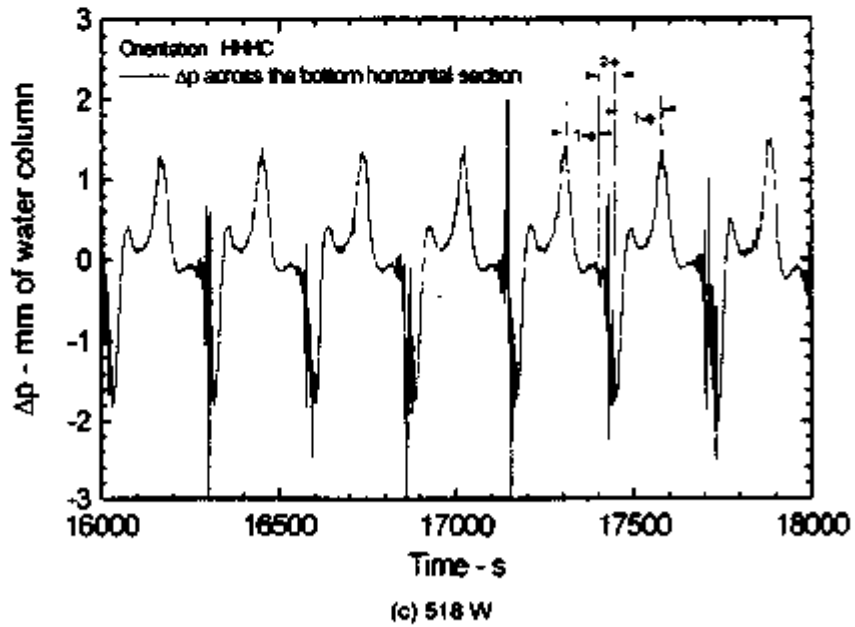

(c) 518 W

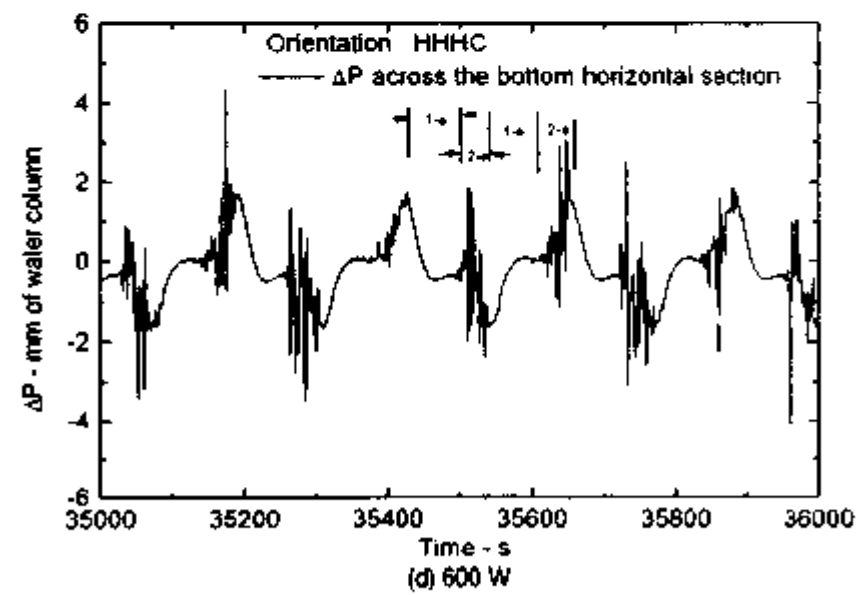

(d) 600 W

Fig.26 : Unstable oscillatory behaviour with subcooled boiling at 5 lpm coolant flow with inlet tempralure 34°C

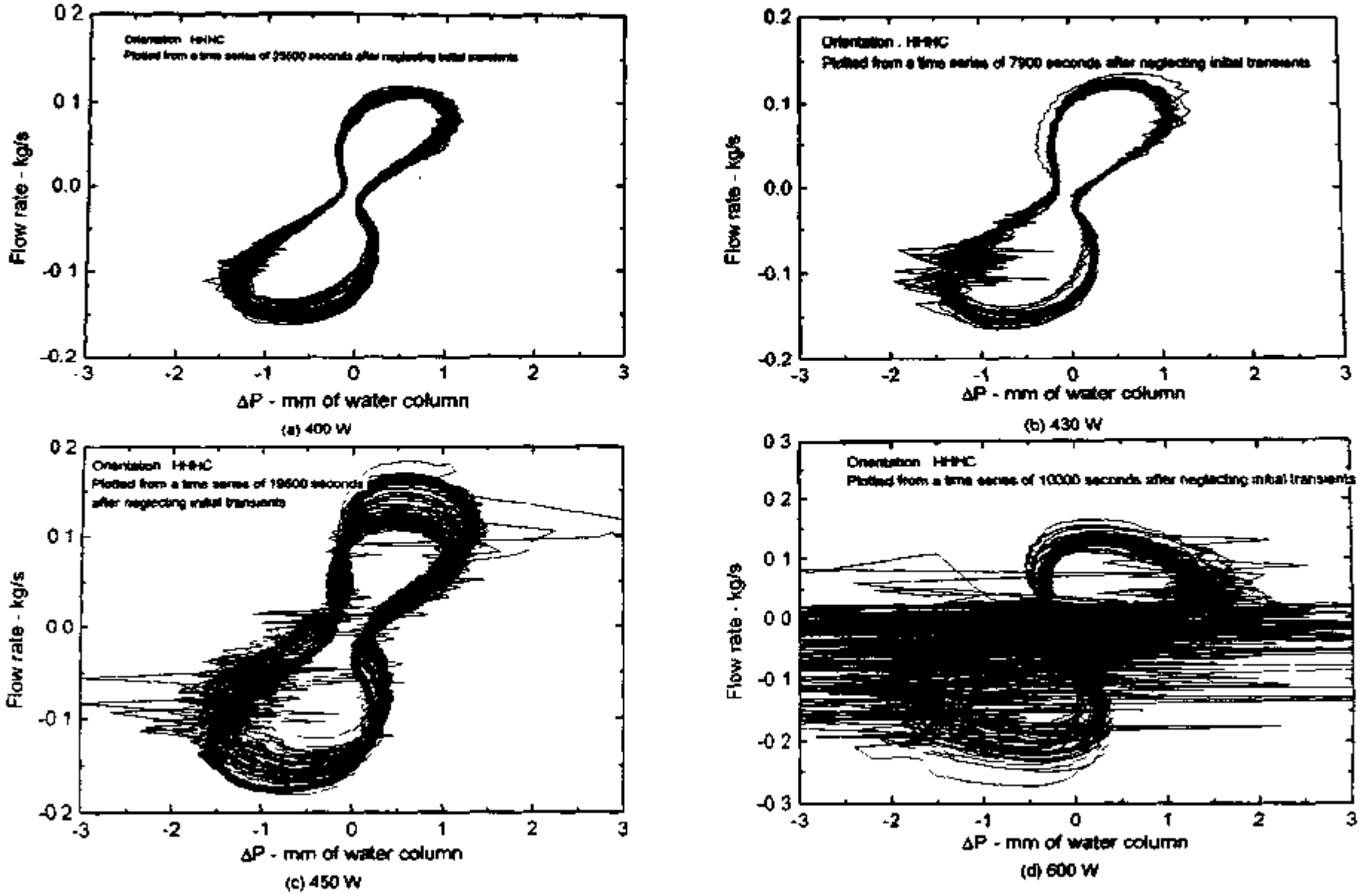

Fig 27 Cusp catastrophe due to subcooled boiling at different powers for 5 lpm coolant flow with inlet temperature of 32 °C

The region above 270 W is unconditionally unstable or simply unstable as it is always unstable independent of the heat addition path

7.2 Stability Margin

Traditionally, the decay ratio (ratio of the amplitudes of the succeeding to the preceding oscillation) is used as the stability margin For all transients that lead to a steady state the amplitude of every succeeding oscillation is lower than that of the preceding one (see Figs 3 & 8) Therefore, it appears that the lower the decay ratio, the faster will be the approach to the steady state This is the rationale behind the adoption of decay ratio as a stability margin

Typical values of the decay ratios for the three heat addition paths are presented in Table-4 It is found from this table, and the corresponding experimental observations given earlier that the amplitude of oscillation for certain operating procedures (power raising from a stable steady state for example) is very small even though the decay ratio is very close to unity For certain other operating conditions, the amplitude of oscillation can be significantly large even though its decay ratio and the operating power are much smaller This is the inadequacy of the decay ratio when used as a stability margin

Table 4: Effect of heating mode on the decay ratio (DR)

Start-up from rest			Decay of instability			Power raising from stable SS*		
Power	DR	ΔP_R^+	Power	DR	ΔP_R^+	Power	DR	ΔP_R^+
45 W	0 81	2 83	200W to 60W	0 88	7.68	60W to 180 W	0 981	1 0
60 W	0 89	2.12	300 W to 60 W	0 84	10 12	80W to 165 W	1 0	1 02
90 W	0 88	2.04	400W to 60 W	0 78	9 78	165W to 260W	0 988	0 96
100 W	0.95	2 11	400 W to 65 W	0 86	5 04	60W to 260 W	1 0	0 98

* SS – steady state . + ΔP_R – ratio of ΔP for first oscillation following the transient to the steady state value

The present experiments have demonstrated the existence of a conditionally stable region near the lower stability threshold Experimentally, a higher threshold value is obtained if we start raising power from a stable steady state However, at powers much less than this threshold (about 4 times less), instability can be encountered if we follow a different operating procedure This suggests that to obtain adequate stability margin an appropriate operating procedure needs to be specified rather than a decay ratio This operating procedure requires the following threshold values to be established

a) Maximum power at which the system can be started up from stagnant initial conditions without encountering instability

b) Maximum step-up in power that is permissible from a given stable steady state operating condition without encountering instability

c) Minimum step back in power required for achieving stability from an unstable operating condition

The first two thresholds are sufficient to safely operate the system without encountering instability The third threshold is required to stabilise the system if it enters an unstable zone of operation Such unintentional landing in an unstable zone can be caused by an operator error or due to an unanticipated transient

7.3 Comparison of the heat transport capability for the stable and unstable cases in the conditionally stable regime

Single-phase natural circulation loops can be stable or unstable depending on the operating conditions. Generally unstable natural circulation is chaotic with associated turbulence. Due to this unstable natural circulation loop can be a better heat transport device than stable natural circulation loop as opined by Bau and Wang (1992). However, to our knowledge, detailed study of the heat transport capability of the stable and unstable loop is not reported. Nevertheless, Misale et al (1999) report higher loop temperatures for the stabilised loop compared to the unstable loop suggesting reduction in heat transport capability in the stabilised loop. Stabilising is usually done by enhancing the hydraulic resistance of the loop. Due to the additional resistance introduced, the stabilised loop has a lower flow rate compared to the time averaged flow in the unstable loop thereby reducing its heat transport capability. Present experiments have established a procedure to achieve stable or unstable operation for the same operating conditions (i.e. heater power, coolant flow and its inlet temperature) in the conditionally stable region. In this section, the heat transport capability of the stable flow is compared with unstable flow.

For this comparison, first the measured flow rates for the stable and unstable modes were compared (see Fig. 28) as the heat transport capability depends on the loop flow (the loop with the larger flow rate has better heat transport capability than the loop with the lower flow rate). Subsequently, the cooler outlet temperature for the stable and unstable cases was compared (see Fig. 29). In both the cases, the power was maintained the same. To make a direct comparison, the time averaged flow and temperature in the unstable case was compared with the corresponding values for the stable case (see Table 5). These results show that the stable case gives more flow and lower temperature compared to the corresponding unstable case. Thus in the conditionally stable region, the unstable loop is found to have less heat transport capability than the stable loop. In contrast, the inference from the reported studies in literature is that the stabilised flow has less heat transport capability compared to the unstable flow (Misale et al. (1999)).

Table-5: Comparison of flow and temperatures for the stable and unstable cases.

S. No	Power - W	Flow Rate - kg/s		Cooler outlet temperature - °C	
		Stable	Unstable[1]	Stable	Unstable[1]
1	80	0.01998	0.0164	34.02	34.16
2	120	0.02066	0.01785	35.36	36.25
3	180	0.026	0.0311	33.13	35.61
4	260	0.06952	0.03807	41.25	43.4

1- Time average of the absolute of instantaneous values

7.4 Mechanism causing the Instability

In figure 24, the instability develops by the growth of small amplitude oscillations whereas in figures 11, 20 and 21 the instability is observed right from the initiation of flow. An amplitude growth is also observed in figures 20 and 21 before switching to bi-directional pulsing. In fact the development of instability via the growth of small amplitude oscillations is observed only when power was increased from an initially stable steady state. Another interesting observation is that growth of small amplitude oscillations as a mechanism of instability is observed for the unconditionally unstable regime (Q_h > 270 W). Further, the observed oscillatory behaviour discarding the initial transients is always bidirectional pulsing for the

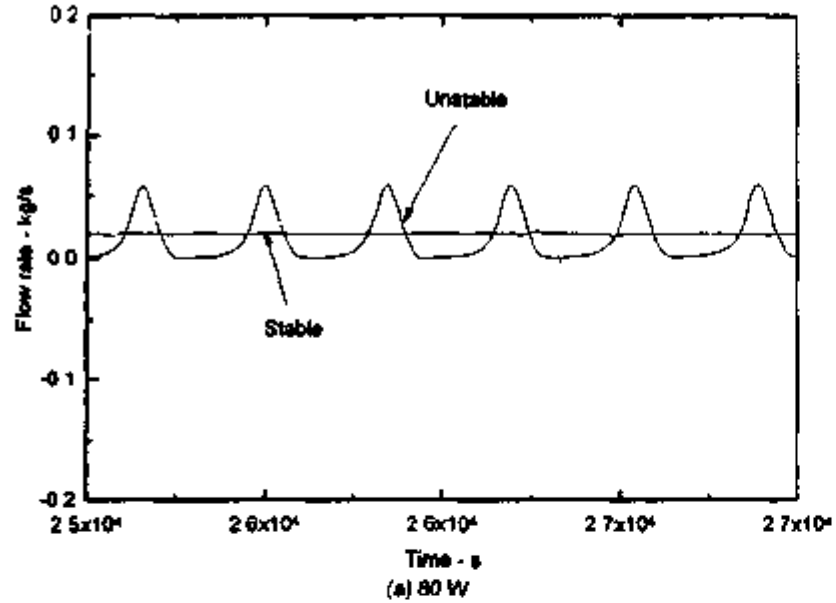

(a) 80 W

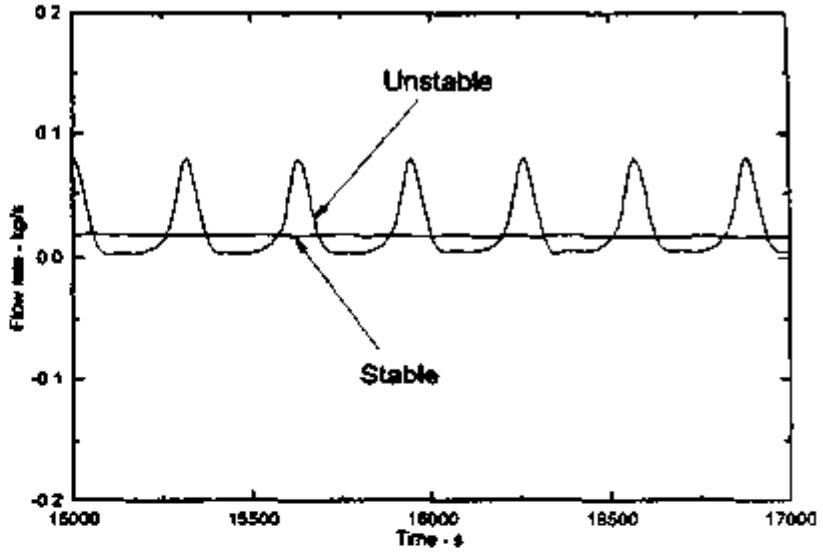

(b) 120 W

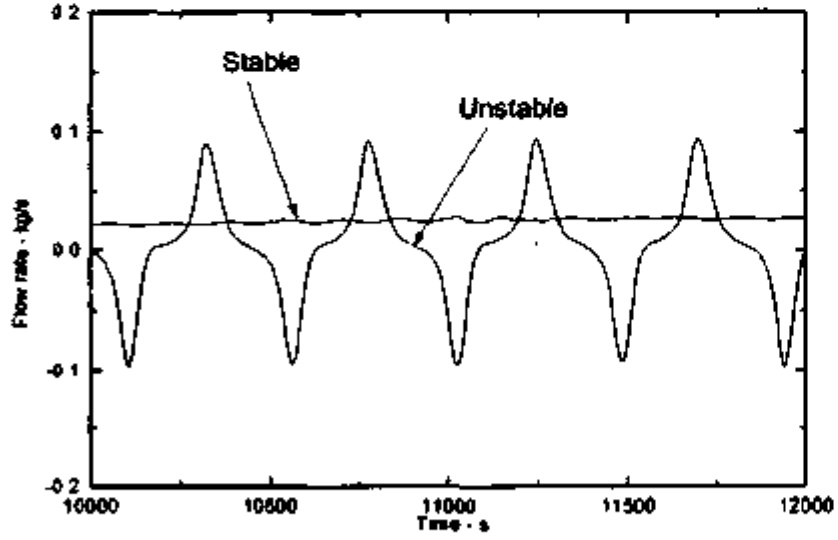

(c) 180 W

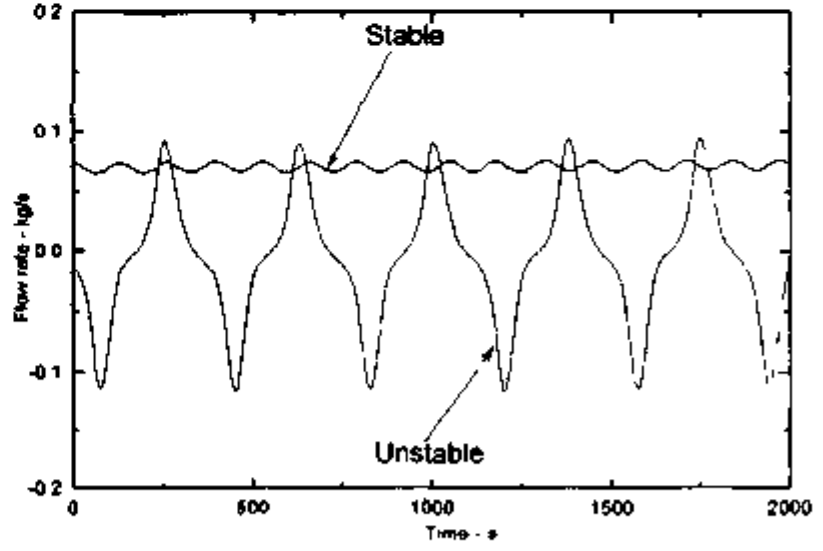

(d) 260 W

Fig 28 : Comparison of Flow rate at different powers with 5 lpm coolant flow at inlet temperature of 32 °C

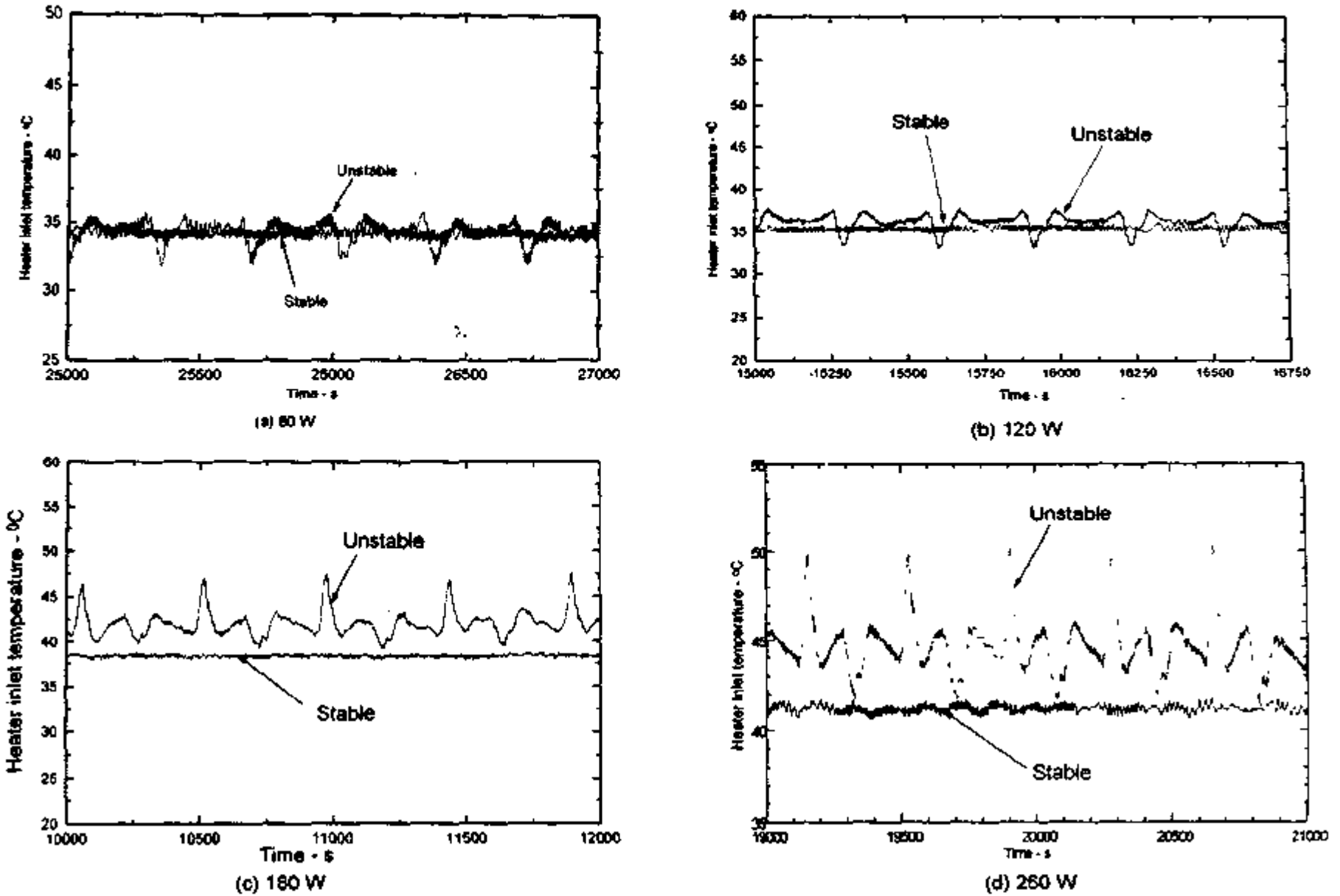

Fig.6 : Comparison of heater inlet temperature for different powers at 5 lpm coolant flow with an inlet temperature of 32 °C

unconditionally unstable regime. Both unidirectional and bidirectional pulsing flows are observed for the conditionally stable regime. However, unidirectional pulsing is observed for the low power region of the conditionally stable regime. Oscillation growth as a mechanism of instability is not applicable for unidirectional pulsing. Here the repetitive pulsing can be explained by the following physical mechanism.

7.4.1 Mechanism for unidirectional pulsing

Following the application of heating during stagnant initial conditions, a hot plug is formed in the heater. Transient conduction calculations show that the temperature in this hot plug is not uniform and shows a peak at the center of the heated section with the ends being relatively cold. Due to the instability associated with the local convection currents, the hot plug lengthens (due to sideward movement), becomes longer than the heated section and eventually covers the entire horizontal section. At the time of flow initiation, the penetration of the hot plug into one of the vertical legs is more than the other (Fig 30a). As the hot plug rises through the vertical leg the flow accelerates due to the increase in the buoyancy force. The flow reaches a peak when the entire hot plug is in the vertical leg, which is much longer than the horizontal leg. During this time, the heater gets filled up with cold water. As the head of

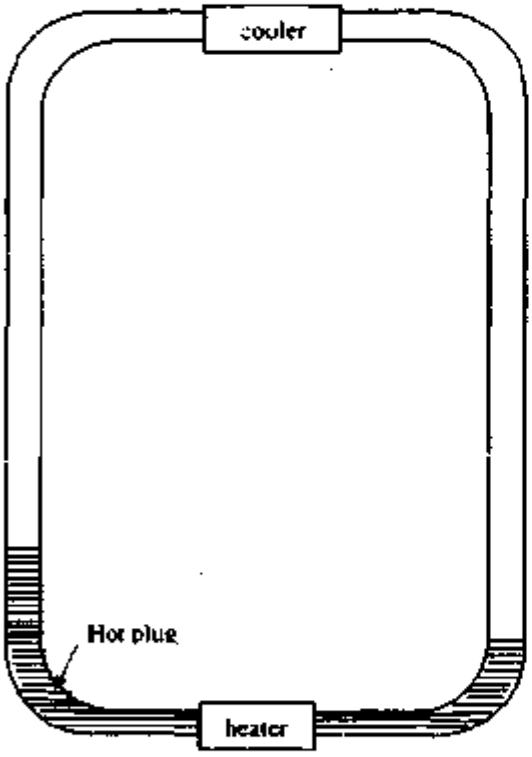

Fig. 30a : Position of hot leg during flow Initiation

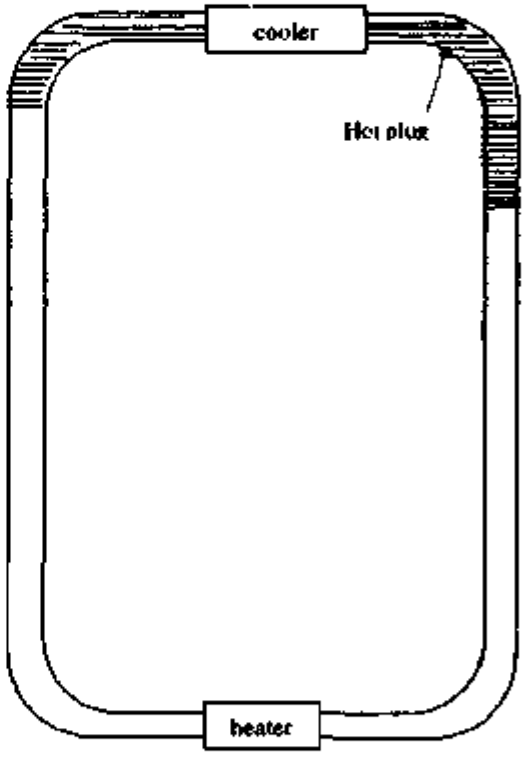

Fig. 30b: Position of hot plug during flow stagnation

the hot plug enters the top horizontal leg, the buoyancy force begins to reduce and the flow tends to decelerate. However, before its tail can go out of the vertical upleg, its head issues out through the vertical downleg (see Fig. 30b). Although, the head of the hot plug has passed through the cooler once, it has not been sufficiently diffused due to the high velocity while passing through the cooler. Due to this, the net buoyancy force reduces rapidly as the hot plug

descends along the vertical downleg leading to rapid reduction in flow This continues till the buoyancy force contribution of the right vertical leg is slightly more than that of the left vertical leg leading to a small reverse flow During the reverse flow (very short duration), part of the hot plug in the vertical downleg returns back to the horizontal leg with the hottest portion getting stranded at the right hand top elbow leading to flow stagnation At the same time, the coldest fluid pocket in the loop occupies the portion on either side of the right hand bottom elbow In the bottom horizontal pipe, the fluid near the left elbow is hotter than the fluid at the right elbow This forms a buoyancy check valve, which only permits forward flow During zero flow, a second hot plug and a cold plug begin to form in the heater and cooler respectively Minor forward and backward oscillations take place as the hot plug in the heater tries to escape into one of the vertical legs During the reverse flow, part of the hot plug returns to the top horizontal leg increasing the forward buoyancy force. During the forward flow, part of the stranded hot plug (in the adiabatic section after the cooler) enters the downleg that tends to reverse the flow The net result is small amplitude forward and backward oscillations for some time (see also Fig 12) During this process, the fluid in the left elbow gets heated more than that at the right elbow (as it was hotter than the right elbow during stagnation) Eventually, the second hot plug enters the vertical leg through the left elbow initiating a pulse in the same direction as the first pulse However, as this second hot plug enters the vertical downleg almost the same situation shown in Fig 30b repeats leading to flow stagnation again Thus each pulse appears to be independent flow initiation from stagnant conditions The process repeats itself giving unidirectional pulsing flow It may be noted that during steady unidirectional pulsing several hot and cold pockets are present, with the dominant peaks in the vertical legs governing the flow

7 4 2 Mechanism for bi-directional pulsing

Welander (1967) has proposed a mechanism for the development of instability through the oscillation growth This mechanism assumes that certain disturbances like a momentary reduction in coolant flow favours the formation of a 'hot pocket' (hotter than normal), which is amplified during every pass through the source and sink eventually leading to flow reversal After flow reversal also, the same scenario is expected to repeat leading to repetitive flow reversals While increasing power from a stable steady state, the Welander mechanism is found to cause the instability always The observed oscillatory behaviour after the first flow reversal, however, is found to differ from Welander's proposition Instead of the amplification taking place in the reverse direction the flow is found to be pulsing periodically with alternate forward and reverse flow pulses

Fig 31 shows a typical bi-directional pulsing behaviour after neglecting the initial transients. Before every large peak a minor peak of the same sign is observed During the minor peaks, the hottest and coldest pockets of fluid are trapped in the horizontal heater and cooler leading to a plateau region of low flow rate, which favours the formation of a very hot plug in the heater and a very cold plug in the cooler Mechanism-wise, bidirectional pulsing is practically similar to that of unidirectional pulsing except that the low flow prevailing during the minor peaks is sufficient enough to position the hot plug in the heater closer to one or the other vertical leg alternatively (see Fig 31) For example, the minor positive peak (after a large negative peak) places the hot plug in the heater closer to the left vertical limb During the minor oscillations in the plateau region, the hot plug issues out through this leg in the clockwise direction Similarly, after a large positive peak a small negative peak is observed which places the hot plug in the heater closer to the right vertical limb During the minor oscillations in the plateau region, the hot plug issues out through this leg in the counter

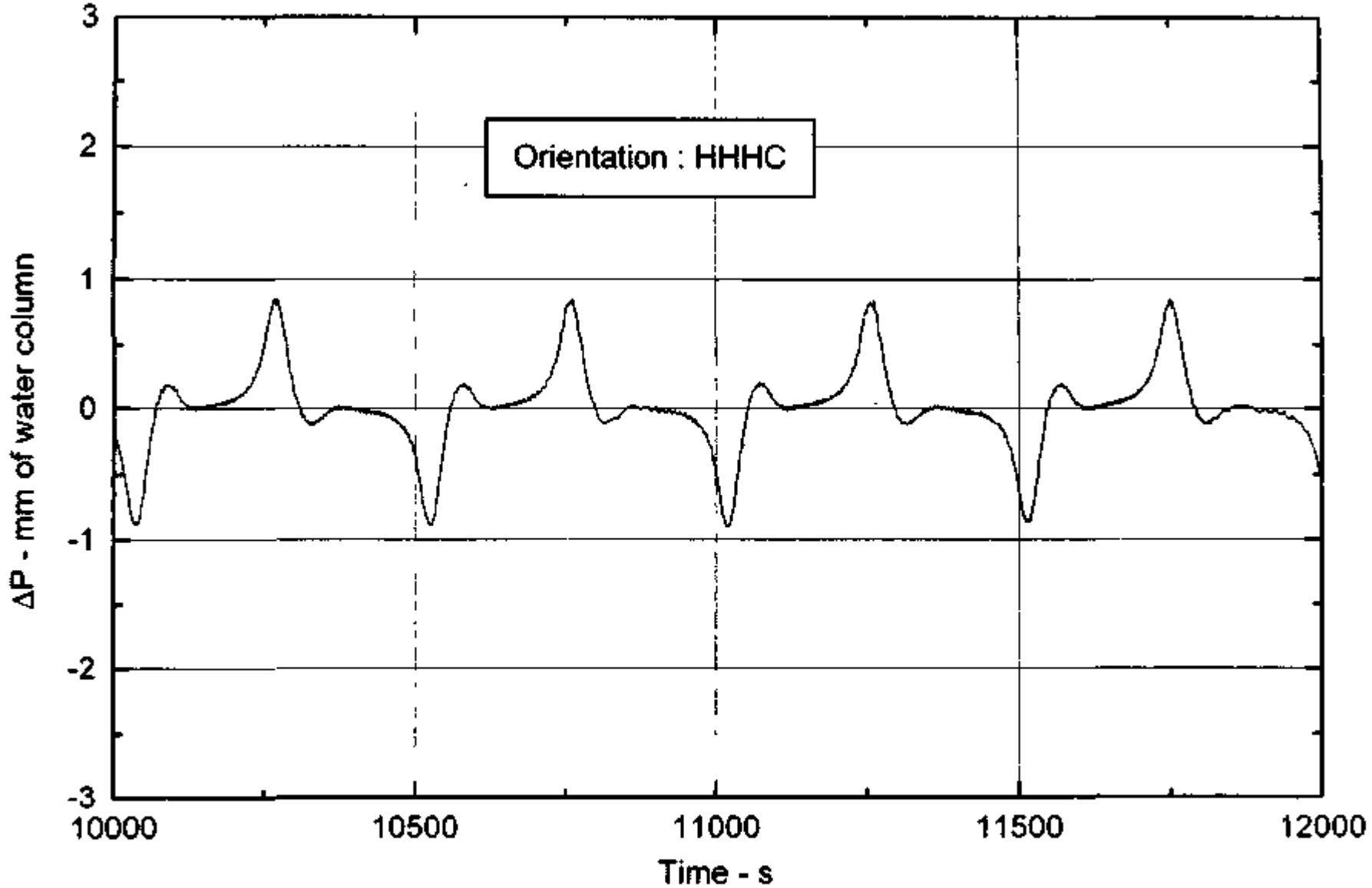

Fig. 31 : Bidirectional pulsing at 180 W and 4.94 lpm coolant flow at 27 ^{0}C

clockwise direction. Thus flow issues out in the clockwise and counter clockwise direction alternatively.

For start-up from rest an oscillation growth mechanism is observed before the flow switches to bi-directional pulsing. During the oscillation growth, the flow remains in the unidirectional pulsing mode with the amplitudes of both the forward and reverse flows increasing with time. Once the reverse flow is sufficient enough to place thhe hot plug in the heater nearer to the right vertical limb the oscillatory behaviour switches to the bi-directional pulsing.

7.5 Oscillation modes and Period n-tupling

7.5.1 Chaotic Switching between the oscillatory modes

An interesting observation is that when the oscillatory mode switches from unidirectional to bidirectional pulsing, the period enhances. On the other hand, when the oscillatory mode switches from bidirectional to unidirectional pulsing, the period reduces. Period doubling is a usual step for transition to chaos (Kapitaniak (2000)). A near period doubling is observed for most cases when the oscillatory mode switches from unidirectional to bidirectional pulsing while a near period halving is observed when switching from bidirectional to unidirectional pulsing (see table-6).

Table -6: Period change during chaotic switching of oscillatory modes

S. No	Power -W	Unidirectional to bidirectional switching			Bidirectional to unidirectional switching		
		T_{UP}^{1} - s	T_{BP}^{2} - s	T_{BP}/T_{UP}	T_{BP}^{1} - s	T_{UP}^{2} - s	T_{UP}/T_{BP}
1	150	275.3	572.1	2.08	635.4	288.5	0.454
2	160	244.35	478.09	1.96	462.2	229.5	0.497
3	160	249.6	495.2	1.99	671.31	316.54	0.471
4	160	243	559.5	2.30	483.23	302.0	0.625
5	160	245	509	2.08	516.0	300.0	0.582
6	165	259.0	5190.0	2.00	505.0	314.8	0.623
7	165	251.0	521.7	2.08	537.9	303.0	0.563
8	170	241.4	497.3	2.06	461.4	236.6	0.513
9	170	240.0	495.8	2.07	471.1	312.7	0.664
10	190	232.3	473.9	2.04	465.8	232.3	0.499

^{1} - Period just before switching ; ^{2} - Period just after switching

7.5 2 First switching from unidirectional to bidirectional pulsing

For start-up from rest, chaotic switching between the oscillatory modes is only observed for $150 < Q_h < 190$ W. Beyond about 196 W, chaotic switching between the oscillatory modes is not observed. However, for all powers above 140 W, unidirectional pulsing is observed initially before switching to bidirectional pulsing. This switching to bidirectional pulsing is always accompanied by a period enhancing process. A near period doubling is observed for powers in the range of 140 to 200 W. At other powers, the period enhancing is less than two (see Table-7).

To check the repeatability of period enhancing reported in Table-7, several tests were carried out at 300 W, the results of which are given in Table-8. From this table, it is observed that although the period values are not reproducible, the period ratio is fairly reproducible.

Table – 7 Period enhancing for the first switching from unidirectional to bidirectional pulsing during start-up from stagnant conditions

S No	Power – W	Period before 1st flow reversal, T_b -s	Period after 1st flow reversal, T_a s	Period ratio T_a/T_b	Remarks
1	140	272 0	534 1	1 96	
2	150	270 0	556 0	2 06	Chaotic switching
3	160	259 0	535 4	2 07	-do-
4	165	270 7	546 8	2 02	-do-
5	170	267 4	537 8	2 01	-do-
6	180	270 8	520 0	1 92	-do-
7	190	268 0	511 4	1 91	-do-
8	196	269 6	557 9	2 07	No chaotic switching
9	200	274 7	552 8	2 01	-do-
10	220	240 9	434 2	1 80	-do-
11	240	259 4	479 1	1 85	-do-
12	280	221 0	387 8	1 75	-do-
13	287	215 5	403 9	1 87	-do-
14	300	244 6	470 7	1 92	-do-
15	330	250 7	460 8	1 84	-do-
16	400	221 7	393 0	1 77	-do-
17	408	197	353 0	1 79	Sporadic boiling
18	430	213 0	336 0	1 58	-do-
19	450	220 9	414 1	1 87	-do-
20	518	242 3	370 5	1 53	Boiling in every cycle

Table – 8 Period enhancing for the first switching from unidirectional to bidirectional pulsing during start-up from stagnant conditions at 300 W

S No	Period before flow reversal, T_b -s	Period after flow reversal, T_a -s	Period ratio T_a/T_b
1	246 2	444 7	1 81
2	244 7	459 6	1 88
3	247 2	443 8	1 80
4	227 2	400 2	1 76
5	235 4	431 2	1 83
6	231 0	406 3	1 76
7	215 5	374 8	1 74
8	227 1	415 4	1 83
9	231 7	416 3	1 80
10	216 4	393 8	1 82

7 5 3 Switching from unidirectional to bidirectional pulsing by oscillation growth

For the small amplitude oscillation growth from conditionally stable region, the period enhancing is significantly more than two (see table 9) Table-9 shows that there is no regular pattern in the observed period enhancement A near period doubling is observed for 280 W, 320 W and 350 W, while a near period tripling is observed at 270 W, 330 W and 480 W

Table - 9 : Period enhancing by small amplitude oscillation growth

S. No.	Power – W	Period before flow reversal, T_b - s	Period after flow reversal, T_a – s	Ratio T_a/T_b
1	270	152.4	453.6	2.98
2	280	182.6	378.6	2.07
3	300	153.3	356.7	2.33
4	320	156.4	313.4	2.00
5	330	140.8	400.6	2.85
6	350	154.6	317.1	2.05
7	385	127.3	331.9	2.61
8	480	117.2	325.8	2.81

7.6 Effect of Coolant flow rate

The results discussed so far are obtained with a constant cooling water flow rate of 5 litres per minute. At higher cooling water flow rates, unidirectional pulsing can be obtained beyond the 135 W observed for 5 lpm flow. Both the stability threshold and the range of power for unidirectional pulsing are found to shift up with cooling water flow rate (see figures 32a and b). With 8 lpm coolant flow, the unidirectional pulsing can be observed for $115 < Q_h < 176$ W. The lower threshold of unidirectional pulsing, however, is less affected by the increase in coolant flow than the upper threshold. The coolant inlet temperature also appears to have the same effect.

7.7 Oscillatory Behaviour of Heater and Cooler Inlet Temperatures

Figs. 33a to d show the oscillatory behaviour of the heater and cooler inlet temperatures measured by the thermocouples TC1 and TC5 (see Fig. 1 for the location of thermocouples TC1 and TC5) for unidirectional pulsing. Figures 34 a to d show similar results for bi-directional pulsing. It is noticed that the fluid temperature oscillations of TC1 and TC5 are out-of-phase by 180^0. Since the locations of thermocouples TC1 and TC5 divide the loop into exactly two halves, the occurrence of the out-of-phase oscillation is an indication of the equality of the period of oscillation to the loop circulation time. Similar results were also obtained earlier by Vijayan et al. (1992).

Comparing figures 33 and 34, we observe the fluctuations in temperature signals are more at low powers than at high powers causing the width of the curve to be more. This is an indication of the significance of the local convection currents at low power, which makes the flow three-dimensional.

7.8 Oscillatory behaviour of ΔT_h

Figures 35 and 36 show typical unstable behaviours of ΔT_h observed for unidirectional and bi-directional pulsing respectively in the present experiments. Again, the minor fluctuations in ΔT_h are found to decrease with power. With increase in power, the frequency of oscillations is found to increase for both unidirectional and bi-directional pulsing.

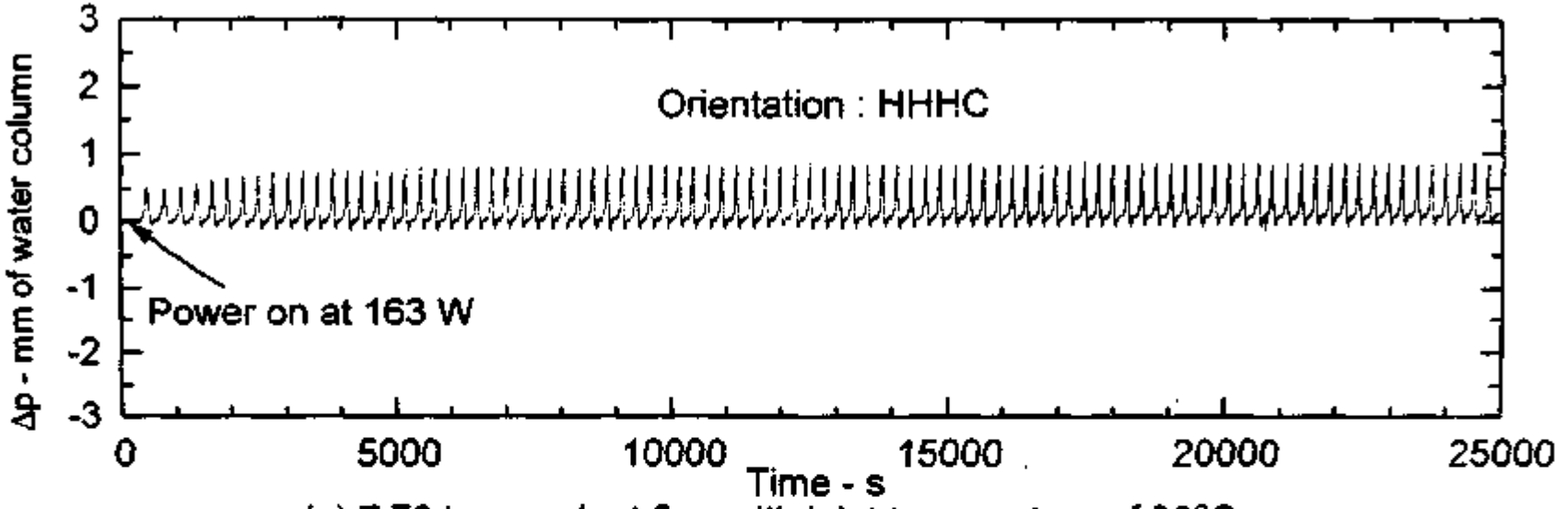

(a) 7.79 lpm coolnat flow with inlet temperature of 30°C

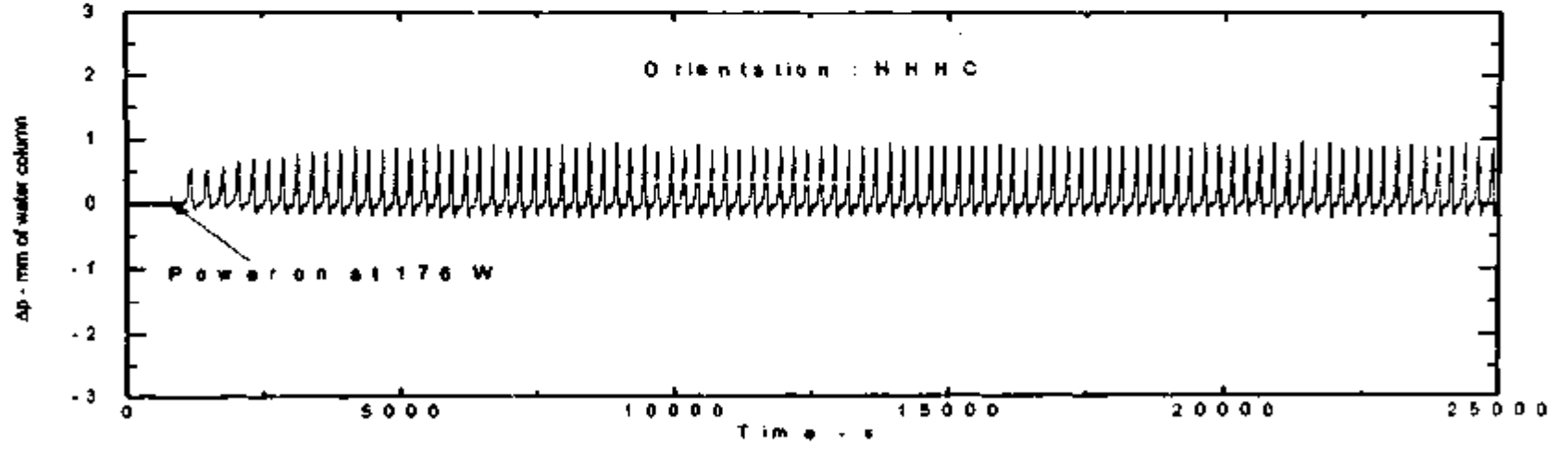

(b) 5.77 lpm coolant flow at inlet temperature of 30 °C

Fig. 32: Effect of coolant flow rate on unidirectional pulsing

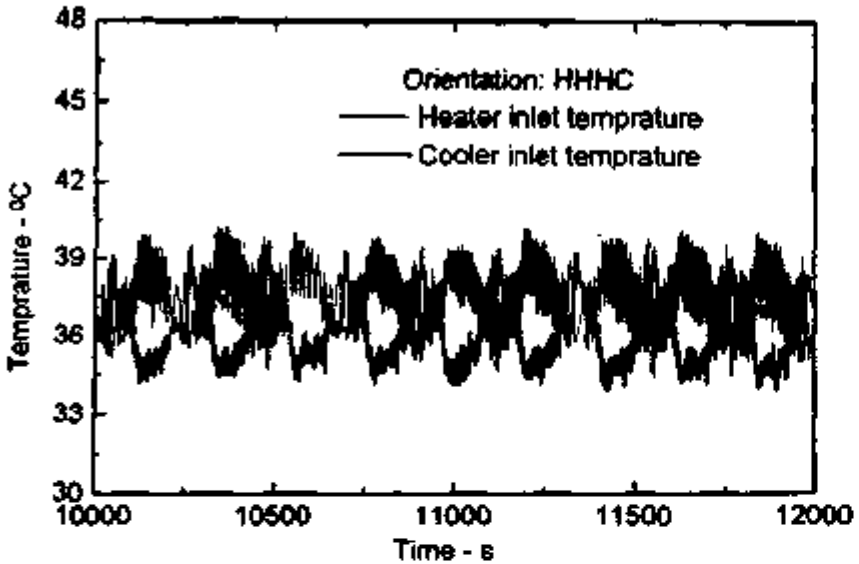

(a) 105 W

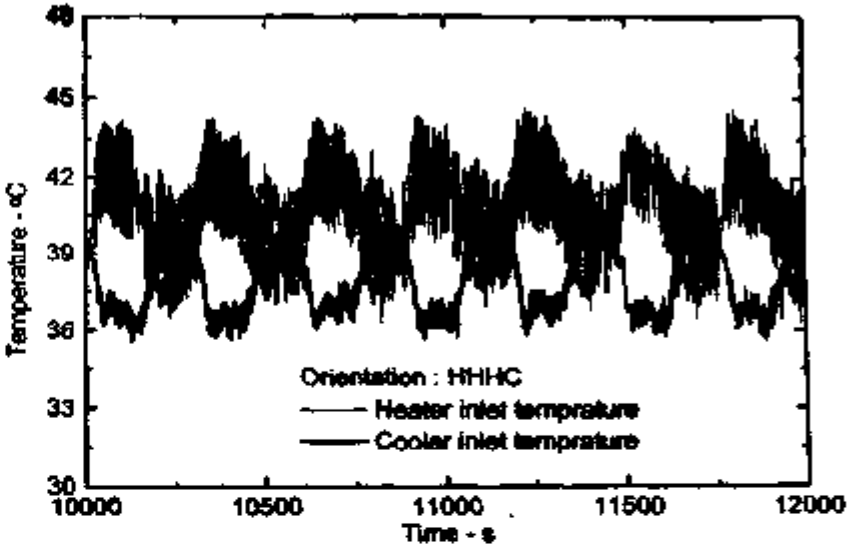

(b) 125 W

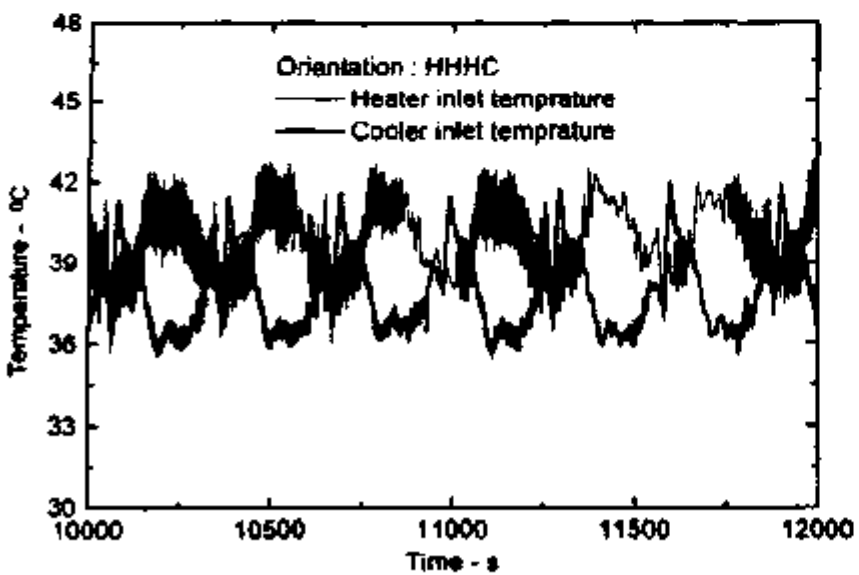

(c) 130 W

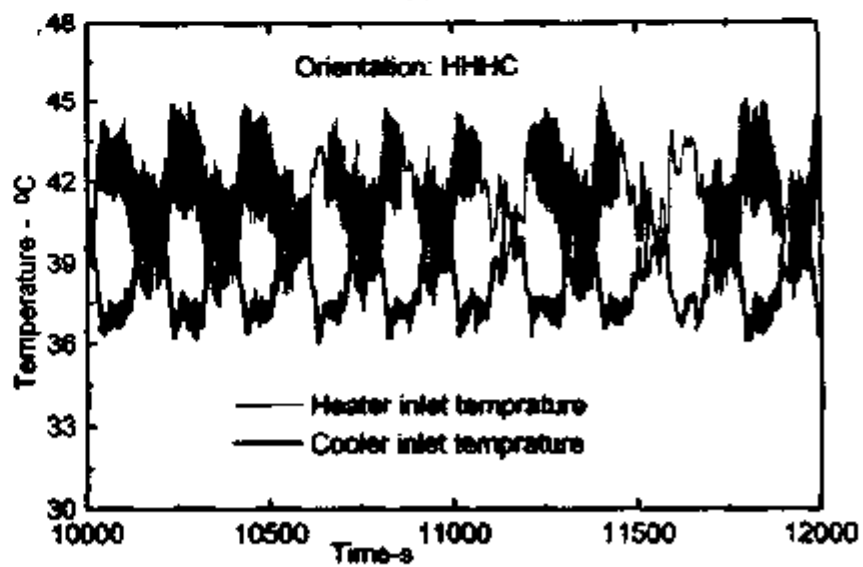

(d) 140 W

Fig. 33. Oscillatory behavior of fluid temperatures during unidirectional pulsing for different powers at 5 lpm at coolant inlet temprature of 34C

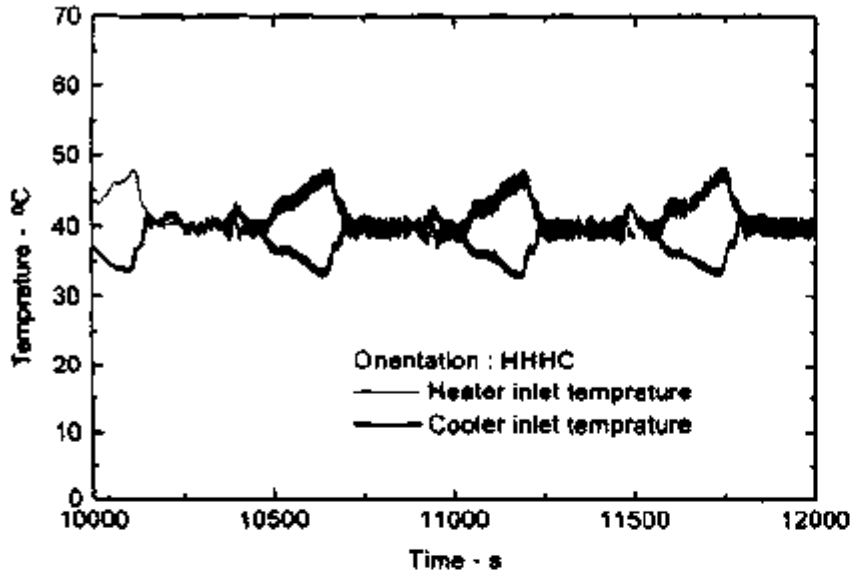

(a) 150 W

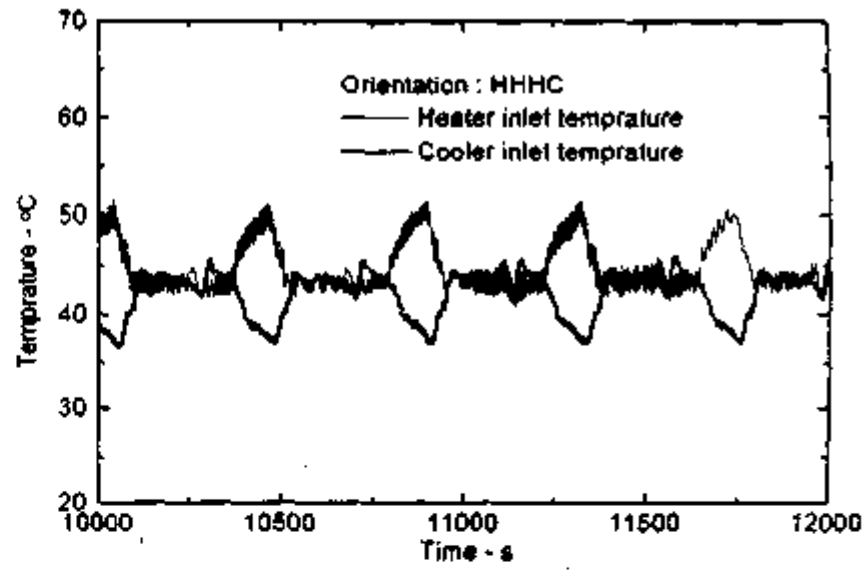

(b) 200 W

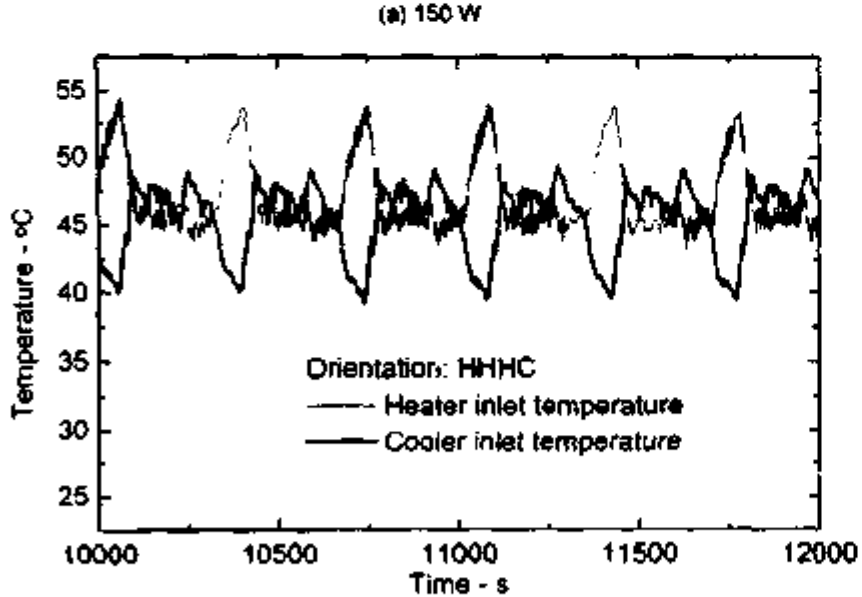

(b) 300 W

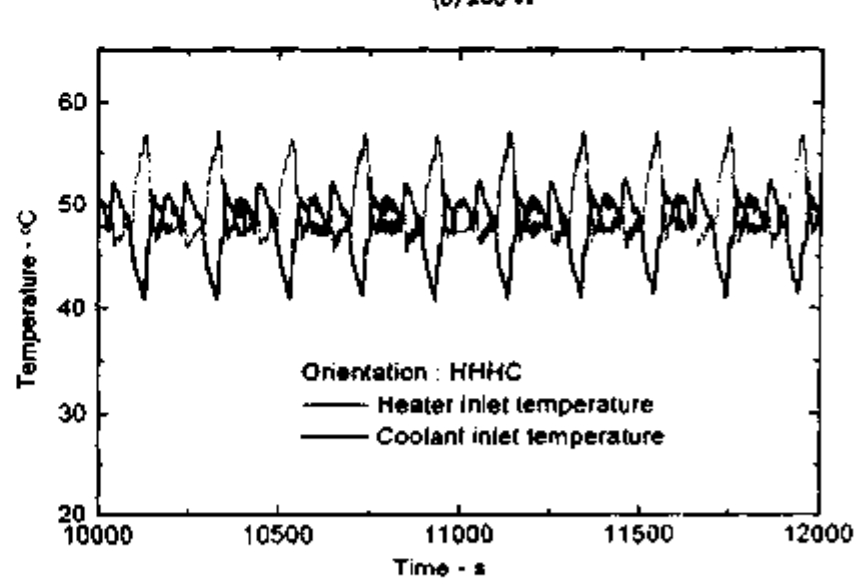

(d) 400 W

Fig. 34 : Oscillatory behaviour of fluid temperatures for bidirectional pulsing flow at 5 lpm coolant flow with inlet temperature of 34 °C

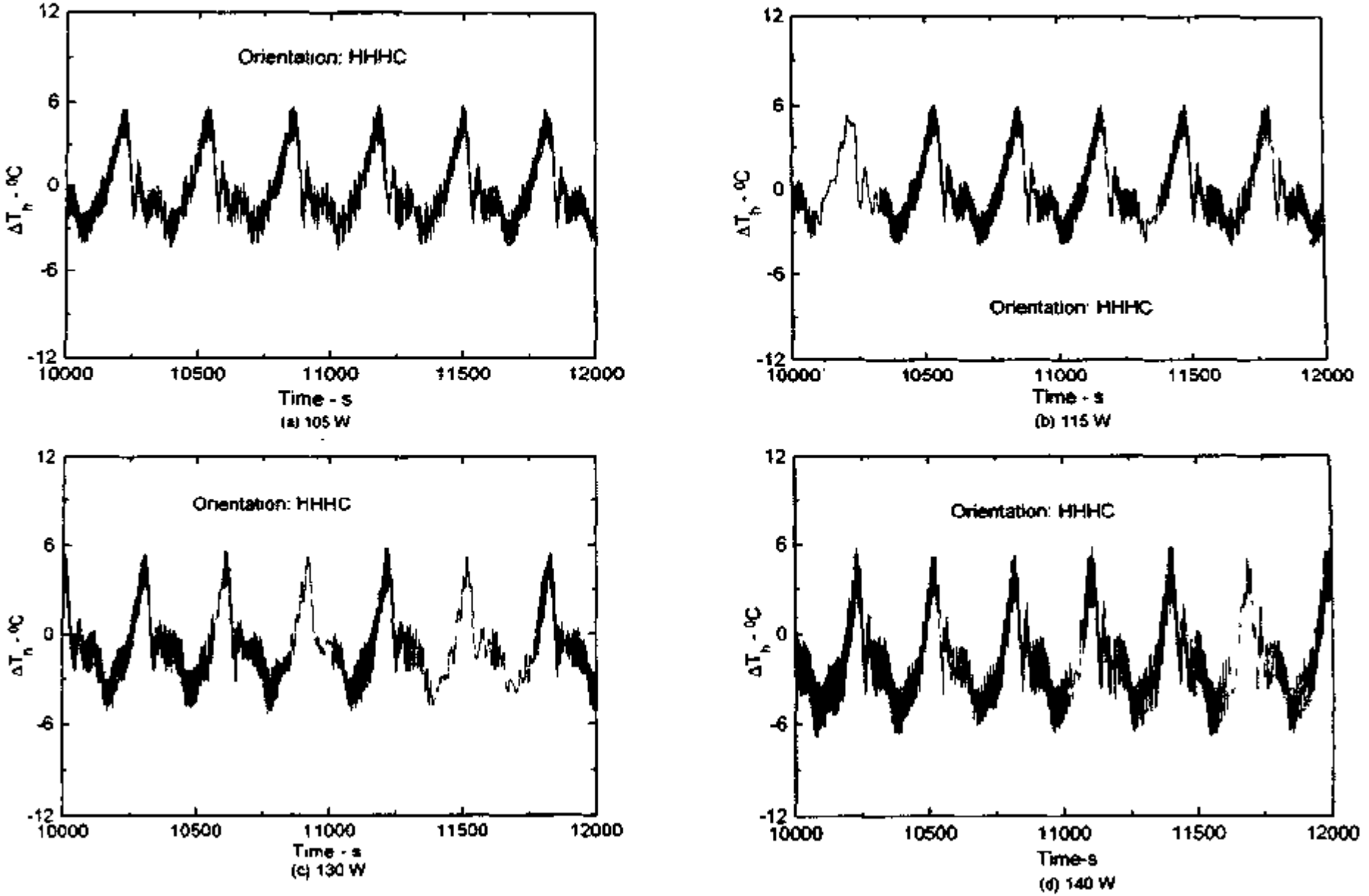

Fig. 35 Oscillatory behavior of ΔT_h for different powers at 5 lpm coolant flow with inlet temprature of 34 ^{0}C

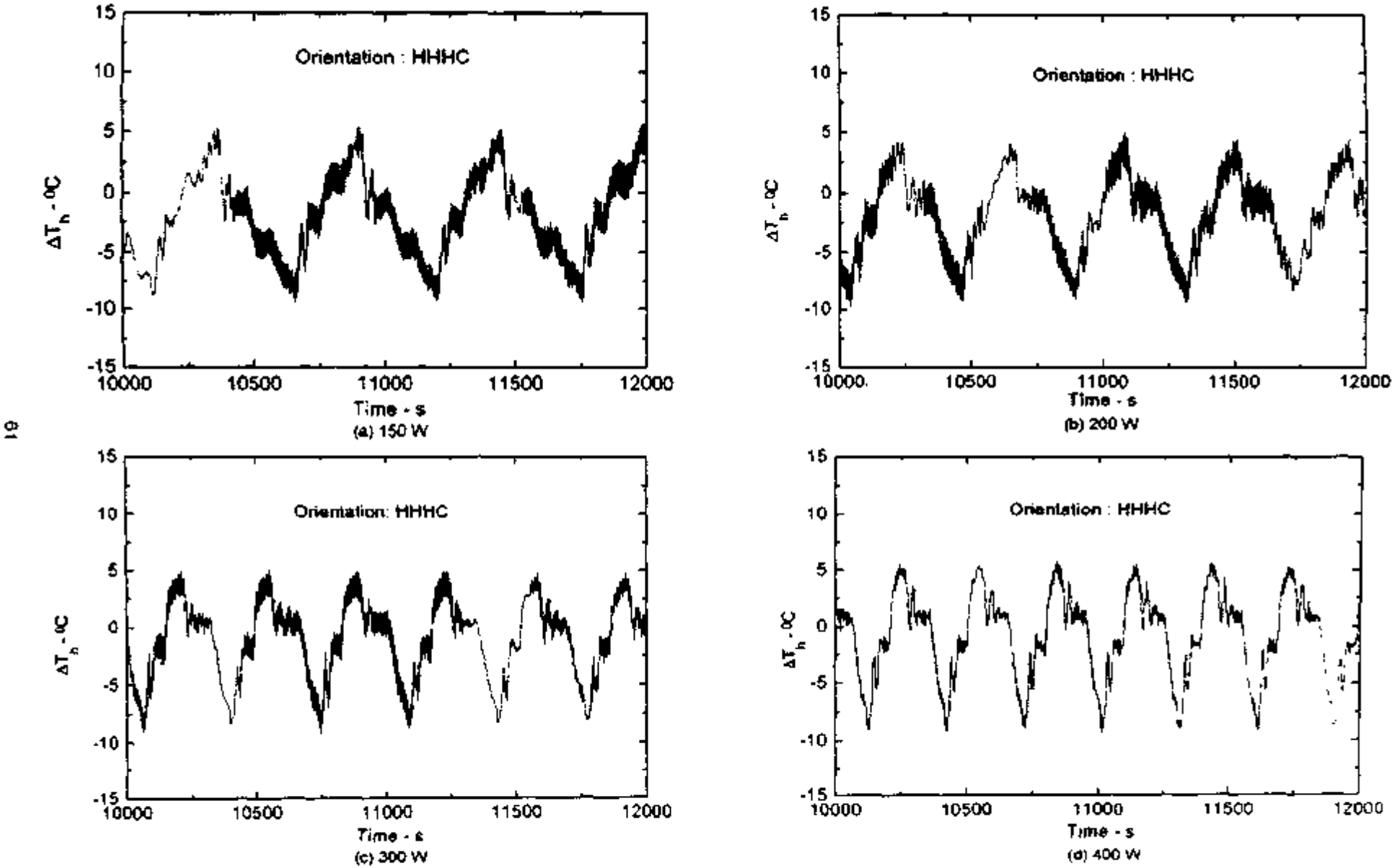

Fig. 36 : Oscillatory behaviour of ΔT_h for bidirectional pulsing at 5 lpm coolant flow and 32 ^{0}C

7.9 Period and Frequency of Oscillation

The oscillation periods for both unidirectional and bi-directional pulsing are not equal to the loop circulation time unlike the oscillations observed in the toroidal loop (Creveling et al. (1975)). Instead, the oscillation periods are equal to the time difference between two successive hot plugs issued out by the heater in the same direction. The cumulative distance travelled by a particle of fluid shown in Fig. 37 proves this. In both cases, the distance travelled by a particle of fluid in one cycle is more than the length of the loop.

From the observed unstable behaviour the average time period and frequency was calculated for different powers and are tabulated in Table 10 and 11 for unidirectional and bi-directional pulsing respectively. It is observed that with increasing power time period decreases and frequency increases for both unidirectional and bi-directional pulsing. Similar result was earlier obtained by Vijayan et al. (1995), Misale et al. (1999) and Nishihara (1997) for other rectangular loops. The results obtained are plotted in Figure 38.

Table 10: Effect of power on the period and frequency of oscillation for unidirectional pulsing

Sr. No.	Power W	Time Period (T) s	Frequency (1/T) Hz	Remarks
1	65	356.1	0.002808	Unidirectional pulsing
2	65	363.3	0.002753	-do-
3	70	363.3	0.002753	-do-
4	80	347.2	0.002880	-do-
5	90	329.1	0.003039	-do-
6	115	313.4	0.003191	-do-
7	120	303.0	0.0033	-do-
8	120	312.4	0.003201	-do-
9	125	292.1	0.003423	-do-
10	125	286	0.003497	-do-
11	130	305.8	0.00327	-do-
12	130	299.6	0.003338	-do-
13	130	295.6	0.003383	-do-
14	140	291.0	0.003436	-do-
15	163	259.7	0.00385	-do-
16	176	247.5	0.00404	-do-

7.10 Phase Plots in other Parameter Spaces

For analysing the instability behaviour, phase plots are often employed. A steady state operating point will be represented by a fixed point on such a plot. Periodic oscillating flow will be represented by a closed curve. There are several ways to make phase plots. Most often, phase plots are made from a time series of any particular parameter by plotting the value at t against the value at $t+\Delta t$. This approach is followed by Bau and Wang (1992), Gorman et al. (1986), etc. The advantage of this method is that a single time series measurement is sufficient to generate such plots. The shape of the phase plot will depend on the chosen Δt. Another way is to select two physical parameters of the system. This approach although involves

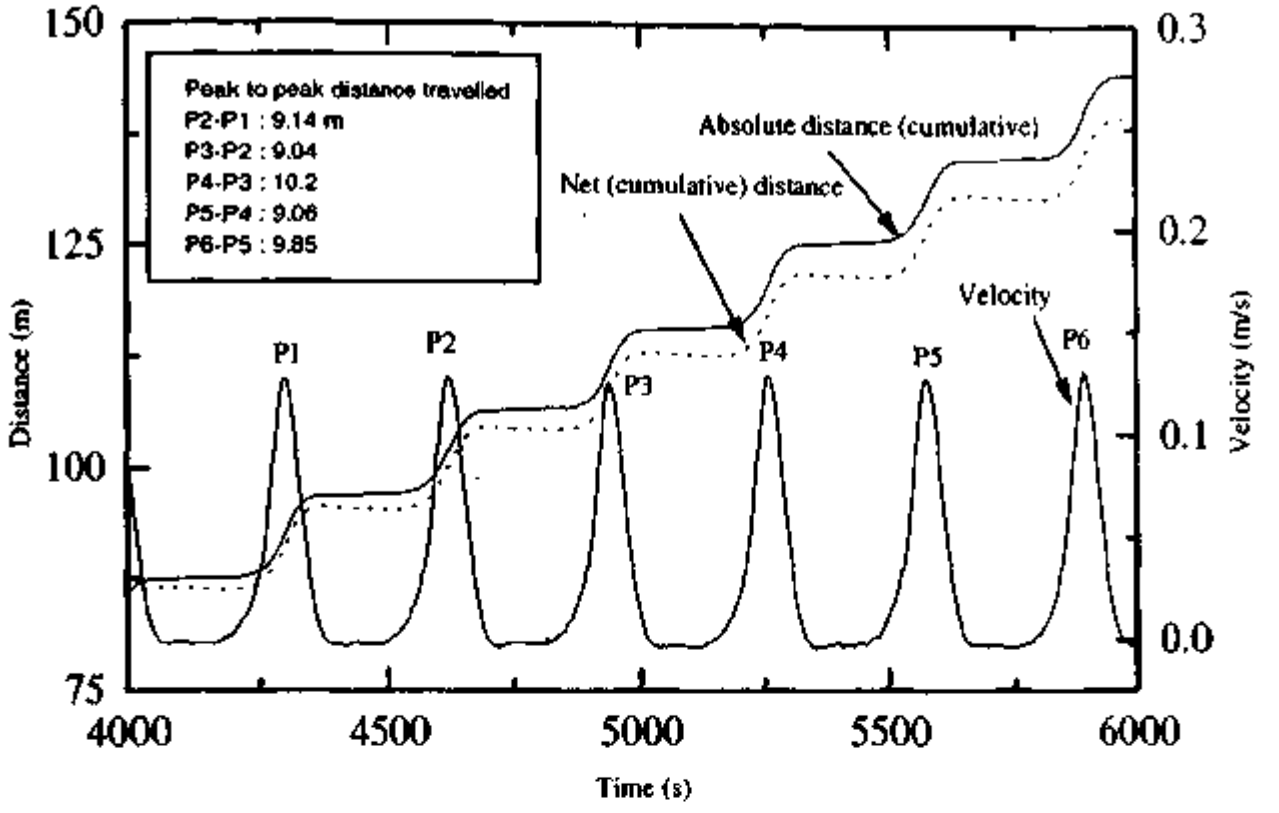

(a) unidirectional pulsing at 120 W

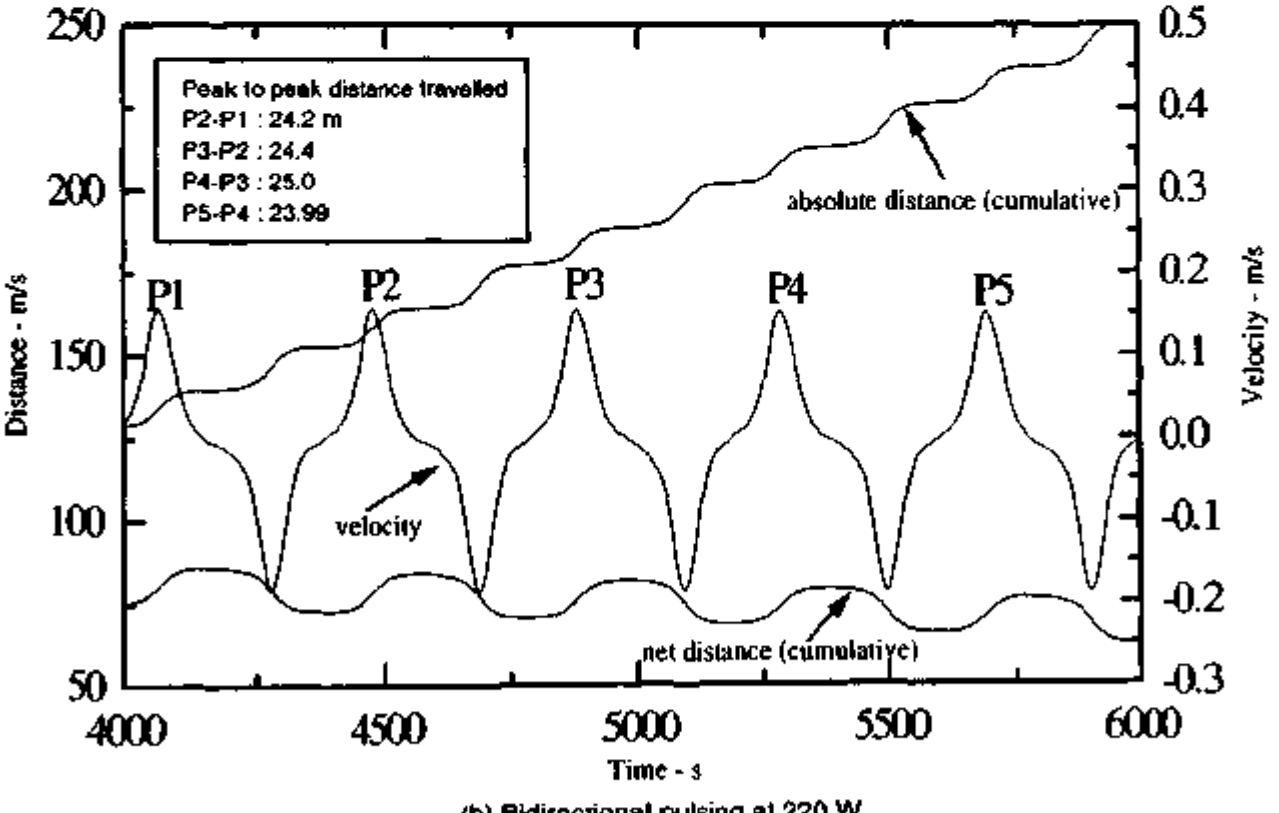

(b) Bidirectional pulsing at 220 W

Fig. 37 : Variation of cumulative distance travelled by the fluid during unstable oscillation

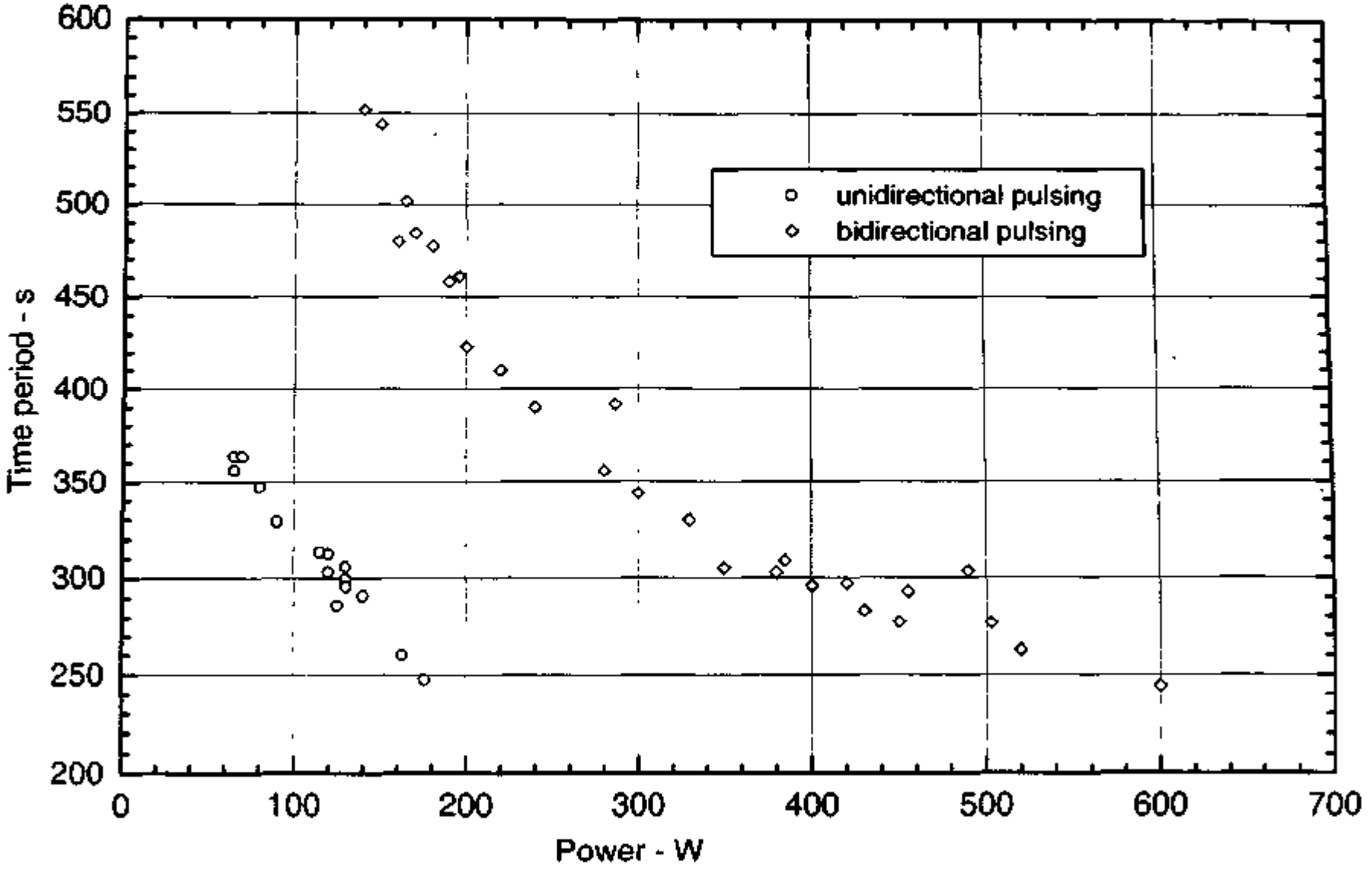

Fig. 38: Variation of oscillation frequency with power

measurement of more than one time series, give a physical picture of the state of the system with respect to the operating parameters Hence this method is adopted in the present report

Table 11: Effect of power on the period and frequency of oscillation for bi-directional pulsing

Sr. No.	Power W	Time Period (T) s	Frequency (1/T) Hz	Remarks
1	140	552.1	0.001811	Bidirectional pulsing
2	150	544.0	0.001838	Chaotic switching between UP and BP
3	160	479.6	0.002085	-do-
4	165	502.	0.001992	-do-
5	170	484.3	0.002065	-do-
6	180	477.2	0.002096	-do-
7	190	458.4	0.002182	-do-
8	196	461.25	0.002168	Bidirectional pulsing
9	200	423.3	0.002362	-do-
10	220	409.9	0.002440	-do-
11	240	389.8	0 002565	-do-
12	280	355.7	0.002811	-do-
13	287	391.6	0.002554	-do-
14	300	343.7	0.002910	-do-
15	330	323.9	0.003087	-do-
16	330	329 65	0.0030335	-do-
17	350	305 0	0 003279	-do-
18	380	302 5	0 003306	-do-
19	385	308.8	0 00324	-do-
20	400	295 9	0.003380	-do-
21	420	297.1	0.003366	BP with sporadic boiling
22	430	282.8	0 003536	-do-
23	450	277 1	0 003609	-do-
24	455	292.8	0 003415	BP with boiling once in a cycle
25	490	303.3	0.003299	-do-
26	503	276.43	0.003618	-do-
27	520	262.3	0 003812	-do-
28	600	244 3	0.004093	BP with boiling twice in a cycle

In general, phase plots can be made between any two operating parameters The shape of the phase plot, however, depends on the parameters chosen. For example, let us take the case of unidirectional pulsing. Fig. 39a shows that in the W-ΔT_h plane, the phase plot resemble more like the jaws of a shark whereas in the ΔT_h-ΔP plane, it looks more or less like the hood of a Cobra (Fig 39b) The phase plot looks like a shoe sole in the T_{ci} - ΔP plane (Fig 39c). The phase plot in the ΔP-W plane for the same case gives a limit cycle (Fig. 39d). Many more shapes are possible to obtain depending on the parameters chosen.

For a typical bidirectional pulsing mode, the phase plot in the W-ΔT_h plane looks like a squirrel (Fig 40a) whereas in the ΔP-ΔT_h plane the phase plot looks like a butterfly (Fig. 40b). The phase plot in the T_{hi} - ΔP plane looks more like a duckling (Fig 40c) whereas in the ΔP-W plane it portrays a dumbbell (Fig. 40d).

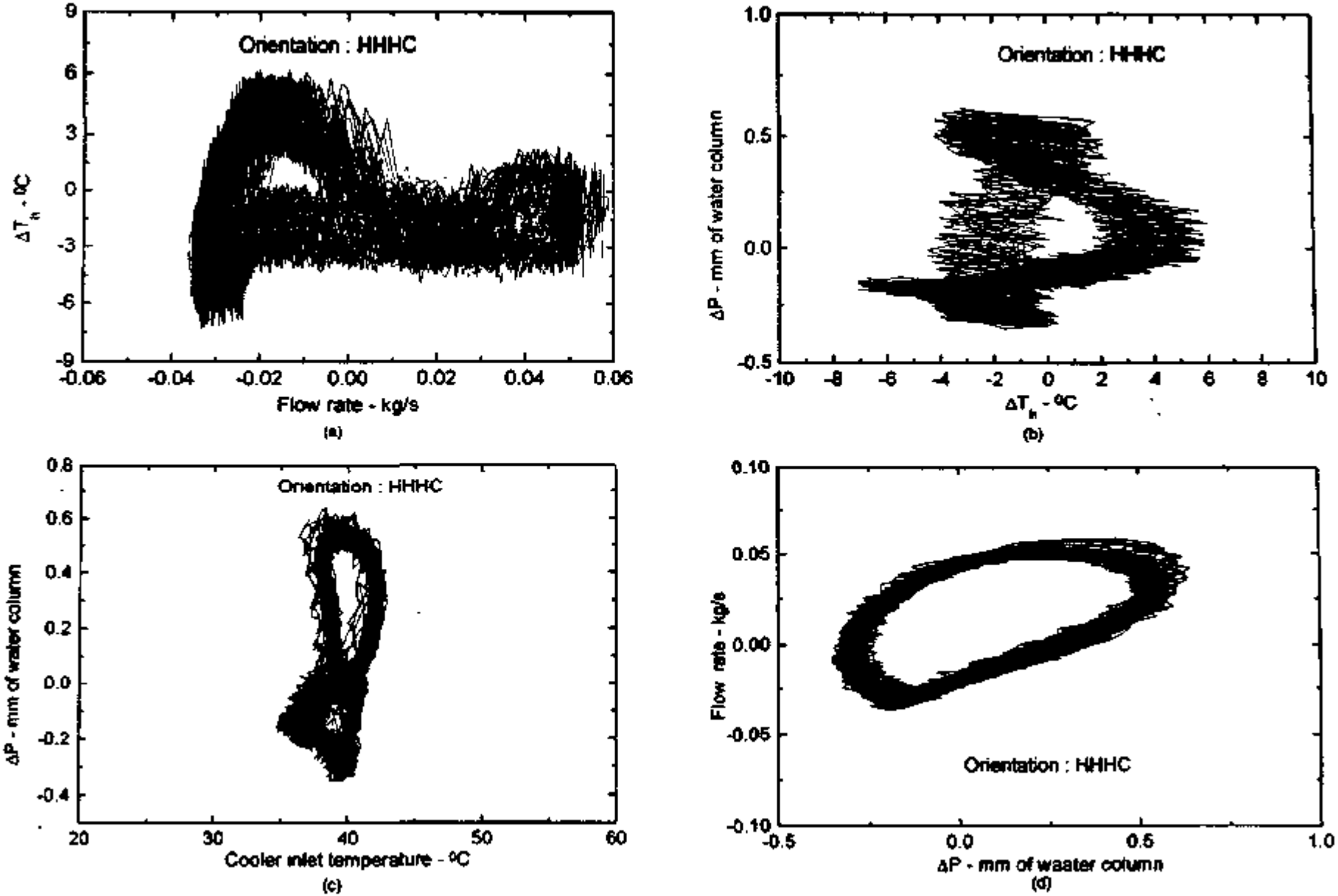

Fig 39 . Pahase plots for unidirectional pulsing at 140 W and 5 lpm coolant flow with inlet temperature of 33°C

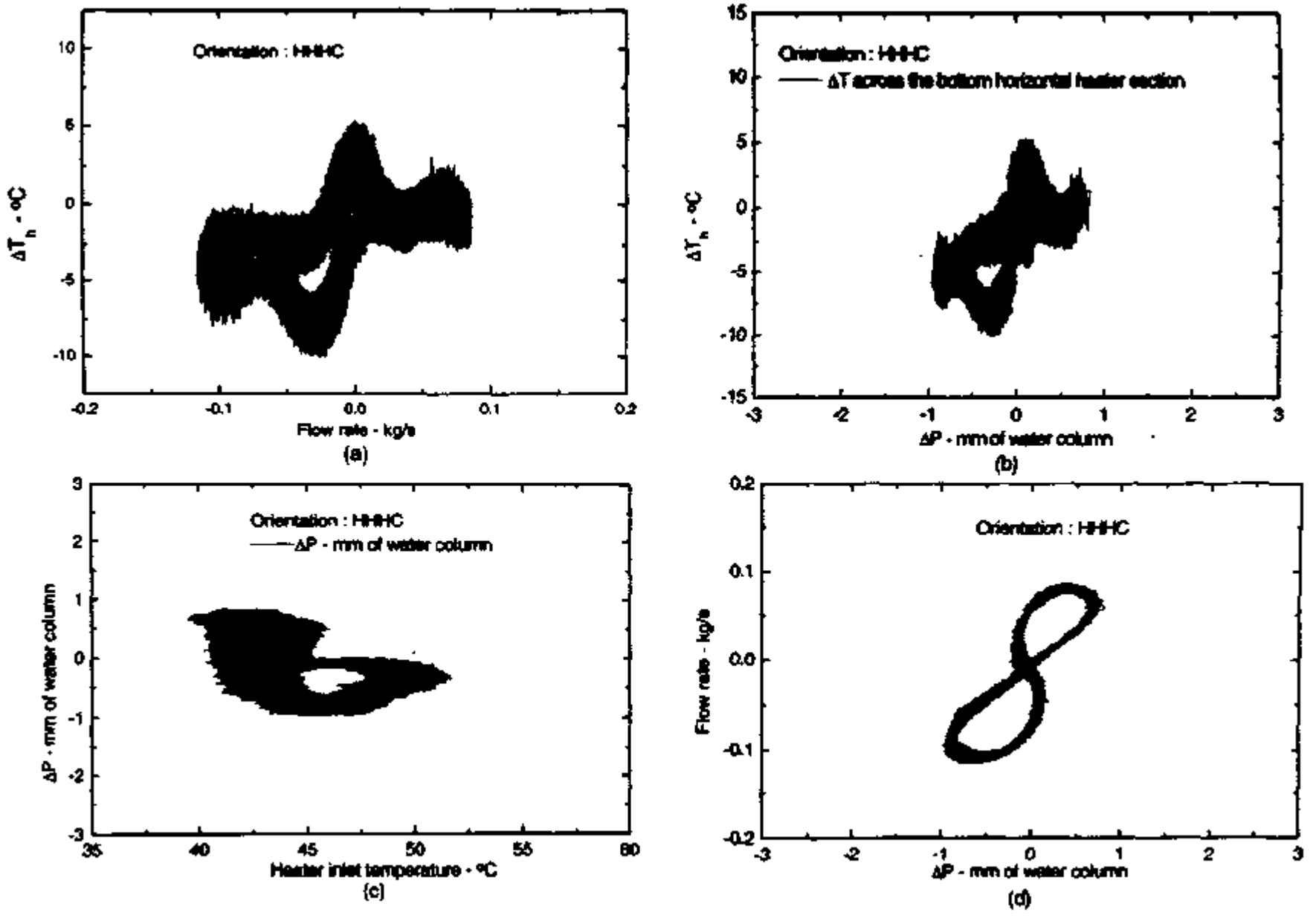

Fig. 40 : Phase space at power 200 W and 5 lpm coolant flow with an inlet temprature of 33 °C

Phase plots made in the ΔP - ΔT_h plane in Fig. 41 (after neglecting the initial transients) show the effect of increasing power on bidirectional pulsing. Phase plots shown in Figures 41a and b resemble a butterfly. For higher power, the shape of the butterfly deforms as shown in figure 41c. For compound instability with subcooled boiling cuspids are observed as shown in Fig. 41d.

7.11 Repeatability of the unstable behaviour

The unstable behaviour is not always completely reproducible. The test results for a case are shown in Fig. 42. Although, the time series looks alike (broadly) the corresponding phase plots are found to be different.

8. STABILITY ANALYSIS

Equation (1) enables us to calculate the steady state flow in a natural circulation loop. However, it does not tell us whether that particular steady state is stable. For example, equation (1) predicts non-zero steady flow rates in the counter-clockwise direction in the present test loop for the HHVC orientation. On the other hand, experiments showed that no steady state is possible with counter-clockwise flow for this orientation. Even though, flow initiated in the counter-clockwise direction for some tests, it eventually reversed itself and stable flow could be obtained only in the clockwise direction. Thus stability analysis is necessary to examine whether a particular steady state is stable. In general, the stability of a natural circulation loop is analysed either by the linear or the non-linear method.

8.1 Linear Stability Method

In this method, the transient momentum and energy equations are perturbed as follows:

$$\omega = \omega_{ss} + \omega' \quad ; \quad \theta = \theta_{ss} + \theta' \tag{13}$$

With these substitutions the perturbed momentum and energy equations obtained are solved to obtain the characteristic equation for the stability behaviour. While detailed derivation is given in Appendix-4, the general form of the characteristic equations obtained for the various orientations of the heater and cooler is

$$n - \frac{Gr_m}{\mathrm{Re}_{ss}^3}\frac{\bar{I}}{\omega} + \frac{p}{\mathrm{Re}_{ss}^b}\frac{L_t}{D}\frac{2-b}{2} = 0 \tag{14}$$

Where $\bar{I} = \oint \bar{\theta} dZ$ and n is a complex number. Replacing Re_{ss} using equation (1), we obtain

$$n - \frac{(p/2)^{1+m}}{(Gr_m)^m (D/L_t)^{1+m}}\left\{I_{ss}\frac{\bar{I}}{\omega} + (2-b)\right\} = 0 \tag{15}$$

Where m=b/(3-b) and the expressions for I_{ss} are given in appendix-1 for various orientations.

The expressions for $\bar{I}/\bar{\omega}$ obtained for flow in the clockwise direction are given below for various orientations.

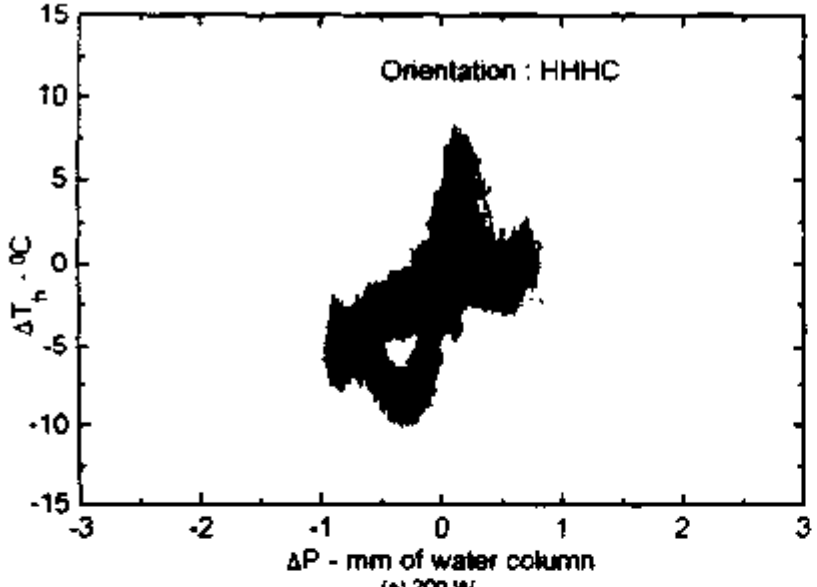

(a) 200 W

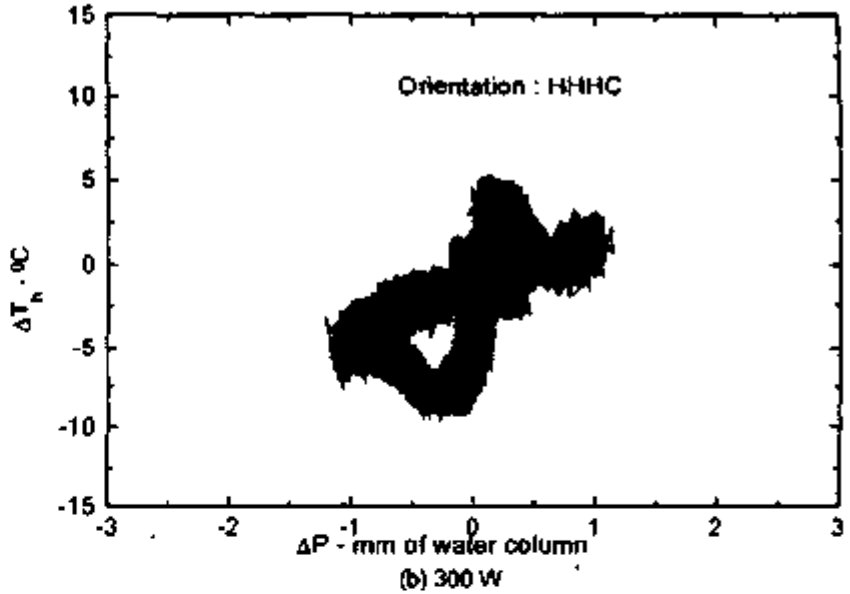

(b) 300 W

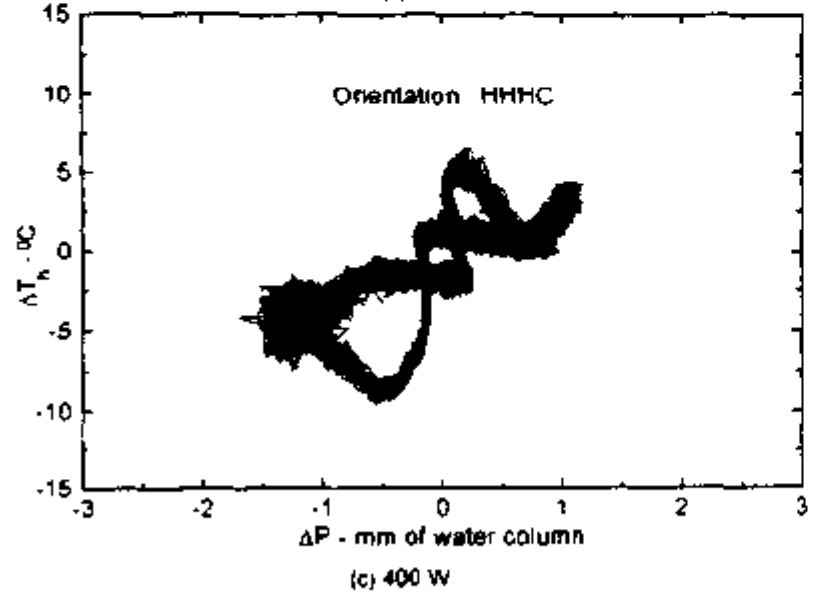

(c) 400 W

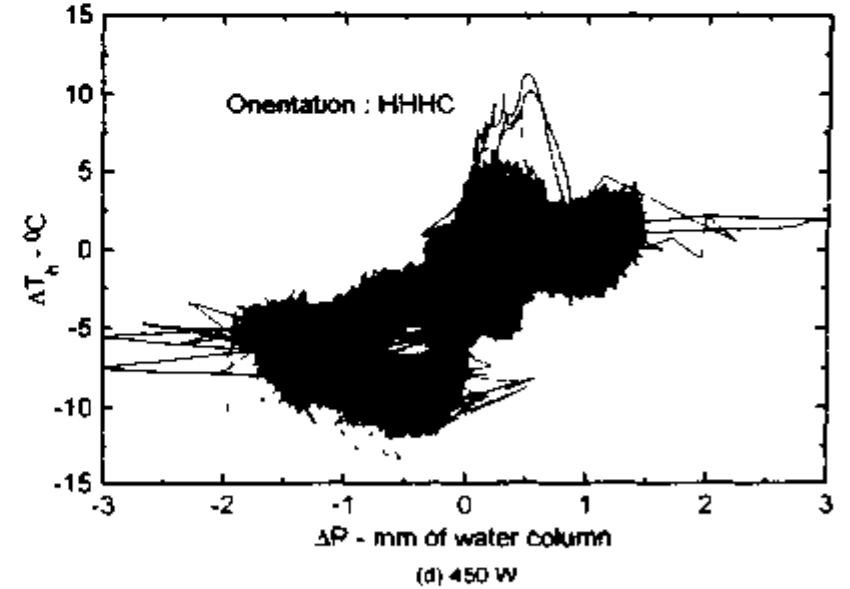

(d) 450 W

Fig. 41 Phase plots at different powers for bidirectional pulsing with 5 lpm coolant flow at inlet temprature of 33 °C

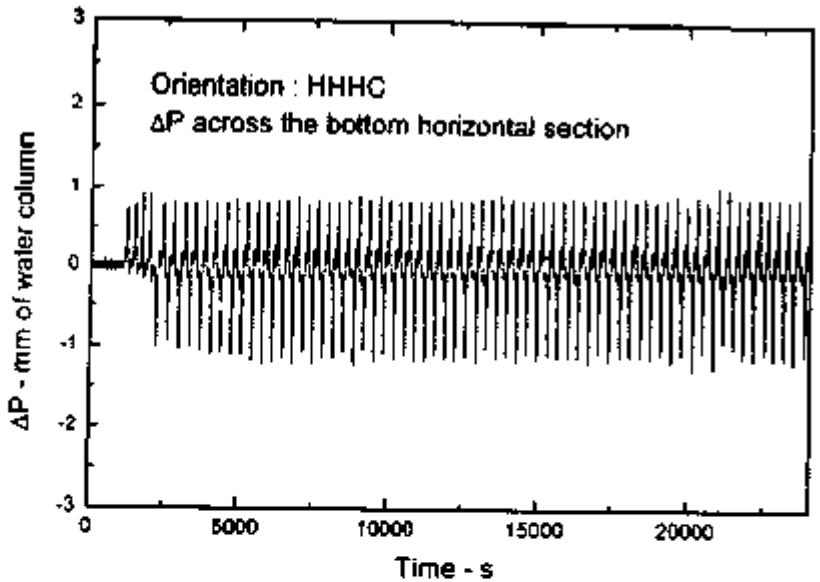

(a) Time series at 300 W (Nov 3, 2000)

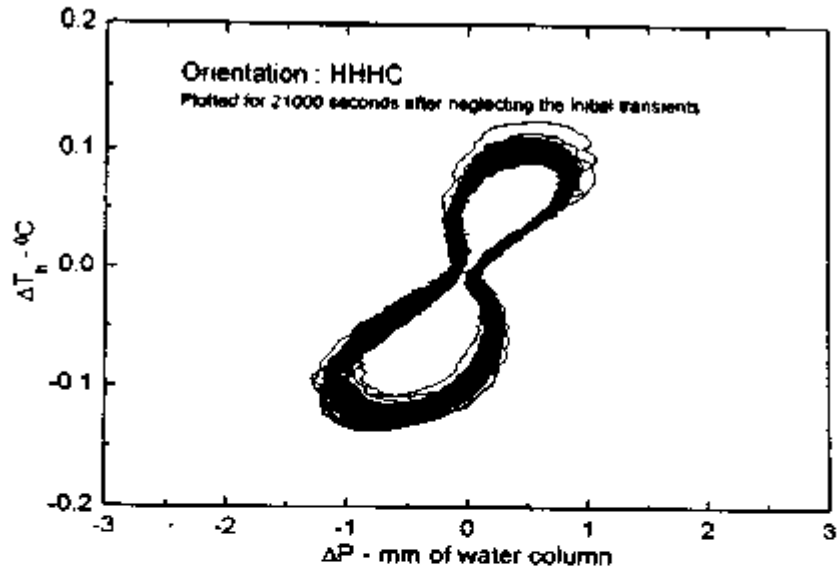

(b) Phase plot corresponding to the time series in (a)

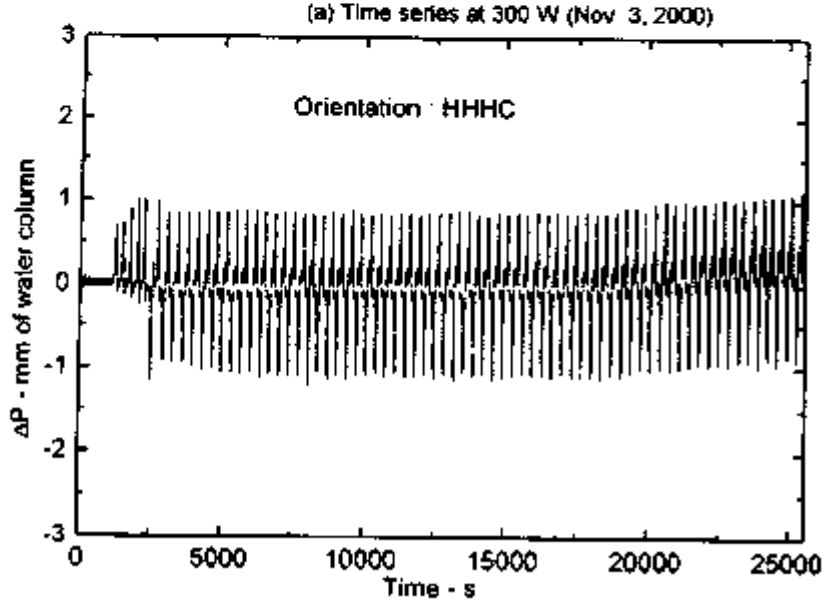

(c) Time series at 300 W (Nov 16, 2000)

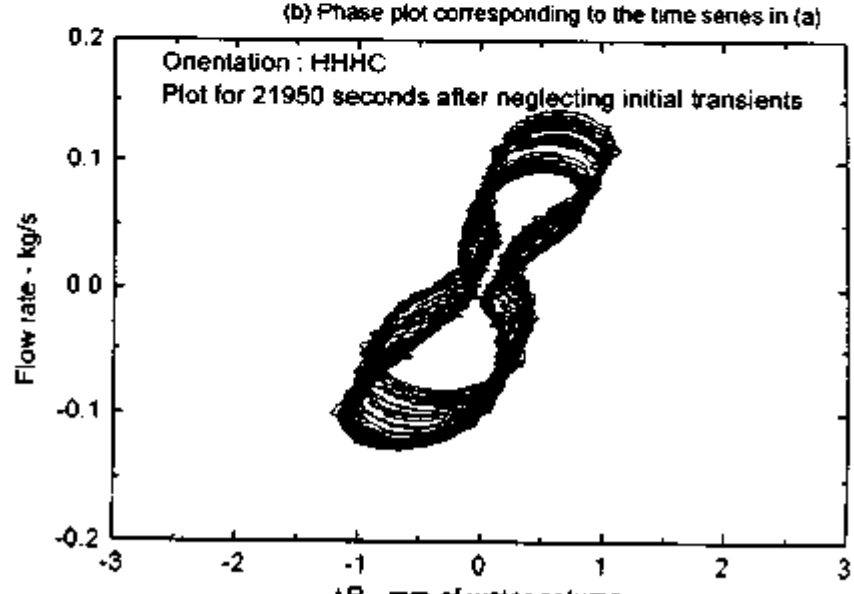

(d) Phase plot corresponding to the time series in (c)

Fig. 42: Reproducibility of the unstable oscillatiry behavior at 300 W and 5 lpm flow rate with coolant inlet temprature of 33 ^{0}C

8.1.1 HHHC Orientation

$$\frac{\bar{I}}{\omega} = \frac{\phi}{n}\left(1 - e^{\frac{-n}{\phi}}\right)\left\{\frac{\overline{\theta_h}}{\omega} e^{\frac{-nL_1}{L_1}} - \frac{\bar{\theta}_c}{\omega} e^{\frac{-nL_3}{L_3}}\right\} \tag{16a}$$

$$\text{Where } \frac{\bar{\theta}_h}{\omega} = \frac{St_m(\theta_{hl})_{st} e^{\frac{nL_2}{L_2}}\left(e^{\frac{nL_1}{L_1}} - 1\right) + \frac{L_1}{L_h}\left(e^{\frac{-nL_h}{L_h}} - 1\right) e^{\frac{(St_m L_1 + nL_1)}{L_1}}}{n\left(e^{\frac{(St_m L_1 + nL_1)}{L_1}} - 1\right)} \tag{16b}$$

$$\text{and } \frac{\bar{\theta}_c}{\omega} = \frac{St_m(\theta_{hl})_{st} e^{n}\left(1 - e^{\frac{-nL_c}{L_c}}\right) + \frac{L_c}{L_h} e^{\frac{nL_{3T}}{L_3}}\left(1 - e^{\frac{nL_h}{L_h}}\right)}{n\left(e^{\frac{St_m L_1 + nL_1}{L_1}} - 1\right)}. \tag{16c}$$

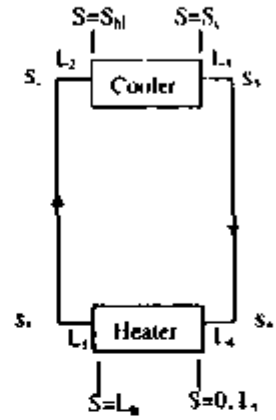

If $L_1=L_3=L_h$, then equation (16a) becomes

$$\frac{\bar{I}}{\omega} = \frac{\phi}{n}\left(1 - e^{\frac{-n}{\phi}}\right) e^{\frac{-nL_2}{L_2}}\left(\frac{\bar{\theta}_h - \bar{\theta}_c}{\omega}\right) \tag{17}$$

8.1.2 HHVC Orientation

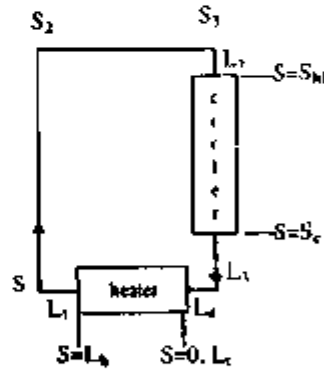

On integration and substitution of limits yield the following equation for $\bar{I}/\bar{\omega}$.

$$\frac{\bar{I}}{\omega} = \frac{\bar{\theta}_h}{\omega}\frac{\phi}{n}\left\{e^{\frac{-nL_1}{L_1}}\left(1 - e^{\frac{-n}{\phi}}\right) + e^{\frac{-nL_{3T}}{L_3}}\left(1 - e^{\frac{nL_2}{L_2}}\right)\right\} +$$

$$\frac{\phi}{n}(\theta_{hl})_{st}\left\{e^{\frac{-St_m L_1}{L_1}} - 1 + \frac{St_m}{n + St_m}\left(1 - e^{-\left(\frac{n+St_m}{L_1}\right)L_1}\right)\right\}$$

$$+\frac{\bar{\theta}_{hl}}{\omega}\left(\frac{\phi}{n + St_m}\right)\left[e^{\frac{-(n+St_m)L_1}{L_1}} - 1\right] + \frac{\bar{\theta}_c}{\omega}\frac{\phi}{n}\left[e^{\frac{-nL_3}{L_3}} - 1\right] \tag{18}$$

The parameters $\bar{\theta}_h/\bar{\omega}$ and $\bar{\theta}_c/\bar{\omega}$ are evaluated using equations (16b) and (16c) respectively while $\bar{\theta}_{hl}/\bar{\omega}$ is obtained from the following equation

$$\frac{\bar{\theta}_{hl}}{\bar{\omega}} = \frac{St_m(\theta_{hl})_{ss}\left(e^{n\frac{L_c}{L_t}}-1\right)+\frac{L_c}{L_h}e^{\frac{St_mL_c+n(L_t-L_{hl})}{L_t}}\left(e^{-n\frac{L_h}{L_t}}-1\right)}{n\left(e^{\frac{St_mL_c+nL_t}{L_t}}-1\right)} \qquad (19)$$

8.1.3 VHHC Orientation

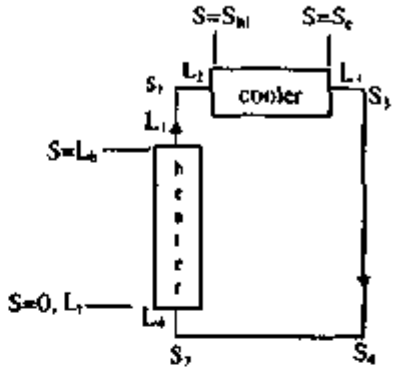

$$\frac{\bar{I}}{\bar{\omega}} = \frac{\bar{\theta}_{cl}}{\bar{\omega}}\frac{\phi}{n}\left(1-e^{\frac{-nL_h}{L_t}}\right)+\frac{L_t}{nL_h}\left\{\frac{\phi}{n}\left(1-e^{\frac{-nL_h}{L_t}}\right)-\frac{L_h}{H}\right\}+$$

$$\frac{\bar{\theta}_h}{\bar{\omega}}\frac{\phi}{n}\left[1-e^{\frac{-nL_h}{L_t}}\right]+\frac{\bar{\theta}_c}{\bar{\omega}}\frac{\phi}{n}\left[\frac{e^{\frac{-nH}{L_t}}-1}{e^{\frac{nL_h}{L_t}}}+\frac{e^{\frac{nL_h}{L_t}}-1}{e^{\frac{nL_{cl}}{L_t}}}\right] \qquad (20)$$

The parameters $\bar{\theta}_h/\bar{\omega}$ and $\bar{\theta}_c/\bar{\omega}$ are evaluated using equations (16b) and (16c) respectively whereas $\bar{\theta}_{cl}/\bar{\omega}$ is evaluated using the following equation.

$$\frac{\bar{\theta}_{cl}}{\bar{\omega}} = \frac{St_m(\theta_{hl})_{ss}e^{\frac{n(L_t-L_{hl})}{L_t}}\left(1-e^{\frac{-nL_c}{L_t}}\right)+\frac{L_c}{L_h}\left(1-e^{\frac{nL_h}{L_t}}\right)}{n\left(e^{\frac{St_mL_c+nL_h}{L_t}}-1\right)} \qquad (21)$$

8.1.4 VHVC Orientation

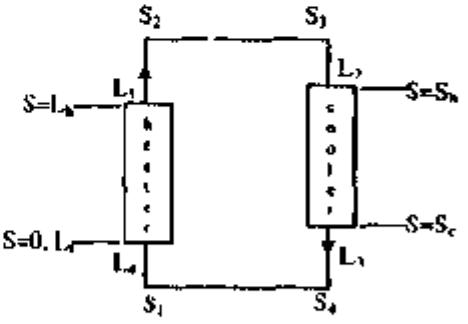

$$\frac{\bar{I}}{\bar{\omega}} = \frac{\bar{\theta}_{cl}}{\bar{\omega}}\frac{\phi}{n}\left(1-e^{\frac{-nL_h}{L_t}}\right)+\frac{L_t^2}{n^2L_hH}\left(1-e^{\frac{-nL_h}{L_t}}-\frac{nL_h}{L_t}\right)$$

$$+\frac{\bar{\theta}_h}{\bar{\omega}}\frac{\phi}{n}\left[1-e^{\frac{-nL_h}{L_t}}+e^{\frac{-nL_h}{L_t}}\left(1-e^{\frac{-nL_2}{L_t}}\right)\right]+$$

$$\frac{\phi(\theta_{hl})_{ss}}{n(n+St_m)}\left[n\left(e^{\frac{-St_mL_c}{L_t}}-1\right)+St_me^{\frac{-St_mL_c}{L_t}}\left(1-e^{\frac{-nL_h}{L_t}}\right)\right]+\frac{\bar{\theta}_{hl}}{\bar{\omega}}\frac{\phi}{n+St_m}\left[e^{\frac{-(n+St_m)L_c}{L_t}}-1\right]+$$

$$\frac{\bar{\theta}_c}{\bar{\omega}}\frac{\phi}{n}\left\{e^{\frac{-nL_2}{L_t}}-1+e^{\frac{-nL_{cl}}{L_t}}\left(e^{\frac{nL_t}{L_t}}-1\right)\right\} \qquad (22)$$

The parameters $\bar{\theta}_s/\bar{\omega}$, $\bar{\theta}_h/\bar{\omega}$, $\bar{\theta}_M/\bar{\omega}$ and $\bar{\theta}_r/\bar{\omega}$ are evaluated using the equations described earlier.

8.1.5 Solution of the characteristic Equation

The roots of the characteristic equation were obtained by the Regula-Falsi method. Stability was judged by the Nyquist Stability Criterion. As per this criterion, if any of the roots of the characteristic equation has a positive real part, then the corresponding operating conditions are unstable. The marginal stability curves, which separate the stable and unstable zones, were obtained in this way for the different orientations. To check the accuracy of the solutions, the marginal stability curves generated earlier by Vijayan et.al. (1994) for the horizontal heater horizontal cooler orientation was reproduced. These results are given in Fig. 43b and c. As expected the results for the various loop diameters gave the same result. However, the results are different for laminar and turbulent flow as expected. Subsequently, a parametric analysis was carried out using the characteristic equations given earlier. From the characteristic equation, it is found that the stability behaviour depends on

$$Stability = f(Gr_m, St_m, orientation, flow\ direction\ and\ length\ scales)$$

The length scales include L_1/H, L_1/D, L_1/L_h, L_c/L_1, L_{h1}/L_h, L_{c1}/L_c, L_1/L_t, L_2/L_t, L_3/L_t and L_4/L_t. The flow directions include both clockwise and counter-clockwise direction. The orientations include HHHC, HHVC, VHHC and VHVC. It may be noted that L_t/D and Gr_m can be combined to obtain a single independent parameter given by $(Gr_m)^m(D/L_t)^{1+m}$. Further, L_1, L_2, L_3 and L_4 may not appear together for all orientations.

8.2 Effect of Orientation

Fig. 44 shows the effect of orientation on the stability behaviour. These calculations were carried out for the loop shown in Fig. 1 with the same total length and diameter for each orientation (see Table-12 for the loop dimensions). With clockwise flow, the VHVC orientation is most stable and HHHC orientation is least stable. For a given heater orientation, the horizontal cooler orientation is less stable compared to the vertical cooler. Similarly, with fixed cooler orientation, the loop with vertical heater is more stable than that with horizontal heater. It may be noted that the stability maps for three different loops with the same length scales for every pipe segment were found to be the same even though their diameters were different (see Fig. 43). However, for the present loop although the total length, diameter and cooler length are the same, stability maps are found to be different. From this it is clear that simulation of the stability behaviour requires not only the simulation of the parameters $(Gr_m)^m(D/L_t)^{1+m}$ and St_m but also the length scales of every pipe segment for a uniform diameter loop.

Table-12: Length scales for various orientations of the test loop

Orientation	Flow direction	Length scales of the loop - m									
		L_1	L_2	L_3	L_4	L_h	L_c	L_{h1}	L_{c1}	H	L_t
HHHC	Clockwise	0.41	0.31	0.305	0.385	0.62	0.8	2.92	2.89	2.2	7.23
HHVC	Clockwise	0.41	0.22	1.18	0.385	0.62	0.8	4.445	1.565	2.2	7.23
VHHC	Clockwise	1.12	0.31	0.305	0.35	0.73	0.8	1.43	4.27	2.2	7.23
VHVC	Clockwise	1.12	0.22	1.18	0.35	0.73	0.8	2.755	3.245	2.2	7.23
HHVC	Anticlockwise	0.385	1.18	0.22	0.41	0.62	0.8	1.565	4.245	2.2	7.23

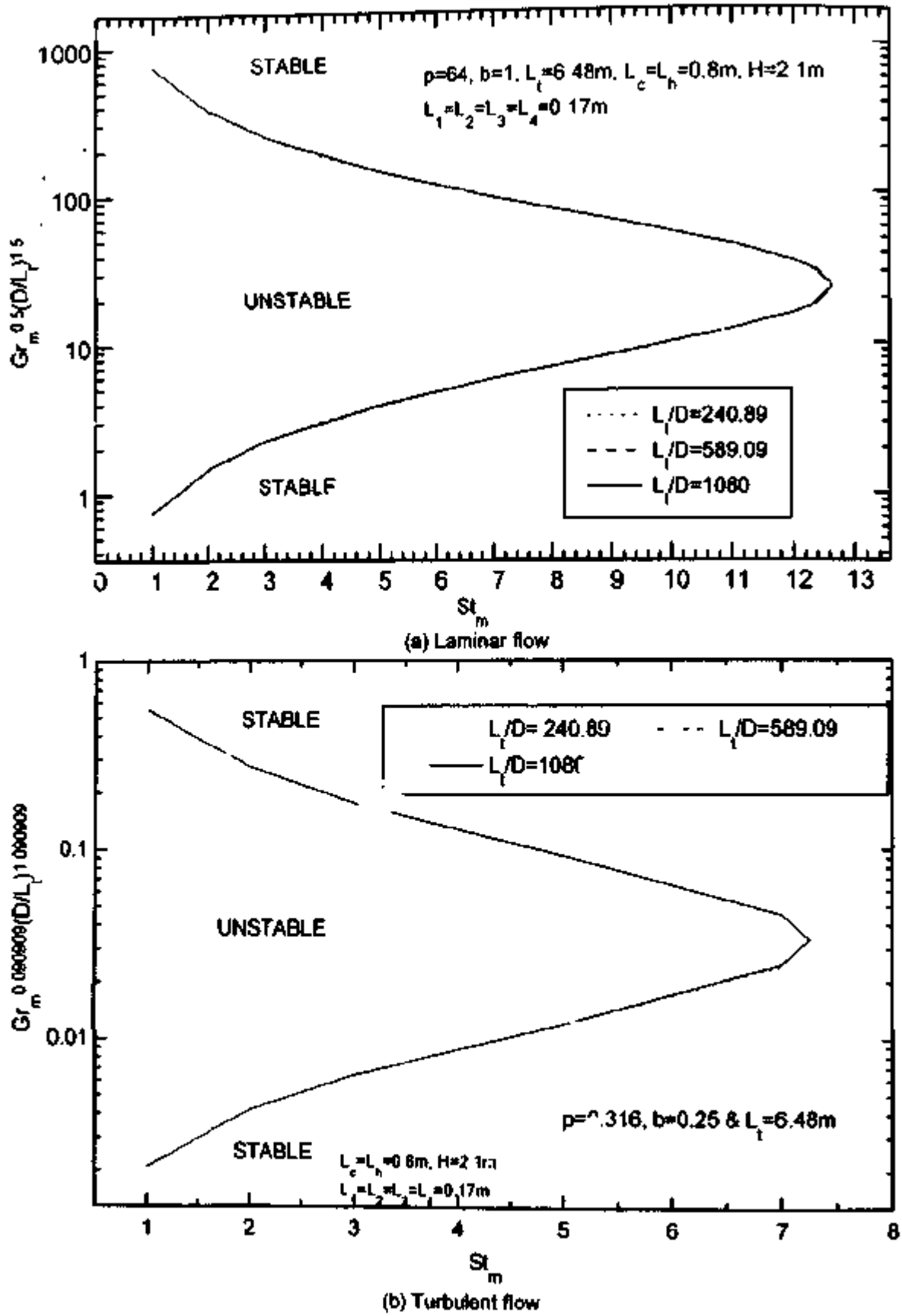

Fig. 43: Stability map for rectangular loops of differing diameters for the HHHC orientation obtained by linear stability analysis

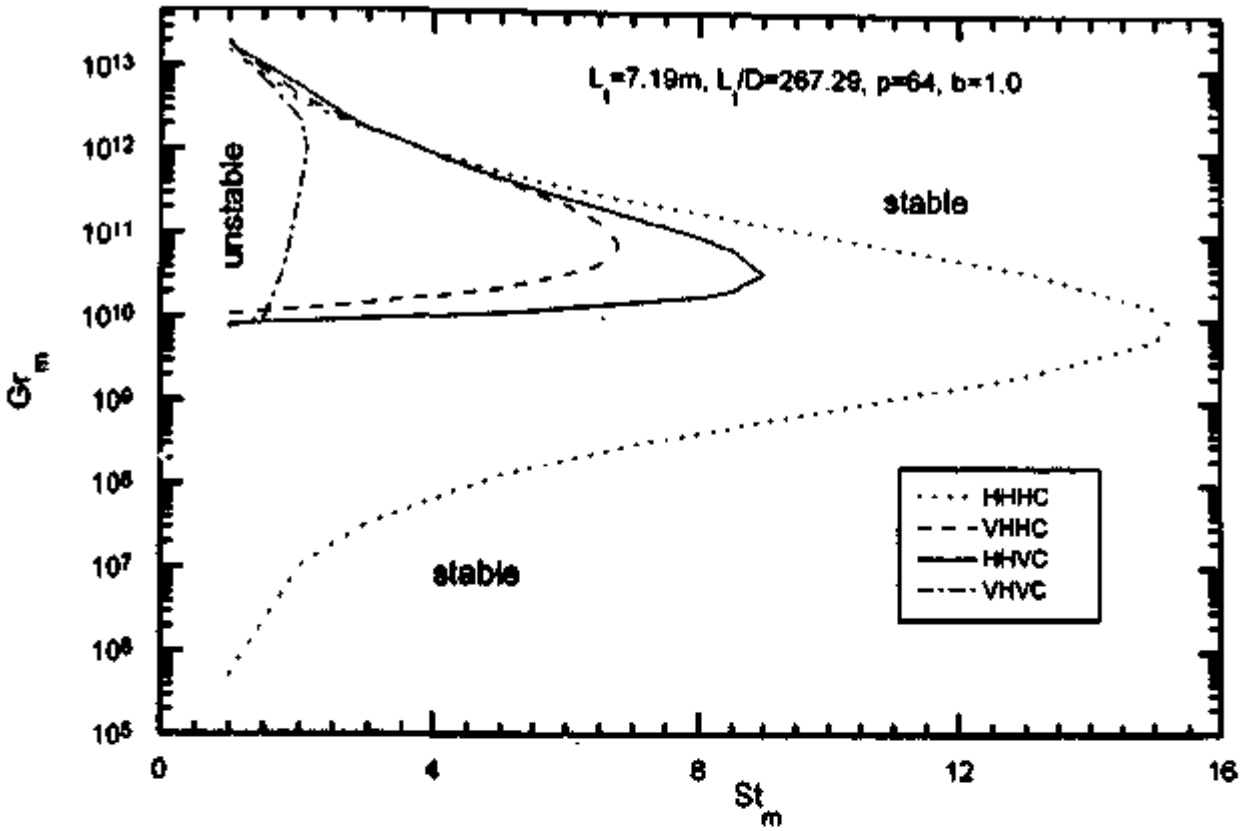

(a) Laminar flow

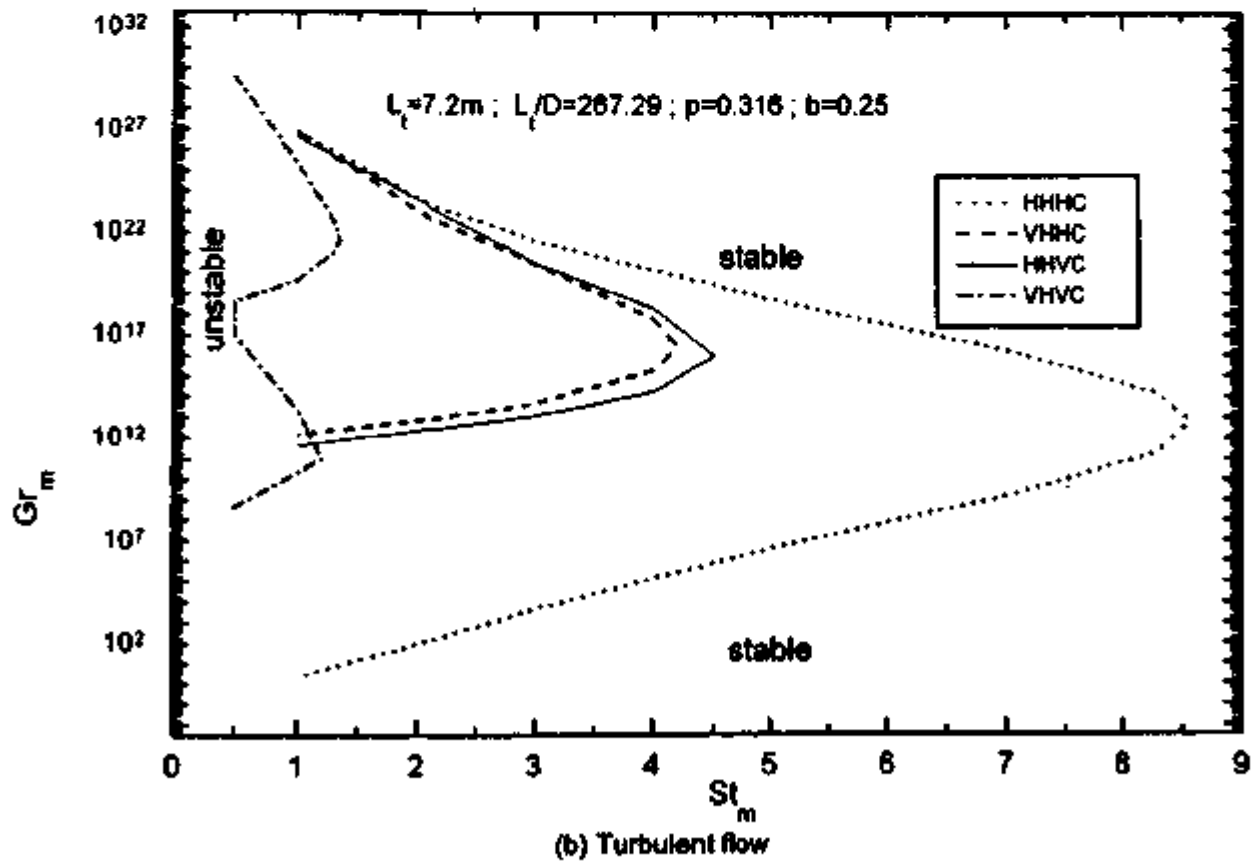

(b) Turbulent flow

Fig.44 : Stability map for Laminar clockwise flow obtained by linear stability method for various orientations

It may be noted that for most part of the lower threshold of the turbulent flow map in Fig. 44b, the flow is not turbulent and hence is only of academic interest. Similar is the case for some part of the upper threshold for laminar flow in Fig. 44a.

8.3 Effect of flow Direction

In case of horizontal heaters, the flow can initiate in either directions, i.e. clock-wise and anti-clock-wise. In case of HHHC orientation with the relative positions of the heater and cooler unchanged no difference is expected with flow direction if the heater and cooler locations are symmetric about the two vertical legs (i.e. L_1=L_4 and $L_2 = L_3$). In case of HHVC orientation, it appears possible from the steady state analysis to have flow in the clock-wise or counter-clockwise direction. Hence, stability of this orientation was studied for both flow directions. The characteristic equation for the stability behaviour (see Appendix-4 for derivation) in the anticlockwise direction is obtained as

$$\frac{\bar{I}}{\omega} = \frac{\bar{\theta}_h}{\omega}\frac{\phi}{n} e^{\frac{-nL_2}{L_1}}\left(1-e^{\frac{-nL_2}{L_1}}\right) + \frac{\phi}{n}\frac{(\theta_{st})_{ss}}{n+St_m}\left\{n\left(1-e^{\frac{-St_m L_1}{L_1}}\right) - St_m e^{\frac{-St_m L_1}{L_1}}\left(1-e^{\frac{-nL_1}{L_1}}\right)\right\} +$$

$$\frac{\bar{\theta}_c}{\omega}\frac{\phi}{n}\left\{1-e^{\frac{-nL_2}{L_1}} + \left(1-e^{\frac{-n}{\phi}}\right)e^{\frac{-n}{L_1}(L_1+L_2+L_3+L_4)}\right\} +$$

$$\frac{\bar{\theta}_{st}}{\omega}\frac{\phi}{n+St_m}\left(1-e^{\frac{-(n+St_m)L_1}{L_1}}\right) \qquad (23)$$

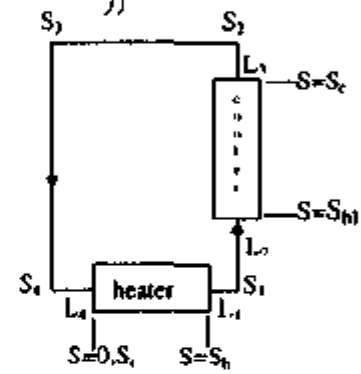

The parameters $\bar{\theta}_h/\bar{\omega}$, $\bar{\theta}_{st}/\bar{\omega}$ and $\bar{\theta}_c/\bar{\omega}$ are evaluated using the equations described early. The marginal stability curve obtained for the counter-clockwise direction is given in Fig. 45. It is found that no stable operation is possible for this case with the current experimental conditions ($0.2 < St_m < 0.6$). Hence, for this orientation, even though the flow initiated in the counter-clockwise direction, flow direction reversed back to clockwise as observed in the experiments (see Fig 4c). The clockwise flow case was found to be completely stable both experimentally and analytically as already mentioned earlier

8.4 Effect of flow direction and symmetry

It appears from the foregoing that the instability can be observed in asymmetric loops. However, in asymmetric loops both the flow directions (i.e. clockwise and anticlockwise) are not equally unstable. One flow direction may be highly stable and another flow direction may be highly unstable. In such cases, even if the flow initiated in the highly unstable direction, it will reverse on its own and revert to the highly stable flow direction. In a symmetric or near symmetric loop both the flow directions can be unstable. In such a loop all the unstable flow regimes described in the paper can be observed. This leads to the conclusion that bi-directional pulsing can be observed in a loop only if both the flow directions are unstable. The unstable flow regime in an asymmetric loop is always unidirectional pulsing (Keller flow regime).

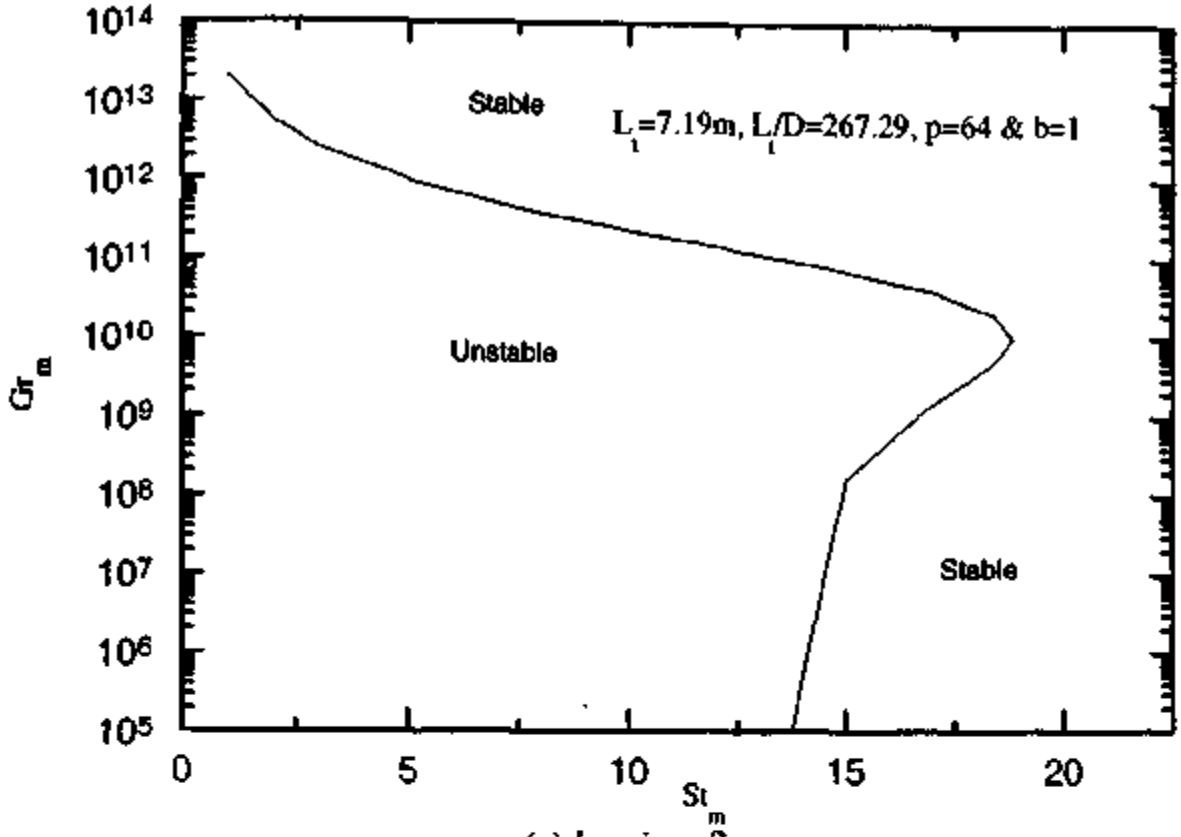

(a) Laminar flow

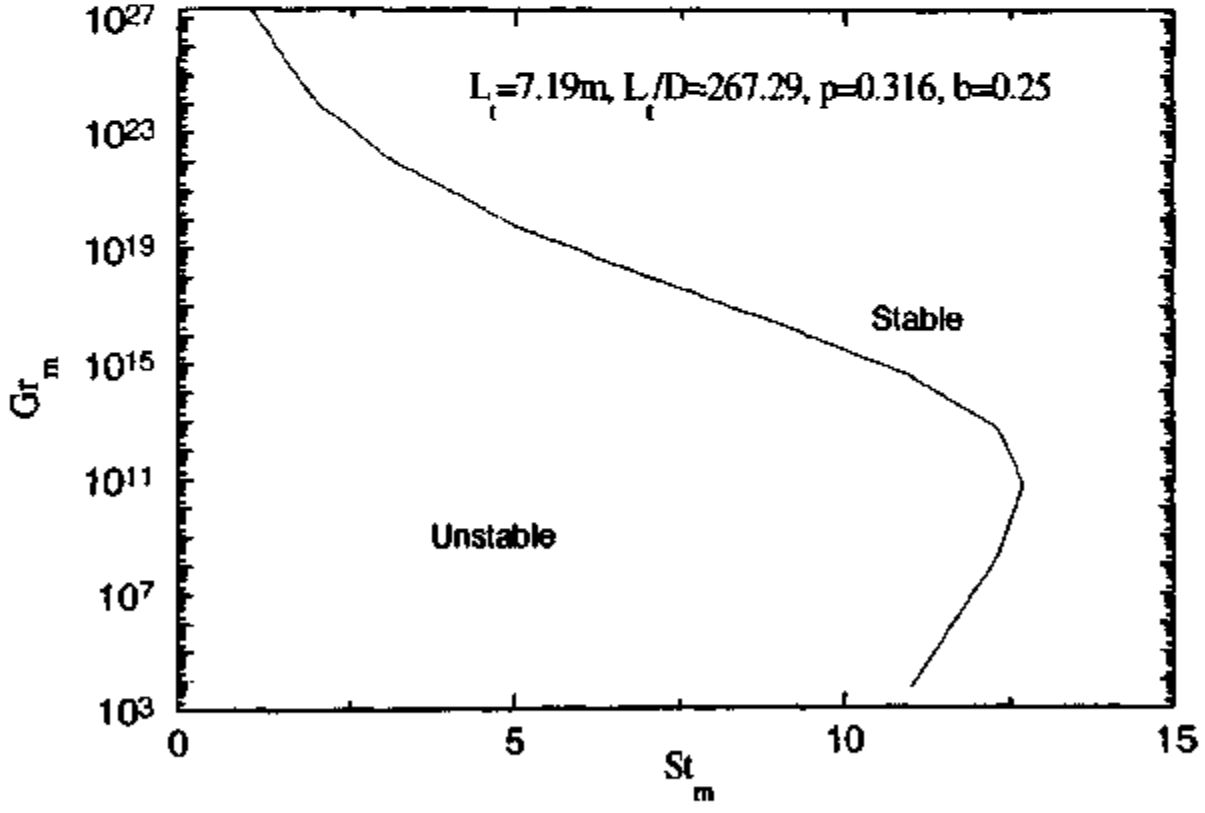

(b) Turbulent flow

Fig. 45: Stability map for anticlockwise flow obtained by the linear stability method for the HHVC orientation

8.5 Effect of Heater and Cooler Length

These studies were carried out for the HHHC orientation with clockwise flow by changing the loop diameter keeping the length scales the same. The results for varying the heater length alone, cooler length alone and simultaneously varying both heater and cooler lengths are given in figures 46a, b and c respectively. It is found that reducing the length of heater as well as cooler has a destabilising effect. However, the heater length has only a marginal effect on the stability behaviour whereas the cooler length has a significant effect. The heater may be considered to be the source of the hot pockets and the cooler is responsible for diffusing these hot pockets. Reducing the length of cooler reduces the heat transfer considerably (and hence the diffusive capability) whereas since the Gr_m is kept the same, the capability of the heat source to produce hot pockets is practically unaffected with reduction in length.

8.6 Effect of L_c/D

Again, these calculations were performed for the HHHC orientation with clockwise flow. If the stability behaviour is plotted in terms of $(Gr_m)^m(D/L_c)^{1+m}$ and St_m then the effect of L_c/D is not visible. However, its effect is important as most techniques for stabilisation results in enhanced L_c/D. A typical example is the introduction of orifices. Hence calculations were done keeping L_c/D as a basic parameter and the results are given in Fig. 47. It is found that increasing L_c/D stabilises the loop flow. Both the lower and upper thresholds are found to increase with L_c/D.

8.7 Comparison with Experimental data

Fig. 48 shows a comparison of the predicted stability map with the experimental data for the present loop. For the VHHC orientation, the experiments did not show instability. For both VHHC and HHHC orientations, the prediction by the linear stability theory is found to be conservative (in that the theory predicts larger unstable zone). The main reason for this is attributed to the fact that the linear stability analysis neglects the influences of the local convection currents, axial conduction, heat losses and the damping effect of the pipe walls. Both the local convection currents (3-D nature of flow) and the axial conduction (in the liquid) appear to play a role in the stability behaviour. Both appear to significantly affect the fluid temperature distribution, especially during the near stagnant conditions.

8.8 Closure

The linear stability method is adequate to conservatively predict the stability threshold. The analysis shows that HHHC orientation is unstable for both flow directions even though the steady state analysis shows that this orientation is capable of the maximum flow rate. For quantitative agreement with test data, the analysis must consider the damping effect of the pipe walls, the heat losses, the axial conduction within the fluid and the 3-D nature of the flow. However, linear analysis cannot provide explanation for the various oscillatory flow regimes observed. The existence of the conditionally stable regime also cannot be verified by this analysis. For this case we resort to nonlinear stability analysis.

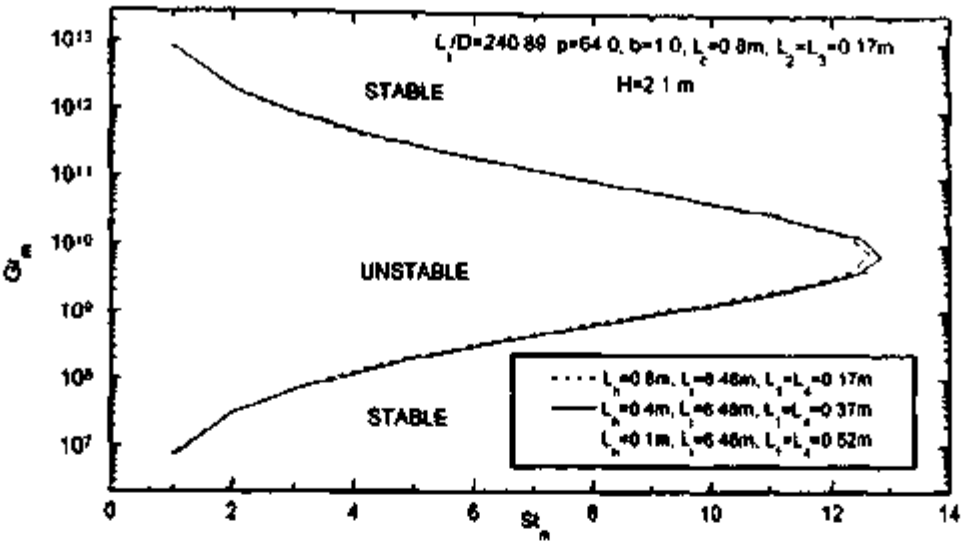

(a) Effect of heater length

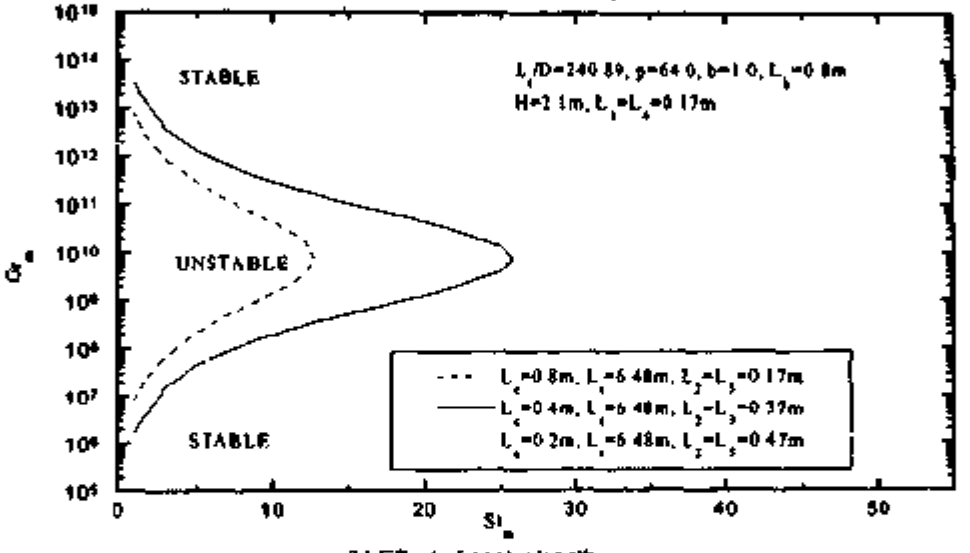

(b) Effect of cooler length

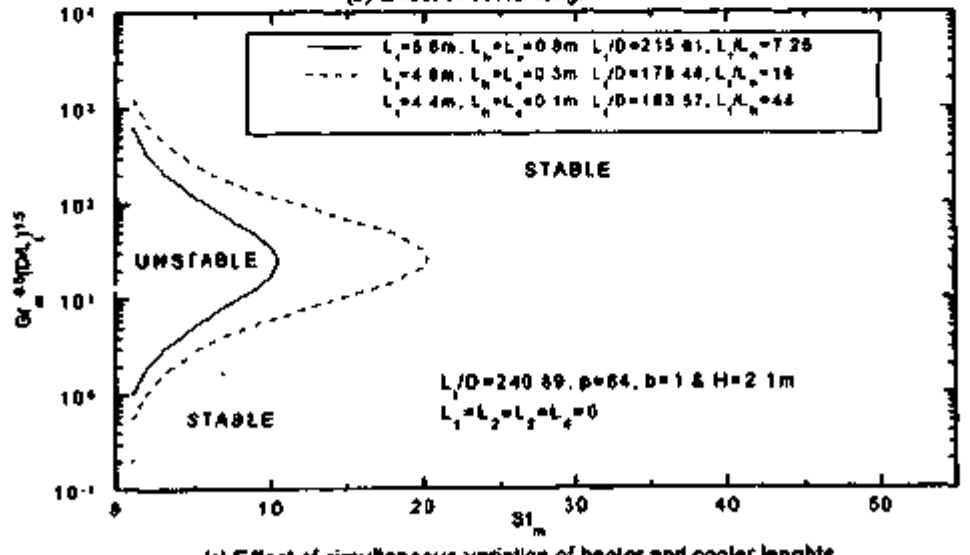

(c) Effect of simultaneous variation of heater and cooler lenghts

Fig. 46 : Effect of heater and cooler lengths on the stability behavior for HHHC orientation (clockwise flow)

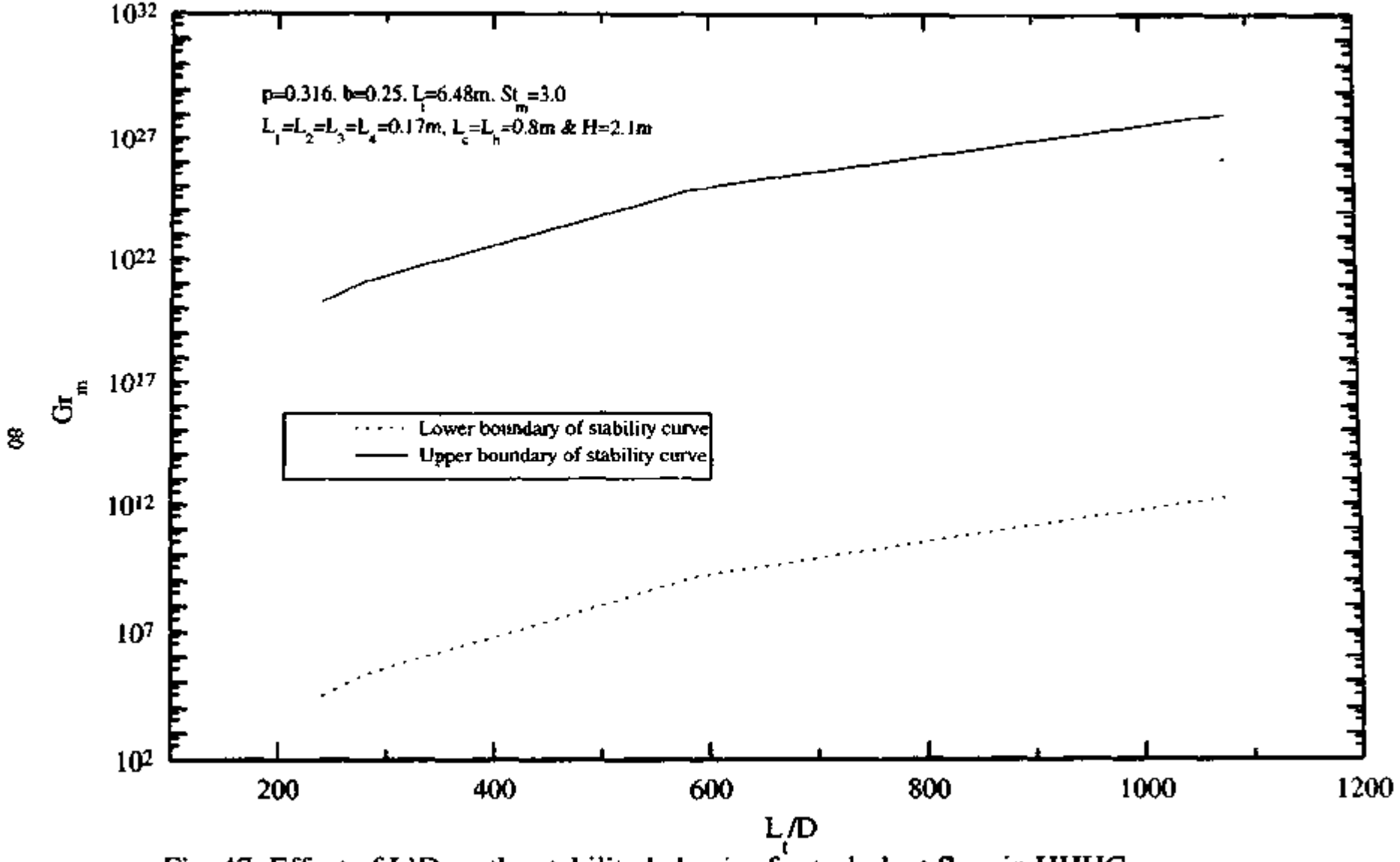

Fig. 47: Effect of L_t\D on the stability behavior for turbulent flow in HHHC orientation using Linear stability analysis.

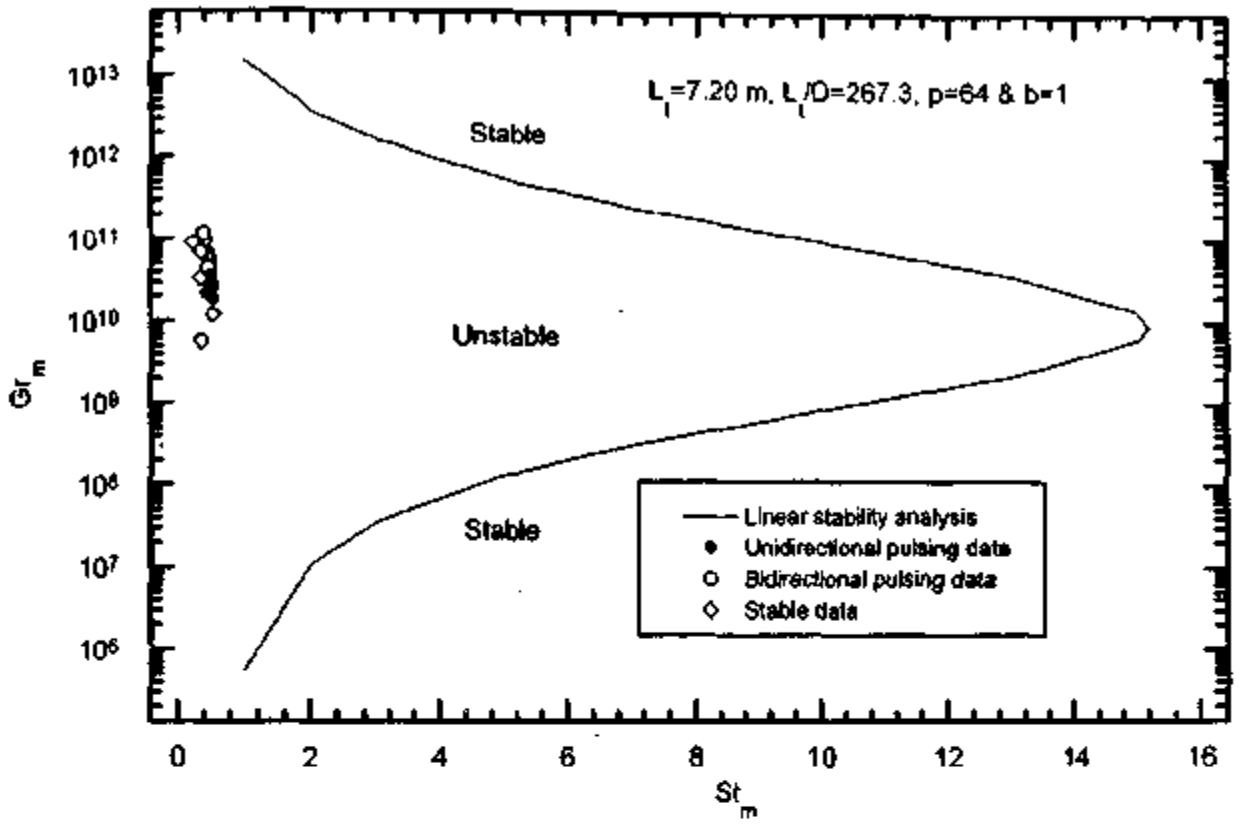

(a) HHHC orientation

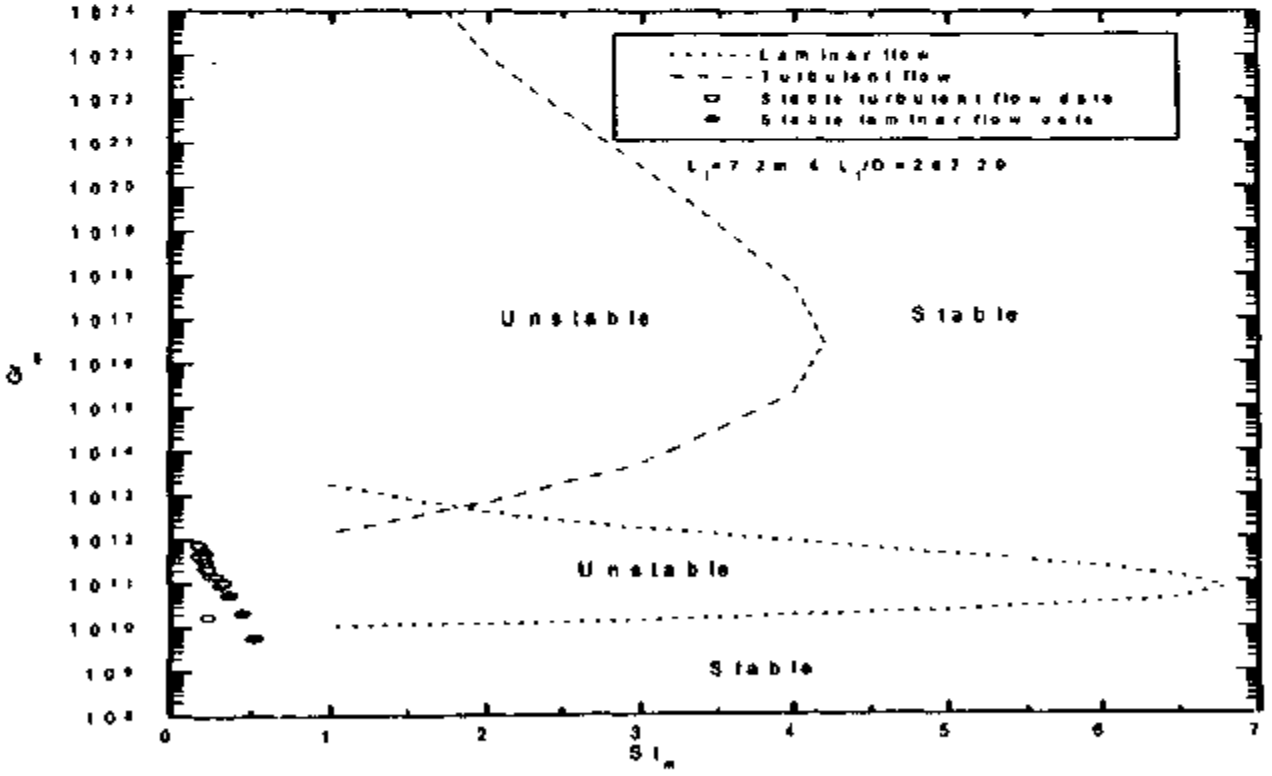

(b) VHHC orientation

Fig. 48: Comparison of the stability maps obtained by the linear stability method with experimental data

9. NONLINEAR STABILITY ANALYSIS

Nonlinear stability analysis is generally carried out by numerically solving the original nonlinear partial differential equations by the finite difference method with continuity of temperature as the boundary condition. Calculations were done for specified initial conditions. Algebraic equations for the governing partial differential equations were obtained using the forward, backward and the central difference formulae for the inertia, convection and diffusion terms respectively. For this calculation, the energy equation was solved explicitly whereas the momentum equation was solved implicitly using the Newton-Raphson method. The temperature integral in the momentum equation was evaluated numerically using the Simpson's rule. The time step was chosen to satisfy the Courant stability criteria. The nodal temperatures were calculated explicitly by marching along the flow direction. When the flow direction changed, the marching direction also was changed. Further details of the numerical scheme employed are given in Appendix-5. Before the actual calculations, it was ensured that the computed results are both grid and time step independent. For these calculations a space step of 1 cm was used. Further details of the code developed are available in Manish et al. (2001).

9.1 Code validation

Comparing the predicted steady state solutions following a transient with the corresponding exact analytical solutions validated the code. Subsequently the code was used to generate the stability map. To enable the predictions to be compared with that of the linear stability method, the initial conditions used in this calculation corresponded to the steady state case with the flow rate perturbed by a small quantity. Stability was judged by the behaviour of the solution. If the perturbation dies down with time, the corresponding operating condition was considered as stable; if the amplitude of perturbation remains the same, then it is neutrally stable and if the amplitude of the perturbation increases with time, then it is considered as unstable. The neutrally stable operating conditions are identified in this way and are compared with that predicted by the linear stability method in Fig. 49. For both laminar and turbulent flows, the predicted stability maps by the linear and the nonlinear analysis are found to be close to each other. Subsequently, numerical experiments were performed to identify the unstable flow regimes.

9.2 The Unstable Flow Regimes

One of the drawbacks of the 1-D formulation used in the nonlinear analysis is that the flow does not start from stagnant conditions with uniform initial temperatures throughout the loop for the HHHC orientation following the start of heating. The same problem manifests itself in another form for an increase in power to an unstable value from stable steady state initial conditions. For this case, instability develops by the Welander mechanism (i.e. growth of small amplitude oscillations) but the flow does not restart after stagnation (at the end of a large pulse) due to the low value of the inertia term at low powers. Hence, the unidirectional pulsing instability could not be simulated in the present loop. To overcome this problem, a very small inclination was given to the horizontal pipes. An upward inclination of 4° was given to the bottom horizontal pipe while a downward inclination of the same magnitude was given to the top horizontal pipe. With this modification, the code is able to predict the various flow regimes observed in the experiment.

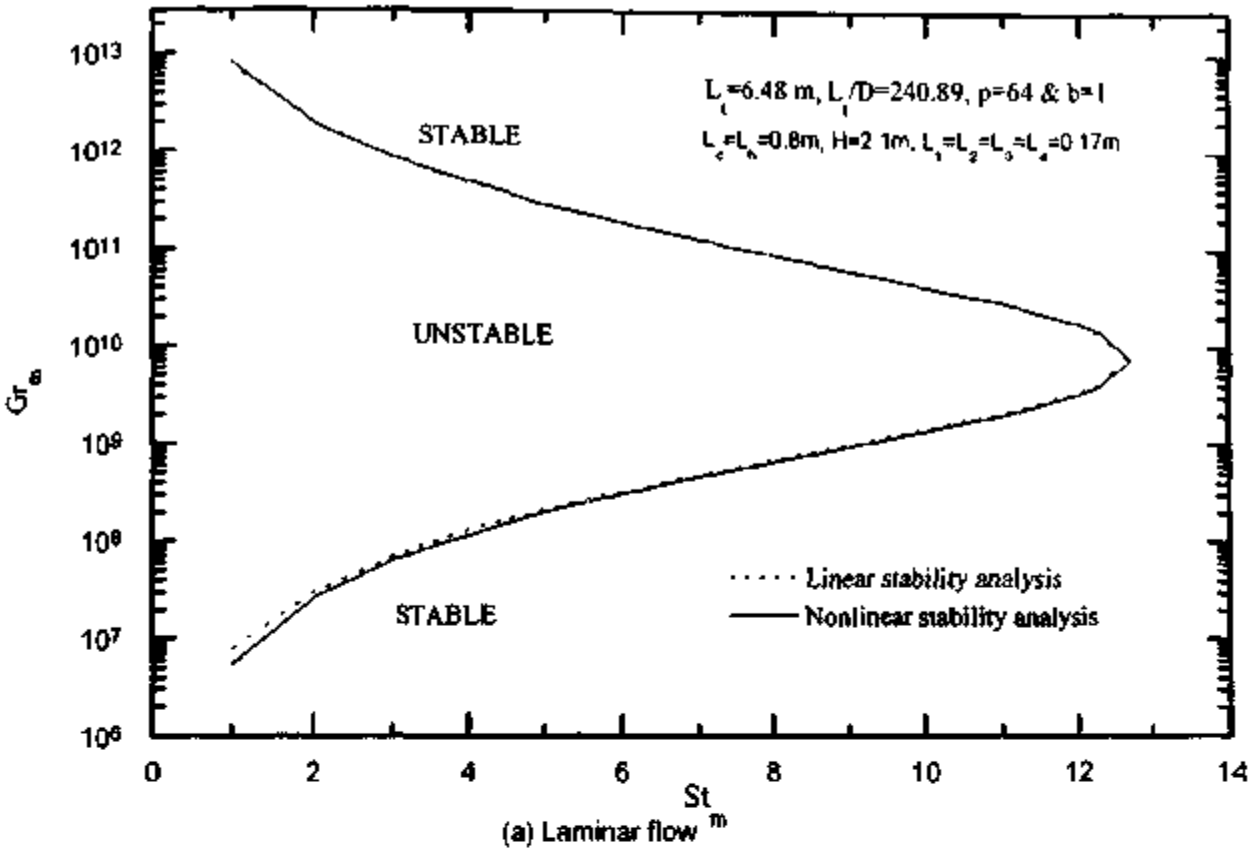

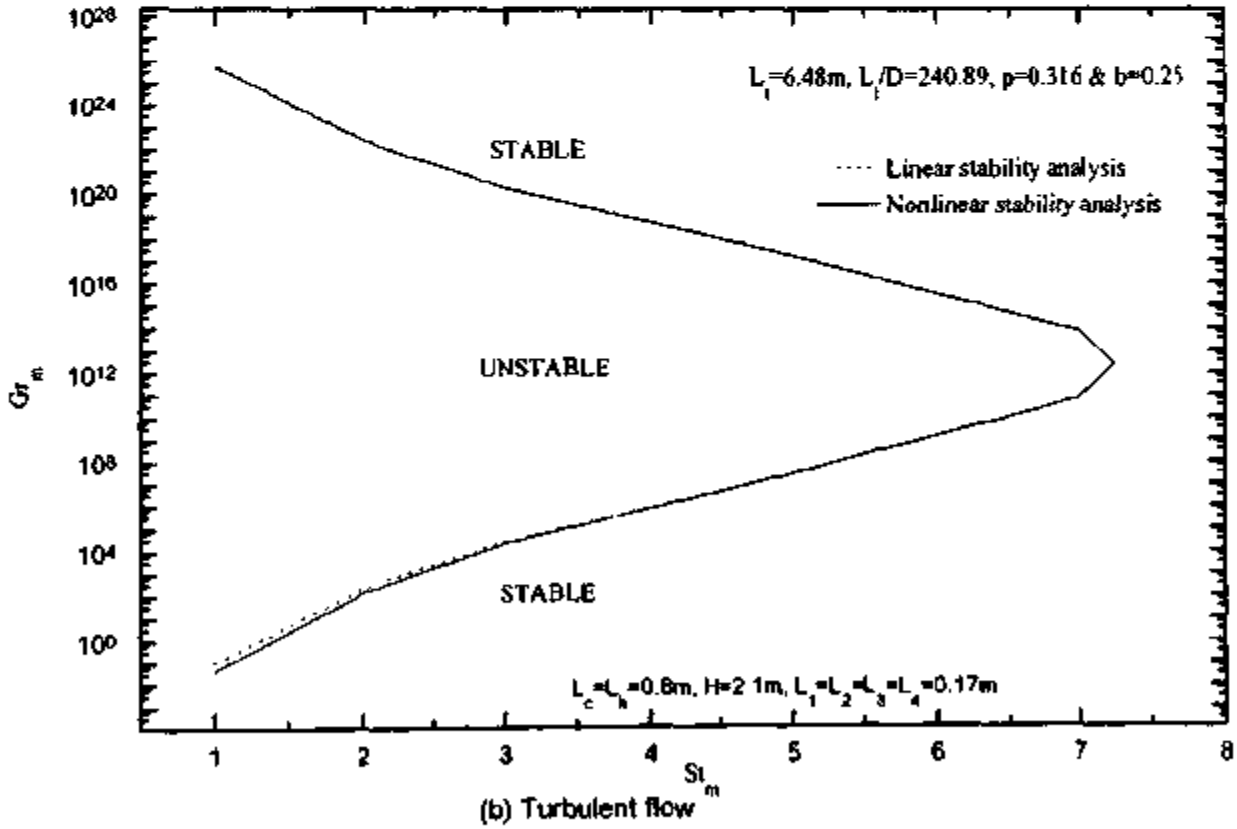

Fig. 49: Comparison of the stability maps obtained by the linear and nonlinear stability analyses for the HHHC orientation.

Fig. 50 shows a typical unidirectional pulsing behaviour predicted with 4° inclination as mentioned above at St_m=6.21. Due to the use of large St_m (the experimental value of St_m is around 0.5), unidirectional pulsing is observed at a significantly larger power than in the experiments. It may be noted that experimentally also, it was found that the effect of increasing the coolant flow rate (equivalent to enhancing the St_m) was to shift the upper threshold of unidirectional pulsing towards higher power (see Fig. 32). Typical chaotic switching predicted for the same St_m is also given in Fig. 50. Typical bi-directional pulsing behaviour predicted for different heater power are shown in Fig 51. Bidirectional pulsing behaviour could be predicted even without considering any inclination of the horizontal legs. This is because of the significance of the inertia effect at the relatively higher power levels at which bi-directional pulsing is observed.

9.3 Mechanism for the Observed Unstable Regimes

The numerical prediction provided an opportunity to verify the mechanisms proposed for unidirectional and bi-directional pulsing based on limited experimental observations.

9.3.1 Unidirectional Pulsing

Typical predicted flow rate for unidirectional pulsing is given in Fig. 52a. The predicted loop temperature distribution corresponding to the different peaks (marked as 1, 2 and 3 in Fig. 52a) is shown in Fig. 52b. These temperature distributions show that there are three dominant hot and cold pockets at any time along with a few minor hot and cold pockets. At τ_1 the hottest and the coolest pockets are in the horizontal heater and cooler respectively. The second hottest pocket is descending through the right vertical leg with its hottest part located right at the elbow. Simultaneously, the second coolest pocket is ascending through the left vertical leg. This leads to near balancing of the buoyancy contribution by each vertical leg resulting in a region of low flow rate. During this time, the hot plug in the heater gets hotter. The small forward flow eventually forces the hot plug to enter the vertical leg assisting forward flow. The peak forward flow is observed when the hottest part of the hottest pocket is near the top of the left vertical leg and the coolest pocket is in the right vertical limb near the bottom elbow. Subsequently, flow reduces as the hottest part of the hot pocket and the coolest pocket begin to enter the top and bottom horizontal tubes respectively. As this pocket emerges from the top horizontal limb and travels a short distance in the vertical downleg, it reverses the flow. The maximum reverse flow is obtained when the hottest pocket gets stranded at the top elbow with its hottest part located just below the elbow in the right vertical leg. Subsequently, the reverse flow reduces and eventually leads to the plateau region with small forward flow due to the 4° inclination considered in the calculation. In the experiment, however, it leads to near flow stagnation which leads to minor forward and backward oscillations as shown in the experimental curve of Fig. 53. These findings are in agreement with the experimentally observed mechanism described in section 7.4.

9.3.2 Bidirectional Pulsing

The predicted temperature distribution corresponding to the peaks of flow rate marked as 1, 2, 3 and 4 in Fig. 54a is shown in Fig. 54b. The temperature distribution shows that there are only three hot and cold pockets in the loop at any time. During the minor peaks (i.e. corresponding to τ_1 and τ_3) the hottest and the coolest pockets are respectively in the heater and the cooler. The remaining two hot and cold pockets are nearly of the same magnitude of which one hot and one cold pocket are in each vertical limb. The locations of these hot and

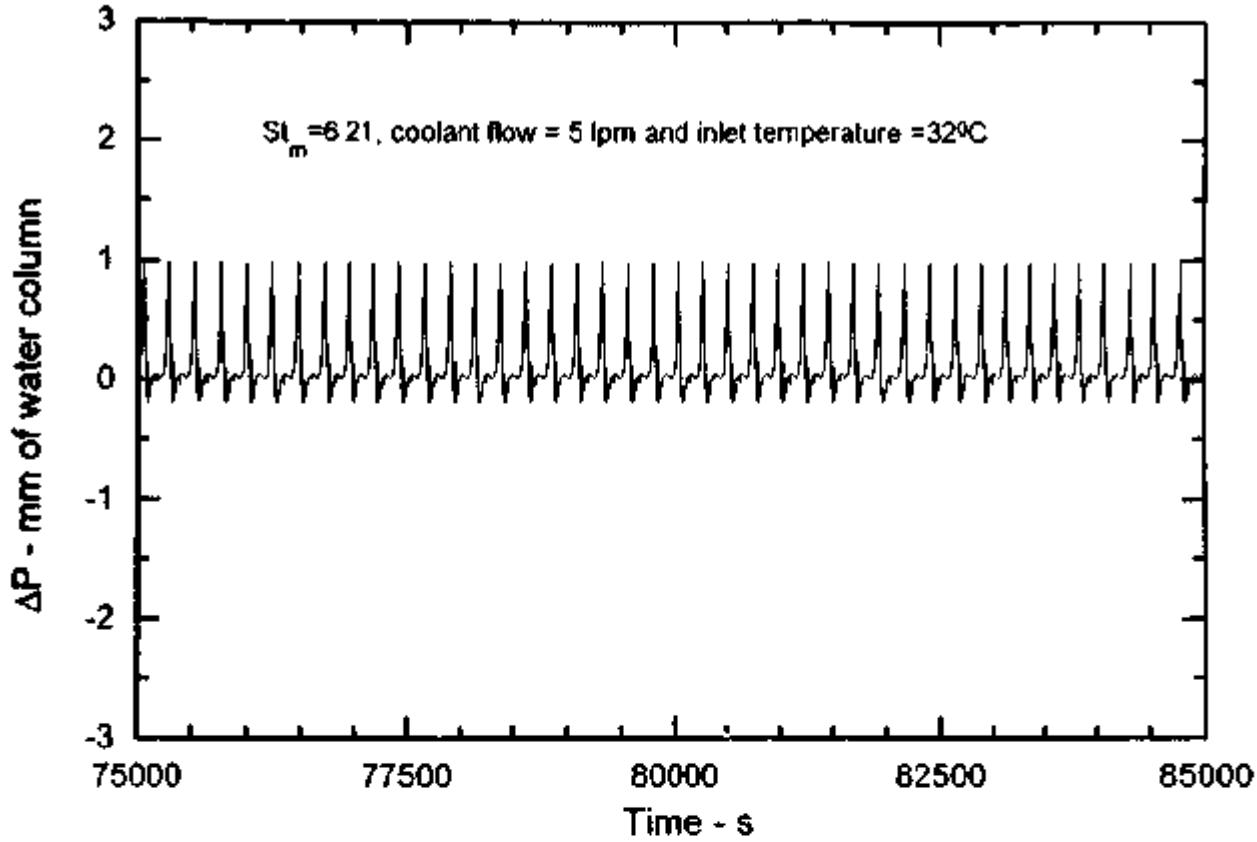

(a) Periodic unidirectional pulsing at 464 W

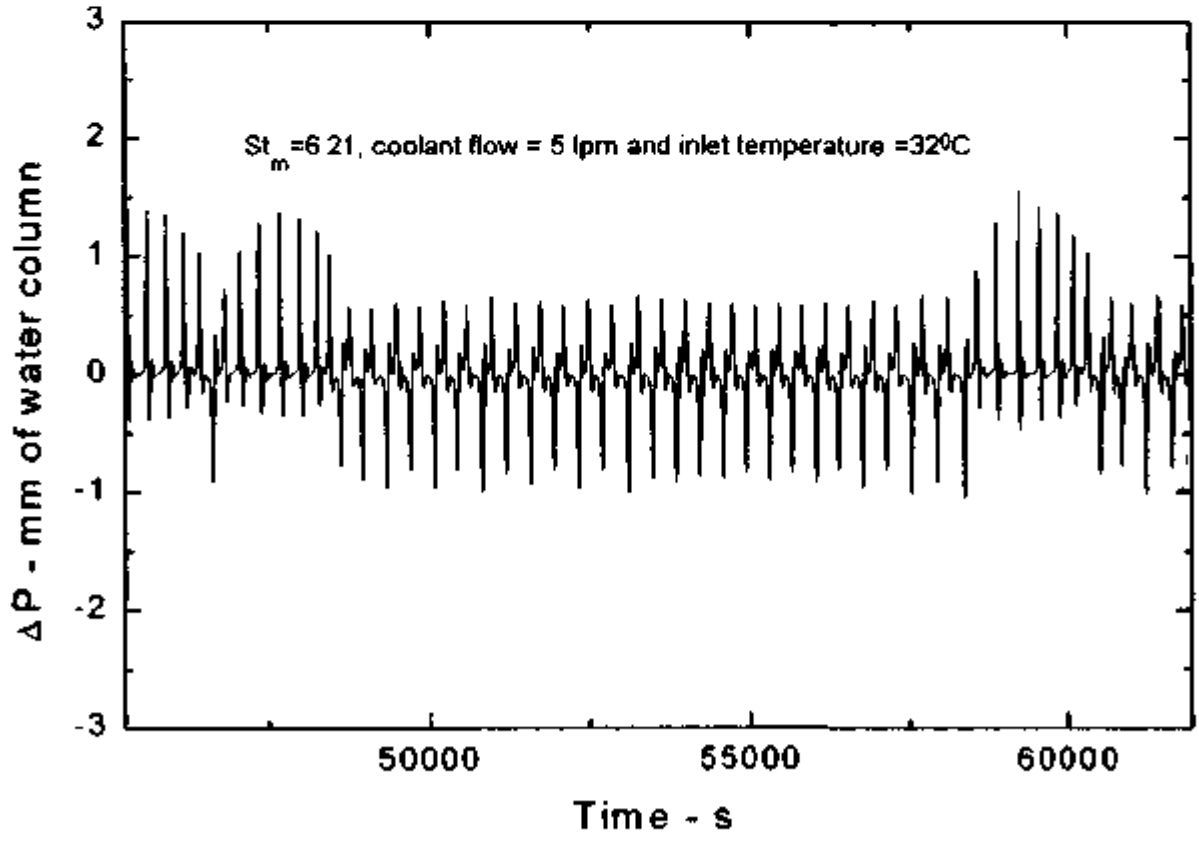

(b) Chaotic switching between unidirectional and bi-directional pulsing at 511 W

Fig. 50: Predicted oscillatory behaviour with 4^0 tilt in horizontal pipes

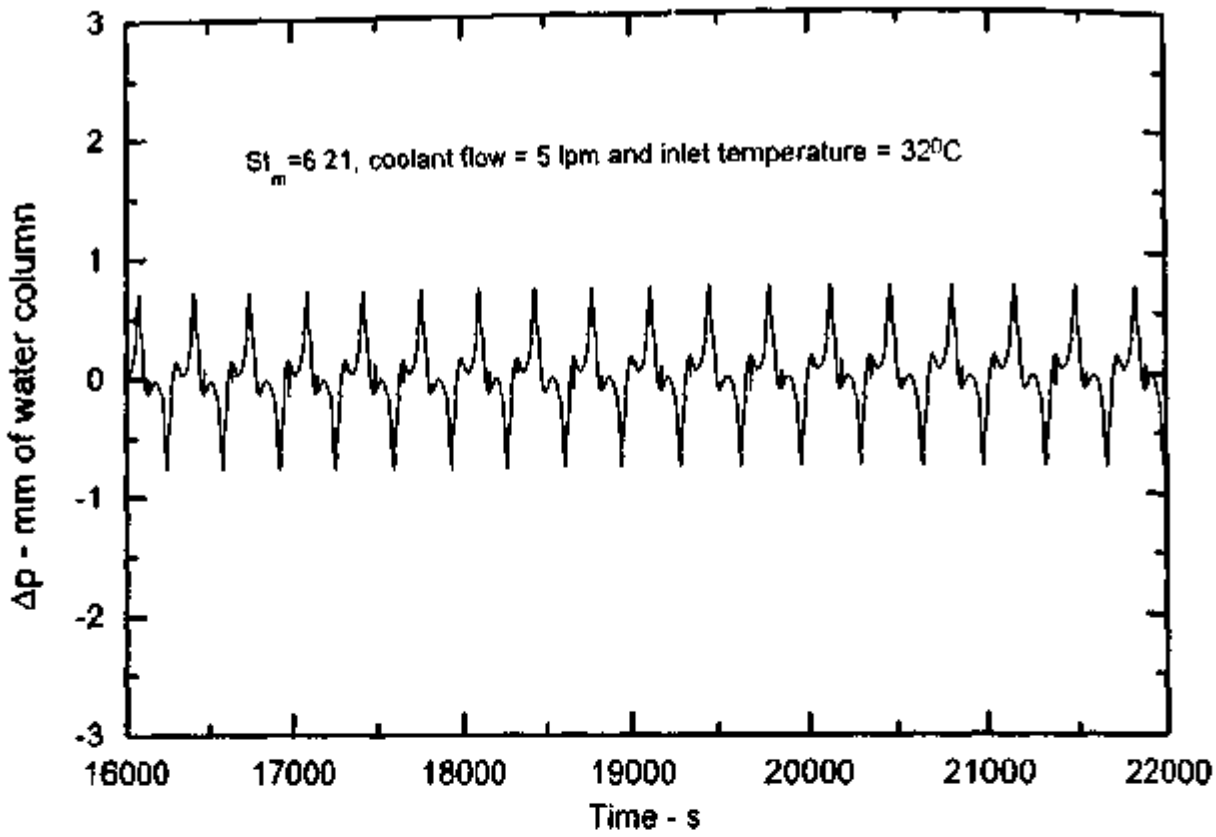

(a) Power = 553 W

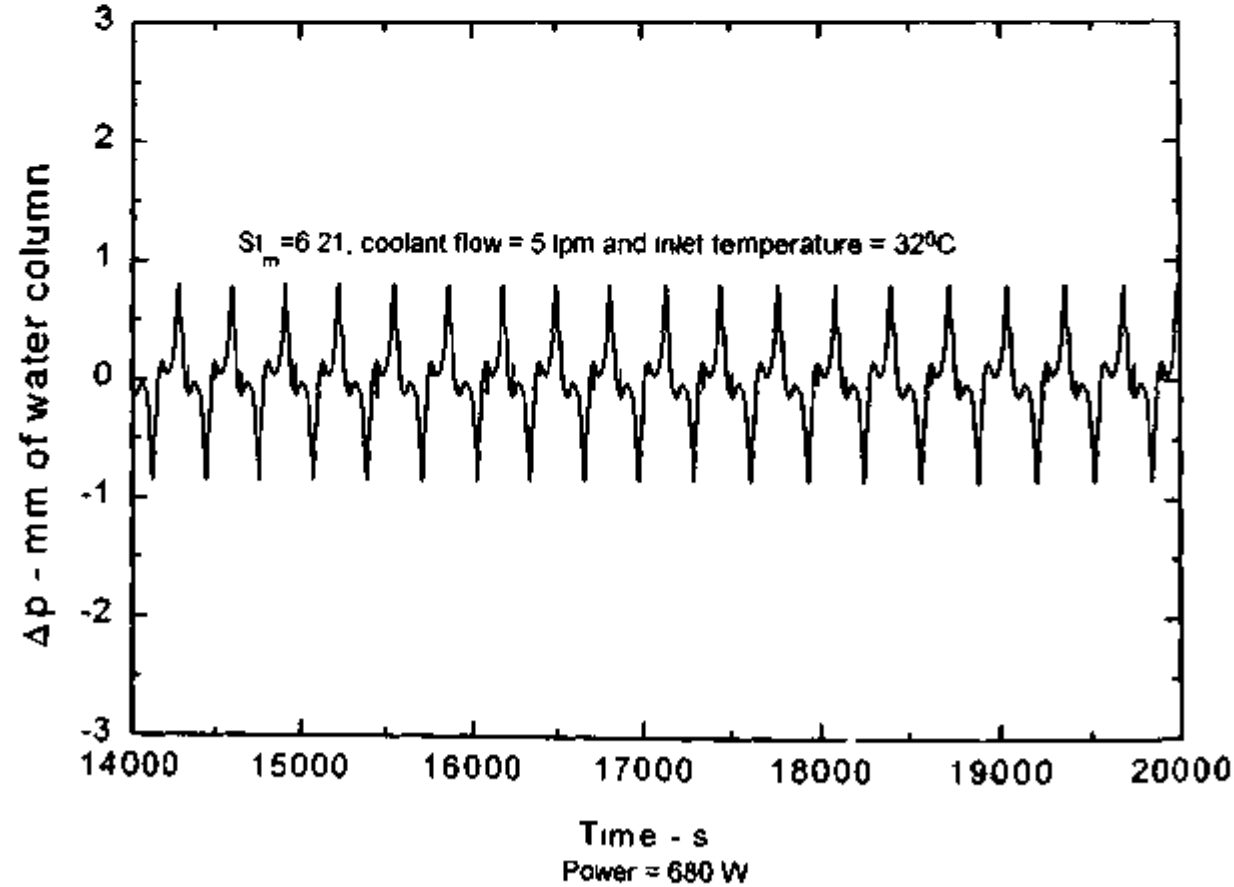

Power = 680 W

Fig 51: Predicted bi-directional pulsing behaviour for different powers without inclination of the horizontal pipes

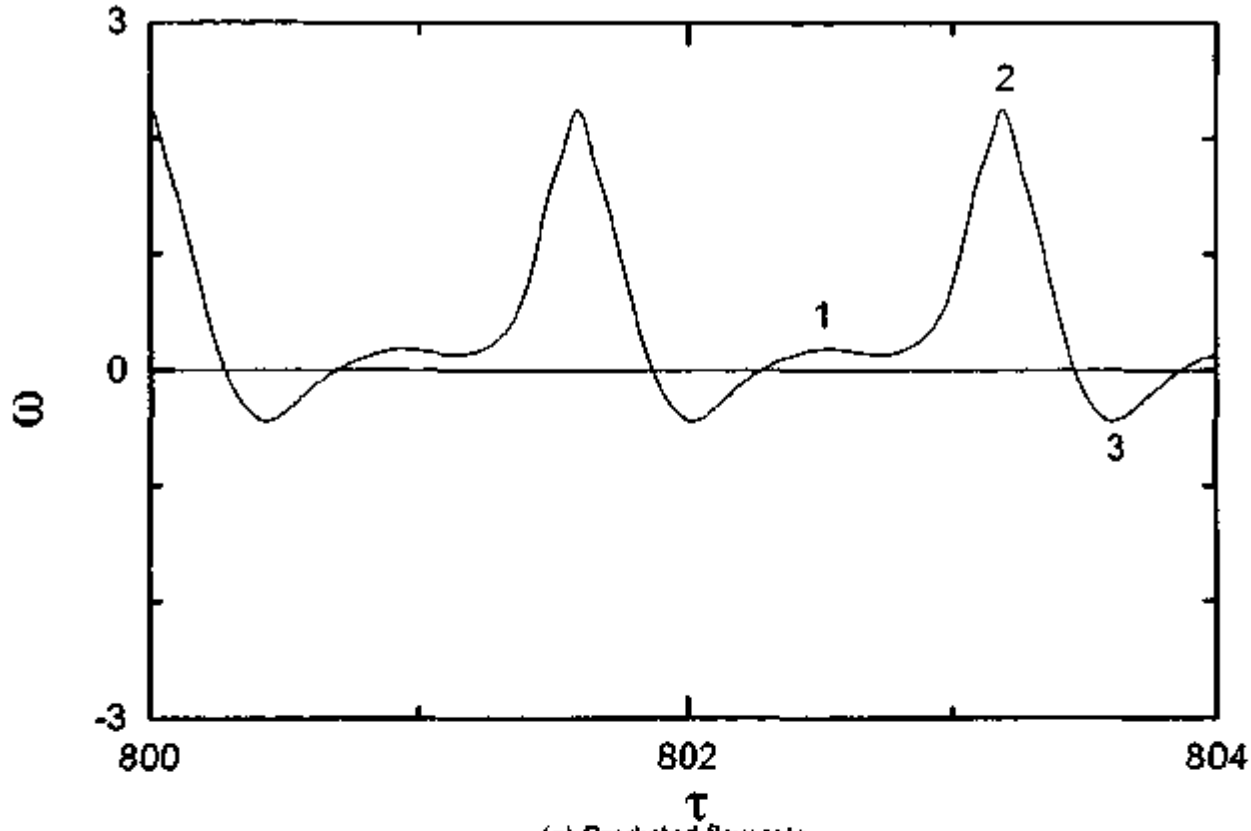

(a) Predicted flow rate

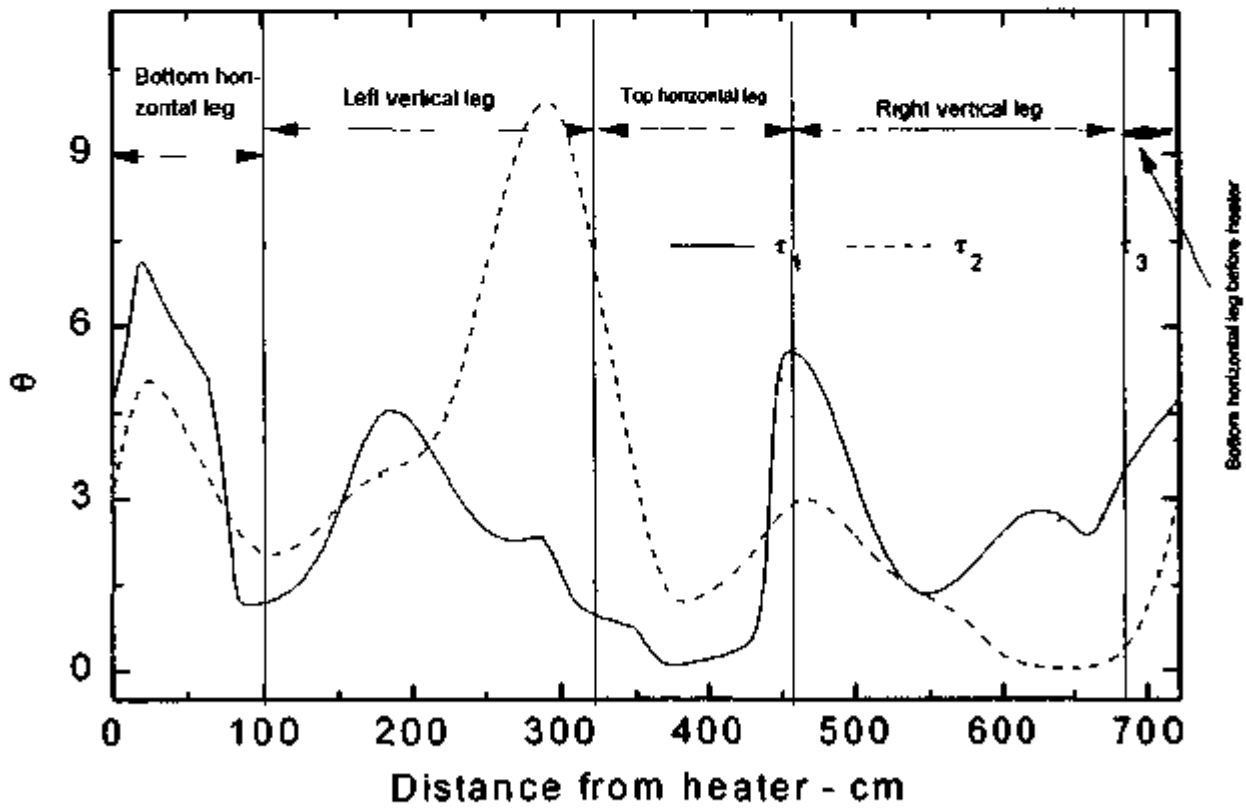

(b) Instantaneous temperature distribution at τ_1, τ_2 and τ_3 corresponding to the peaks in (a)

Fig. 52 : Flow and temperature variation for typical unidirectional pulsing

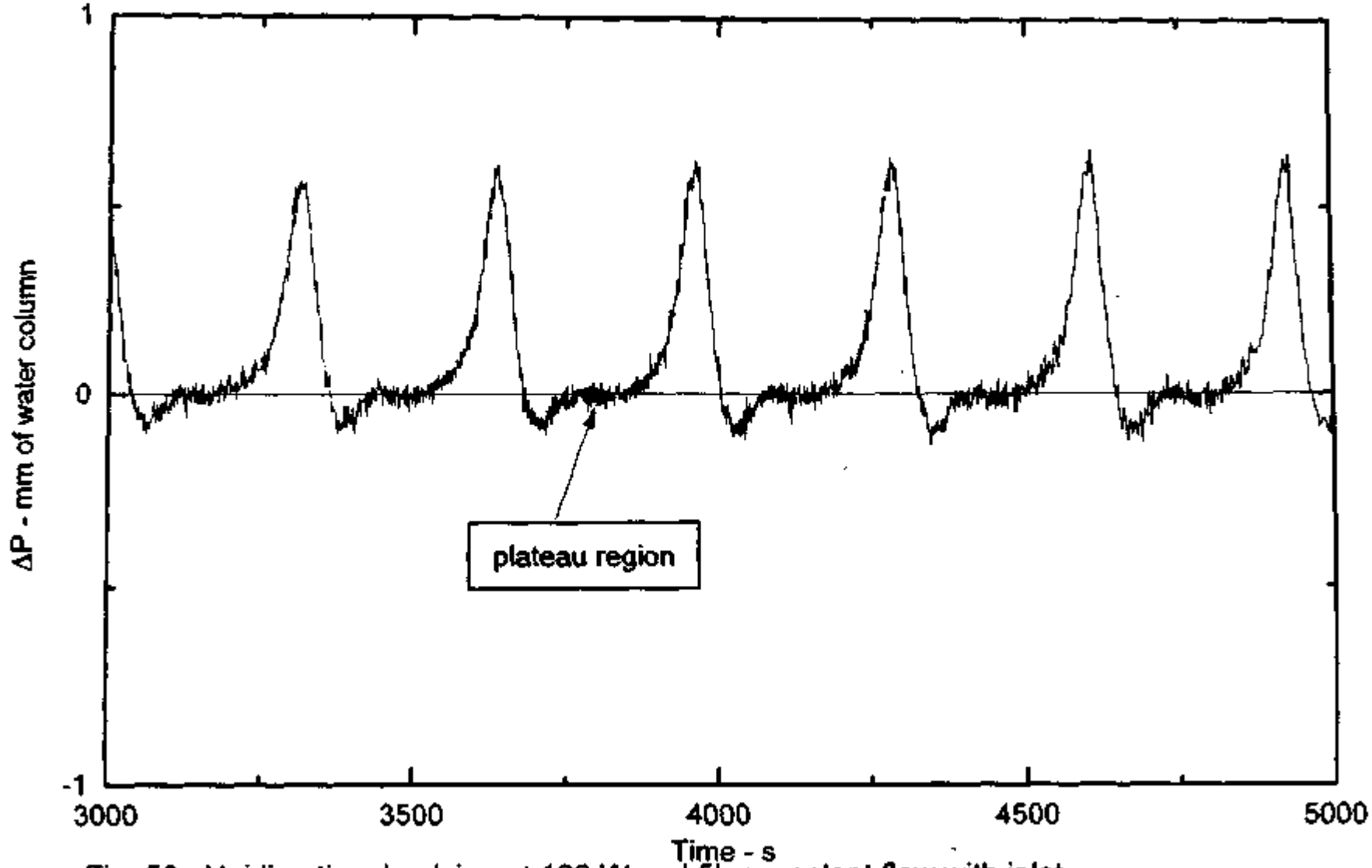

Fig. 53 : Unidirectional pulsing at 120 W and 5lpm coolant flow with inlet temperature of 35 ^{0}C

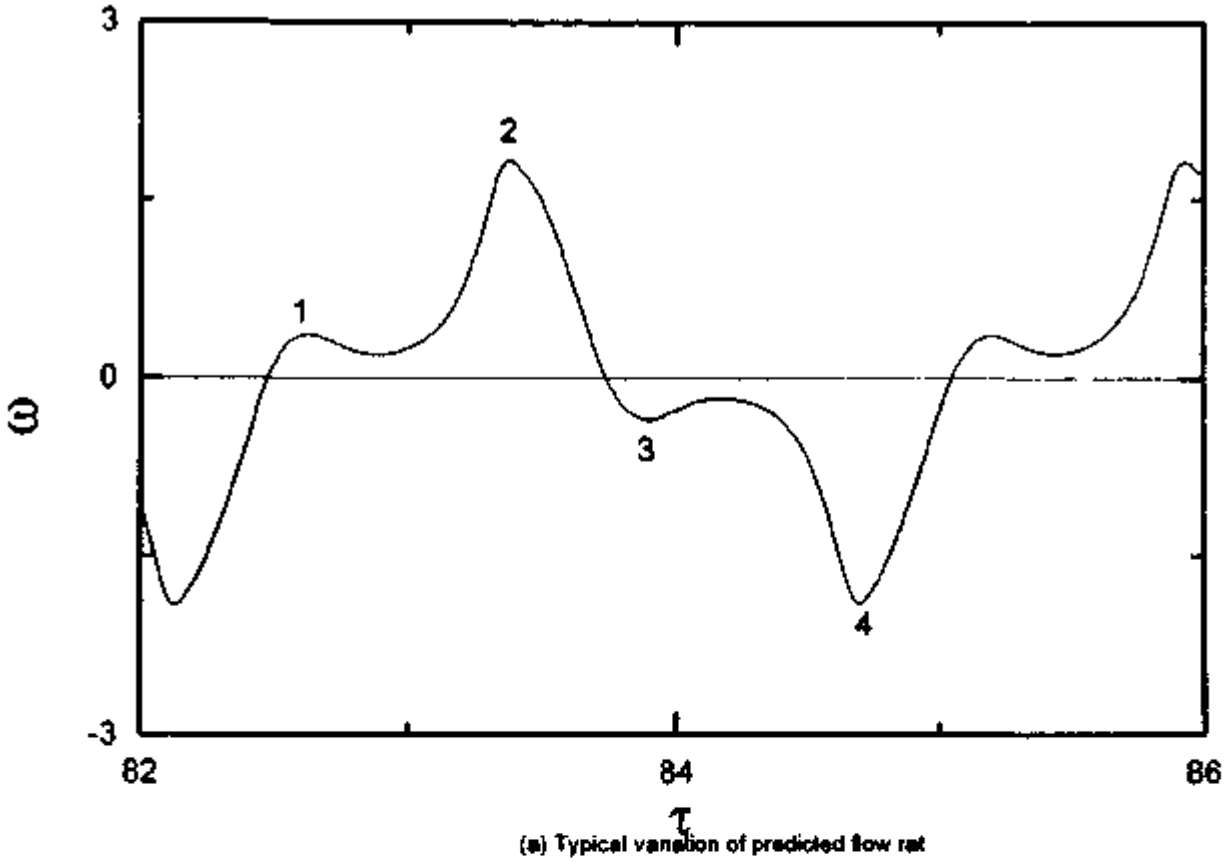

(a) Typical variation of predicted flow rat

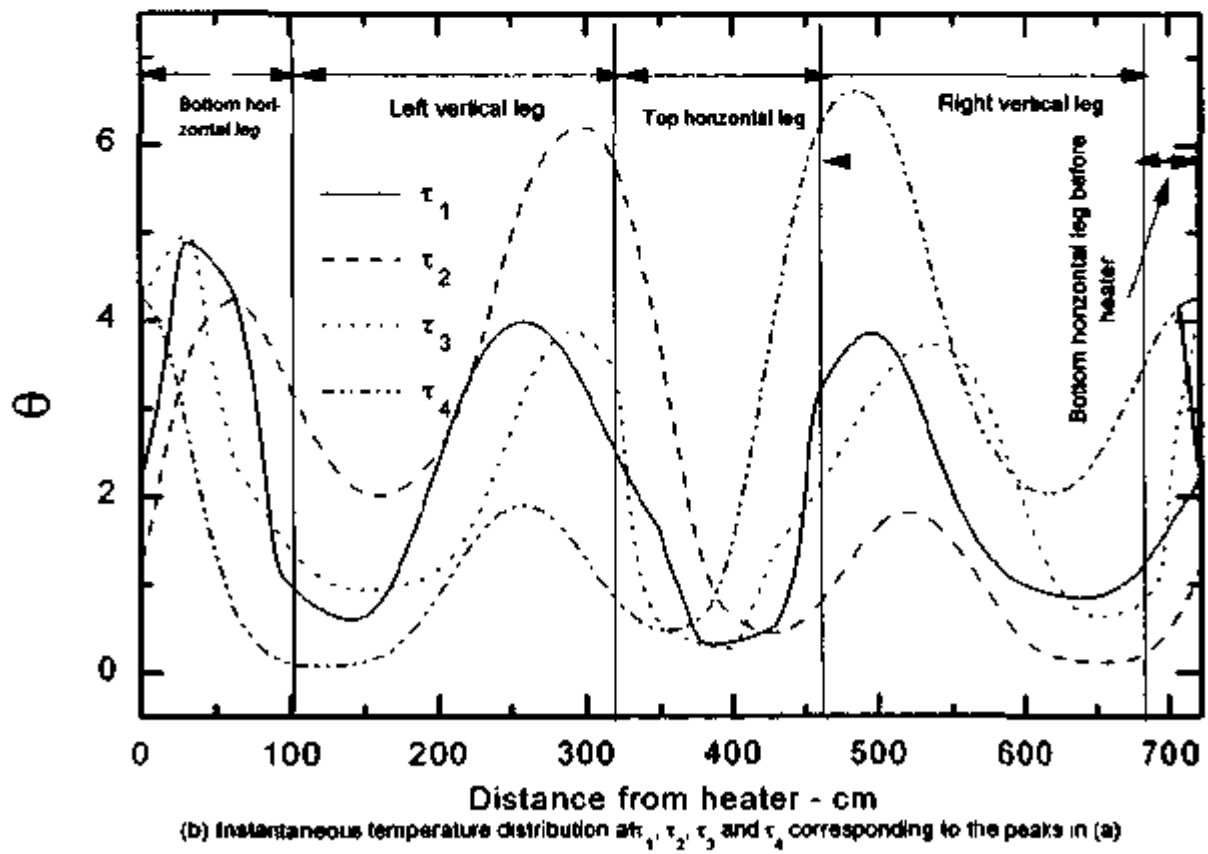

(b) Instantaneous temperature distribution at τ_1, τ_2, τ_3 and τ_4 corresponding to the peaks in (a)

Fig. 54 : Flow and temperature variation in typical bidirectional pulsing

cold pockets of fluid are such that at τ_1, the hot and cold pockets are respectively near to the top and bottom of the left and right vertical legs. The rising cold pocket in the left vertical leg and the descending hot pocket in the right vertical limb oppose the clockwise flow reducing it to a very small value. This makes the hot pocket in the heater hotter and cold pocket in the cooler colder. The slight forward flow forces these hot and cold pockets to enter the left and right vertical legs respectively, thereby increasing the forward buoyancy force initiating the large forward flow peak at τ_2. At τ_3 the situation is similar as at τ_1. But the prevailing small reverse flow forces the hot plug in the heater to release in the right vertical limb thereby causing a large increase in the reverse buoyancy force initiating the large reverse flow peak at τ_4. These are in agreement with the proposed mechanism given in section 7.4 based on the temperature measurements at a few locations in the loop.

During the large flow rate peaks (τ_2 and τ_4) one hot and one cold pocket are dominant compared to the others and they are respectively located near the top and bottom elbows of the upleg and downleg. The two smaller hot pockets are also clearly unequal in magnitude as seen from Fig. 54b. The dominant hot pocket at τ_4 is slightly greater than that at τ_2. Accordingly a small difference in peak flow rate is also noted in Fig. 54a. This difference is attributed to the heater location, which is not exactly at the centre of the bottom horizontal tube.

9.4 Other flow regimes

It might be noted that the unstable flow regimes observed are near to the lower stability boundary. With power increase, subcooled boiling starts in the experimental loop. Hence, pure single-phase unstable flow regimes far way from the lower threshold could not be experimentally studied. The nonlinear code, however, provided an opportunity to investigate these flow regimes. Figures 55, 56 and 57 show that several other flow regimes are possible with different combinations of Gr_m and St_m for the HHHC orientation. Investigating the temperature distribution can provide insights into the mechanisms causing these regimes to occur.

9.5 The existence of the conditionally stable regime

The following three initial conditions were studied.

(a) Steady state initial conditions
(b) Start-up from rest with uniform initial temperatures and
(c) Decay of instability due to a power decrease

9.6 Steady State Initial Conditions

This case has already been described in section 9.1. The instability threshold was found to be insensitive to the magnitude of the initial perturbation. The stability map obtained by the nonlinear stability method with this initial condition for the present experimental loop is given in Fig. 58 as curve 'a'. The nature of the observed oscillatory behaviour was studied and found to be always bi-directional pulsing (see Fig. 51). With this initial condition, the instability always develops by the Welander mechanism as shown in Fig. 59. The same is true for the experimental curves shown in Fig. 24.

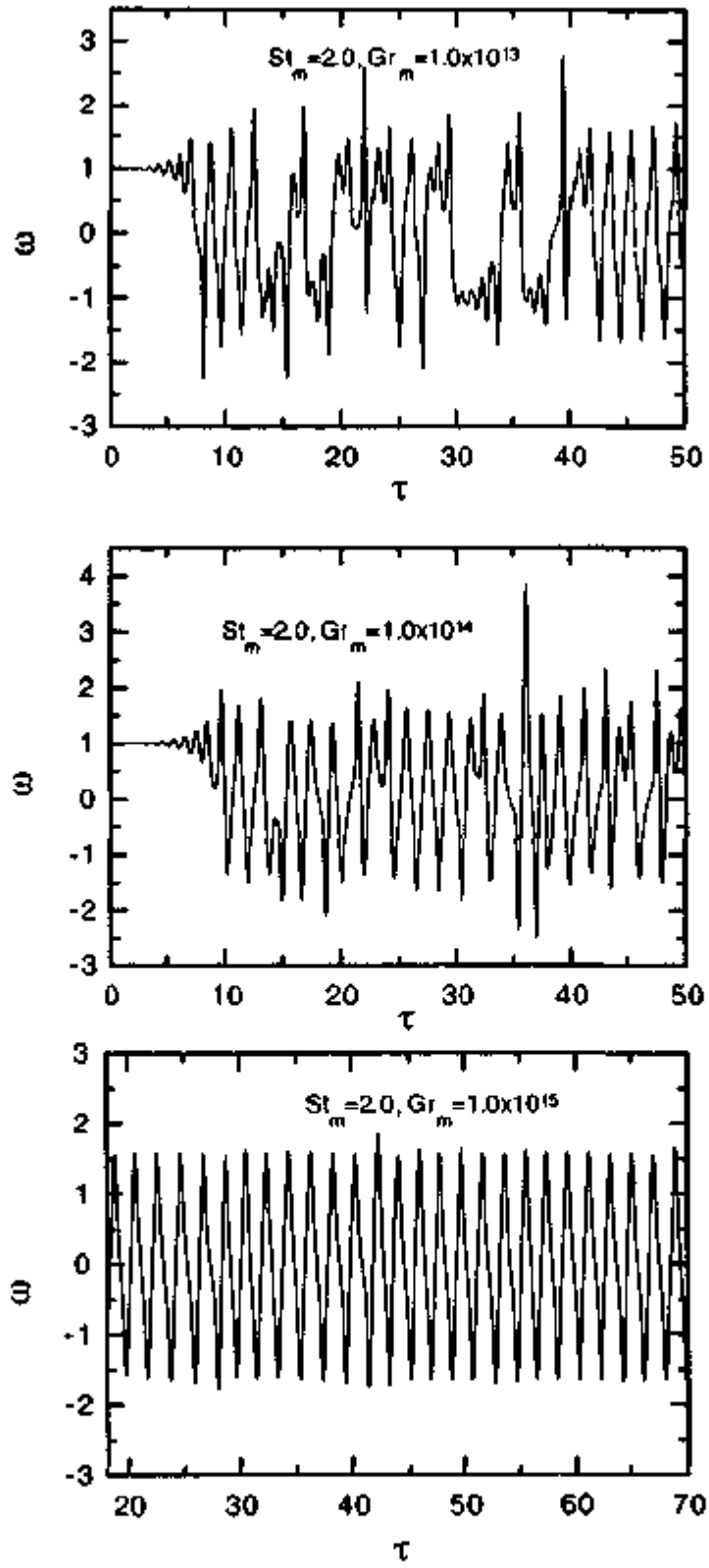

Fig 55: Variation of unstable oscillatory regimes observed without axial conduction and 4^0 inclination

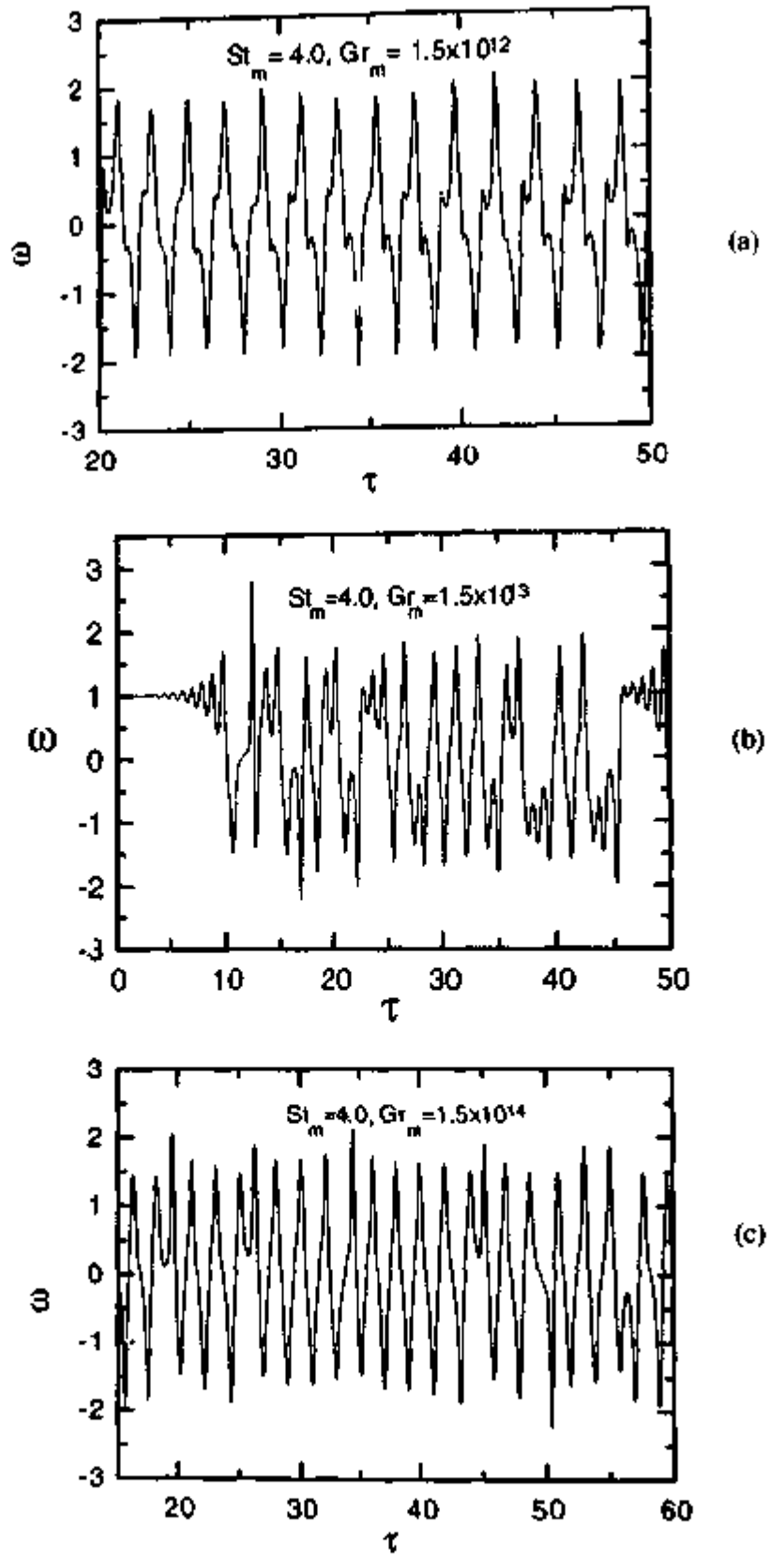

Fig 56: Variation of unstable oscillatory regimes observed without axial conduction and 4^0 inclination

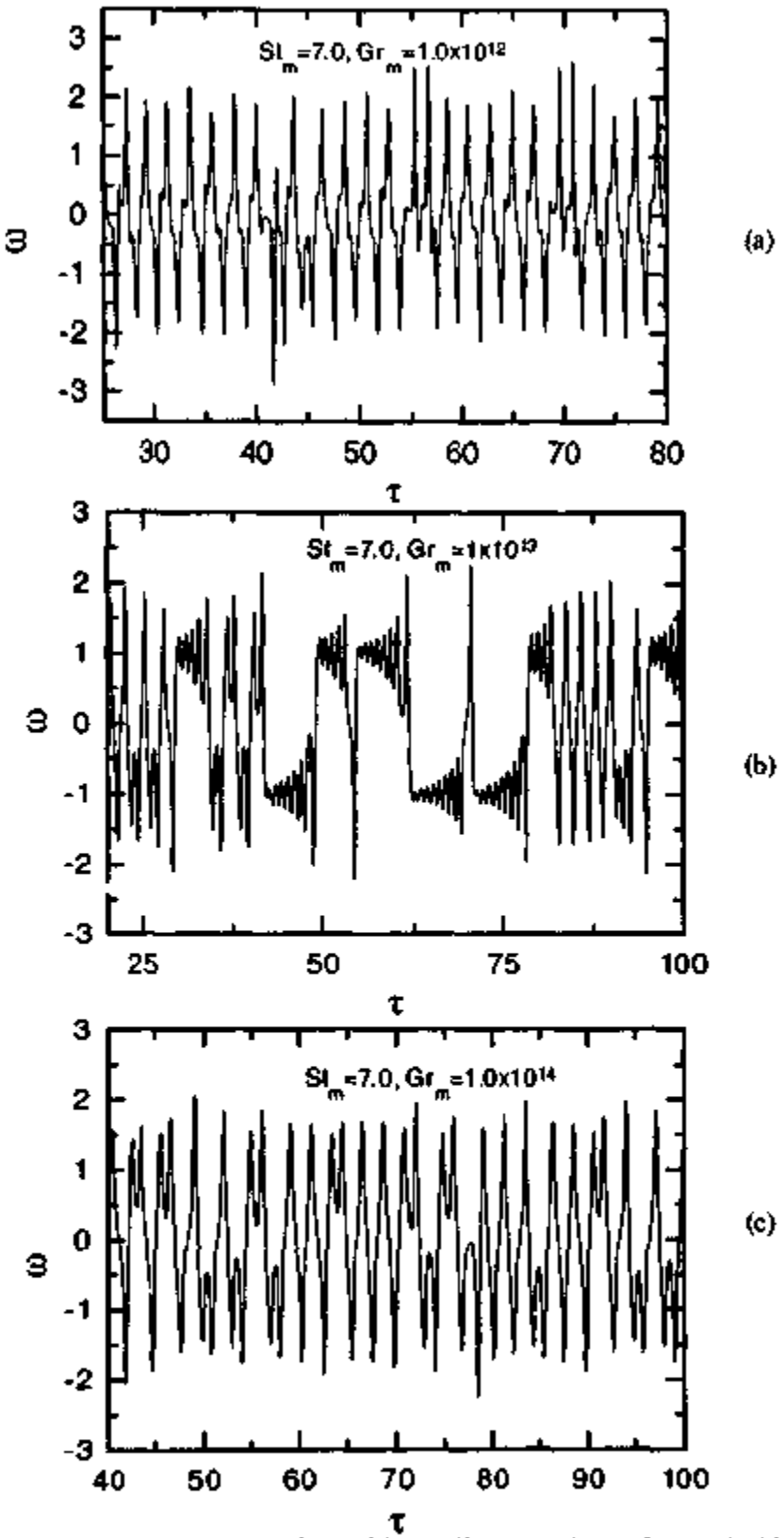

Fig 57: Variation of unstable oscillatory regimes observed without conduction and 4^0 inclination

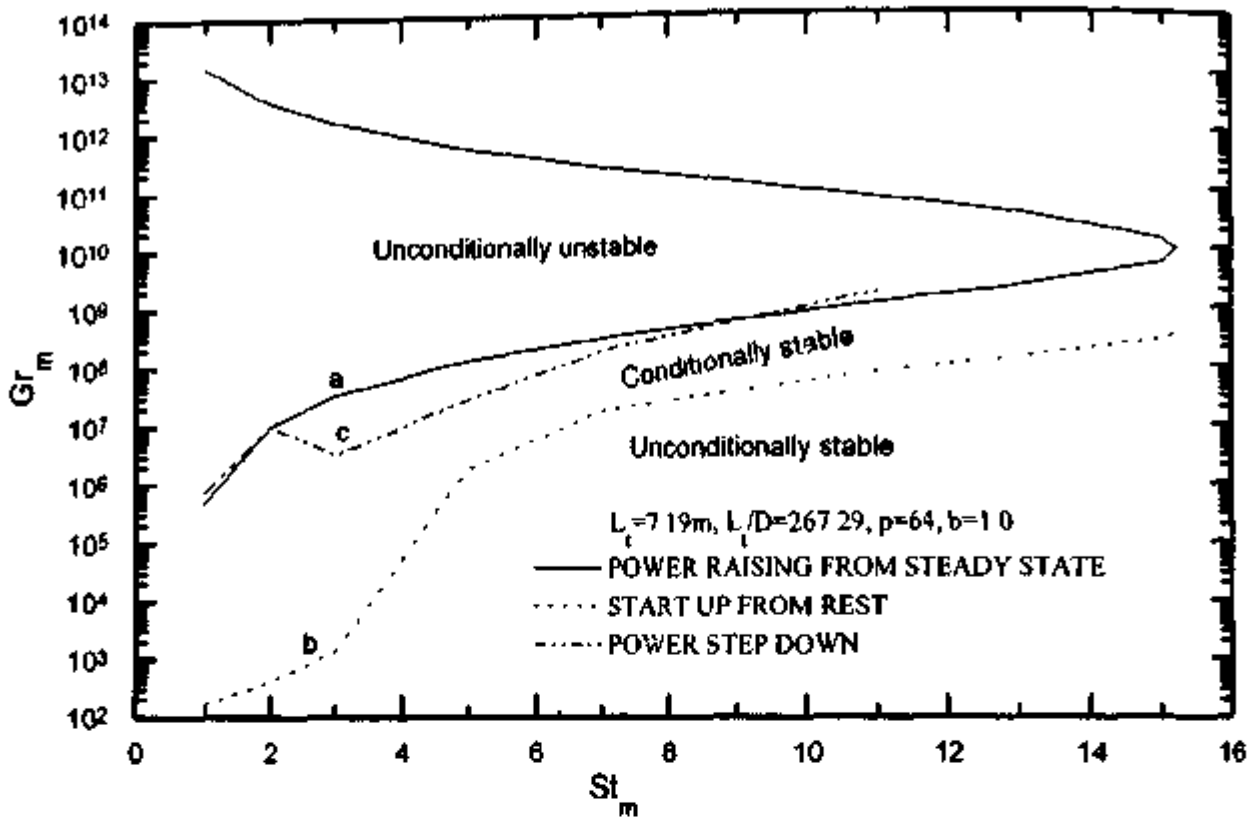

(a) Laminar flow

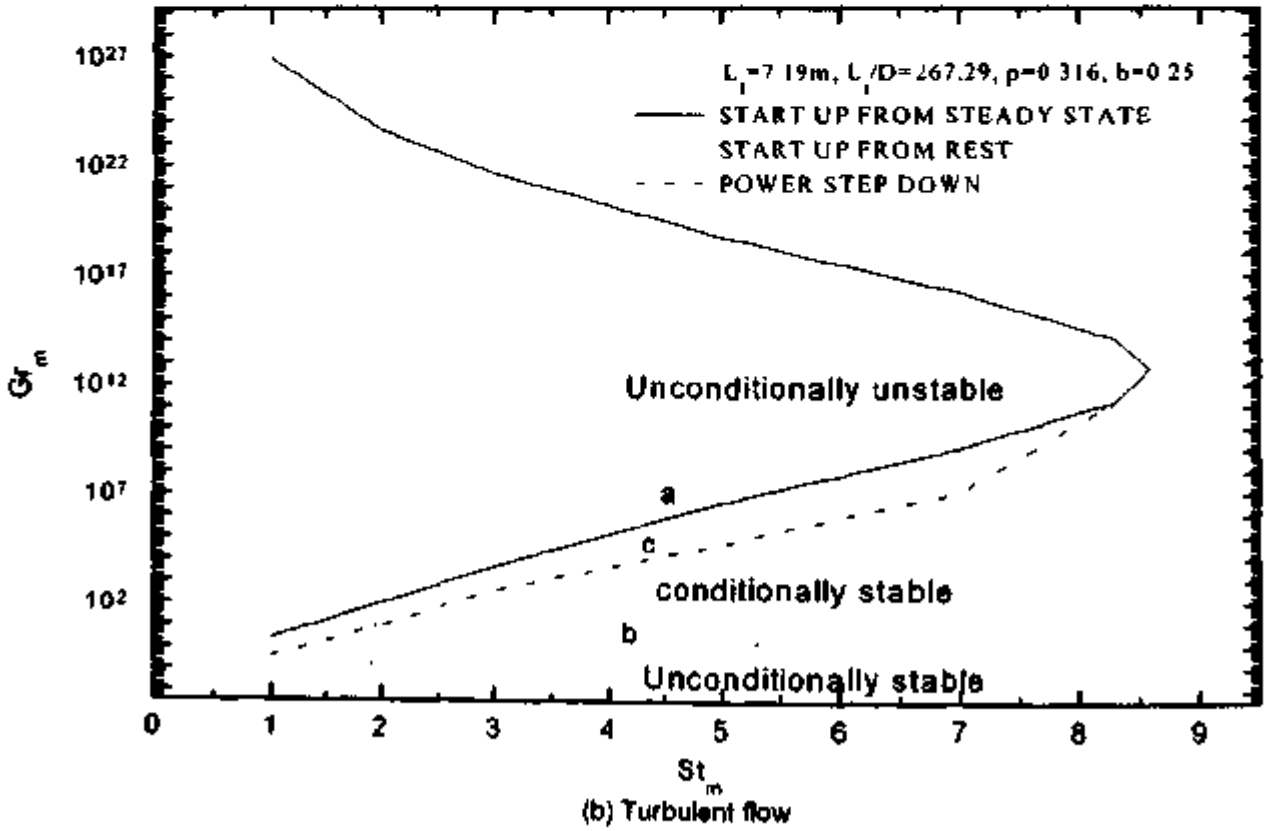

(b) Turbulent flow

Fig. 58: Conditionally stable regime for the HHHC orientation

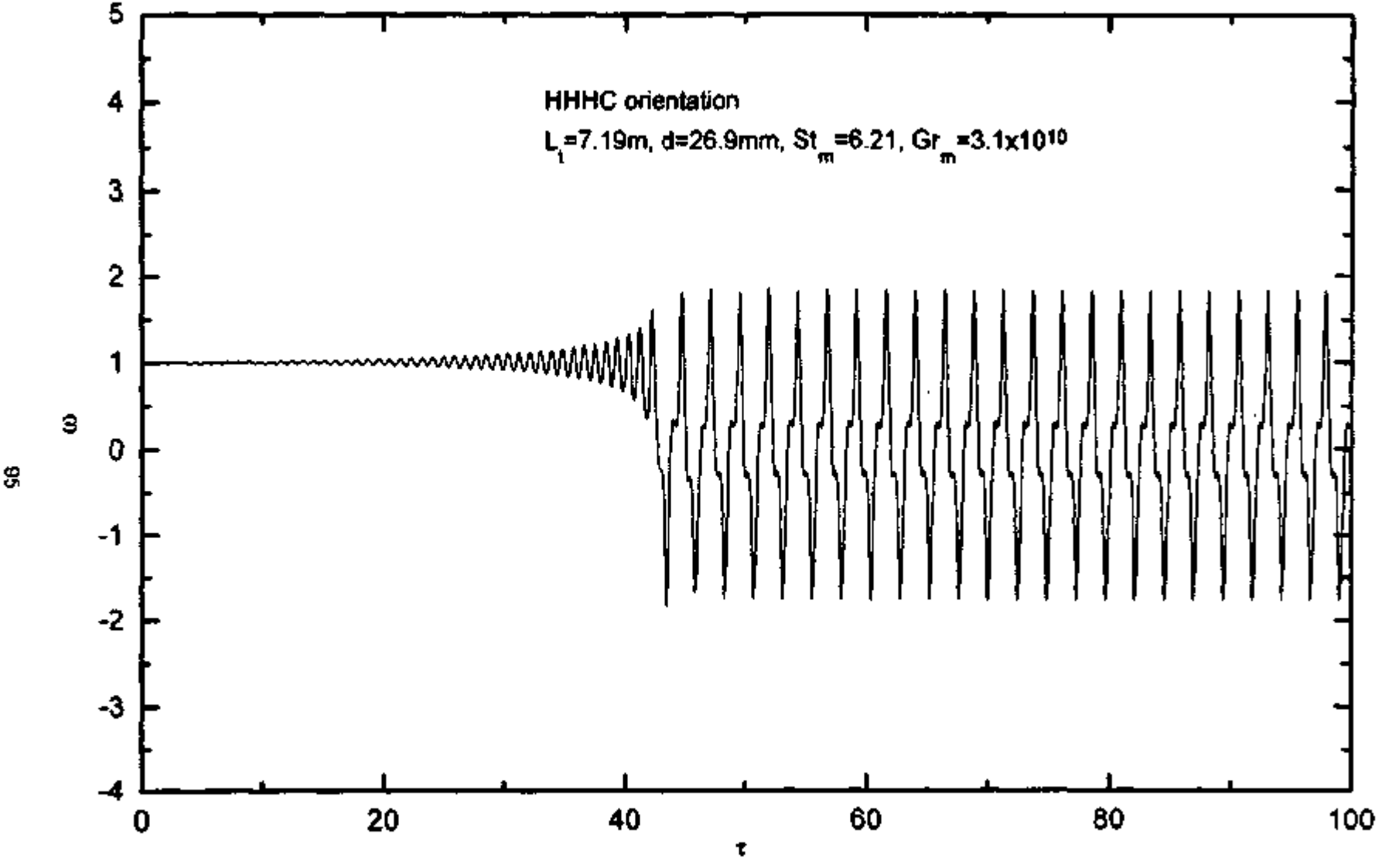

Fig. 59: Development of instability by the Welander mechanism from steady state initial conditions

9.7 Start-up from rest with uniform initial temperatures

This condition cannot be simulated as it is with the code for the HHHC orientation, as starting from zero flow; there is no way to initiate the flow. To overcome this, we included the axial conduction effect in the numerical calculations. To initiate flow in a given direction, the unheated length on one side of the heater was kept small in the calculations. For example clockwise flow is obtained if the unheated length near the left vertical leg is small while anticlockwise flow is obtained if the unheated length is small near the right vertical limb. For these calculations no inclination was considered for the horizontal pipes. The calculations were conducted with increasing initial power till the occurrence of instability starting with the flow initiation (see Fig. 60). Fig. 60 also shows a case where the oscillatory behaviour switches to bi-directional pulsing. These results are in general agreement with the trends observed in the experiments. However, the experimental results are obtained at much higher Gr_m. The range of power for the occurrence of unidirectional and bi-directional pulsing can be established in this way. The locus of all points that just lead to instability is found to be below the neutral stability curve obtained in section 9.1 (see curve 'b' in Fig. 58). From Fig. 58, it is found that the curve 'b' is considerably below the curve 'a' and the region between curve 'a' and 'b' can be termed as the conditionally stable region.

9.8 Decay of instability due to power step back

In this case, the instability was first established by the procedure discussed in section 9.1. After the initial transients died out the calculation was continued with a sudden decrease in the power. The calculations were continued till the instability decays into a steady state. If the steady state is unachievable, then the power is further decreased till a steady state is achieved. The objective was to test the existence of the hysteresis phenomenon. Typical results are shown in Fig. 61. The locus of all neutrally stable points obtained in this way is curve 'c' in Fig. 58. Curve 'c' is found to be above curve 'b' contrary to the experimental findings. This may be attributed to the simplified modelling of the cooler with a constant secondary side temperature. In reality, the cooler operates in parallel and counter flow mode due to repetitive flow reversals during the unstable flow in the loop. Prior simulation with the computer code ATHLET has shown that the counter flow mode is little more efficient than the parallel flow mode (Vijayan et al. (1995)), which can sustain the hot and cold pockets at much lower power.

9.9 Effect of other Orientations

With HHVC orientation, experiments did not show any stable steady state with anticlockwise flow. To check the code behaviour, predictions were carried out with the HHVC orientation with steady state anticlockwise flow as the initial condition. As expected the anticlockwise direction is found to be unstable leading to stable clockwise flow following an auto-flow reversal (see Fig. 62).

9.10 Closure

The existence of different oscillatory flow regimes and a conditionally stable region could be established with the help of the non-linear stability analysis. The mechanisms proposed for the unidirectional and bi-directional pulsing could also be verified.

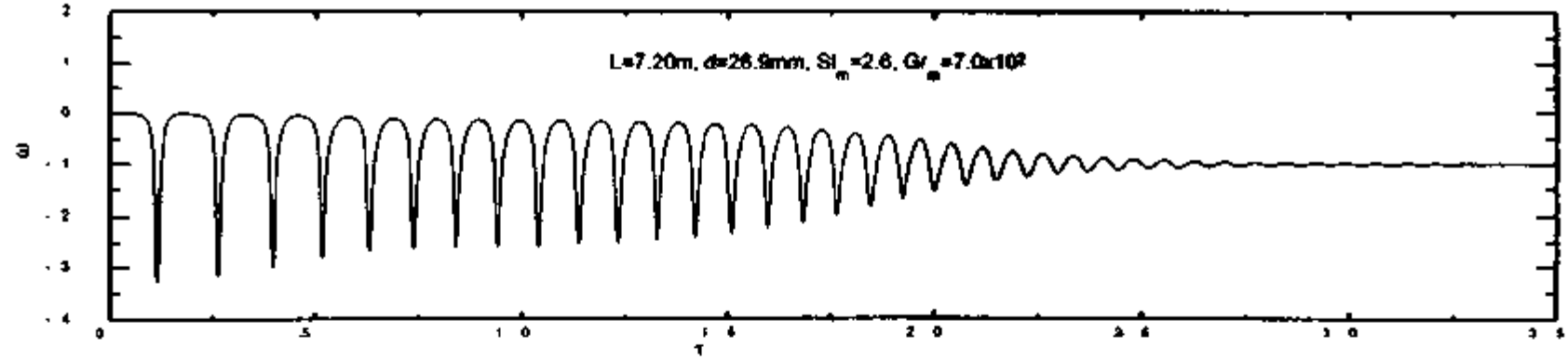

(a) Stable start-up

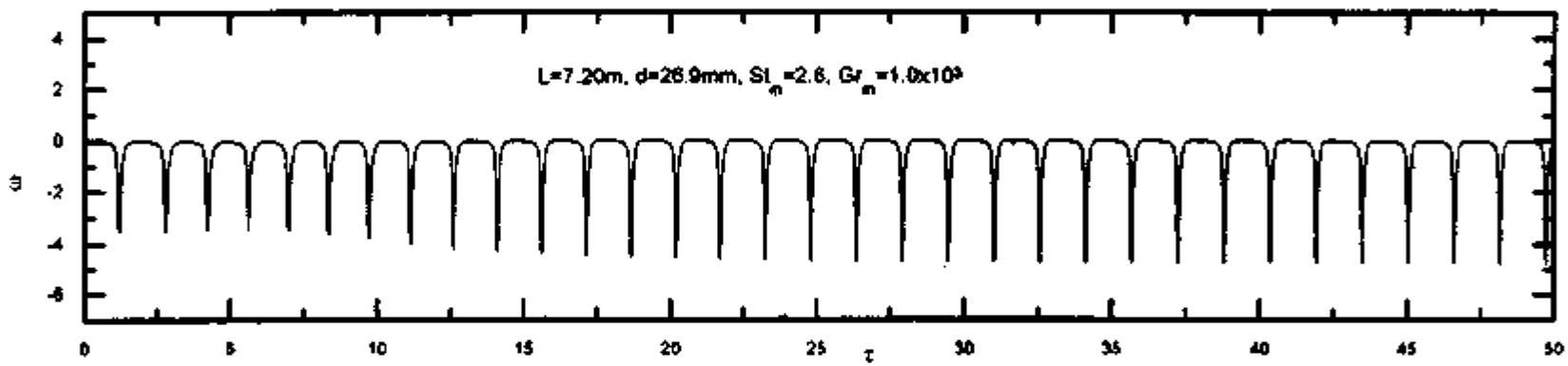

(b) Unidirectional pulsing flow

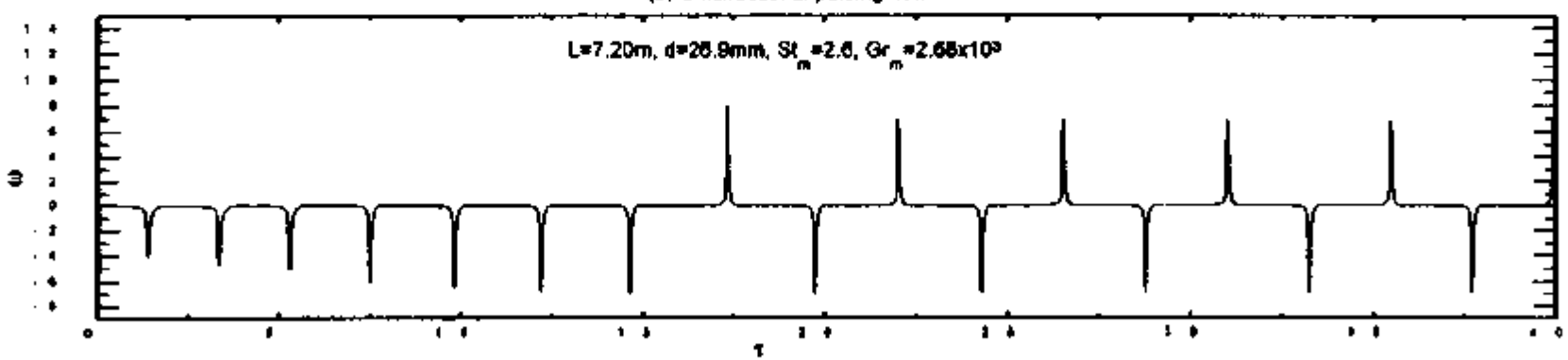

(c) Switching to bidirectional pulsing

Fig 60 : Various flow regimes for start-up from rest with anticlockwise flow

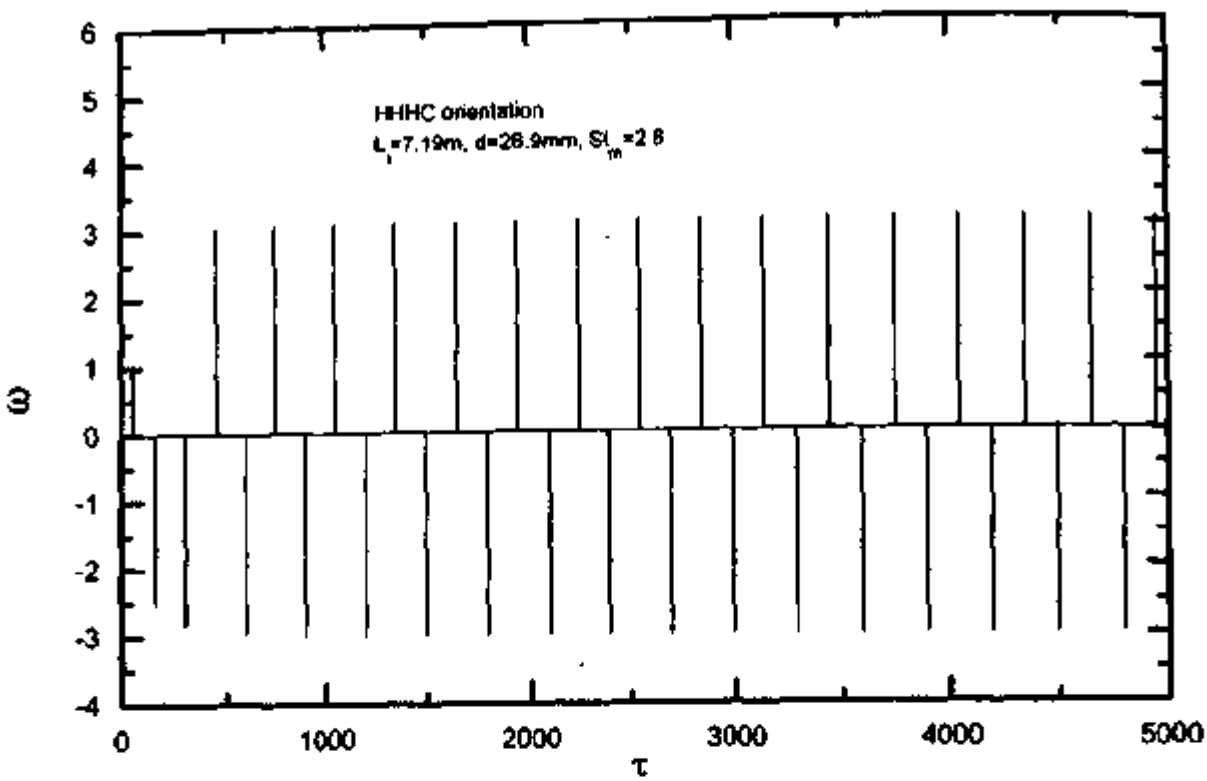

(a) Unstable behaviour for Gr_m reduced from $6.7x10^7$ to $4.69x10^5$ at τ=50

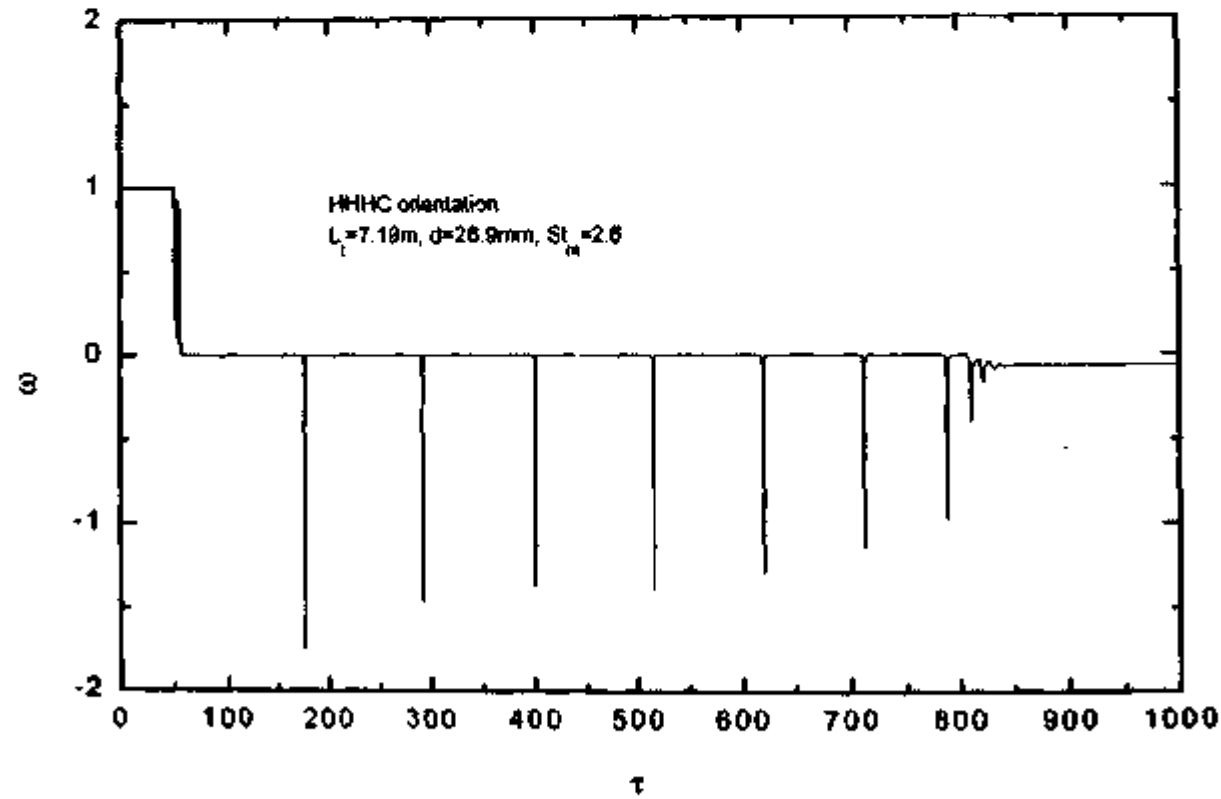

(b) Stable behaviour for Gr_m reduced from $6.7x10^7$ to $2.68x10^5$ at τ=50

Fig. 61: Typical results for decay of instability due to power step back

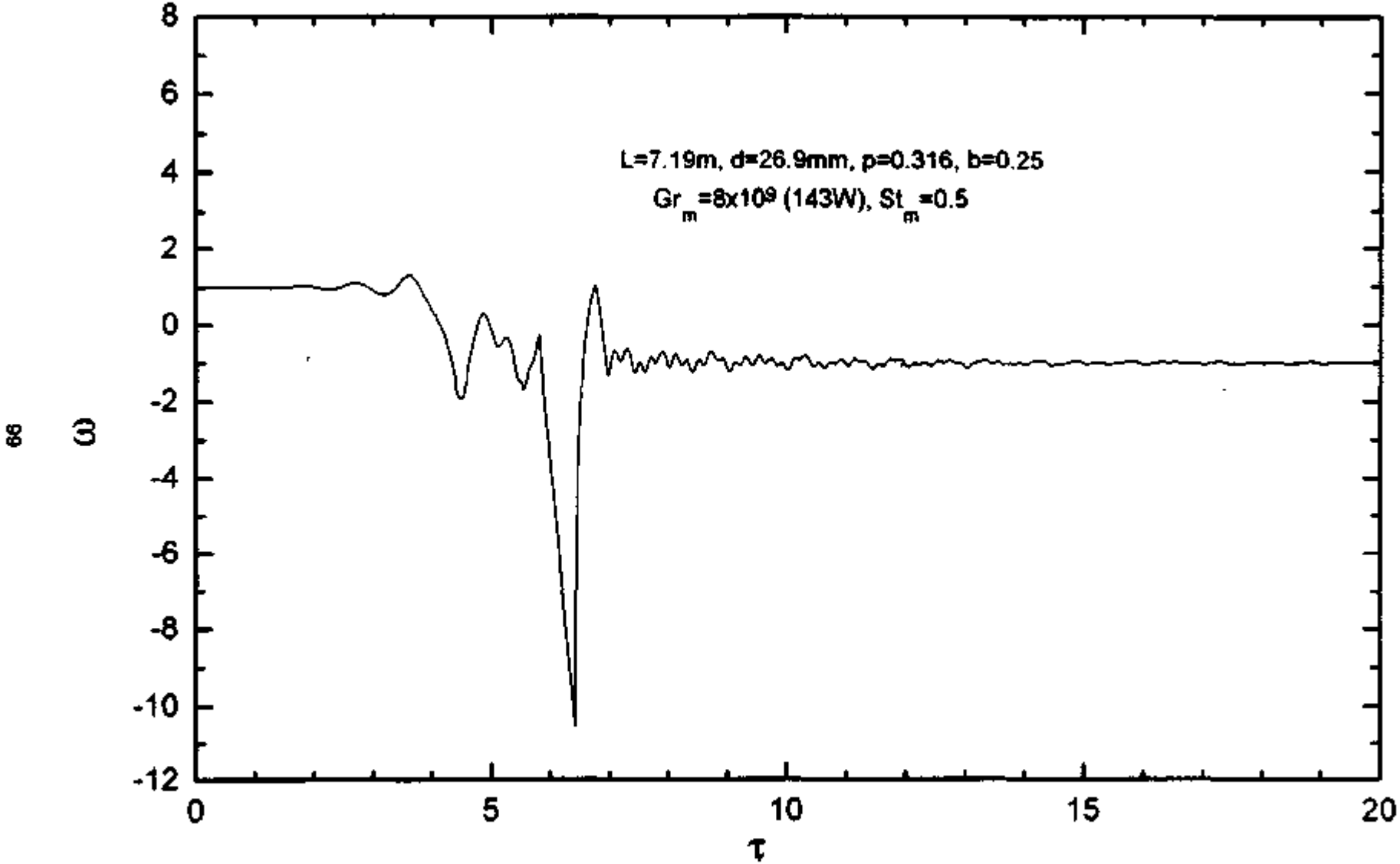

Fig. 62: Autoflow reversal for HHVC orientation with initial steady anticlockwise flow

10. CONCLUSIONS

This report deals with the experimental investigations on the single-phase natural circulation in a rectangular loop with emphasis on the following topics

1) Validation of generalised correlation for the steady state flow for different orientations of the heater and cooler

2) Experimental investigations on the start-up transients with different orientations of the heater and cooler

3) Effect of heater and cooler orientation and heat addition paths on the stability

4) Characteristics of the unstable flow regimes,

5) Linear stability analysis to study the parametric effects of heater and cooler orientations, heater and cooler length and length to diameter ratio

6) Nonlinear stability analysis for the horizontal heater and cooler orientation using the finite difference technique to understand the mechanism leading to the unstable behaviour

10.1 Validation of the Generalised Correlation

The generalised correlations for the steady state flow in single-phase NCLs were tested with experimental data generated in the present loop for the following orientations of heater and cooler

1) Horizontal Heater and Horizontal Cooler (HHHC)
2) Horizontal Heater and Vertical Cooler (HHVC)
3) Vertical Heater and Horizontal Cooler (VHHC)
4) Vertical Heater and Vertical Cooler (VHVC)

The same generalised correlation is found to be valid for all the orientations of the heater and the cooler Linear approximation for the variation of temperature in the cooler is adequate for all orientations as it leads to less than 1% error The experimental steady state data belonged to both laminar and turbulent regimes in the following parameter range

$2.5 \times 10^7 < Gr_m/N_G < 9.2 \times 10^9$ and $735 < Re_m < 11614$

10.2 Start-up Transients

The nature of flow initiation transient in horizontal and vertical heating is observed to be different In vertical heating, a temperature difference between the vertical legs and hence a buoyancy force is created almost instantaneously following the application of heating However, in horizontal heating the flow initiates after considerable dead time, which depends upon the applied power For the HHVC orientation, stable steady state was observed only with flow in the clockwise direction Even if the flow initiated in the counter clockwise direction, it was found to reverse leading to stable clockwise flow

10.3 Conditionally Stable Regime

Instability was observed only for the HHHC orientation. The existence of a metastable (also known as conditionally stable) regime was confirmed, where the instability threshold depends on the path followed to vary the heater power. In the present experiments, conditionally stable regime was observed for 65 W < heater power < 270 W and above 270 W the system was unconditionally unstable. The heat transport capability of the unstable loop is found to be inferior to the stable loop in the conditionally stable region.

The significance of the conditionally stable regime is that a theoretically obtained stability threshold (by the linear analysis) alone is not sufficient to ensure adequate stability margin. To ensure this, an appropriate operating procedure needs to be established. The experiments also show that the amplitude of oscillation for neutrally stable condition for certain heat addition paths is very small. For certain other operating procedures even though the decay ratio is much less than unity, the amplitude of oscillation is much larger. Thus with certain operating procedures it is possible to operate at or very close to the threshold of instability. An operating procedure to avoid instability requires the establishment of the following three thresholds:

a) Maximum power at which the system can be started up from stagnant initial conditions without encountering instability.

b) Maximum step-up in power that is permissible for a given stable steady state operating condition without encountering instability.

c) Minimum step back in power required for achieving stability from an unstable operating condition.

It may be noted that the thresholds mentioned at (a) and (b) above are sufficient to safely operate the system without encountering instability. The third threshold is required to stabilise the system if it enters an unstable zone of operation. Such unintentional landing in an unstable zone can be caused by an operator error or due to an unanticipated transient.

10.4 Natural Circulation Flow Regimes

With proper choice of heat addition paths and the heater power, the following distinctive flow regimes were observed:

1) Stable unidirectional flow,
2) Unidirectional pulsing flow,
3) Chaotic switching between unidirectional and bi-directional pulsing flow,
4) Bidirectional pulsing flow and
5) Compound single-phase two-phase instability.

Flow regimes (2) and (3) mentioned above were not observed when power was raised from a stable steady state. The oscillatory regime observed during the compound instability is bi-directional in nature although the oscillations are increasingly more chaotic. Under compound single-phase two-phase instability also different regimes are observed as described below:

1) Bidirectional pulsing with sporadic boiling,
2) Bidirectional pulsing with subcooled boiling once in every cycle and

3) Bidirectional pulsing with subcooled boiling twice in every cycle

The switchover from unidirectional to the bi-directional pulsing takes place by a near period doubling bifurcation Similarly while switching back from bi-directional to unidirectional pulsing a near period halving is observed For power raising from a stable steady state even period tripling is observed for specific heater power For a given oscillatory mode the frequency was found to increase with power The oscillations of temperature at the inlets of heater and cooler are out-of-phase by almost 180^0

Phase plots for unidirectional pulsing in the ΔP-W plane depict a bean shaped limit cycle whereas for bi-directional pulsing the phase plot is dumbbell shaped With chaotic switching some spread is observed around the dumbbell shaped phase trajectory With inception of subcooled boiling, a dumbbell shaped trajectory with cusps is obtained The shape of the phase trajectory is found to depend on the chosen parameter space

10.5 Stability Analysis

Stability analysis has been carried out for all the four orientations using the linear method. The analysis showed that the orientation with both heater and cooler vertical is most stable and the orientation with both cooler and heater horizontal is least stable For a given heater orientation, the loop with vertical cooler is more stable than the one with horizontal cooler For a specified cooler orientation, the loop with heater vertical is more stable than the one with heater horizontal Effect of the heater and cooler lengths on the stability behaviour was studied using the linear method for the orientation with both heater and cooler horizontal The heater length is found to have only a marginal effect on the stability whereas the effect of cooler length is significant Increasing the length of both heater and cooler is found to enhance stability

Linear and nonlinear analyses using the same boundary conditions give almost identical stability maps With the nonlinear analysis code, it is possible to reproduce the different oscillatory regimes observed in the experiment However, there is significant deviation in the power level at which the different oscillatory regimes are obtained in the experiment and in the prediction Comparison of the data with the predicted stability maps showed that the analysis is conservative (in that it predicts larger unstable zone than experimentally observed)

Another significant finding from the theoretical model as well as the experiment is that the instability is due to thermal stratification, which causes the hot plug to remain stranded just below the elbow in the vertical down leg Therefore, locating the cooler just below the elbow in the vertical down leg enhances stability Other methods to suppress the instability are to enhance the L_f/D and St_m Enhancing the St_m beyond a certain value can completely eliminate the instability However, enhancing the L_f/D can only shift the unstable zone but cannot eliminate it altogether

NOMENCLATURE

A - flow area, m^2
a_r - dimensionless flow area, A_f/A_r
b - constant in equation (2)
C - constant in equation (1)

C_p - specific heat, J/kgK
D - hydraulic diameter, m
d_i - dimensionless hydraulic diameter, D_i/D_r
f - Darcy-Weisbach friction coefficient
g - gravitational acceleration, m/s^2
Gr_m - modified Grashof number, $D^3\rho^2\beta g\Delta T_r/\mu^2$
H - loop height, m
K - local pressure loss coefficient
k - thermal conductivity, W/mK
l_i - dimensionless length, L_i/L_t
L - length, m
N - total number of pipe segments
Nu_m - modified Nusselt number, U_tL_t/k
N_G - dimensionless parameter defined by Eq. (3)
Pr - Prandtl number, $C_p\mu/k$
p - constant in Eq. (2)
Q - total heat input rate, W
r - constant in equation (1)
Re - Reynolds number, $DW/A\mu$
S - dimensionless co-ordinate around the loop, s/H
s - co-ordinate around the loop, m
St_m - modified Stanton number, $4Nu_m/Re_{ss}Pr$
T - temperature, K
ΔT_r - reference temperature difference ($QH/A\mu C_p$), K
W - mass flow rate, kg/s
Δz - centre line elevation difference between cooler and heater, m

Greek Symbols

β - thermal expansion coefficient, K^{-1}
μ - dynamic viscosity, Ns/m^2
θ - dimensionless temperature
ρ_0 - reference density, kg/m^3
τ - dimensionless time
ϕ - dimensionless circulation length, L_t/H
ω - dimensionless mass flow rate

Subscripts

c - cooler
cl - cold leg
e - equivalent
eff - effective
h - heater
hl - hot leg
i - i^{th} segment
r - reference value
ss - steady state
t - total

REFERENCES

Ambrosini, W. and Ferreri, J.C. (1998) The effect of truncation error on the numerical prediction of linear stability boundaries in a natural circulation single-phase loop, Nuclear Engineering and Design *181* 53-76.

Bade, M.H. (2000) Development of generalised correlation for steady state behaviour of single-phase natural circulation loops and investigation on the suppression of instability using helical wire inserts, ME Thesis, Department of Mechanical Engineering, Walchand College of Engineering, Sangli 416 415, Maharashtra, India.

Bau, H.H. and Torrance, K.E. (1981) Transient and steady state behaviour of an open, symmetrically heated, free convection loop, Int. J. Heat Mass Transfer 24 597-609.

Bau, H.H. and Wang, Y. Chaos: a heat transfer perspective, in C.L. Tien (ed.) Annual Review of Heat Transfer, Vol.4, 1992.

Bernier, M.A. and Baliga, B.R (1992) A 1-D/2-D model and experimental results for a closed-loop thermosyphon with vertical heat transfer sections, Int. J. Heat Mass Transfer 35 2969-2982.

Chen, K. (1985) On the Oscillatory Instability of Closed-Loop Thermosyphons, Trans. ASME, J. Heat Transfer 107 826-832.

Creveling, H.F. De Paz, J.Y. Baladi and R.J. Schoenhals, (1975) Stability characteristics of a single-phase free convection loop, J. Fluid Mech. 67 65-84.

D'Auria, F. and Frogheri, M. (1999) Use of a natural circulation flow map for assessing PWR performance, Misale, M and Mayinger F (Eds.), 407-416, Proceedings of Eurotherm Seminar N° 63 on Single and Two-phase Natural Circulation, 6-8 September, Genoa, Italy.

Delmastro, D.F, (2000), Thermal-hydraulic aspects of CAREM reactor, IAEA Technical Committee Meeting on Natural circulation data and innovative nuclear power plant design, July 18-21, Vienna, Austria.

Gorman, M, Widmann P.J. and Robbins, K.A, (1986) Nonlinear dynamics of a convection loop: a quantitative comparison of experiment with theory, Physica D 19 255-267.

Guteeva, L.V., Egorov, V.V, Kuul' V.S, Malamud V.A, Mitenkov F.M, and Samoilov O.B. (1989) Realisation of AST-500 Plant passive safety principles, IAEA TCM on Passive safety features in current and future water-cooled reactors, March 21-24, Moscow, USSR.

Hart J.E (1984), A new analysis of the closed loop thermosyphon, Int. J. Heat Mass Transfer, 27, pp. 125-136

Hart J. E. (1985), A note on the loop thermosyphon with mixed boundary conditions, Int. J. Heat Mass Transfer, 28 pp.939-947.

Ho, C.J, Chiou, S.P. and Hu, C.S (1997) Heat transfer characteristics of a rectangular natural circulation loop containing water near its density extreme, Int. J Heat Mass Transfer, Vol 40 3553-3558

Holman J.P and Boggs, J.H. (1960) Heat transfer to freon 12 near the critical state in a natural circulation loop, J. Heat Transfer 82 221-226.

Huang, B.J. and R. Zelaya (1988) Heat transfer behaviour of a rectangular thermosyphon loop, J. Heat Transfer 110 487-493.

Kapitaniak, T, Chaos for engineers, Theory, applications and control, p 69-86, 2nd revised edition, Springer - Verlag, Berlin 2000.

Keller, J.B. (1966) Periodic oscillations in a model of thermal convection, J. Fluid Mech. Vol. 26, pp. 599-606.

Lorenz E.N, 1963, Deterministic non-periodic flow, J. atmos. Sci 20, 130-141.

Misale, M, Frogheri M and D'Auria F, Experiments in natural circulation: Influence of scale factor on the stability behaviour, Misale, M and Mayinger F (Eds.), 109-114, Proceedings of Eurotherm Seminar N° 63 on Single and Two-phase Natural Circulation, 6-8 September 1999, Genoa, Italy.

Misale, M, Frogheri, M and Ruffino, P (1998) Steady-state and stability behaviour of a single-phase natural circulation loop, *Heat Transfer 1998, Proceedings of 11th IHTC, vol. 3 August* 23-28, Kyongju, Korea.

Misale, M. Tagliafico, L. and Tanda, G. (1991) Experiments in a free convection rectangular loop. Proceedings of the fourth International Symposium on Transport phenomena in heat and mass transfer, Sydney (Australia), 14-19 July, p. 203-211.

Nishihara, T. (1997) Oscillatory instability of a single-phase natural circulation loop, NURETH-8, Kyoto, Japan, *September 30-October 4.*

Streeter, V.L. and Wylie, E.B. Fluid Mechanics, p. 243-245, McGraw-Hill Book Company, Singapore, 1983.

Vijayan, P.K. Investigations on the single-phase thermosyphon phenomenon in a figure-of-eight loop relevant to pressurised heavy water reactors, Ph. D. thesis, Indian Institute of Technology, Bombay, 1988.

Vijayan, P.K. Experimental observations on the general trends of the steady state and stability behaviour of single-phase natural circulation loops, Invited talk, M. Misale and F.Mayinger, (Eds.) 3-16, 1999, Proceedings of EUROTHERM SEMINAR N°. 63 on Single and Two-Phase Natural Circulation, 6-8 September 1999, Genoa, Italy.

Vijayan P.K, H.Austregesilo and V. Teschendorff (1995) 'Simulation of the unstable oscillatory behaviour of single-phase natural circulation with repetitive flow reversals in a rectangular loop using the computer code ATHLET', Nuclear Engineering Design 155 623-641.

Vijayan, P.K and Austregesilo, H. (1994) Scaling laws for single-phase natural circulation loops, Nuclear Engineering and Design 152 331-347.

Vijayan, P.K and Date A W (1992) The limits of conditional stability for single-phase natural circulation with throughflow in a figure-of-eight loop, Nucl. Eng. Des. 136 361-380.

Vijayan, P.K, Nayak, A.K, Pilkhwal, D.S, Saha, D. and Venkat Raj, V (1992) Effect of loop diameter on the stability of single-phase natural circulation in rectangular loops, Proc. 5th Int. Topical Meet. on Reactor Thermalhydraulics, NURETH-5, Salt Lake City, UT, Vol.1, 261-267.

Welander, P (1967) On the oscillatory instability of a differentially heated loop, J. Fluid Mech. 29 17-30.

Widmann, P.J, Gorman M. and Robbins K.A (1989) Nonlinear Dynamics of a convection loop II. Chaos in laminar and turbulent flows, Physica D 36 157-166.

APPENDIX-1: Derivation of the integral in the momentum equation

The integral in the momentum equation is evaluated in this appendix for the different orientations and flow directions Steady flow in both the clockwise and anticlockwise directions is possible only with horizontal heaters For the HHHC orientation, however, the integral is the same for both flow directions Therefore, the integral is evaluated for both flow directions for the HHVC orientation only

HHHC Orientation

The geometry and coordinate system adopted is shown in Fig A-1 1 L_1, L_2, L_3 and L_4 are the lengths of the respective horizontal unheated sections in the figure L_h, L_{hl}, L_c and L_{cl} are respectively the lengths of the heater, hot leg, cooler and cold leg The pipe between end of the heated section and the beginning of the cooled section is the hot leg Similarly, the pipe between the end of the cooler and the beginning of the heater is the cold leg The nondimensional lengths S_h, S_{hl}, S_c and S_{cl} are the cumulative distances from the origin, which is taken as the beginning of the heated section The nondimensional length S_1, S_2, S_3 and S_4 are the cumulative distances from the origin to the four corners of the rectangular loop

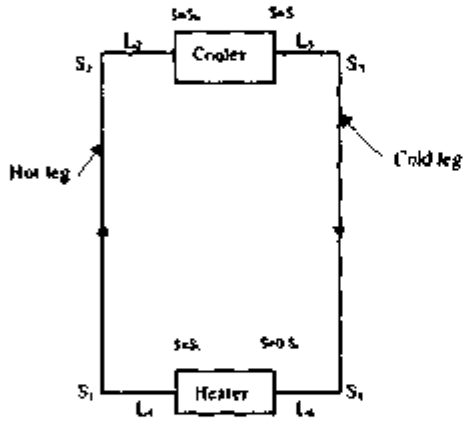

Fig A-1 1 Loop Geometry and co-ordinates for the HHHC orientation

Since dZ=0 for horizontal sections, the integral in the momentum equation can be written as

$$I_{ss} = \oint [\theta(S)]_{ss}\, dZ = \int_{S_2}^{S_3} (\theta_{hl})_{cs}\, dZ + \int_{S_4}^{S_1} (\theta_{cl})_{cs}\, dZ \qquad \text{(A-1 1)}$$

For the upleg dZ=dS and for the downleg dZ = -dS Also, $S_2 = S_1+1$ and $S_4=S_3+1$ since lengths are nondimensionalised using H (i e loop height) Hence

$$\oint [\theta(S)]_{ss}\, dZ = \int_{S_1}^{S_1+1} (\theta_{hl})_{cs}\, dS - \int_{S_3}^{S_3+1} (\theta_{cl})_{cs}\, dS \qquad \text{(A-1 2)}$$

Which can be written as

$$\oint [\theta(S)]_{ss} dZ = (\theta_{hl})_{ss} - (\theta_{cl})_{ss} \qquad \text{(A-1.3)}$$

From equation (A-1.3b) we obtain $(\theta_{hl})_{ss} - (\theta_{cl})_{ss} = 1$. Therefore, for the HHHC orientation we get

$$I_{ss} = \oint [\theta(S)]_{ss} dZ = 1 \qquad \text{(A-1.4)}$$

HHVC Orientation

The geometry and co-ordinate system adopted for the HHVC orientation is given in Fig. A-1.2.

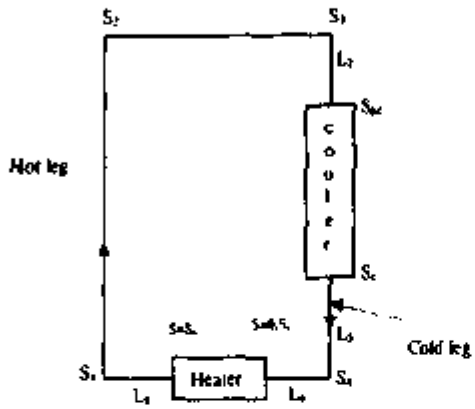

Fig. A-1.2: Loop Geometry and co-ordinates for the HHVC orientation

The integral can be evaluated as

$$I_{ss} = \int_{S_1}^{S_2=1} (\theta_{hl})_{ss} dS - \int_{S_3}^{S_W} (\theta_{hl})_{ss} dS - \int_{S_W}^{S_4} (\theta_{hl})_{ss} e^{\frac{St_m}{\phi}(S_W - S)} dS - \int_{S_4}^{S_1} (\theta_{cl})_{ss} dS \qquad \text{(A-1.5)}$$

After integrating and substituting the limits we get

$$I_{ss} = (\theta_{hl})_{ss} - (\theta_{hl})_{ss} \frac{L_2}{H} + (\theta_{hl})_{ss} \frac{\phi}{St_m} \left[e^{\frac{-St_m L_3}{L_3}} - 1 \right] - (\theta_{cl})_{ss} \frac{L_3}{H} \qquad \text{(A-1.6)}$$

Noting that $\theta_{hl} = \theta_{cl} + 1$ and using equations (A-1.4a) and (A-1.4b) we get

$$I_{ss} = \frac{H - L_2 - L_3}{H\left(e^{\frac{St_m L_3}{L_3}} - 1 \right)} + \left(1 - \frac{L_2}{H} \right) - \frac{L_3}{St_m H} \qquad \text{(A-1.7)}$$

Since $L_c = (H - L_2 - L_3)$, we obtain

$$I_{ss} = \frac{L_c}{H}\left[1 + \frac{1}{e^{\frac{St_m L_c}{L_h}} - 1}\right] + \frac{L_2}{H} - \frac{L_1}{St_m H} = \frac{L_h}{H}\left[\frac{1}{1 - e^{\frac{-St_m L_c}{L_h}}}\right] + \frac{L_2}{H} - \frac{L_1}{St_m H} \qquad \text{(A-1 8)}$$

VHHC Orientation

The loop geometry and co-ordinate system for this case is shown in Fig A-1.3. The integral in the momentum equation can be written as

$$I_{ss} = \int_0^{S_h}\left((\theta_{cl})_{ss} + \frac{H}{L_h}S\right)dS + \int_{S_h}^{S_3}(\theta_{hl})_{ss}\,dS - \int_{S_4}^{S_5}(\theta_{cl})_{ss}\,dS + \int_{S_5}^{S_7}(\theta_{cl})_{ss}\,dS \qquad \text{(A-1.9)}$$

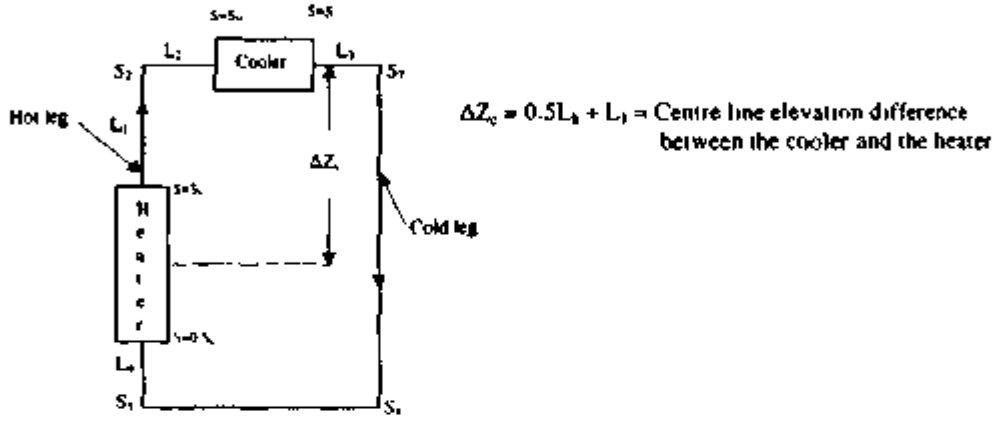

Fig. A-1.3: Loop Geometry and co-ordinates for the VHHC orientation

Integration of Equation (A-1 9) and substituting the limits yields

$$I_{ss} = (\theta_{cl})_{ss}\left(\frac{L_h}{H} - 1 + \frac{L_4}{H} + \frac{L_1}{H}\right) + \frac{L_h}{2H} + \frac{L_1}{H} \qquad \text{(A-1 10)}$$

Where $(\theta_{hl})_{ss} = (\theta_{cl})_{ss}+1$ has been used Noting that $H=L_h+L_1+L_4$ we obtain

$$I_{ss} = \frac{L_1 + 0.5L_h}{H} = \frac{\Delta Z_c}{H} \qquad \text{(A-1.11)}$$

VHVC Orientation

The loop geometry and co-ordinate system for this case is shown in Fig. A-1 4. The integral in the momentum equation can be written as

$$I_{ss} = \int_0^{S_h}\left((\theta_{cl})_{ss} + \frac{H}{L_h}S\right)dS + \int_{S_4}^{S_3}(\theta_{hl})_{ss}\,dS - \int_{S_1}^{S_2}(\theta_{hl})_{ss}\,dS - \int_{S_{hc}}^{S_1}(\theta_{hl})_{ss}\,e^{\frac{St_m(S_{hc}-S)}{L_h}}\,dS - \int_{S}^{S_7}(\theta_{cl})_{ss}\,dS + \int_{S_7}^{S_1}(\theta_{cl})_{ss}\,dS$$

Which on integration and substitution of the limits leads to

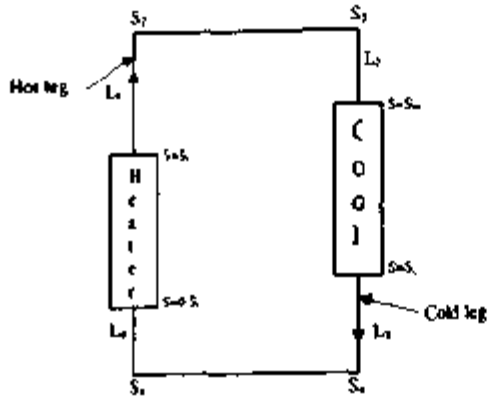

Fig. A-1.4: Loop Geometry and co-ordinates for the VHVC orientation

$$I_{ss} = (\theta_{cl})_{ss}\left(\frac{L_h}{H} - \frac{L_1}{H} + \frac{L_4}{H}\right) + \frac{L_h}{2H} + (\theta_{hl})_{ss}\left(\frac{L_1}{H} - \frac{L_2}{H}\right) + \frac{\phi}{St_m}\left(\frac{e^{\frac{-St_m L_c}{L_c}} - 1}{1 - e^{\frac{-St_m L_c}{L_c}}}\right) \qquad \text{(A-1.12)}$$

Where Eq. (A-1.4b) has been used. Noting that $\theta_{hl} = \theta_{cl}+1$, we obtain

$$I_{ss} = (\theta_{cl})_{ss}\left[\frac{L_h + L_1 + L_4}{H} - \frac{L_1 + L_2}{H}\right] + \frac{0.5L_h + L_1 - L_2 - L_c / St_m}{H} \qquad \text{(A-1.13)}$$

which can be rewritten as

$$I_{ss} = [\theta_{cl}]_{ss}\left[1 - \left(\frac{L_1 + L_2}{H}\right)\right] + \frac{0.5L_h + L_1 - L_2 - L_c / St_m}{H} \qquad \text{(A-1.14)}$$

Which can be rewritten as

$$I_{ss} = \frac{L_c}{H\left(e^{\frac{St_m L_c}{L_c}} - 1\right)} + \frac{0.5L_h + L_1 - L_2 - L_c / St_m}{H} \qquad \text{(A-1.15)}$$

HHVC Orientation with anticlockwise flow

The geometry and coordinates with this flow direction are given in Fig. A-1.5.

$$I_{ss} = \oint [\theta(S)]_{ss}\, dZ = \int_{S_4}^{S_H} (\theta_H)_{ss}\, dS + \int_{S_H}^{S_2} (\theta_{hl})_{ss} e^{\frac{St_m (S_H - S)}{*}} dS + \int_{S_2}^{S_3} (\theta_{cl})_{ss}\, dS - \int_{S_4}^{S_3} (\theta_{cl})_{ss}\, dS \qquad \text{(A-1.16)}$$

Upon integration and substituting the limits we get

$$I_{ss} = (\theta_M)_{ss}\frac{L_2}{H} + \frac{\phi}{St_m}(\theta_M)_{ss}\left(1 - e^{\frac{-St_m L_c}{L}}\right) + (\theta_{cl})_{ss}\left(\frac{L_3}{H} - 1\right) \quad \text{(A-1.17)}$$

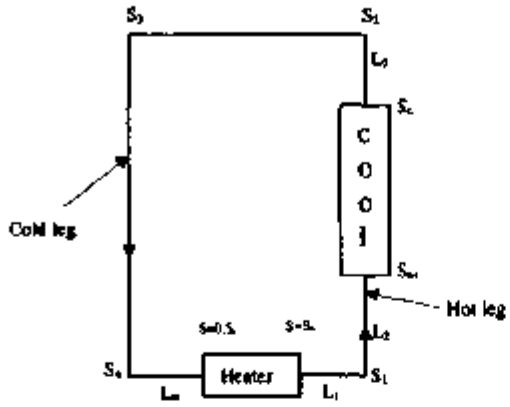

Fig. A-1.5: Loop Geometry and co-ordinates for the HHVC orientation with flow in the anticlockwise direction

Noting that H-(L_1+L_2) =L_c and using equations (A-1.4b) and (A-1.3b) we get

$$I_{ss} = -(\theta_{cl})_{ss}\left(\frac{H - L_2 - L_3}{H}\right) + \frac{L_2}{H} + \frac{L_t}{HSt_m} \quad \text{(A-1.18)}$$

which can be rearranged as

$$I_{ss} = \left(\frac{1}{1 - e^{\frac{St_m L_c}{L}}}\right)\left(\frac{L_c}{H}\right) + \frac{L_2}{H} + \frac{L_t}{HSt_m} \quad \text{(A-1.19)}$$

APPENDIX-2:
Error of the linear temperature approximation in the cooler

It is a usual practice to assume the temperature variation in the cooler to be linear in many analyses of natural circulation The advantage of such an assumption is that the integral in the momentum equation becomes unity if we use the center line elevation difference between the cooler and the heater (ΔZ_c) for nondimensionalisation so that the steady state flow rate can be expressed as

$$Re_{ss} = \left[\frac{2}{p}(Gr_m)_{\Delta Z}\ \frac{D}{L_t}\right]^{\frac{1}{3-b}} \qquad \text{(A-2 1)}$$

Where $(Gr_m)_{\Delta Z_c}$ is based on the ΔZ_c This can be related to the usual Gr_m based on the loop height H by the following equation

$$Re_{ss} = \left[\frac{2}{p} Gr_m \frac{D}{L_t} I_{ss}\right]^{\frac{1}{3-b}} = \left[\frac{2}{p}(Gr_m)_{\Delta Z_c} \frac{D}{L_t}\right]^{\frac{1}{3-b}} \left[\frac{H}{\Delta Z_c} I_{ss}\right]^{\frac{1}{3-b}} \qquad \text{(A 2 2)}$$

It is easy to see that the error of approximation E is given by

$$E = \left[\frac{H}{\Delta Z_c} I_{ss}\right]^{\frac{1}{3-b}} \qquad \text{(A-2 3)}$$

From the above expression, it is easy to see that if E=1, then no error is introduced For both the HHHC (ΔZ_c = H and I_{ss}=1) and VHHC orientation (I_{ss}= ΔZ_c/H) no error would be introduced For the VHVC and HHVC orientations on the other hand some error will be introduced and it would be interesting to quantify it For this we make a plot of the RHS of Eq (A-2 3) against St_m (see figures A-2 1 and A-2 2) While making such a plot the I_{ss} expression derived in Appendix –2 is used For convenience it is reproduced below

$$I_{ss} = \frac{L_c}{H}\left[1 + \frac{1}{e^{\frac{St_m L_t}{L_t}} - 1}\right] + \frac{L_3}{H} - \frac{L_t}{St_m H} \qquad \text{HHVC orientation} \qquad \text{(A-2 4)}$$

$$I_{ss} = \frac{L_t}{H\left(e^{\frac{St_m L_t}{L_t}} - 1\right)} + \frac{0.5L_h + L_3 - L_c - L_t/St_m}{H} \qquad \text{VHVC orientation} \qquad \text{(A-2 5)}$$

From figures A-2 1 and A-2 2 it is found that the error in the approximation is less than 1% for both HHVC and VHVC orientations if the $St_m \leq 1$ The normal operating value in the present test loop is $0.2 < St_m < 0.6$ The error is less than 4% even at St_m=10 However, the plots in figures A-2 1 and A-2 2 were made using the geometric dimensions of the present loop Hence the results cannot be generalized to cover all natural circulation loops

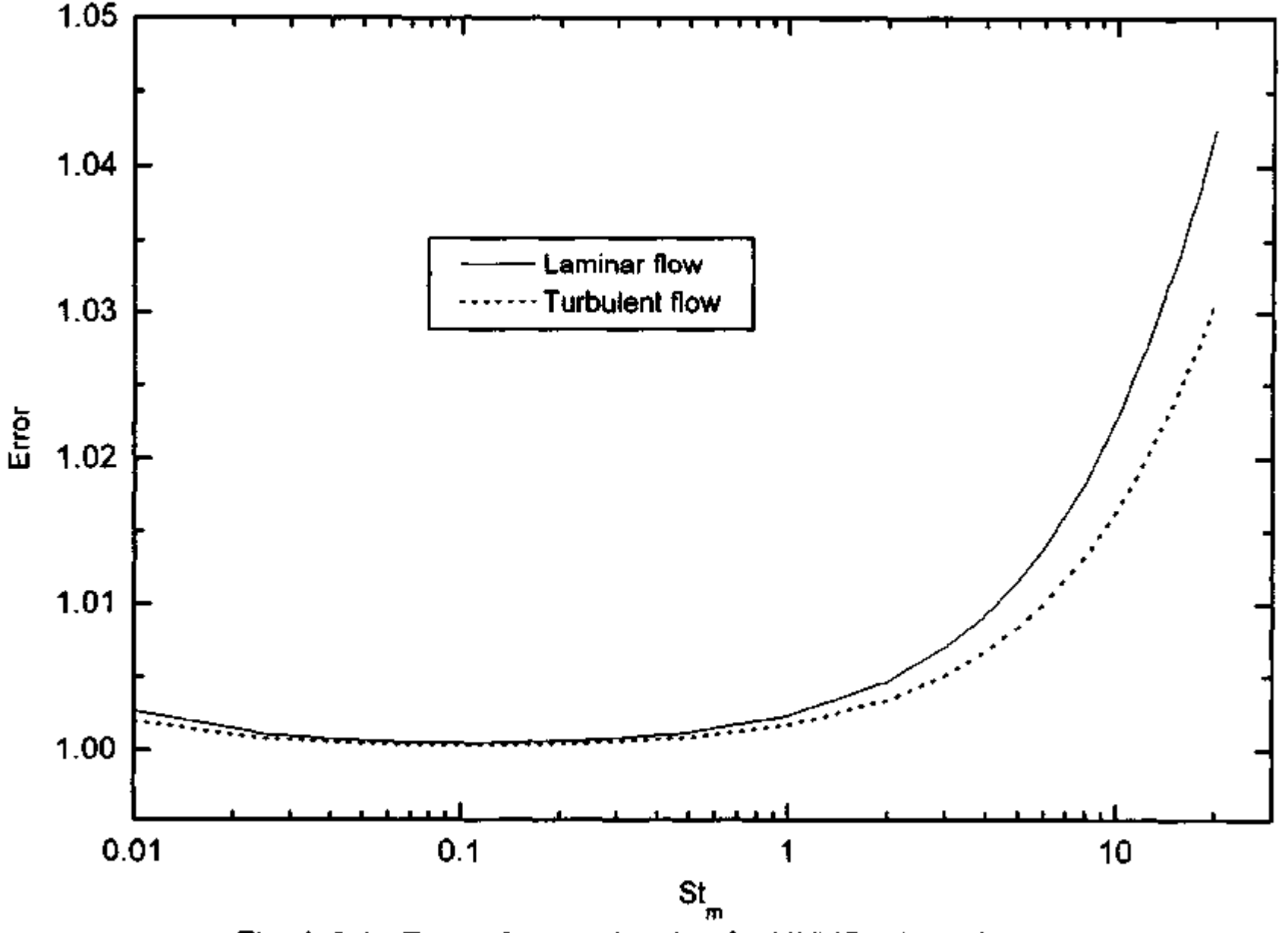

Fig. A-2.1 : Error of approximation for HHVC orientation

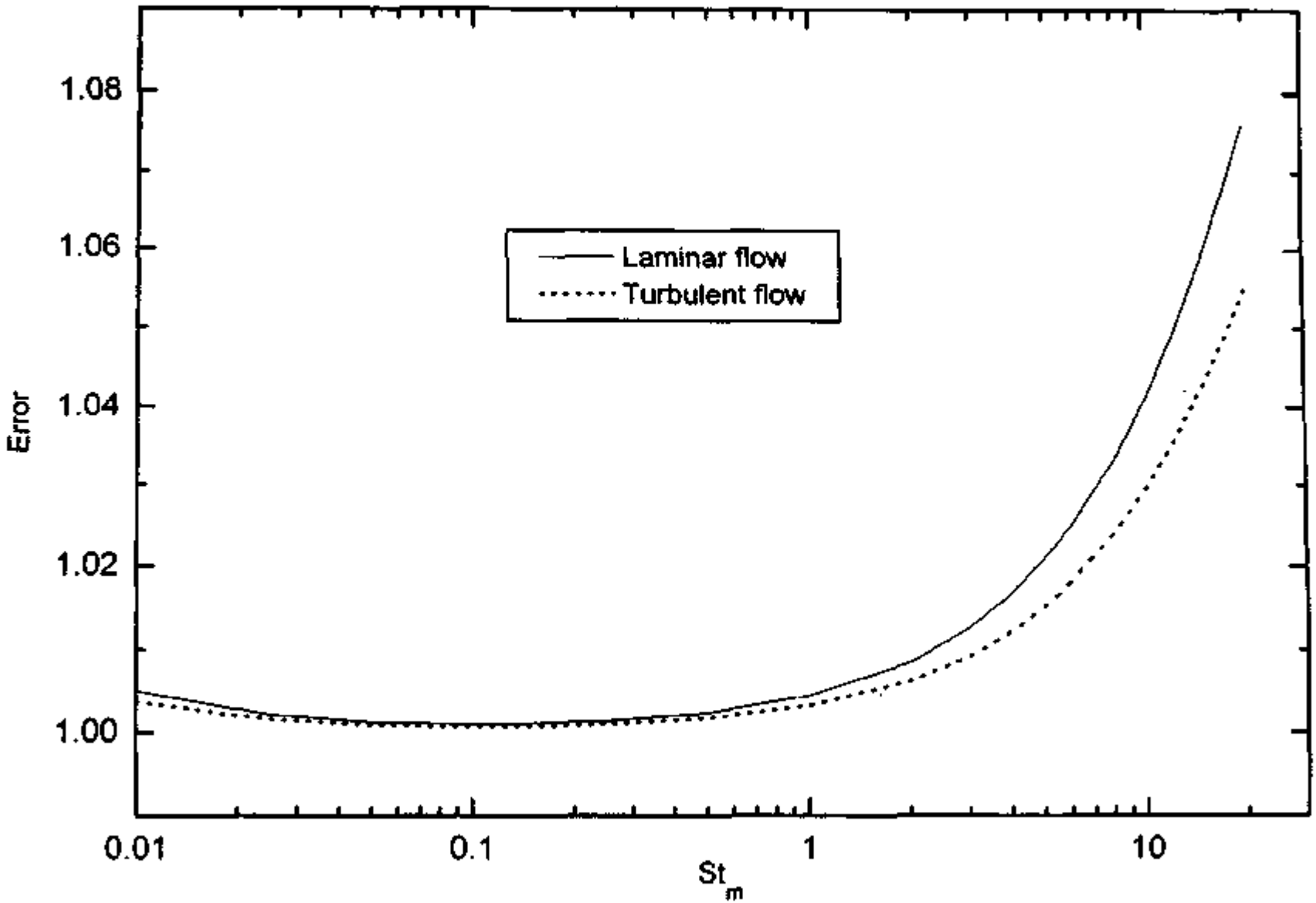

Fig. A-2.2 : Error of approximation for VHVC orientation

APPENDIX-3 :
Steady state experimental data generated for the various orientations of the heater and cooler

For the HHHC orientation (see Table A-3.1) steady state was not possible for powers greater than ≈270 W. For the HHVC orientation, continuous formation of steam bubbles began at the top surface of the horizontal heater leading to subcooled boiling above 600 W. Hence steady state data are available only upto 585 W (see Table A-3.2). For the remaining orientations (i.e. VHHC and VHVC) steady state single-phase natural circulation data were collected upto 1000 W (maximum power in the current experiments) These data are given in Tables A-3.3 and A-3.4 respectively.

Table : A-3.1: Steady state data for the HHHC orientation

Q_h - W	T_m - ^{0}C	ΔT_h - ^{0}C	W_{ss} - kg/s	Gr_m	$Gr_m(D/L_c)$	Re_{ss}
.55000E+02	.29760E+02	57000E+00	.23090E-01	.56258E+10	.21025E+08	13643E+04
.10500E+03	.30880E+02	18000E+01	.13961E-01	11928E+11	.44578E+08	84487E+03
20800E+03	.34700E+02	20800E+01	.23943E-01	33735E+11	.12383E+09	15683E+04
25700E+03	41400E+02	28000E+01	21981E-01	69711E+11	26053E+09	16404E+04
30200E+03	39440E+02	29100E+01	24853E-01	70598E+11	.26384E+09	17872E+04
.30800E+03	42100E+02	18700E+01	.39443E-01	.87992E+11	32885E+09	29823E+04

Table : A-3.2: Steady state data for the HHVC orientation

Q_h - W	T_m - ^{0}C	ΔT_h - ^{0}C	W_{ss} - kg/s	Gr_m	$Gr_m(D/L_c)$	Re_{ss}
.10500E+03	.29750E+02	14400E+01	.17447E-01	.77583E+10	28995E+08	.10307E+04
.21500E+03	.34710E+02	19000E+01	.27091E-01	.24785E+11	.92629E+08	.17748E+04
.29500E+03	.40810E+02	24100E+01	.29313E-01	55360E+11	.20689E+09	.21635E+04
.41400E+03	.46140E+02	27800E+01	.35661E-01	.11401E+12	42608E+09	29015E+04
.53700E+03	.49100E+02	.30500E+01	42155E-01	18043E+12	67430E+09	36119E+04
58500E+03	.54810E+02	.28800E+01	.48614E-01	28157E+12	10523E+10	.45808E+04

Table : A-3.3: Steady state data for the VHHC orientation

Q_h - W	T_m - °C	ΔT_h - °C	W_m - kg/s	Gr_m	$Gr_m(D/L_t)$	Re_m
.10000E+03	.28100E+02	16700E+01	.14325E-01	59578E+10	22266E+08	81641E+03
.15000E+03	.38290E+02	20200E+01	17783E-01	21932E+11	81964E+08	12507E+04
.19800E+03	.32360E+02	13200E+01	35906E-01	17604E+11	65792E+08	22415E+04
.25000E+03	44390E+02	.27000E+01	22172E-01	.57650E+11	.21546E+09	17483E+04
.30800E+03	.40530E+02	.33000E+01	22351E-01	.53546E+11	.20012E+09	16410E+04
.35000E+03	46205E+02	30800E+01	27209E-01	91598E+11	.34233E+09	22164E+04
.42800E+03	45500E+02	41000E+01	.24996E-01	10669E+12	39872E+09	20107E+04
.45300E+03	49730E+02	.31200E+01	34757E-01	15004E+12	56075E+09	30102E+04
.50600E+03	.47900E+02	.39800E+01	.30438E-01	.14855E+12	.55516E+09	25544E+04
.57200E+03	52620E+02	.37200E+01	36800E-01	.22771E+12	.85102E+09	33457E+04
.59500E+03	51560E+02	38700E+01	.36799E-01	.22162E+12	.82824E+09	32872E+04
.63900E+03	.55350E+02	.38600E+01	39607E-01	.30055E+12	.11232E+10	37647E+04
.71000E+03	.56600E+02	39000E+01	.43564E-01	.35981E+12	.13447E+10	42242E+04
.73000E+03	.59100E+02	35400E+01	.49316E-01	.42747E+12	.15976E+10	.49726E+04
80200E+03	58350E+02	.47000E+01	.40810E-01	.44986E+12	.16813E+10	.40674E+04
.84700E+03	.61490E+02	.46100E+01	.43924E-01	.56714E+12	.21195E+10	.45933E+04
.90000E+03	61360E+02	.47500E+01	.45298E-01	.59831E+12	22360E+10	.47277E+04
.95200E+03	.63480E+02	.43900E+01	51829E-01	.71056E+12	26555E+10	55832E+04
.10100E+04	.64600E+02	45900E+01	52579E-01	.80037E+12	.29912E+10	57578E+04

Table : A-3.4: Steady state data for the VHVC orientation

Q_h - W	T_m - °C	ΔT_h °C	W_m - kg/s	Gr_m	$Gr_m(D/L_t)$	Re_m
10500E+03	29400E+02	20000E+01	12561E-01	42266E+10	15796E+08	73646E+03
.15000E+03	.40430E+02	.17500E+01	20527E-01	15407E+11	57581E+08	15042E+04
20600E+03	.34350E+02	.35000E+01	14091E-01	12974E+11	48487E+08	91646E+03
25500E+03	.44820E+02	.27400E+01	.22286E-01	.36086E+11	13486E+09	17710E+04
.30500E+03	.38820E+02	40000E+01	.18260E-01	.27676E+11	10343E+09	12975E+04
.34500E+03	49210E+02	.43700E+01	.18901E-01	.65761E+11	24577E+09	16225E+04
.40500E+03	43540E+02	41600E+01	.23314E-01	.52331E+11	19557E+09	18101E+04
.44800E+03	.53320E+02	47500E+01	.22572E-01	.11089E+12	41441E+09	20759E+04
.51200E+03	.47770E+02	.50650E+01	.24203E-01	.88710E+11	33153E+09	20265E+04
.55200E+03	.57180E+02	.49530E+01	.26661E-01	.17226E+12	64379E+09	.26090E+04
.60500E+03	.53730E+02	42500E+01	.34067E-01	.15357E+12	57394E+09	31543E+04
.64000E+03	.60230E+02	.46400E+01	32986E-01	.23786E+12	.88896E+09	33842E+04
.74000E+03	.63130E+02	54700E+01	.32340E-01	.32271E+12	.12061E+10	34658E+04
.80500E+03	.62400E+02	52200E+01	.36867E-01	.33737E+12	12609E+10	39083E+04
.84500E+03	.66870E+02	54900E+01	36769E-01	44905E+12	16782E+10	.41605E+04
.92200E+03	.65840E+02	.62300E+01	.35367E-01	46449E+12	.17359E+10	39432E+04
.92500E+03	.69030E+02	56800E+01	.38895E-01	54895E+12	20516E+10	45372E+04
.10150E+04	.72380E+02	.64700E+01	37449E-01	71095E+12	26570E+10	45742E+04

APPENDIX-4: Linear Stability analysis

For uniform diameter loops the governing momentum and energy conservation equations in nondimensional form can be expressed as

$$\frac{d\omega}{d\tau} = \frac{Gr_m}{\mathrm{Re}_{ss}^3}\oint\theta\, dZ - \frac{pL_t\omega^{2-b}}{2D\,\mathrm{Re}_{ss}^b} \qquad \text{(A-4.1)}$$

$$\frac{\partial\theta}{\partial\tau} + \phi\omega\frac{\partial\theta}{\partial S} = \frac{L_t}{L_h} \qquad \text{heater (for } 0 < S \le S_h\text{)} \qquad \text{(A-4.2a)}$$

$$\frac{\partial\theta}{\partial\tau} + \phi\omega\frac{\partial\theta}{\partial S} = 0 \qquad \text{pipes (for } S_h < S \le S_{hl} \text{ and } S_c < S \le S_t\text{)} \qquad \text{(A-4.2b)}$$

$$\frac{\partial\theta}{\partial\tau} + \phi\omega\frac{\partial\theta}{\partial S} = -St_m\theta \qquad \text{cooler (for } S_{hl} < S \le S_c\text{)} \qquad \text{(A-4.2c)}$$

Where ϕ is a non-dimensional parameter given by $\phi = L_t / H$. The steady state solution for the momentum and energy equations can be obtained by setting $\omega_{ss} = 1$ and $\partial\omega/\partial\tau = \partial\theta/\partial\tau = 0$. The solution of the energy equation for the various segments of the loop can be written as

$$\theta = \theta_{cl} + \frac{\pi}{L_m} S \qquad \text{heater } (0<S\le S_h) \qquad \text{(A-4.3a)}$$

Where the boundary condition that at S=0, $\theta = \theta_{cl}$ has been used. Similarly for the hot leg (by setting $S=S_h$ in the above equation) we get

$$\theta = \theta_{cl} + 1 = \theta_{hl} \qquad \text{hot leg } (S_h<S\le S_{hl}) \qquad \text{(A-4.3b)}$$

For the cooler we get

$$\theta = \theta_{hl} e^{\frac{St_m}{\phi}(S_{hl}-S)} \qquad \text{cooler } (S_{hl}<S\le S_c \qquad \text{(A-4.3c)}$$

Where the boundary condition that at $S=S_{hl}$, $\theta = \theta_{hl}$ has been used. For the cold leg (by setting that at $S=S_c$, $\theta = \theta_{cl}$) we get

$$\theta = \theta_{hl} e^{\frac{-St_m L_c}{L_t}} = \theta_{cl} \qquad \text{cold leg } (S_c<S\le S_t) \qquad \text{(A-4.3d)}$$

From the above equations explicit equations for the cold leg and hot leg temperatures can be obtained as

$$\theta_{cl} = \frac{1}{e^{\frac{St_m L_c}{L_t}} - 1} \qquad \text{(A-4.4a)}$$

$$\theta_{ss} = \frac{1}{1 - e^{-St_m \frac{L_c}{L_t}}} \qquad \text{(A-4.4b)}$$

The steady state solution of the momentum equation can be written as

$$\mathrm{Re}_{ss} = \left[\frac{2}{p} Gr_m \frac{D}{L_t} I_{ss}\right]^{\frac{1}{3-b}} \qquad \text{(A-4.5)}$$

Where $I_{ss} = \oint \theta_{ss} dZ$. Using Eq. (A-4.3), expressions for I_{ss} applicable for the various orientations can be obtained as given in Appendix-I. The stability analysis is performed by perturbing θ and ω as

$$\theta = \theta_{ss} + \theta' \text{ and } \omega = \omega_{ss} + \omega' \qquad \text{(A-4.6)}$$

Where θ' and ω' are small perturbations over the steady state values. With these substitutions, the perturbed momentum equation can be written as

$$\frac{d\omega'}{d\tau} = \frac{Gr_m}{\mathrm{Re}_{ss}^3} \oint \theta' dZ - \frac{pL_t(2-b)\omega'}{2D\,\mathrm{Re}_{ss}^b} \qquad \text{(A-4.7)}$$

Where $(\omega_{ss} + \omega')^{2-b} = (1 + \omega')^{2-b}$ and was replaced by 1+(2-b)ω' which is valid for small values of ω' (from binomial theorem neglecting the higher order terms). The perturbed energy equation for the various segments of the loop become

$$\frac{\partial \theta'}{\partial \tau} + \phi \frac{\partial \theta'}{\partial S} + \frac{L_t}{L_h}\omega' = 0 \qquad \text{Heater } (0<S\le S_h) \qquad \text{(A-4.8a)}$$

$$\frac{\partial \theta'}{\partial \tau} + \phi \frac{\partial \theta'}{\partial S} = 0 \qquad \text{Pipes } (S_h<S\le S_{ul} \text{ and } S_c<S\le S_t) \qquad \text{(A-4.8b)}$$

$$\frac{\partial \theta'}{\partial \tau} + \phi \frac{\partial \theta'}{\partial S} + St_m(\theta' - \omega'\theta_{ss}) = 0 \qquad \text{Cooler } (S_{ul}<S\le S_c) \qquad \text{(A-4.8c)}$$

The small perturbations ω' and θ' can be expressed as

$$\omega' = \bar{\omega}\varepsilon e^{n\tau} \text{ and } \theta' = \bar{\theta}(S)\varepsilon e^{n\tau} \qquad \text{(A-4.9)}$$

Where ε is a small quantity and n is the stability parameter so that $\partial\theta'/\partial\tau = \bar{\theta}(S)n\varepsilon e^{n\tau}$, $\partial\theta'/\partial S = \varepsilon e^{n\tau}\partial\bar{\theta}(S)/\partial S$ and $d\omega'/d\tau = \bar{\omega}n\varepsilon e^{n\tau}$. Using these in equation (A-4.7) and (A-4.8) we get

$$n\bar{\omega} - \frac{Gr_m}{\mathrm{Re}_{ss}^3} \oint \bar{\theta}(S) dZ - \frac{pL_t(2-b)\bar{\omega}}{2D\,\mathrm{Re}_{ss}^b} = 0 \qquad \text{(A-4.10a)}$$

which can be rewritten as

$$n - \frac{Gr_m}{\mathrm{Re}_{ss}^3}\frac{\bar{I}}{\omega} - \frac{pL_t(2-b)}{2D\mathrm{Re}_{ss}^b} = 0 \qquad \text{(A-4.10b)}$$

Where $\bar{I} = \oint \bar{\theta} dZ$.

$$\frac{d\bar{\theta}(S)}{dS} + \frac{n}{\phi}\bar{\theta}(S) + \frac{L_t\bar{\omega}}{\phi L_h} = 0 \qquad \text{heater } (0<S\leq S_h) \qquad \text{(A-4.11a)}$$

$$\frac{d\bar{\theta}(S)}{dS} + \frac{n}{\phi}\bar{\theta}(S) = 0 \qquad \text{pipes } (S_h<S\leq S_{hl} \text{ and } S_c<S\leq S_t) \qquad \text{(A-4.11b)}$$

$$\frac{d\bar{\theta}(S)}{dS} + \left(\frac{n+St_m}{\phi}\right)\bar{\theta}(S) - \frac{St_m\theta_{ss}\bar{\omega}}{\phi} = 0 \qquad \text{cooler } (S_{hl}<S\leq S_c) \qquad \text{(A-4.11c)}$$

The above equations are of the form $dy/dx + py = Q$, whose solution can be expressed as $ye^{\int pdx} = \int Qe^{\int pdx} + C$. Hence, for each segment of the loop we obtain

$$\bar{\theta}(S) = \left[\bar{\theta}_{cl} + \frac{\bar{\omega}L_t}{nL_h}\right]e^{\frac{-nS}{\phi}} - \frac{L_t}{L_h}\frac{\bar{\omega}}{n} \qquad \text{heater } (0<S\leq S_h) \qquad \text{(A-4.12)}$$

Where the boundary condition that at S=0, $\bar{\theta}(S) = \bar{\theta}_{cl}$ has been used. Similarly we get the following equation for the hot leg

$$\bar{\theta}(S) = \bar{\theta}_h e^{\frac{n}{\phi}(S_h - S)} \qquad (S_h<S\leq S_{hl}) \qquad \text{(A-4.13)}$$

Where the boundary condition that at S=S_h, $\bar{\theta}(S) = \bar{\theta}_h$ has been used. Similarly we get the following equation for the cold leg

$$\bar{\theta}(S) = \bar{\theta}_c e^{\frac{n}{\phi}(S_c - S)} \qquad (S_c<S\leq S_t) \qquad \text{(A-4.14)}$$

Where the boundary condition that at S=S_c, $\bar{\theta}(S) = \bar{\theta}_c$ has been used. For the cooler the following equation can be obtained

$$\bar{\theta}(S) = \frac{\bar{\omega}}{n}St_m(\theta_{hl})_{ss}\left[e^{\frac{St_m}{\phi}(S_{hl}-S)} - e^{\frac{n+St_m}{\phi}(S_{hl}-S)}\right] + \bar{\theta}_{hl}e^{\frac{n+St_m}{\phi}(S_{hl}-S)} \qquad (S_{hl}<S\leq S_c) \qquad \text{(A-4.15)}$$

Where the boundary condition that at S=S_{hl}, $\bar{\theta}(S) = \bar{\theta}_{hl}$ has been used. The parameters $\bar{\theta}_{cl}$, $\bar{\theta}_h$, $\bar{\theta}_c$ and $\bar{\theta}_{hl}$ can be evaluated from the above equations by using appropriate boundary conditions. For example use of the boundary condition that at S=S_h, $\bar{\theta}(S) = \bar{\theta}_h$ in the equation for the heater gives

$$\bar{\theta}_h = \left[\bar{\theta}_{cl} + \frac{\bar{\omega}}{n}\frac{L_c}{L_h}\right] e^{\frac{-nL_h}{L_c}} - \frac{L_c}{L_h}\frac{\bar{\omega}}{n} \qquad \text{(A-4.16a)}$$

Substituting in (A-4.13) we get the following equation for the hot leg

$$\bar{\theta}(S) = \left[\bar{\theta}_{cl} + \frac{\bar{\omega}}{n}\frac{L_c}{L_h}\right] e^{\frac{-nS}{\phi}} - \frac{L_c}{L_h}\frac{\bar{\omega}}{n} e^{\frac{n}{\phi}(S_h - S)} \qquad \text{(for } S_h < S \le S_{hl}\text{)} \qquad \text{(A-4.16b)}$$

At $S = S_{hl}$, $\bar{\theta}(S) = \bar{\theta}_{hl}$. Hence

$$\bar{\theta}_{hl} = \left[\bar{\theta}_{cl} + \frac{\bar{\omega}}{n}\frac{L_c}{L_h}\right] e^{\frac{-n(L_h + L_{hl})}{L_c}} - \frac{L_c}{L_h}\frac{\bar{\omega}}{n} e^{\frac{-nL_{hl}}{L_c}} \qquad \text{(A-4.16c)}$$

Substituting this in the equation for the cooler, we get

$$\bar{\theta}(S) = \frac{\bar{\omega}}{n} St_m (\theta_{hl})_{cl} \left[e^{\frac{St_m}{\phi}(S_{hl} - S)} - e^{\frac{n + St_m}{\phi}(S_{hl} - S)} \right] + \left[\bar{\theta}_{cl} + \frac{\bar{\omega}}{n}\frac{L_c}{L_h}\right] e^{\frac{-(n + St_m)S + St_m S_{hl}}{\phi}}$$

$$- \frac{L_c}{L_h}\frac{\bar{\omega}}{n} e^{\frac{n(S_h - S) + St_m (S_{hl} - S)}{\phi}} \qquad \text{(for } S_{hl} < S \le S_c\text{)} \qquad \text{(A-4.16d)}$$

From the above using the boundary condition that at S=S$_c$, $\bar{\theta}(S) = \bar{\theta}_c$, we get

$$\bar{\theta}_c = \frac{\bar{\omega}}{n} St_m (\theta_{hl})_{cl} \left(e^{\frac{-St_m L_c}{L_c}} - e^{\frac{-(n + St_m)L_c}{L_c}} \right) + \left(\bar{\theta}_{cl} + \frac{\bar{\omega}}{n}\frac{L_c}{L_h} \right) e^{-\left| \frac{St_m L_c + n(L_h + L_{hl} + L_c)}{L_c} \right|}$$

$$- \frac{L_c}{L_h}\frac{\bar{\omega}}{n} e^{\left| \frac{nL_{hl} + (n + St_m)L_c}{L_c} \right|} \qquad \text{(A-4.16e)}$$

Using this in Eq. (A-4.14) the cold leg equation can be written as

$$\bar{\theta}(S) = \frac{\bar{\omega}}{n} St_m (\theta_{hl})_{cl} \left[e^{\frac{St_m (S_{hl} - S_c) + n(S_c - S)}{\phi}} - e^{\frac{St_m (S_{hl} - S_c) + n(S_{hl} - S)}{\phi}} \right] + \left(\bar{\theta}_{cl} + \frac{\bar{\omega}}{n}\frac{L_c}{L_h} \right) e^{\frac{St_m (S_{hl} - S_c) + nS}{\phi}}$$

$$- \frac{L_c}{L_h}\frac{\bar{\omega}}{n} e^{\frac{n(S_c - S) + St_m (S_{hl} - S_c)}{\phi}} \qquad \text{(for } S_c < S \le S_l\text{)} \qquad \text{(A-4.16f)}$$

Using the boundary condition that at S=S$_c$, $\bar{\theta}(S) = \bar{\theta}_{cl}$, we can get the following expression for $\bar{\theta}_{cl}$.

$$\bar{\theta}_{rl} = \frac{\bar{\omega}}{n}\left[\frac{St_m(\theta_{hl})_{ss}\, e^{\frac{n(L_1-L_{sl})}{L_1}}\left(1-e^{\frac{-nL_r}{L_1}}\right)+\frac{L_1}{L_h}\left(1-e^{\frac{nL_h}{L_1}}\right)}{e^{\frac{St_m L_1+nL_h}{L_1}}-1}\right] \qquad \text{(A-4.17a)}$$

From this, $\bar{\theta}_{rl}/\bar{\omega}$ can be written as

$$\frac{\bar{\theta}_{rl}}{\bar{\omega}} = \frac{St_m(\theta_{hl})_{ss}\, e^{\frac{n(L_1-L_{sl})}{L_1}}\left(1-e^{\frac{-nL_r}{L_1}}\right)+\frac{L_1}{L_h}\left(1-e^{\frac{nL_h}{L_1}}\right)}{n\left(e^{\frac{St_m L_1+nL_h}{L_1}}-1\right)} \qquad \text{(A-4.17b)}$$

Expressions for $\bar{\theta}_h/\bar{\omega}$, $\bar{\theta}_{hl}/\bar{\omega}$ and $\bar{\theta}_r/\bar{\omega}$ can be obtained by using the above expression for $\bar{\theta}_{rl}/\bar{\omega}$ in equations (A-4.16a), (A-4.16c) and (A-4.16e) as follows:

$$\frac{\bar{\theta}_h}{\bar{\omega}} = \frac{St_m(\theta_{hl})_{ss}\, e^{\frac{nL_{hl}}{L_1}}\left(e^{\frac{nL_h}{L_1}}-1\right)+\frac{L_1}{L_h}\left(e^{\frac{-nL_h}{L_1}}-1\right)e^{\frac{(St_m L_1+nL_h)}{L_1}}}{n\left(e^{\frac{(St_m L_1+nL_h)}{L_1}}-1\right)} \qquad \text{(A-4.17c)}$$

$$\frac{\bar{\theta}_{hl}}{\bar{\omega}} = \frac{St_m(\theta_{hl})_{ss}\left(e^{n\frac{L_h}{L_1}}-1\right)+\frac{L_1}{L_h}e^{\frac{St_m L_1+n(L_h-L_{hl})}{L_1}}\left(e^{-n\frac{L_h}{L_1}}-1\right)}{n\left(e^{\frac{St_m L_1+nL_h}{L_1}}-1\right)} \qquad \text{(A-4.17d)}$$

$$\frac{\bar{\theta}_r}{\bar{\omega}} = \frac{St_m(\theta_{hl})_{ss}\, e^{n}\left(1-e^{\frac{-nL_r}{L_1}}\right)+\frac{L_1}{L_h}e^{\frac{nL_{sl}}{L_1}}\left(1-e^{\frac{nL_h}{L_1}}\right)}{n\left(e^{\frac{St_m L_1+nL_h}{L_1}}-1\right)} \qquad \text{(A-4.17e)}$$

Using the expressions (A-4.12) to (A-4.15), we can find the integral $\oint\bar{\theta}(S)dZ$. Substituting this in Eq. (A-4.10b) we obtain the characteristic equation for stability. However, the value of the integral is different for different orientations.

HHJC Orientation

For evaluating the integral consider the figure A-1.1 with the various distances marked as shown in the direction of flow. The relations between the various lengths are given below:

$$L_t = L_h + L_M + L_r + L_{sl} = L_h + L_r + 2H + L_1 + L_2 + L_3 + L_4 \qquad \text{(A-4.18)}$$

$$L_{hl} = L_1 + H + L_2 \text{ and } L_{cl} = L_3 + H + L_4 \qquad \text{(A-4.19)}$$

The breadth of the loop, B, can be expressed as

$$B = L_1 + L_h + L_4 = L_2 + L_c + L_3 \qquad \text{(A-4.20)}$$

For generality, the lengths L_1, L_2, L_3 and L_4 are considered to be unequal. The cumulative lengths, s_1, s_2, s_3 and s_4 can be expressed as

$$s_1 = L_h + L_1 \; ; \; s_2 = s_1 + H \; ; \; s_3 = s_2 + B = s_c + L_3 = L_h + L_{hl} + L_c + L_3 \; \& \; s_4 = s_3 + H \qquad \text{(A-4.21)}$$

The nondimensional lengths S_2 and S_4 can be expressed as

$$S_2 = S_1 + 1 \text{ and } S_4 = S_3 + 1 \qquad \text{(A-4.22)}$$

The integral $\oint \bar{\theta}(S)\, dZ$ can be expressed as

$$\oint \bar{\theta}(S)\, dZ = \int_{S_1}^{S_2} \left\{\bar{\theta}(S)\right\}_{hot\ leg} dZ + \int_{S_3}^{S_4} \left\{\bar{\theta}(S)\right\}_{cold\ leg} dZ \qquad \text{(A-4.23)}$$

For the hot leg dZ=dS and for the cold leg dZ= -dS. Hence, using (A-4.13) and (A-4.14) we can obtain

$$\oint \bar{\theta}(S)\, dZ = \int_{S_1}^{S_1+1} \bar{\theta}_h e^{-\frac{n(S_1 - S)}{\phi}}\, dS - \int_{S_3}^{S_3+1} \bar{\theta}_c e^{-\frac{n(S_3 - S)}{\phi}}\, dS \qquad \text{(A-4.24)}$$

Integrating and substituting the limits yield

$$\oint \bar{\theta}(S)\, dZ = \frac{\phi}{n}\left(1 - e^{-\frac{n}{\phi}}\right)\left\{\bar{\theta}_h e^{-\frac{nl_2}{l_c}} - \bar{\theta}_c e^{-\frac{nl_1}{l_c}}\right\} \qquad \text{(A-4.25)}$$

$$\frac{\bar{I}}{\omega} = \frac{1}{\omega}\oint \bar{\theta}(S)\, dZ = \frac{\phi}{n}\left(1 - e^{-\frac{n}{\phi}}\right)\left\{\frac{\bar{\theta}_h}{\omega} e^{-\frac{nl_2}{l_c}} - \frac{\bar{\theta}_c}{\omega} e^{-\frac{nl_1}{l_c}}\right\} \qquad \text{(A-4.26)}$$

$\bar{\theta}_h / \bar{\omega}$ and $\bar{\theta}_c / \bar{\omega}$ are obtained from Eq. (A-4.17c) and (A-4.17e) respectively. If $L_1 = L_2 = L_c$, then this reduces to

$$\frac{\bar{I}}{\omega} = \frac{1}{\omega}\oint \bar{\theta}(S)\, dZ = \frac{\phi}{n}\left(1 - e^{-\frac{n}{\phi}}\right)\left(e^{-\frac{nl_c}{l_c}}\right)\left\{\frac{\bar{\theta}_h - \bar{\theta}_c}{\bar{\omega}}\right\} \qquad \text{(A-4.27)}$$

Using Eqs (A-4.17c) and (A-4.17e), the following expression for $(\bar{\theta}_h - \bar{\theta}_c)/\bar{\omega}$ can be obtained as

$$\frac{\bar{\theta}_h - \bar{\theta}_c}{\bar{\omega}} = \frac{St_m(\theta_{hl})_{in}\left\{e^{\frac{nl_{hl}}{l_c}}\left(e^{\frac{nl_c}{l_c}} - 1\right) - e^{n}\left(1 - e^{-\frac{nl_c}{l_c}}\right)\right\} + \frac{l_{cl}}{l_h}\left\{e^{\frac{(l_h + l_{hl} + nl_c}{l_c}}\left(e^{-\frac{nl_h}{l_c}} - 1\right) - e^{\frac{nl_{cl}}{l_c}}\left(1 - e^{\frac{nl_h}{l_c}}\right)\right\}}{n\left(e^{\frac{St_m l_c + nl_c}{l_c}} - 1\right)}$$

HHVC Orientation

Refer to Fig. A-1.2 for the geometry and co-ordinate system considered. For S_1 to S_2 dZ = dS, and for S_3 to S_4, dZ= - dS. Hence

$$\oint\bar{\theta}(S)dZ = \int_{S_1}^{S_1+1}\bar{\theta}_h e^{\frac{n(S_h-S)}{\phi}}dS - \int_{S_2}^{S_h}\bar{\theta}_h e^{\frac{n(S_h-S)}{\phi}}dS - \int_{S_4}^{S_t}\bar{\theta}_{hl} e^{\frac{n+St_m(S_{hl}-S)}{\phi}}dS - \frac{\bar{\omega}}{n}St_m(\theta_{hl})_{ll}\int_{S_{hl}}^{S_t}\left(e^{\frac{St_m(S_{hl}-S)}{\phi}} - e^{\frac{n+St_m(S_{hl}-S)}{\phi}}\right)dS - \int_{S_t}^{S_3}\bar{\theta}_c e^{\frac{n(S_c-S)}{\phi}}dS \quad \text{(A-4.28)}$$

On integration and substitution of limits yield the following equation for $\bar{I}/\bar{\omega}$.

$$\frac{\bar{I}}{\bar{\omega}} = \frac{\bar{\theta}_h}{\bar{\omega}}\frac{\phi}{n}\left\{e^{\frac{-nL_t}{L_t}}\left(1-e^{\frac{-n}{\phi}}\right)+e^{\frac{-nL_{hl}}{L_t}}\left(1-e^{\frac{nL_h}{L_t}}\right)\right\}+\frac{\phi}{n}(\theta_{hl})_{ll}\left\{e^{\frac{-St_mL_t}{L_t}}-1+\frac{St_m}{n+St_m}\left(1-e^{-\left(\frac{n+St_m}{L_t}\right)L_t}\right)\right\}$$

$$+\frac{\bar{\theta}_{hl}}{\bar{\omega}}\left(\frac{\phi}{n+St_m}\right)\left[e^{\frac{-(n+St_m)L_h}{L_t}}-1\right]+\frac{\bar{\theta}_c}{\bar{\omega}}\frac{\phi}{n}\left[e^{\frac{-nL_3}{L_t}}-1\right] \quad \text{(A-4.29)}$$

The parameters $\bar{\theta}_h/\bar{\omega}$, $\bar{\theta}_{hl}/\bar{\omega}$, and $\bar{\theta}_c/\bar{\omega}$ are evaluated using equations (A-4.17c), (A-4.17d) and (A-4.17e) respectively.

VHHC Orientation

Refer to Fig. A-1.3 for the geometry and co-ordinate system considered. For S_1 to S_2 dZ = dS, and for S_3 to S_4, dZ= - dS. Hence,

$$\oint\bar{\theta}(S)dZ = \int_0^{S_t}\left[\left(\bar{\theta}_{cl}+\frac{\bar{\omega}}{n}\frac{L_t}{L_h}\right)e^{\frac{-nS}{\phi}}-\frac{\bar{\omega}}{n}\frac{L_t}{L_h}\right]dS+\int_{S_h}^{S_t}\bar{\theta}_h e^{\frac{n(S_h-S)}{\phi}}dS-\int_{S_3}^{S_3+1}\bar{\theta}_c e^{\frac{n(S_c-S)}{\phi}}dS$$

$$+\int_{S_1}^{S_t}\bar{\theta}_c e^{\frac{n(S_c-S)}{\phi}}dS \quad \text{(A-4.30)}$$

$$\frac{\bar{I}}{\bar{\omega}} = \frac{\bar{\theta}_{cl}}{\bar{\omega}}\frac{\phi}{n}\left(1-e^{\frac{-nL_h}{L_t}}\right)+\frac{L_t}{nL_h}\left\{\frac{\phi}{n}\left(1-e^{\frac{-nL_h}{L_t}}\right)-\frac{L_h}{H}\right\}+\frac{\bar{\theta}_h}{\bar{\omega}}\frac{\phi}{n}\left[1-e^{\frac{-nL_h}{L_t}}\right]$$

$$+\frac{\bar{\theta}_c}{\bar{\omega}}\frac{\phi}{n}\left[\frac{e^{\frac{-nH}{L_t}}-1}{e^{\frac{nL_3}{L_t}}}+\frac{e^{\frac{nL_h}{L_t}}-1}{e^{\frac{nL_{hl}}{L_t}}}\right] \quad \text{(A-4.31)}$$

The parameters $\bar{\theta}_{cl}/\bar{\omega}$, $\bar{\theta}_h/\bar{\omega}$ and $\bar{\theta}_c/\bar{\omega}$ are evaluated using equations (A-4.17b), (A-4.17c) and (A-4.17e) respectively.

VHVC Orientation

Refer to Fig A-1.4 for the geometry and co-ordinate system considered. For S_1 to S_2 dZ = dS, and for S_3 to S_4, dZ= - dS. Hence,

$$\bar{I} = \int_0^{S_1}\left\{\left(\bar{\theta}_{c1} + \frac{\bar{\omega}}{n}\frac{L_c}{L_h}\right)e^{\frac{-nS}{\phi}} - \frac{\bar{\omega}}{n}\frac{L_c}{L_h}\right\}dS + \int_{S_2}^{S_3}\bar{\theta}_h e^{\frac{n}{\phi}(S_3-S)}dS - \int_{S_1}^{S_M}\bar{\theta}_h e^{\frac{n}{\phi}(S_2-S)}dS$$

$$-\int_{S_M}^{S_4}\left\{\frac{\bar{\omega}}{n}St_m(\theta_M)_{s1}\left(e^{\frac{St_m(S_M-S)}{\phi}} - e^{\frac{n+St_m}{\phi}(S_M-S)}\right) + \bar{\theta}_M e^{\frac{(n+St_m)}{\phi}(S_M-S)}\right\}dS - \int_{S_4}^{S_3}\bar{\theta}_c e^{\frac{n}{\phi}(S_c-S)}dS$$

$$-\int_{S_3}^{S_2}\bar{\theta}_c e^{\frac{n}{\phi}(S_c-S)}dS \qquad \text{(A-4.32)}$$

After integration and substitution of limits we obtain

$$\frac{\bar{I}}{\bar{\omega}} = \frac{\bar{\theta}_{c1}}{\bar{\omega}}\frac{\phi}{n}\left(1-e^{\frac{-nL_h}{L_t}}\right) + \frac{L_t^2}{n^2L_hH}\left(1-e^{\frac{-nL_h}{L_t}} - \frac{nL_h}{L_t}\right) + \frac{\bar{\theta}_h}{\bar{\omega}}\frac{\phi}{n}\left[1-e^{\frac{-nL_1}{L_t}} + e^{\frac{-nL_M}{L_t}}\left(1-e^{\frac{-nL_2}{L_t}}\right)\right] +$$

$$\frac{\phi(\theta_M)_{s1}}{n(n+St_m)}\left[n\left(e^{\frac{-St_mL_c}{L_t}}-1\right) + St_m e^{\frac{-St_mL_c}{L_t}}\left(1-e^{\frac{-nL_c}{L_t}}\right)\right] + \frac{\bar{\theta}_M}{\bar{\omega}}\frac{\phi}{n+St_m}\left[e^{\frac{-(n+St_m)L_c}{L_t}}-1\right] +$$

$$\frac{\bar{\theta}_c}{\bar{\omega}}\frac{\phi}{n}\left\{e^{\frac{-nL_3}{L_t}} - 1 + e^{\frac{-nL_c}{L_t}}\left(e^{\frac{nL_c}{L_t}}-1\right)\right\} \qquad \text{(A-4.33)}$$

The parameters $\bar{\theta}_{c1}/\bar{\omega}$, $\bar{\theta}_h/\bar{\omega}$, $\bar{\theta}_M/\bar{\omega}$ and $\bar{\theta}_c/\bar{\omega}$ are evaluated using equations (A-4.17b), (A-4.17c), (A-4.17d) and (A-4.17e) respectively.

HHVC Orientation with anticlockwise flow

Refer to Fig. A-1.5 for the geometry and co-ordinate system considered. For S_1 to S_2 dZ = dS, and for S_3 to S_4, dZ= - dS. Hence,

$$\oint\bar{\theta}(S)dZ = \int_{S_1}^{S_M}\bar{\theta}_h e^{\frac{n}{\phi}(S_2-S)}dS + \int_{S_M}^{S_2}\left\{\frac{\bar{\omega}}{n}St_m(\theta_M)_{s1}\left(e^{\frac{St_m(S_M-S)}{\phi}} - e^{\frac{n+St_m}{\phi}(S_M-S)}\right) + \bar{\theta}_M e^{\frac{(n+St_m)}{\phi}(S_M-S)}\right\}dS$$

$$+\int_{S_2}^{S_3}\bar{\theta}_c e^{\frac{n}{\phi}(S_c-S)}dS = \int_{S_3}^{S_{1'}}\bar{\theta}_c e^{\frac{n}{\phi}(S_c-S)}dS \qquad \text{(A-4.34)}$$

After integration and substitution of the limits and simplifying we obtain

$$\frac{\bar{I}}{\bar{\omega}} = \frac{\bar{\theta}_h}{\bar{\omega}}\frac{\phi}{n}e^{\frac{-nL_2}{L_1}}\left(1-e^{\frac{-nL_2}{L_1}}\right)+\frac{\phi}{n}\frac{(\theta_N)_{ss}}{n+St_m}\left\{n\left(1-e^{\frac{-St_m L_2}{L_1}}\right)-St_m e^{\frac{-St_m L_2}{L_1}}\left(1-e^{\frac{-nL_2}{L_1}}\right)\right\}$$

$$+\frac{\bar{\theta}_c}{\bar{\omega}}\frac{\phi}{n}\left\{1-e^{\frac{-nL_2}{L_1}}+\left(1-e^{\frac{-n}{\phi}}\right)e^{\frac{-n}{L_1}(L_2+L_1+L_3+L_4)}\right\}+\frac{\bar{\theta}_M}{\bar{\omega}}\frac{\phi}{n+St_m}\left(1-e^{\frac{-(n+St_m)L_2}{L_1}}\right) \qquad \text{(A-4.35)}$$

The parameters $\bar{\theta}_h/\bar{\omega}$, $\bar{\theta}_N/\bar{\omega}$ and $\bar{\theta}_c/\bar{\omega}$ are evaluated using equations (A-4.17c), (A-4.17d) and (A-4.17e) respectively.

APPENDIX – 5: Nonlinear stability analysis

Nonlinear stability analysis is carried out using the finite difference method by solving the nonlinear governing equations directly. Before the calculations can commence the loop is divided into a number of small segments. A node separates two such segments (see Figs. A-5.1 and A-5.2). The energy equation for the various segments of the loop is discretised to obtain the following equations for the temperature of the i^{th} node at the new time step (i.e. n+1) as a function of the old (i.e. n^{th}) nodal temperatures at the i^{th} and $(i-1)^{th}$ nodes.

$$\theta_i^{n+1} = \theta_i^n\left[1-\phi\omega_n\frac{\Delta\tau}{\Delta S}\right]+\theta_{i-1}^n\left[\phi\omega_n\frac{\Delta\tau}{\Delta S}\right]+\frac{L_t\Delta\tau}{L_h} \qquad 1<N\le N_h \text{ (heater)} \qquad \text{(A-5.1)}$$

$$\theta_i^{n+1} = \theta_i^n\left[1-\phi\omega_n\frac{\Delta\tau}{\Delta S}\right]+\theta_{i-1}^n\left[\phi\omega_n\frac{\Delta\tau}{\Delta S}\right] \qquad N_h+1<N\le N_H \text{ and } N_c+1<N\le N_t \quad \text{(A-5.2)}$$

$$\theta_i^{n+1} = \theta_i^n\left[1-\phi\omega_n\frac{\Delta\tau}{\Delta S}-St_m\Delta\tau\right]+\theta_{i-1}^n\left[\phi\omega_n\frac{\Delta\tau}{\Delta S}\right] \qquad N_H+1<N\le N_c \qquad \text{(A-5.3)}$$

Similarly, the momentum equation can be discretised implicitly as

$$\omega_{n+1}+\frac{pL_t\Delta\tau}{2\mathrm{Re}_{st}^b}\omega_{n+1}^{2-b}=\omega_n+\frac{Gr_m\Delta\tau}{\mathrm{Re}_{st}^b}\theta_f \qquad \text{(A-5.4)}$$

$$\text{Where } \theta_f=\oint\theta_i^{n+1}dZ=\int_{Z_{N1}}^{Z_{N3}}\theta_i^{n+1}dZ-\int_{Z_{N3}}^{Z_{N4}}\theta_i^{n+1}dZ \qquad \text{(A-5.5)}$$

The limits Z_{N1}, Z_{N2}, Z_{N3} and Z_{N4} correspond to the elevation at nodes N_1, N_2, N_3 and N_4 respectively (see Fig. A-5.1 and A-5.2). The explicit scheme has been used for the energy equation for which the stability criterion satisfying equations A-5.1 to A-5.3 is

$$\Delta\tau\le\frac{1}{\frac{\phi\omega_n}{\Delta S}+St_m} \qquad \text{(A-5.6)}$$

To ensure stability, the calculated time step was multiplied with a number less than unity in the present calculations.

Calculation Procedure

A uniform segment length of 1 cm was considered for the present calculations. For clockwise flow, the marching calculations started with node 1 and (first node in the heater) equation (A-5.1) was used to calculate the nodal temperatures for $1<N\le N_h$. From $N_h+1<N\le N_H$ equation (A-5.2) was used. Similarly, equation (A-5.3) was used for $N_H+1<N\le N_c$. For the cold leg equation (A-5.2) was used for $N_c+1<N\le N_t$. Once all the nodal temperatures are calculated ω_{n+1} is calculated using equation (A-5.4) after evaluating the temperature integral numerically by Simpson's rule. For the HHHC

orientation, flow direction could be clockwise or anticlockwise. For flow in the anticlockwise direction the marching direction was reversed keeping the same sign for ω in equations (A-5.1) to (A-5.3). The flow rate so calculated will always be positive. To identify the flow direction, the calculated flow is multiplied by the following parameter

$$N_{sign} = N_{sign} x(-1) \qquad \text{(A-5.7)}$$

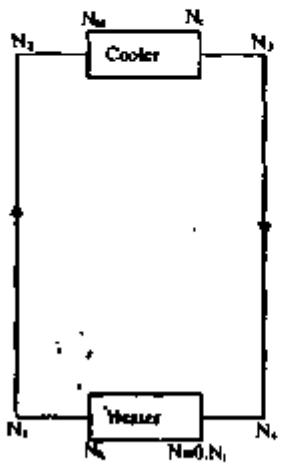

Fig. A-5.1 Nodalisation for clockwise flow

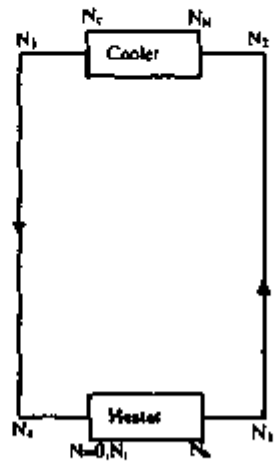

Fig. A-5.2: Nodalisation for anticlockwise flow

The starting value of $N_{sign} = 1$ for clockwise flow. Whenever, the calculated value of ω is negative, then the value of N_{sign} is changed as per the above equation so that instantaneous value of ω is obtained as

$$\omega = N_{sign}\omega \qquad \text{(A-5.8)}$$

The node number for anticlockwise flow (denoted with superscript 'a') has the following relation to the node number in clockwise flow (denoted without superscript)

$$N_4^a = N_4 \qquad \text{(A-5.9a)}$$

$$N_1^a = N_4^a + N_c - N_4 \qquad \text{(A-5.9b)}$$

$$N_2^a = N_1^a + N_3 - N_3 \qquad \text{(A-5.9c)}$$

$$N_N^a = N_2^a + N_3 - N_c \qquad \text{(A-5.9d)}$$

$$N_c^a = N_N^a + N_c - N_N \qquad \text{(A-5.9e)}$$

$$N_3^a = N_c^a + N_N - N_2 \qquad \text{(A-5.9f)}$$

$$N_4^a = N_3^a + N_2 - N_1 \qquad \text{(A-5.9g)}$$

$$N_i^n = N_d^n + N_1 - N_h = N_i \qquad \text{(A-5.9h)}$$

The adequacy of the nonlinear formulation was checked by comparing with the analytical steady state equations. Also, the stability threshold predicted by the code was compared with the corresponding threshold obtained by the linear method. For this comparison, the initial conditions corresponded to the steady state value for the orientation considered.

Effect of axial conduction

Effect of axial conduction is negligible at high flows but can be significant at low flows. If it is considered, then the governing differential equations become

$$\frac{\partial\theta}{\partial\tau} + \phi\omega\frac{\partial\theta}{\partial S} - \frac{L_t D}{\mathrm{Re}_{rr}\,\mathrm{Pr}\,H^2}\frac{\partial^2\theta}{\partial S^2} = \frac{L_t}{L_h} \qquad 0<S\leq S_h \quad \text{heater} \qquad \text{(A-5.10a)}$$

$$\frac{\partial\theta}{\partial\tau} + \phi\omega\frac{\partial\theta}{\partial S} - \frac{L_t D}{\mathrm{Re}_{rr}\,\mathrm{Pr}\,H^2}\frac{\partial^2\theta}{\partial S^2} = 0 \qquad S_h<S\leq S_{hl} \text{ and } S_c<S\leq S_t \text{ pipes} \qquad \text{(A-5.10b)}$$

$$\frac{\partial\theta}{\partial\tau} + \phi\omega\frac{\partial\theta}{\partial S} - \frac{L_t D}{\mathrm{Re}_{rr}\,\mathrm{Pr}\,H^2}\frac{\partial^2\theta}{\partial S^2} = -St_m\theta \qquad S_{hl}<S\leq S_c \quad \text{cooler} \qquad \text{(A-5..10c)}$$

The above equations can be discretised to obtain the following finite difference equations

$$\theta_i^{n+1} = \theta_i^n\left[1 - \phi\omega_n\frac{\Delta\tau}{\Delta S} - \frac{2L_t D}{\mathrm{Re}_{rr}\,\mathrm{Pr}\,H^2}\frac{\Delta\tau}{\Delta S^2}\right] + \theta_{i-1}^n\left[\phi\omega_n\frac{\Delta\tau}{\Delta S} + \frac{L_t D}{\mathrm{Re}_{rr}\,\mathrm{Pr}\,H^2}\frac{\Delta\tau}{\Delta S^2}\right] + \theta_{i+1}^n\left[\frac{L_t D}{\mathrm{Re}_{rr}\,\mathrm{Pr}\,H^2}\frac{\Delta\tau}{\Delta S^2}\right] + \frac{L_t\Delta\tau}{L_h} \qquad \text{(A-5.11a)}$$

$$\theta_i^{n+1} = \theta_i^n\left[1 - \phi\omega_n\frac{\Delta\tau}{\Delta S} - \frac{2L_t D}{\mathrm{Re}_{rr}\,\mathrm{Pr}\,H^2}\frac{\Delta\tau}{\Delta S^2}\right] + \theta_{i-1}^n\left[\phi\omega_n\frac{\Delta\tau}{\Delta S} + \frac{L_t D}{\mathrm{Re}_{rr}\,\mathrm{Pr}\,H^2}\frac{\Delta\tau}{\Delta S^2}\right] + \theta_{i+1}^n\left[\frac{L_t D}{\mathrm{Re}_{rr}\,\mathrm{Pr}\,H^2}\frac{\Delta\tau}{\Delta S^2}\right] \qquad \text{(A-5.11b)}$$

$$\theta_i^{n+1} = \theta_i^n\left[1 - \phi\omega_n\frac{\Delta\tau}{\Delta S} - \frac{2L_t D}{\mathrm{Re}_{rr}\,\mathrm{Pr}\,H^2}\frac{\Delta\tau}{\Delta S^2} - St_m\Delta\tau\right] + \theta_{i-1}^n\left[\phi\omega_n\frac{\Delta\tau}{\Delta S} + \frac{L_t D}{\mathrm{Re}_{rr}\,\mathrm{Pr}\,H^2}\frac{\Delta\tau}{\Delta S^2}\right] + \theta_{i+1}^n\left[\frac{L_t D}{\mathrm{Re}_{rr}\,\mathrm{Pr}\,H^2}\frac{\Delta\tau}{\Delta S^2}\right] \qquad \text{(A-5.11c)}$$

The effect of axial conduction is considered for start-up from rest. To facilitate flow initiation in a particular flow direction, the unheated length before one of the vertical limbs was made smaller compared to the other

Published by : Dr. Vijai Kumar, Head Library & Information Services Division
Bhabha Atomic Research Centre, Mumbai - 400 085, India.